Role of Supplementary Cementitious Materials in Mitigating Alkali-Silica Reaction

by

Marie Joshua Tapas

Supervisors:
Dr Kirk Vessalas
Dr Paul Thomas
Prof. Vute Sirivivatnanon

This thesis is submitted in fulfilment of the requirements for the degree of

Doctor of Philosophy

School of Civil and Environmental Engineering
Faculty of Engineering and Information Technology
University of Technology Sydney

April 2020

Certificate of Original Authorship

I, *Marie Joshua Tapas,* declare that this thesis, is submitted in fulfilment of the requirements for the award of Doctor of Philosophy, in the School of Civil and Environmental Engineering, Faculty of Engineering and Information Technology at the University of Technology Sydney.

This thesis is wholly my own work unless otherwise referenced or acknowledged. In addition, I certify that all information sources and literature used are indicated in the thesis.

This document has not been submitted for qualifications at any other academic institution.

This research is supported by the Australian Government Research Training Program.

Production Note:
Signature removed prior to publication.

Signature: Marie Joshua Tapas
Date: April 16, 2020

Acknowledgements

This study will not be possible without the support of my supervisors, Dr Kirk Vessalas, Dr Paul Thomas and Prof. Vute Sirivivatnanon. I am deeply grateful to them for giving me the opportunity to do my PhD in Sydney and for allowing me the freedom to carry out the research work in the manner I see best, while providing comments and recommendations on how to further improve. Likewise, I am deeply grateful for their generosity and support. I was indeed privileged and blessed that during the course of my PhD I was able to attend technical trainings, local and international conferences and even do part of my research overseas for seven months at EPFL, Switzerland. I am also thankful to Dr Nadarajah Gowripalan for fruitful and insightful discussions, which allowed me to learn even beyond the scope of my PhD.

I am also extremely thankful to Prof. Karen Scrivener for giving me the opportunity to work at the Laboratory of Construction Materials (LMC), EPFL, providing me access to all LMC equipment and resources at no cost and even allowing me to attend relevant meetings for my own learning. This work would not have been possible without the facilities and equipment provided by LMC. Likewise, I am thankful to Mr. Lionel Sofia for his incredible support to my ASR work at EPFL. Also, my thanks to all EPFL friends who've made my stay memorable, most especially to Ms. Mahsa Bagheri, who've been so kind to extend a helping hand every time I need to ensure that I complete all required work and deliver the most out of my short stay. I am also thankful to UTS Research collaboration fund for giving me the financial support to do my exchange overseas. It was definitely the most memorable part of my PhD journey.

Likewise, my thanks to UTS Science for providing facilities and equipment for most of my characterization work and to UTS Concrete and Mortar lab for providing my casting work requirements. Most notably, I would like to extend my sincerest thanks to Mr. Muller Hailu for providing support to most of my experimental work and for always lending a helping hand with a smile.

I am also thankful to all my ASR research teammates for the fruitful discussions, fun moments, and laughter. My sincerest thanks to Mr. Jinsong Cao for so generously providing support to some of my experimental work.

I am also thankful to all the friends I've met in UTS for making my PhD very fun and memorable. More than the PhD, I have gained lifelong friends that I will forever treasure. Likewise, my gratitude to all my friends outside the University for giving me my work-life balance.

I am also extremely grateful to my parents for their unwavering support in my every endeavour, and most especially to my mother, for her unconditional love and for always reminding me that I can be whatever I want to be.

Lastly, I would like to thank Cement Concrete and Aggregates Australia (CCAA) and the Australian Research Council Research Hub for Nanoscience Based Construction Materials Manufacturing (NANOCOMM) for providing financial support for this project.

List of Publications

- Tapas, M.J., Vessalas, K., Thomas, P. and Sirivivatnanon, V., "Mechanistic Role of SCM Composition in ASR Mitigation" accepted for oral presentation in Concrete 2019 "Concrete in Practice-Progress Through Knowledge", September 8-11, 2019 Sydney, Australia

- Tapas, M.J., Vessalas, K., Thomas, P. and Sirivivatnanon, V., "An AMBT Study on the Effect of Limestone on ASR Mitigation: Ground Limestone vs. Interground Limestone in Cements", 2nd RILEM Spring Convention & International Conference on Sustainable Materials, Systems and Structures (SMSS2019), March 18-22, 2019 Rovinj, Croatia

- Tapas, M.J., Brenner, J., Vessalas, K., Thomas, P. and Sirivivatnanon, V., "Effect of Limestone Content in Cement on Alkali-Silica Reaction Using Accelerated Mortar Bar Test" Concrete In Australia, Vol 44 (2): 41-47, June 2018

- Tapas, M.J., Vessalas, K., Thomas, P. and Sirivivatnanon, V., "Role of SCM Composition in ASR Mitigation" accepted for oral presentation in Concrete 2017 "Advances in Materials and Structures in Adelaide, Australia held October 23-25, 2017

- Tapas, M.J., Sofia, L., Vessalas, K., Thomas, P., Scrivener, K., " The Ability of Supplementary Cementitious Materials to Mitigate Alkali-Silica Reaction (ASR) in Cements of Higher Alkali Contents and their Effect on ASR Gel Composition," submitted to Cement and Concrete Research, October 2019 (under review)

- Tapas, M.J., Vessalas, K., Thomas, P., Sirivivatnanon, V., "Accelerated mortar bar test investigation of blended cements containing limestone mineral addition," submitted to Cement and Concrete Research, October 2019 (under review)

Table of Contents

List of Figures

List of Tables

List of Abbreviations

AFm	aluminate ferrite monosulfate
AFt	Al_2O_3-Fe_2O_3-trisulfate
Al/Ca	aluminium/calcium
Al/Si	aluminium/silicon
Al_2O_3	alumina
AMBT	accelerated mortar bar test
AS	Australian standards
ASR	alkali silica reaction
C_2S	belite
C_3A	tricalcium aluminate
C_3S	alite
C_4AF	tetracalcium aluminoferrite
Ca/Si	calcium/silicon
$CaCO_3$	calcium carbonate
C-A-S-H	calcium aluminosilicate hydrate
CH	portlandite
CPT	concrete prism test
C-S-H	calcium silicate hydrate
EDS	energy dispersive spectroscopy
FA	fly ash
GGBFS	ground granulate blast furnace slag
GP	General Portland
ICP-MS	inductively coupled plasma mass spectrometry
ICP-OES	inductively coupled plasma - optical emission spectrometry
K	potassium

K_2O	potassium oxide
MK	metakaolin
Na	sodium
Na_2O	sodium oxide
Na_2O_{eq}	sodium equivalent
N-A-S-H	sodium aluminosilicate hydrates
PC	Portland cement
RH	relative humidity
SCM	supplementary cementitious material
SEM	scanning electron microscope
SF	silica fume
SiO_2	silica
SL	slag or ground granulated blast furnace slag
TG	thermogravimetry
XRD	X-ray diffraction

Abstract

Alkali-silica reaction (ASR) describes reactions between certain forms of silica and the high alkaline pore solution of concrete that form an ASR gel product that causes the concrete to expand and crack. ASR poses a threat to concrete stability particularly in cases where the formation of cracks leads to a loss in the mechanical performance and properties of the concrete. The addition of supplementary cementitious materials (SCMs) such as fly ash and slag for the partial replacement of Portland cement in concrete is considered to be the most economical option in mitigating the occurrence of ASR. However, the closure of coal-fired power stations and increased recycling of steel threaten the supply of fly ash and slag.

In order to be able to identify future SCMs for use in ASR mitigation, there is a need to understand the mechanisms by which conventional SCMs mitigate ASR. At present, the mitigation mechanisms are still poorly understood. Furthermore, the influence of other components of the binder system on the efficacy of SCMs in ASR mitigation such as limestone (which is a standard cement addition) and cement itself (the introduction of higher alkali contents) also warrant investigation. Currently, there is an ongoing interest in Australia to increase the limestone content in General Purpose (GP) cement from 7.5% to 12% in order to reduce CO_2 emissions associated with cement production. In addition, there is a requirement to increase the alkali limits in cement, which is currently set at 0.6% Na_2O_{eq} (sodium equivalent), in order to minimize the amount of raw materials thrown to waste. Sodium equivalent is equal to the sum of alkali oxides in the cement ($Na_2O + 0.658K_2O$).

In this study, the accelerated mortar bar test (AMBT) was carried out to assess the efficacy of traditional SCMs in mitigating ASR as a function of SCM type (fly ash, slag, metakaolin and silica fume) and dosage in binder systems with various limestone contents (0%, 8%, 12% and 17%). The effect of SCM type, SCM replacement level and limestone addition on the portlandite amount, the pore solution alkalinity and the composition of the calcium silicate hydrate (main cement hydration product) as well as the dissolution of SCMs in an alkali environment were investigated and compared with the expansion results. To be able to assess the effect of cement alkalinity on the efficacy of the SCMs in ASR mitigation, the expansion of concrete prisms was studied by immersion of concrete prisms in simulated pore solution derived from the 28-day pore solution of pastes with equivalent composition of the binder used in the concrete. This alternative testing method addresses the limitations of the conventional ASR testing methods of AMBT (excessive alkali) and CPT (alkali leaching) for assessing the effect of binder alkalinity on the level of ASR expansion.

The results demonstrate that SCMs at recommended dosages work effectively to mitigate ASR even in cements with effective alkali content of 1% Na_2O_{eq}. The efficacy of SCMs in reducing ASR expansion is related to their ability to release silicon and aluminium in solution, consume portlandite, reduce pore solution alkali concentration and modify the calcium silicate hydrate (C-S-H) composition. Thus, siliceous materials, aluminosilicates and even pure aluminium present a potential to mitigate ASR. Limestone (98% $CaCO_3$) does not aggravate ASR and has no detrimental effect on the efficacy of SCMs in mitigating ASR. Moreover, experimental findings indicate that limestone has no capability to actively mitigate ASR as it does not modify the C-S-H composition and does not actively reduce the pore solution alkali concentration like SCMs.

1 Introduction

Concrete outperforms other construction materials due to its low cost, versatility, strength, and durability. It is, in fact, the most widely used construction material in the world and the second most used substance on earth after water (Scrivener, John & Gartner 2016). Due to the critical role it plays in infrastructure, concrete demands a high level of stability over its service life. Concrete durability can, however, be affected by several processes that can, in turn, lead to its premature degradation. Typical causes of concrete deterioration include acid attack, sulphate attack, delayed ettringite formation (DEF), alkali-aggregate reactions, corrosion of embedded metals, freezing and thawing, abrasion and erosion, de-icer salt scaling, and many others.

Alkali-aggregate reactions (AAR) are of two types: alkali-silica reactions (ASR) and alkali-carbonate reactions (ACR). To date, ACR, which occurs when alkali in concrete reacts with certain argillaceous dolomitic limestone aggregates, has not been identified in Australia (Standards Australia 2015). This study is particularly interested in ASR.

Stanton first reported the occurrence of ASR in 1940. The first case of ASR is that of a concrete pavement in California (Stanton 1940). In Australia, a number of concrete structures including dams, bridges and concrete railway sleepers have also been identified as suffering from various levels of ASR. The 1st case of ASR in a bridge structure was reported in 1983 (Shayan, Diggins & Ivanusec 1996b).

ASR can occur in concrete if all three factors are present: reactive silica in the aggregate, high alkali pore solution, and sufficient moisture. High alkali pore solution, which may be present in certain types of cements, will dissolve certain silica phases in the aggregate and once dissolved, bind calcium (Ca^{2+}) and alkali ions (Na^{+}, K^{+}) in the pore solution to form the ASR product (alkali calcium silicate hydrate gel) which can induce pressure build up, resulting in expansion, and eventual cracking of the concrete (Chatterji 2005; Rajabipour et al. 2015). The cracking either leads to premature failure of the concrete structure or helps facilitate water ingress leading to other concrete failure mechanisms such as reinforcement corrosion and freeze thaw damage.

The elimination or depletion of any of the essential factors (reactive aggregate, alkali and moisture) will inhibit ASR. The total alkali content, also referred to as the sodium equivalent ($\%Na_2O_{eq}$), is calculated as the $\%Na_2O + 0.658(\%K_2O)$, where Na_2O and K_2O are derived from the cement oxide composition. In Australia, the risk of damage due to ASR is minimised in concrete mixes with an alkali content less than 2.8 kg/m^3. Further, a strict, 0.6% sodium equivalent (Na_2O_{eq}) alkali limit is imposed for Australian cements in order to minimize the occurrence of ASR (Standards Australia 2015). The use of a non-reactive aggregate is also one possible solution to prevent the occurrence of ASR. However, due to geographical constraints or local unavailability, the option of using non-reactive aggregates is not always viable. At present, the addition of supplementary cementitious materials (SCMs) to concrete is considered the most economical option in mitigating the occurrence of ASR. Traditional SCMs include fly ash, ground granulated blast furnace slag (GGBFS or slag), metakaolin and silica fume. In Australia, the most common method of mitigating ASR is the

incorporation of fly ash or slag into the concrete mix. The use of silica fume and metakaolin is very limited for reasons of cost (Standards Australia 2015).

Two test methods are widely used to assess aggregate reactivity and the efficacy of SCMs in ASR mitigation: the accelerated mortar bar test (AMBT) and the concrete prism test (CPT). The more rapid test method AMBT involves monitoring expansion in mortar specimens immersed in 1M NaOH at 80 °C while the generally acknowledged and more reliable yet longer test method CPT involves measuring expansion in concrete specimens boosted with alkali to reach 1.25% Na_2O_{eq} and stored at 38 °C in a humid environment. Alkali boosting is carried out by adding NaOH to elevate the original cement alkali level to 1.25% Na_2O_{eq}. The most popular versions of these test methods include American standards ASTM C1567 AMBT and ASTM C1293 CPT. Australia also uses its own version of test methods, AS 1141.60.1 AMBT and AS 1141.60.2 CPT, which are very similar to the American standards but differ with changes in the test limits.

ASR mitigation in Australia varies by region. In Queensland, testing of aggregate for ASR potential is not mandatory, but all mixes are required to have a minimum content of 20% fly ash. In New South Wales, all aggregates need to be assessed for ASR using AMBT procedure at least annually, and aggregates assessed as slowly reactive may be used with the addition of 25% fly ash. However, if the aggregates are assessed as reactive (i.e., the expansion exceeds 0.1% at 10 days), the specification recommendation is that an alternative aggregate be used or that a proposed mitigative measure is proven in testing by the RMS T364 method, a concrete prism test which uses a higher adjusted cement alkali of 1.38% Na_2Oeq. In Victoria, all aggregates are

to be assessed for ASR using the AMBT on a three-yearly basis and if aggregates are assessed as reactive, (either 'slowly reactive' or 'reactive' in the AMBT classification), the 'deemed to comply' levels of SCMs given in HB79 (Standards Australia 2015).

Most commonly used SCMs, fly ash and ground granulated blast furnace slag (GGBFS), are industrial by-products and foreseen to be scarce in the future. Fly ash is generated from the burning of coal in electrical power stations while GGBFS or simply, slag is a by-product of iron production used for steelmaking (Thomas 2013).

Globally, the shortage of fly ash supply is fueled by the closure of coal-fired power plants in favour of greener sources of energy. Coal-fired power stations pollute the environment heavily due to significant production of greenhouse gases that can lead to global warming. Although carbon dioxide (CO_2) emissions are typically the biggest point of concern, other emissions like sulfur dioxide SO_2, nitrogen oxide (NO_x) as well as fine particulate matter also pose significant health hazards (ECRC 2017; Thomson, Huelsman & Ong 2018). Between 2010 and the first quarter of 2019, U.S. power companies announced the retirement of more than 546 coal-fired power units (Johnson & Chau 2019). Moreover, Europe has a continent-wide move away from coal-fired power, with some coal-fired power plants due to close or switch to biomass (Nalbandian-Sugden 2015). Australia is no exception with around one-third of its coal-fired power stations closed during 2012-2017, with remaining expected to close as well in the coming decades (Burke, Best & Jotzo 2018).

Increasing recycling of steel lowers the availability of slag. Currently, the amount of slag available is only about 8% by mass of total cement production worldwide and

even expected to further decrease in the coming years (Scrivener, John & Gartner 2016).

In order to be able to identify future SCMs for ASR mitigation that are both sustainable and locally available, there is a need to understand the mechanisms by which traditional SCMs mitigate ASR. At present, the mitigation mechanisms are still poorly understood. Further, the influence of other components of the binder on the efficacy of SCMs in ASR mitigation, such as limestone (which is a standard cement addition) and cement itself (higher alkali contents), also warrant an investigation.

Adding limestone mineral addition is a way to reduce CO_2 emissions associated with cement production. Thus, currently, there is a drive to increase limestone content in Australian GP cement from 7.5% to 12%. Whereas, the effect of limestone on the mechanical properties of concrete has been evaluated, its effect on ASR still remains to be investigated.

Since alkalis drive the dissolution of silica phases of aggregates, one way to control ASR is to limit the alkali content of cements. Thus, Australian cements are limited to have maximum alkali content of 0.6% Na_2O_{eq}. Strict alkali limits on cement however result in a lot of raw materials being thrown out due to unsuitability.

1.1 Research Objectives

This study has three main objectives distributed into three results and discussion chapters. The objectives of each chapter are outlined below.

Chapter 4 Mechanistic Role of SCMs in ASR Mitigation

This chapter aims to uncover the mechanisms by which SCMs mitigate ASR by correlating the efficacy of various SCMs (FA, SL, MK and SF) in reducing ASR expansion with their ability to release silicon and aluminium in solution, consume portlandite, reduce alkali pore solution concentration, and modify calcium silicate hydrate (C-S-H) composition. In particular, this chapter aims to understand why effective dosage requirements for ASR mitigation vary as a function of SCM type, and based on generated understanding of the mechanisms, develop a basis for identifying potential SCMs for ASR mitigation.

Chapter 5 Pore Solution Method for Assessing the Efficacy of SCMs to Mitigate ASR in Cements of Higher Alkali Contents

This chapter investigates the ability of SCMs (fly ash and slag) to mitigate ASR when used in conjunction with cements with up to 1% Na_2O_{eq} effective alkali content using an alternative ASR testing method. The method, developed at the laboratory of construction materials, EPFL Switzerland makes use of simulated pore solution (based

on 28 days pore solution alkali concentration of the binder of interest) as a storage solution for concrete prisms. The new method addresses the limitations of conventional testing methods AMBT and CPT in assessing the effect of cement alkalinity on ASR mitigation. The formation of ASR gel as well as the effect of SCM addition on C-S-H composition, alkali uptake in the C-S-H and ASR gel composition, are also investigated.

Chapter 6 Influence of Limestone on the Efficacy of SCMs in ASR Mitigation

This chapter investigates the effect of limestone addition (up to 17%) on the efficacy of SCMs in ASR mitigation. The effect of limestone addition on portlandite content, phase development, pore solution alkalinity, and C-S-H composition are also reported.

1.2 Significance of the Study

The findings of this study are useful to ensure the sustainable production of ASR-free concrete in Australia. The ability to determine suitable alternative SCMs that are abundant and locally available will ensure sustainable mitigation of ASR irrespective of the availability of traditional SCMs fly ash and slag. Moreover, if increased limestone and cement alkali contents will be shown to not affect the efficacy of SCMs in ASR mitigation, then this will provide additional supporting data to the proposed increase in limestone and alkali contents in Australian cements thereby reducing the environmental impact of cement production.

2 Literature Review

2.1 Chemistry of Cement and Concrete

Portland cement is produced by burning limestone and clay minerals to a temperature of about 1450 °C. The resulting clinker is cooled rapidly, mixed with gypsum (calcium sulfate), and then finely ground to produce cement (Taylor 1997). The clinker is composed of four major phases: alite, belite, tricalcium aluminate and tetracalcium aluminoferrite. These phases play an integral role in the strength development of hydrated cement.

Alite or tricalcium silicate (Ca_3SiO_5) constitutes 50-70% of the clinker and is mainly responsible for strength development at ages up to 28 days. Belite or dicalcium silicate (Ca_2SiO_4) which represents 15-30% reacts slowly with water, and hence does not contribute much to strength development up to 28 days but is essential for later age strength development. Tricalcium aluminate ($Ca_3Al_2O_6$) which makes up 5-10% of the clinker reacts rapidly with water and liberates a lot of heat, which results in fast setting. Gypsum slows down the hydration of tricalcium aluminate and controls the rate of set. Tetracalcium aluminoferrite (Ca_2AlFeO_5) makes up 5-10% of the clinker and also does not contribute much to strength (Taylor 1997).

Simplified notations based on the sum of oxides are typically employed to name cement compounds. Tricalcium silicate (Ca_3SiO_5), for instance can be expressed as $3CaO + SiO_2$. Tables 2-1 and 2-2 list cement chemistry notation for oxides and cement phases.

Table 2-1 Cement chemistry notation for oxides

CaO	C
SiO_2	S
$A1_2O_3$	A
Fe_2O_3	F
SO_3	S
H_2O	H
CO_2	C
Na_2O	N
K_2O	K
SO_3	$\bar{S}$

Table 2-2 Cement chemistry notation for cement phases

$3CaO•SiO_2$ or Ca_3SiO_5	C_3S
$2CaO•SiO_2$ or Ca_2SiO_4	C_2S
$3CaO•Al_2O_3$ or $Ca_3Al_2O_6$	C_3A
$4CaO•Al_2O_3•Fe_2O_3$ or $Ca_4Al_2Fe_2O_{10}$/ Ca_2AlFeO_5	C_4AF

When cement is mixed with water, the silicate phases (C_3S and C_2S) react to form calcium silicate hydrate (C-S-H), which is the main binding phase of cement and produces calcium hydroxide (CH) as a by-product (Equations 2-1 and 2-2). The stoichiometry of C-S-H is variable and depends on the actual composition of the cement. Typically, the Ca/Si ratio has a range of 1.5-2 (Thomas 2013). The aluminate phases on the other hand, react with water and gypsum producing ettringite ($C_6A\bar{S}_3H_{32}$) as the primary product (Equation 2-3). Once gypsum is depleted, some of the excess C_3A react with the formed ettringite to produce monosulfate ($3C_4A\bar{S}H_{12}$), as shown in Equation 2-4 (Beaudoin & Odler 2003).

Equation 2-1 $C_3S + 5.3H \rightarrow C_{1.7}SH_4 + 1.3CH$

Equation 2-2 $C_2S + 4.3H \rightarrow C_{1.7}SH_4 + 0.3CH$

Equation 2-3 $C_3A + 3C\bar{S}H_2 + 26H \rightarrow C_6A\bar{S}_3H_{32}$

Equation 2-4 $2C_3A + C_6A\bar{S}_3H_{32} + 4H \rightarrow 3C_4A\bar{S}H_{12}$

Cement, in combination with water and aggregates produces concrete, which is the second most used substance on earth after water (Scrivener, John & Gartner 2016). Owing to its durability, versatility and low cost, concrete is the material of choice for most structures. However, although concrete is highly durable, there are processes and certain environmental conditions that may lead to its premature degradation. Table 2-3 lists the common causes of concrete deterioration. This study will focus on one type of alkali-aggregate reaction, known as alkali-silica reaction (ASR), which will be discussed in the next section.

Table 2-3 Common causes of concrete deterioration (Thomas 2013)

Chemical	**Physical**
Acid Attack	Freezing and thawing
Sulfate Attack	De-icer salt scaling
Delayed ettringite formation	Abrasion and erosion
Corrosion of embedded metals	Fire
Alkali-aggregate reactions	Physical salt attack
Carbonation	

2.2 Alkali-Silica Reaction: Factors and Mechanisms

Alkali-silica reaction (ASR) results from the dissolution of silica (SiO_2) present in aggregates and swelling of the hygroscopic gel that forms. In alkaline environment which is typical in concrete, hydroxyl ions (OH^-) attack the (≡Si-O-Si≡) linkages, resulting in the dissolution of silica network as in Equation 2-5. The dissolved silicate ions are negatively charged and therefore react with available potassium (K^+) and sodium ions (Na^+) in the system forming alkali silicates (Chatterji 2005). The network

dissolution of silica, as well as its reaction with dissolved alkali ions, effectively reduces the pH in the system resulting in the polymerization of the silicate ions, producing silica gel. Some of the alkalis incorporated in silica gel may be replaced by calcium ions resulting in the formation of alkali calcium silicate hydrate ((N,K)-C-S-H) gel, known as the ASR gel (Rajabipour et al. 2015). Moreover, this exchange also results in the recycling of the alkalis back into concrete pore solution and to calcium deficiency of the pore solution which promotes further dissolution of portlandite, which again results in the increase of pH and continued ASR cycle (Rajabipour et al. 2015).

Equation 2-5 $\equiv Si\text{-}O\text{-}Si\equiv + 2OH^- \rightarrow 2\equiv SiO^- + H_2O$

The reaction mechanism for ASR can be summarized as follows: 1) hydroxyl attack breaking the Si-O-Si bonds and forming silanol (Si-OH) bonds; 2) reaction of silanol groups with OH^- in the solution forming negatively charged sites on the silicate surface; 3) binding of the sodium ions (Na^+) and potassium ions (K^+) as a form of charge compensation; and 4) calcium ions (Ca^{2+}) substituting some of the alkali cations to form the ASR gel, alkali calcium silicate hydrate ((Na,K)-Ca-SiO_2-H_2O) (Glasser & Kataoka 1981).

The ASR gel is porous with a high surface area and bears many hydrophilic groups which increases its adsorption capacity and makes the gel prone to swelling (Rajabipour et al. 2015). Gel swelling can induce pressure build up, resulting to expansion, and eventual cracking of the concrete. The cracking can either lead to premature failure of the concrete structure or help facilitate water ingress leading to

other concrete failure mechanisms such as reinforcement corrosion and freeze thaw damage.

There are three essential requirements for alkali-silica reaction in concrete to take place: reactive aggregate, high alkali pore solution and sufficient moisture. It follows then that elimination of any of the three factors will prevent the occurrence of deleterious ASR.

2.2.1 Alkali-Reactive Aggregates

Alkali-reactive aggregates contain 'reactive silica' which is a form of silica that is either poorly crystalline (i.e. contains many lattice defects and or dislocations) or is amorphous/glassy. SiO_2 stability decreases with increasing disorder in its structure. SiO_4 tetrahedra are the building blocks of silica and the structure of silica minerals depend on how the SiO_4 tetrahedra are interconnected (Smith 1997). Atoms that have no long-range order and instead form a random network are referred to as amorphous. Amorphous SiO_2 is known to be the most reactive form of SiO_2 (Rajabipour et al. 2015). Aside from reactive SiO_2 content, porosity and presence of internal defects such as cracks also contribute to aggregate reactivity.

2.2.2 Pore Solution Alkalinity

The potential for ASR increases with increasing pH or alkalinity of the pore solution due to increase in the solubility of silica, facilitating the formation of alkali-silica gel. Even more stable forms of silica can dissolve at higher alkali concentrations.

Cement is considered to be the major source of alkali content in concrete. AS 3972 General Purpose and Blended Cements (Standards Australia 2010) provides a guide to calculate the total alkali content ($\%Na_2O_{eq}$) of a Portland cement as shown in Equation 2-6.

Equation 2-6 $\%Na_2O_{eq} = \%Na_2O + 0.658\ \%K_2O$

Sodium oxide ($\%Na_2O$) and potassium oxide ($\%K_2O$) are derived from the cement oxide composition analysis. The 0.658 correction factor accounts for the difference in molecular weight between Na_2O and K_2O. Figure 2-1 illustrates the relationship between hydroxyl ion concentration of pastes ($w/c \sim 0.5$) and the alkali content of the cement (Thomas 2013).

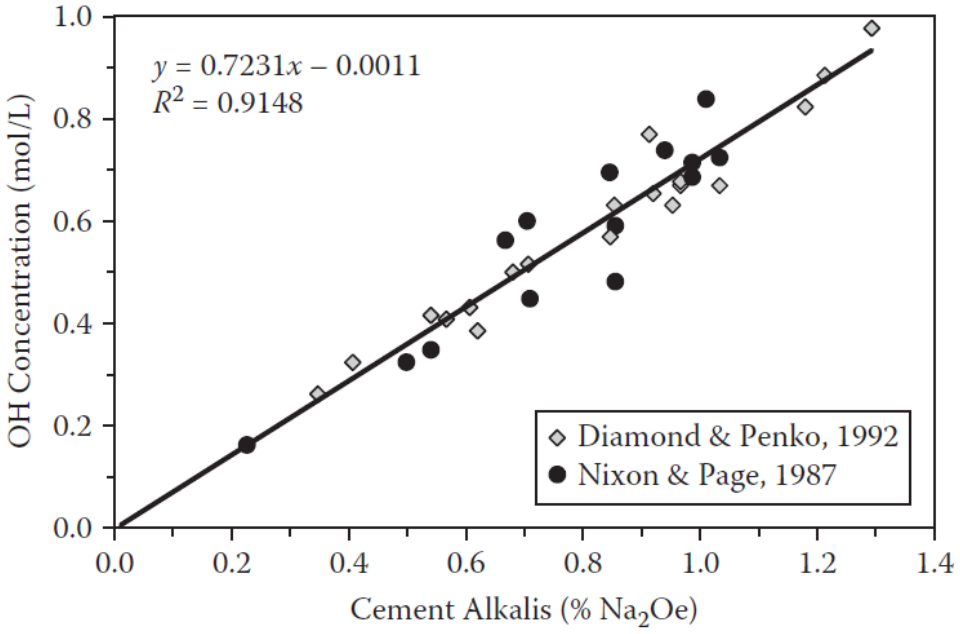

Figure 2-1 Relationship between the hydroxyl ion concentration of the pore solution and the alkali content of the Portland cement (Thomas 2013)

Whereas cement serves as the major source of alkali, aggregates and SCMs can also supply alkalis into the pore solution. In addition, external sources can also increase the alkalinity of the concrete (Rajabipour et al. 2015). During cement hydration reactions, certain amount of alkali ions can be released from the aggregates (Constantiner & Diamond 2003; Drolet, Duchesne & Fournier 2017) and SCMs and carried into the pore solution of concrete (Shehata, Thomas & Bleszynski 1999).

One way to mitigate ASR is to control the alkali content of the concrete. The proposed limit on alkalis in concrete varies in different parts of the world and ranges between 2 and 5 kg Na_2O_{eq}/m^3 of concrete. In Australia, the risk of damage due to ASR is considered minimised in concrete mixes with alkali content ($\%Na_2O_{eq}$) less than 2.8 kg/m^3. The use of low alkali cement or cement not having a total alkali content greater

than 0.6% sodium equivalent (Na_2O_{eq}) is also a standard requirement (*ATIC SP43 Cementitious Material for Concrete* 2017; Standards Australia 2015).

2.2.3 Moisture Requirement

ASR does not occur in concretes that are dry in service because moisture is necessary to allow the migration of alkali ions into the reaction sites. Further, the ASR gel also absorbs moisture (Juenger & Ostertag 2004), resulting for it to swell and to further aggravate ASR-induced damage. The risk for ASR is minimized when the humidity level is below 80 percent (Standards Australia 2015). Moisture conditions, is however dependent on field exposure conditions and thus, hard to control.

2.3 ASR Mitigation Using Supplementary Cementitious Materials (SCMs)

The use of a non-reactive aggregate is the safest mitigation approach to prevent the occurrence of deleterious ASR. However, due to geographical constraints or local unavailability, the option of using non-reactive aggregates is not always possible.

Incorporating traditional supplementary cementitious materials (SCMs) such as fly ash, ground granulated blast furnace slag (GGBS or slag), metakaolin and silica fume in the concrete mix is widely regarded as the most economical means of preventing ASR. The presence of SCMs allows the use of aggregates that are otherwise not

suitable for concrete structures. In Australian context, SCM mitigation involves the use of fly ash and slag in concrete mixes with reactive aggregates. The use of more expensive SCMs like metakaolin and silica fume is very limited due to reasons of cost.

Although SCMs are proven to be effective in preventing ASR, the mechanisms behind mitigation are still poorly understood and a subject of controversy among researchers worldwide. Due to the foreseen scarcity of SCMs, understanding of the mechanisms of mitigation is critical in the identification of other potential SCMs for ASR mitigation.

The succeeding sections cover the origin and composition of traditional SCMs as well as proposed mechanisms from literature on how SCMs mitigate ASR.

2.3.1 Origin of SCMs

Fly ash is a by-product of burning coal in power generating stations. Fly ash comes from non-combustible inorganics of the coal melt forming small liquid droplets. The flue gases carry the droplets away from the burning zone and cooled rapidly, resulting in the formation of spherical particles with high amorphous content (Thomas 2013).

Metakaolin is a dehydroxylated form of the clay mineral kaolinite and is produced by the thermal activation of kaolin clay through heat treatment. The calcination process breaks down the structure of kaolin, resulting for it to lose its long-range order (Rashad

2013). The hydroxyl bonds between the platy clay structures are driven off and there is a substantial re-organisation of the basic building units resulting in a highly amorphous material that behaves as a highly reactive pozzolan (Ramlochan, Thomas & Gruber 2000). The dehydroxylation reaction of kaolinite is shown in Equation 2-7.

Equation 2-7 $Al_2Si_2O_5(OH)_4 \rightarrow Al_2Si_2O_7 + 2H_2O$

Ground granulated blast furnace slag (GGBFS), or simply slag is a by-product of iron production from iron ore. The iron is then further processed to produce steel. Molten iron and molten slag are produced when combination of iron ore, coke and limestone are subjected to blast furnace at about 1500 °C. The molten slag is cooled rapidly from around 1500 °C (2700 °F) resulting in the formation of granulated slag with a glassy structure (Thomas 2013). The granulated slag is ground to a very fine powder, producing GGBFS (Siddique & Khan 2011).

Silica fume is a by-product from the production of silicon metals and ferrosilicon alloys (Thomas 2013). High-purity quartz (SiO_2) is reduced to silicon metal at temperatures of about 2,000 °C, producing SiO_2 vapours, which condense in the low temperature zone producing tiny particles consisting of amorphous silica (Siddique & Khan 2011). Silica fume is a highly reactive pozzolan due to its very small particle size (averages at 0.1 μm) and high amorphous silica composition. (Boddy, Hooton & Thomas 2003).

2.3.2 Composition of SCMs

The reactivity of SCMs in cement mainly depends on their composition, size and crystal structure. Figure 2-2 shows the typical composition of conventional SCMs. Fly ash, metakaolin and slag contain significant amount of silica (SiO_2) and alumina (Al_2O_3). Metakaolin typically with more Al_2O_3 than fly ash and slag with higher calcium (CaO) content than both metakaolin and fly ash.

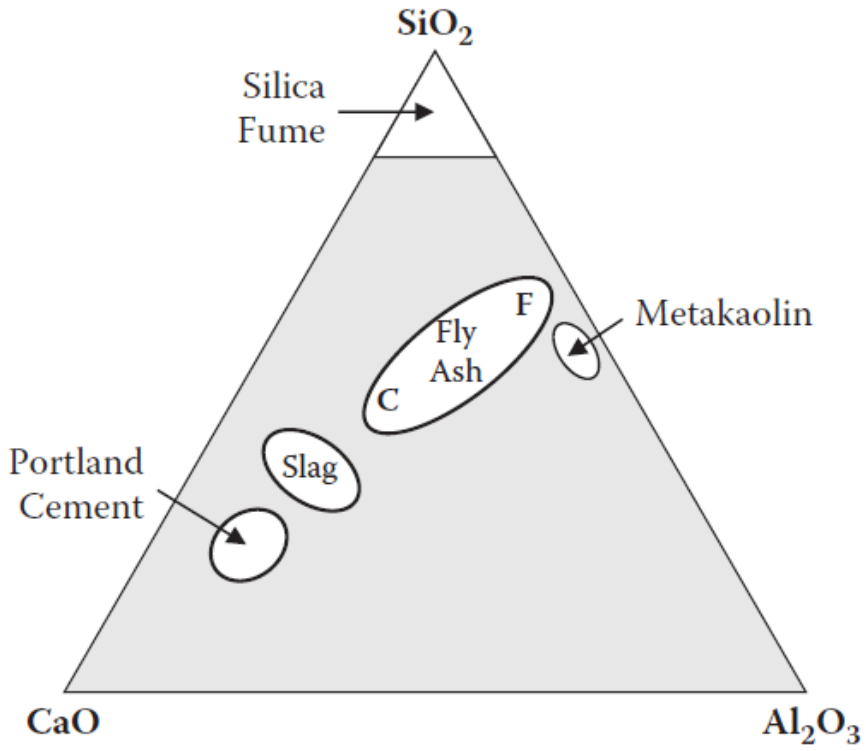

Figure 2-2 Chemical composition of conventional SCMs (Thomas 2013)

Fly ash varies widely in composition and may be classified as Class F (high CaO content) or Class C (low CaO content). ASTM C618 classifies fly ash to be Class F if

$SiO_2+Al_2O_3+Fe_2O_3 \geq 70\%$ and Class C if $SiO_2+Al_2O_3+Fe_2O_3 \geq 50\%$ (ASTM International 2015). Australian standard AS/NZS 3582.1 however, only allows fly ash with a composition of $SiO_2+Al_2O_3+Fe_2O_3 \geq 70\%$ to be suitable for use.

Silica fume is almost entirely composed of amorphous silica, making it highly pozzolanic. Pozzolanic materials contain a high amount of silica that chemically react with calcium hydroxide (portlandite) at ordinary temperature to form cementitious hydrates that help improve the durability of concrete (Thomas 2013).

In Australia, AS/NZS 3582.3 requires silica fume or amorphous silica to contain at least 85% silica to be suitable for use as a cementitious material in concrete, mortar, and related applications. Slag, on the other hand, has a composition relatively close to that of portland cement, i.e. has relatively high calcium content and is hydraulic in nature with little or no pozzolanic behaviour (Lothenbach, Scrivener & Hooton 2011a; Thomas 2013). Hydraulic materials readily react with water to form cementitious compounds.

Figure 2-3 shows typical x-ray diffraction (XRD) patterns of silica fume, slag and fly ash. XRD pattern of fly ash shows presence of both crystalline and amorphous glassy phase. The major crystalline peaks in fly ash are quartz (silica) and mullite (aluminosilicate). The presence of an amorphous phase is indicated by a broad hump in the XRD pattern at about 2Θ=15-30°. The amorphous content dictates the reactivity of a fly ash material, however like composition, this also varies according to coal source, combustion temperature and other process parameters (Durdziński et al. 2015).

The XRD patterns of slag and silica fume both show absence of crystalline peaks and presence of a broad hump confirming their primarily amorphous/glassy nature (Gebregziabiher, Thomas & Peethamparan 2016). In general, blast furnace slag may be described as $CaO\text{-}SiO_2\text{-}Al_2O_3\text{-}MgO$ glass with about 95% glassy content (Kolani et al. 2012; Ye & Radlińska 2016).

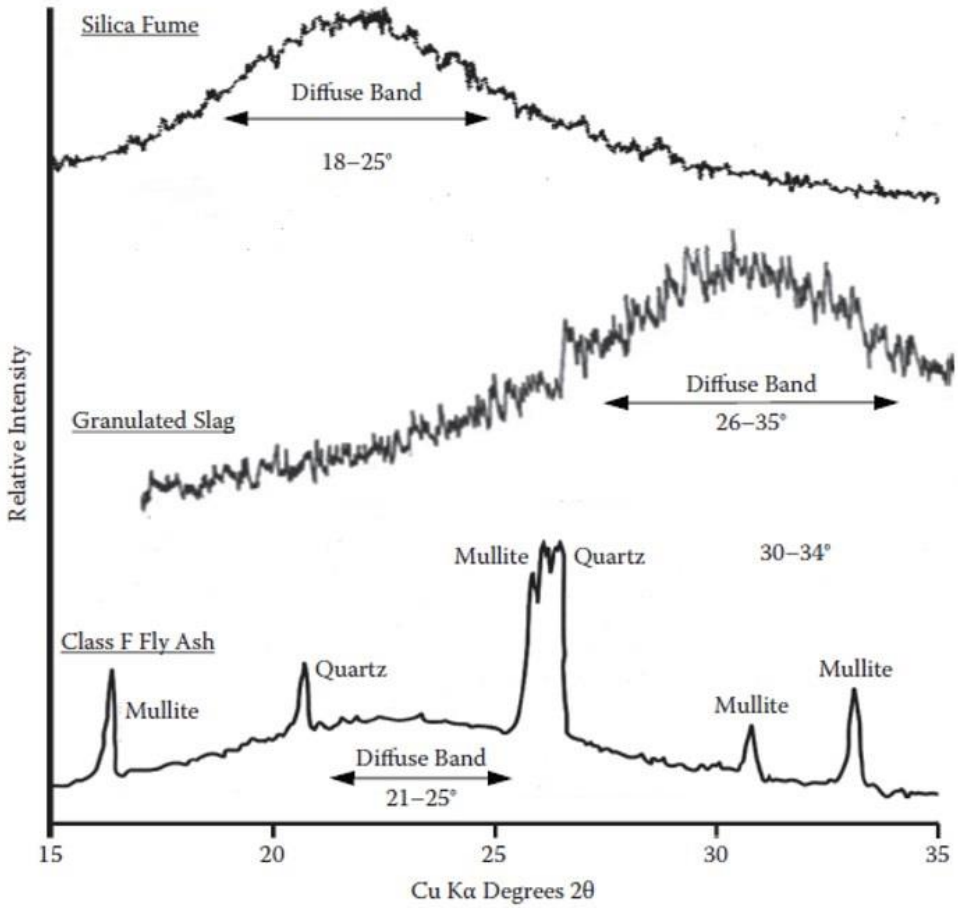

Figure 2-3 XRD patterns of common SCMs (Thomas 2013)

The metakaolin crystal structure depends on the purity of the kaolinite and the calcination temperature. Figure 2-4 shows the effect of calcination temperature on the disappearance of kaolinite peaks (unfired raw material) (Fabbri, Gualtieri & Leonardi

2013). The very high calcination temperature required to transform kaolinite into amorphous aluminosilicate makes metakaolin a relatively expensive SCM.

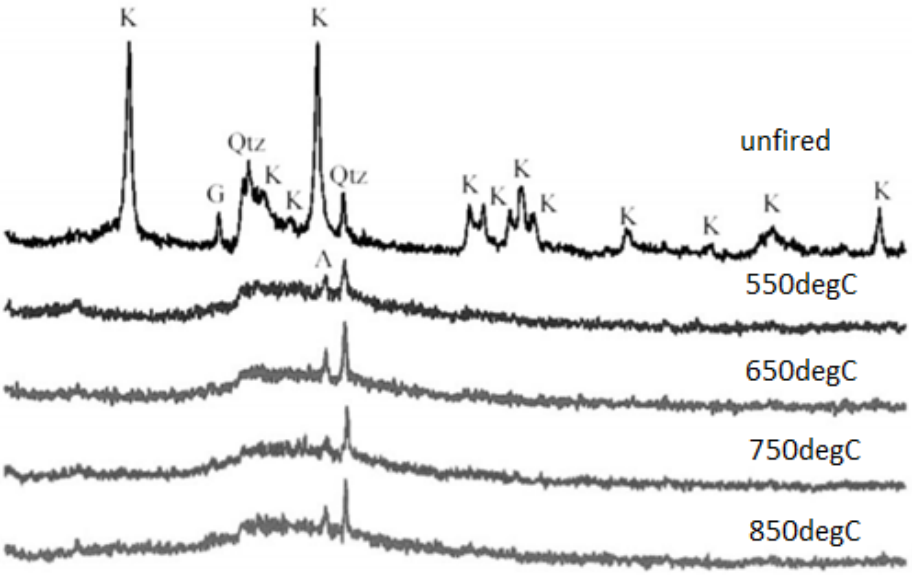

Figure 2-4 Effect of calcination temperature on XRD pattern of metakaolin where K=kaolinite, Qtz= quartz and G=Gibbsite (Fabbri, Gualtieri & Leonardi 2013)

2.3.3 Reaction Mechanisms of SCMs in Concrete

The alite (C_3S) and belite (C_2S) phases of cements react with water producing calcium silicate hydrate (C-S-H) and calcium hydroxide (CH). When SCMs such as fly ash, metakaolin and silica fume are present, the silica component reacts with the CH from cement hydration and this reaction can be represented by Equation 2-8 (Thomas 2013). The formation of secondary C-S-H reduces total porosity and refines the pore structure which result in increased strength and decrease in the permeability of the cementitious matrix (Siddique & Khan 2011).

Equation 2-8 $xCH + yS + zH \rightarrow C_xS_yH_z$

The alumina present will also react to form a variety of alumina-containing phases, including strätlingite (C_2ASH_8) and hydrogarnet (C_3AH_6), calcium aluminate hydrate (C_4AH_{13}), ettringite ($C_3A{\cdot}3C\bar{S}{\cdot}H_{32}$), calcium monosulfoaluminate ($C_3A{\cdot}C\bar{S}{\cdot}H_{12}$), and calcium carboaluminate ($C_3A{\cdot}CC{\cdot}H_{12}$) (Siddique & Khan 2011; Thomas 2013).

Slag hydrates when mixed with water but the reaction rate is relatively slow (Kolani et al. 2012). This is because the hydration products form a thin Si-rich layer on the surface of the slag grains, which essentially prevents any further hydration. An alkaline activator has to be used to raise the pH (>12) and prevent the formation of an impermeable layer, thereby allowing the continued dissolution of the glass. As cement is inherently basic, it is a good activator for slag. The main products formed in a mixture of Portland cement and slag are similar to those that form in a pure Portland cement mix: calcium silicate hydrate (C-S-H), calcium hydroxide (CH), AFm (aluminate ferrite monosulfate), and AFt (Al_2O_3-Fe_2O_3-trisulfate).

When cement is in combination with slag, the quantity of CH that is formed is lower than the amount that would be produced by the hydration of Portland cement (PC) alone, indicating that CH is partly consumed in the hydration reaction of slag (Thomas 2013). The C-S-H formed in Portland cement-slag blends has a lower Ca/Si ratio and a higher Al/Si ratio than pure PC (Lothenbach, Scrivener & Hooton 2011b).

2.3.4 Proposed Mechanisms for ASR Mitigation

In almost 80 years of ASR research, several theories have been proposed on how SCMs work to mitigate ASR. This section discusses the most widely accepted theories (pozzolanic reactions leading to alkali binding, reduction in porosity and microstructure refinement) as well as a recent proposed mechanism which is still subject of interest worldwide (formation of aluminosilicates).

2.3.4.1 Alkali Binding

The widely accepted mechanism by which SCMs mitigate ASR is by reducing the alkalinity of the pore solution (Duchesne & Berube 1994b). The 'reactive silica' present in SCMs reacts with the hydroxyl ions in the pore solution and portlandite (CH) to produce C-S-H phases (Durand et al. 1990; Gebregziabiher, Thomas & Peethamparan 2016; Kim, Olek & Jeong 2015). The C-S-H phases formed from pozzolanic reactions have a decreased Ca/Si ratio which causes more alkali ions to be entrapped in the hydrates (Duchesne & Berube 1994b; Hong & Glasser 1999).

The C-S-H present in Portland cement typically has a composition of ~1.5-1.9$CaO \cdot SiO_2 \cdot nH_2O$, but reduced Ca/Si ratios are observed when SCMs are used (Lothenbach, Scrivener & Hooton 2011b). When the Ca/Si ratio is lower than about 1.2-1.3, the surface charge of C-S-H becomes negative and alkali cations (Na^+ and K^+) are incorporated in the C-S-H (Hong & Glasser 1999; Monteiro et al. 1997). Alkalis

are adsorbed into C-S-H at deprotonated silanol, Si–OH, sites. This sorption increases as the volume of the silanol bonds increases. Both the number and acidity of the sites increase as the Ca/Si ratio of C-S-H decrease (Hong & Glasser 2002).

A study by Hong and Glasser suggests that the aluminium in the SCMs can also dissolve into the pore solution and be further incorporated into the pozzolanic reactions to form C-A-S-H (also known as Al-modified C-S-H) gel which has enhanced alkali binding capacity (Hong & Glasser 2002; Lothenbach, Scrivener & Hooton 2011b). The incorporated aluminium in the silanol layer leads to a free negative valence, resulting in the compensation of this charge by the positive alkali ions Na^+ and K^+ (Figure 2-5). This suggests that aluminium-rich SCMs like fly ash and metakaolin have added benefit for mitigation.

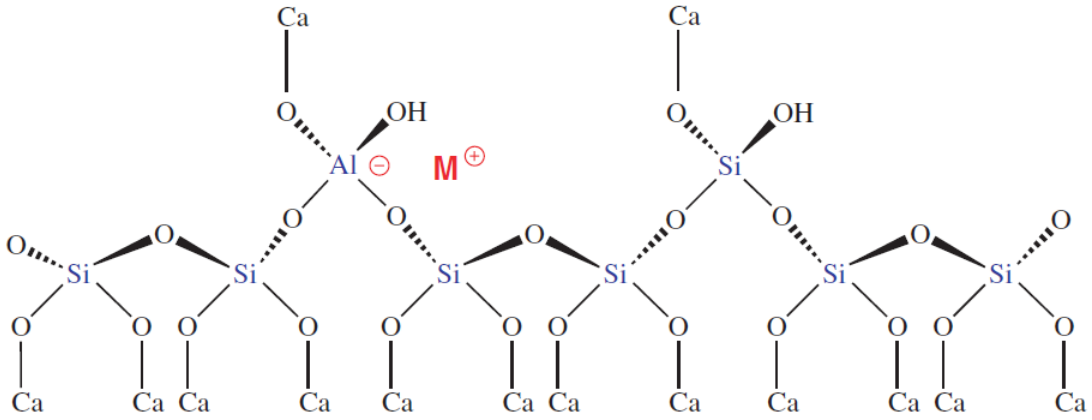

Figure 2-5 Schematic representation of the incorporation of Al in the bridging site of an octameric chain of SiO_4/AlO_4 tetrahedra (Skibsted & Andersen 2013)

Several studies suggest that aluminium-rich SCMs, such as fly ash, slag or metakaolin are more efficient against ASR than pure silica additions which only have a delaying effect on ASR expansion (Berube & Duchesne 1993). The expansion observed in SF mixes at later ages is attributed to the slow release of entrapped alkalis in C-S-H because they remain mobile. Thus, it is argued that silica fume does not have a high capacity to retain alkalis in its hydration products (Shehata & Thomas 2006). Pastes samples as shown in Figure 2-6 containing silica fume achieved low pore solution alkalinity at early ages. After 28 days, a slow but sustained increase in the alkalinity up to 2 or 3 years was observed (Shehata & Thomas 2002).

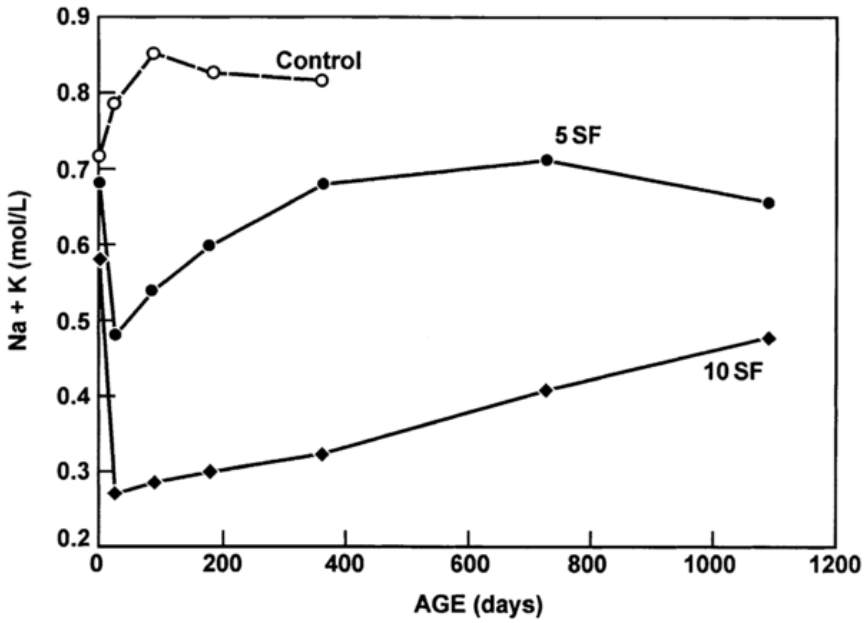

Figure 2-6 Effect of silica fume on the alkalinity of the pore solution of pastes, represented by the sum of alkali cations in the pore solution (Shehata & Thomas 2002)

When silica fume and fly ash were used in combination, the low pore solution alkalinity of the samples remained unchanged up to the age of 3 years as shown in Figure 2-7 (Shehata & Thomas 2002). The reductions in alkalinity remain stable when alumina-bearing SCMs such as fly ash are used, possibly due to the formation of C-A-S-H, which is reported to better retain alkalis than C-S-H (Lothenbach, Scrivener & Hooton 2011b). When Al substitutes for Si in the C-S-H, this creates a charge deficit, which is charge balanced by the incorporation of a monovalent metal ion (M^+, i.e., Na^+ or K^+) (Skibsted & Andersen 2013). This, in turn, results in better binding of the alkalis.

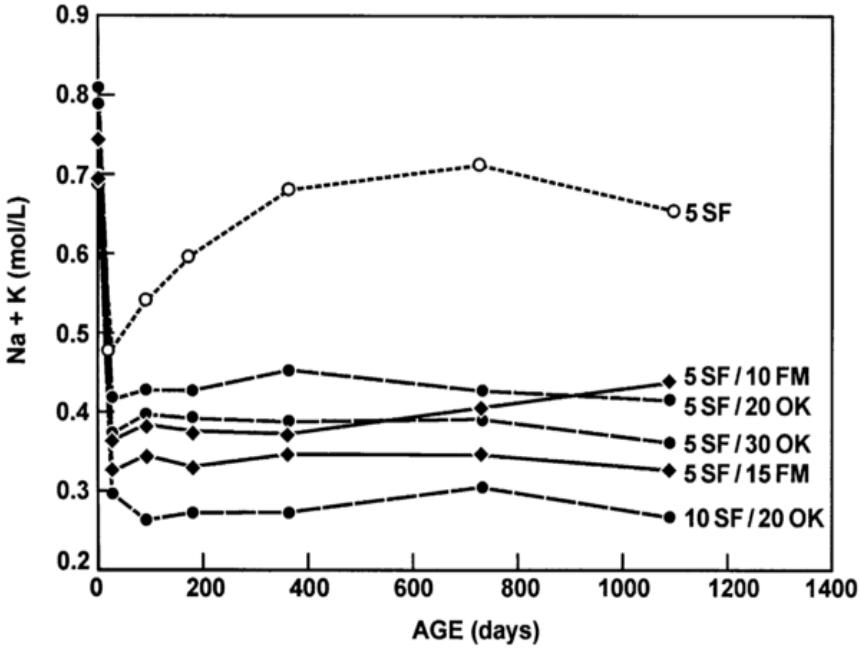

Figure 2-7 Effect of silica fume/fly ash combinations on the alkalinity of pore solution of paste, represented by the sum of alkali cations in the pore solution (FM, OK are both types of fly ash) (Shehata & Thomas 2002)

The theory on the increased alkali fixation with aluminium is however challenged by another study which reported that the incorporation of aluminium does not increase the alkali fixation of the C-S-H found in real cementitious materials, and that the greater effectiveness of SCMs containing alumina is due to the formation of aluminosilicates (Chappex & Scrivener 2012a).

2.3.4.2 Reduction in Porosity and Microstructure Refinement

Pozzolanic reactions increase the volume fraction of C-S-H leading to a lower permeability and much slower migration of alkalis towards the reactive aggregate. SCMs were reported to have positive impact on pore refinement and interfacial transition zone (ITZ) enhancement of concrete, especially at later curing stages (Duana et al. 2013). Mortars with fly ash after three days submersion in 1M NaOH 80 °C (ASTM C1567) exhibit higher tensile and compressive strength than control mortars. Higher strength delays the formation of cracks which can promote immediate access of the NaOH solution to the interior of the specimen (Shafaatian et al. 2013). The high early-age strength is attributed to increased rate of pozzolanic reactions due to higher temperature and alkalinity. Under normal curing conditions, SCMs also increase strength, but this takes longer time because of much slower pozzolanic reactions (Juenger & Siddique 2015).

2.3.4.3 Formation of aluminosilicates

Aluminium reportedly reacts with the silica components of the aggregates, forming aluminosilicates that are stable under alkali. The aluminosilicates formed on the surface of aggregates act as a passivation layer, preventing further dissolution of the reactive silica and inhibiting ASR (Chappex & Scrivener 2012b). A study involving fused silica plates showed that the aluminium-treated portion shows less dissolution pits than the untreated side. Thus, the pre-treatment with aluminium was enough to stabilize the surface of silica (Chappex & Scrivener 2013). X-ray photoelectron spectroscopy analysis shows that the aluminium species are incorporated into the silica framework of amorphous silica (Chappex & Scrivener 2013).

Another study has reported that reactive aggregates exposed to alkaline solutions (0.3M or 0.6M sodium hydroxide and excess calcium hydroxide) with no aluminium has shown cracking while that in saturated aluminium hydroxide has shown little cracking over 300 days (Chappex & Scrivener 2012b). The authors cited adsorption of aluminium in the silicate network as the reason for the reduction of dissolution rate observed. The negatively charged aluminosilicate surface sites formed, repel OH^- ions, and thus limit their attack on the silica structure (Bickmore et al. 2006; Rajabipour et al. 2015). This is consistent with an earlier study on the effect of the presence of aluminium on the dissolution of soda-lime silicate glass in water at 90 °C which reported that formation of more stable aluminosilicate groups, rather than ion exchange, resulted in the retardation of silica dissolution (Sang, Jakubik & Barkatt 1994).

The result for mass dissolution of the glass rods in NaOH solutions in Figure 2-8 shows that adding aluminium into 1N NaOH significantly reduced the dissolution of the glass rod. The results imply that a small concentration of dissolved aluminium in the concrete pore solution could be effective in limiting the dissolution of reactive aggregates (Hay & Ostertag 2019). A study of Bickmore et al. confirmed that $Al(OH)_4^-$ depressed the dissolution rate of quartz, and this is due $Al(OH)_4^-$ and Na^+ co-adsorbing on silanol sites and passivating the surrounding quartz surface (Bickmore et al. 2006).

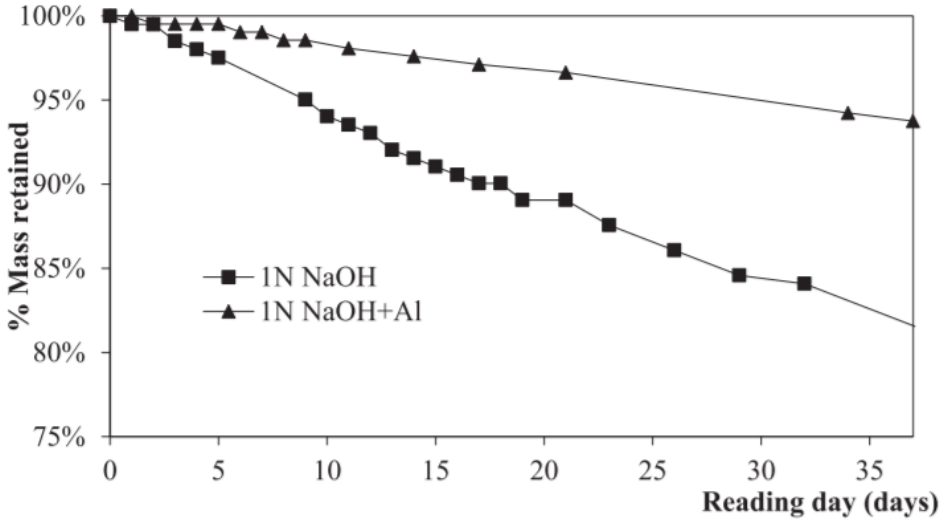

Figure 2-8 Mass dissolution of borosilicate rod in 1N NaOH solution (Hay & Ostertag 2019)

2.3.4.4 Increased SiO_2 surface area

It is also reported that by increasing the accessible silicate surface area, the SCM reduces the effective concentration of OH^- at the surface of aggregates; and as such,

reduces the aggregate dissolution rate. In an experiment where glass slides were immersed in alkali with and without fly ash in solution, it was observed that the rate of mass loss from glass slides is higher in the system without fly ash. The authors attribute this to a drastic increase in the silicate surface area to solution volume ratio as a result of the silicate area provided by the fly ash resulting in a much lower concentration of OH^- ions per unit silicate surface area (Shafaatian et al. 2013).

2.3.5 Typical Dosage Requirements for Effective ASR Mitigation

Replacing a portion of the cement with SCMs is an effective way of mitigating ASR. Silica fume is widely accepted as the most effective SCM in reducing expansion in terms of dosage requirement closely followed by metakaolin, Class F fly ash, Class C fly ash and blast furnace slag (Thomas 2011). Studies show that 5-10% replacement by silica fume (Boddy, Hooton & Thomas 2003; Durand et al. 1990) and 10-20% replacement by metakaolin and 20-30% replacement by Class F Fly Ash is adequate to prevent expansion due to ASR (Hobbs 1986; Ramlochan, Thomas & Gruber 2000; Shehata & Thomas 2000; Thomas 2011; Thomas et al. 2011). Higher replacement is required for Class C fly ash at 45-60% (Shehata & Thomas 2000). Similarly, for slag, a replacement level of at least 50% is recommended (Duchesne & Berube 2001; Hobbs 1986; Rasheeduzzafar & Hussain 1991).

The minimum replacement level required to mitigate ASR depends on a number of factors, including aggregate reactivity, type of SCM, concrete alkali content, and exposure conditions (Thomas 2013). In general, higher SCM replacement level results in lower expansion.

In Australia, SA HB 79:2015 provides recommended levels of SCM replacement to mitigate ASR as shown in Table 2-4. Slag requires the highest amount of replacement at 65%, followed by fly ash (Class F) at 25%, metakaolin at ≤15% and silica fume at 10%. The difference in dosage requirement as a function of SCM type suggests that SCM composition plays an essential role in the ability of SCMs to mitigate ASR.

Table 2-4 Recommended SCM Replacement Levels in Australia

SCM	Recommended SCM content in binder for ASR mitigation (%)
Fly ash	~25
Silica fume	~10
Slag (GGBFS)	~65
Metakaolin	≤15

2.4 Effect of High Alkali Cements on ASR Mitigation

Cement is the biggest contributor to the alkali content of the concrete and thus, the strict limit imposed on cement alkali contents. Australian cement alkali limit is currently set at 0.6% sodium equivalent (%Na_2O_{eq}) (Standards Australia 2015). Low

cement alkali limit however result in an enormous amount of limestone rejected on the basis of its alkali content. As SCMs are proven to reduce pore solution alkalinity and thereby prevent ASR, the possibility of increasing cement alkali limits in concrete mixes with SCMs offers a more sustainable and cost-effective cement production.

2.4.1 Influence of High Alkali Cements on SCM Efficacy

There are limited reported field studies on the effectiveness of SCMs in minimizing ASR when used with high alkali cements. One example where a fly ash concrete performed well with no indications of ASR damage after more than 30 years of service is the Lower Notch Dam in Ontario, Canada that was completed in 1971. The concrete made use of highly reactive greywacke-argillite coarse aggregates and high alkali cement (1.08% Na_2O_{eq}) in combination with 20% and 30% low CaO fly ash in the structural and mass concrete respectively (Thomas et al. 2006; Thomas 1996).

In another study, concrete made with high-alkali cement (> 0.8%) and no protective measures cracked at the age of 5 years when stored outdoors in the Canadian climate. However, when the high-alkali cement was replaced with 25% GGBFS or 18% Class F fly ash, expansion was considerably less, and only very minor cracking occurred. When sufficient levels of SCMs were used (50% GGBFS, or 25% slag + 3.8% silica fume interground with a high-alkali portland cement), there was no sign of ASR or cracking after 20 years (Hooton et al. 2013). Moreover, in a study where 45 concrete blocks (915 x 915 x 815 mm or 350 mm cubes) containing alkali-silica reactive

aggregates, and high alkali cement (K_2O= 1.10%, Na_2O= 0.43%) were placed on an outdoor exposure site in England for a period of up to 18 years to determine the efficacy of fly ash in controlling damaging alkali-silica reaction (ASR), fly ash used at replacement levels of 25% and 40% was effective in significantly reducing expansion and cracking with all three flint aggregates at all levels of alkali (Thomas et al. 2011). Figure 2-9 shows photos of the blocks in the exposure site. The block without fly ash is extensively cracked with crack widths exceeding 10 mm in some locations. No cracking was observed in any of the blocks with fly ash.

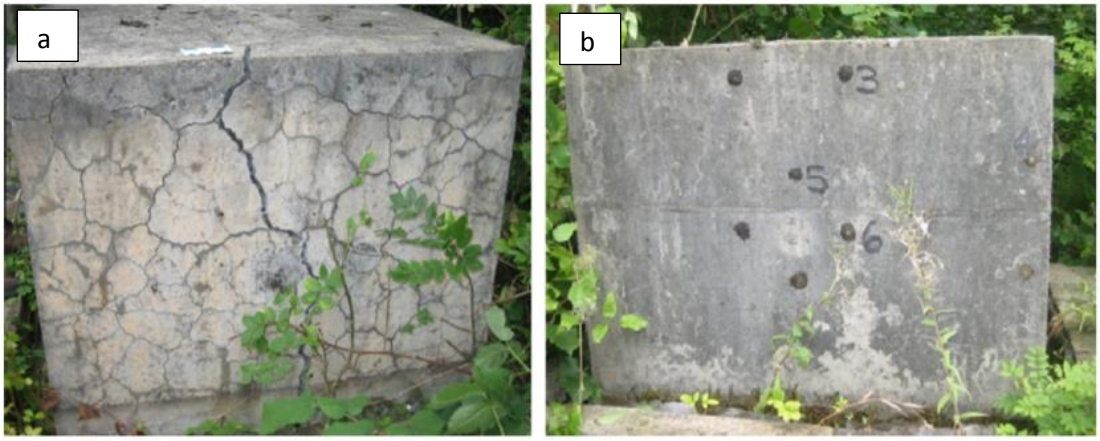

Figure 2-9 Photographs of 915 mm blocks a) with and b) without 25% fly ash after 18 years on the exposure site at BRE (Thomas et al. 2011)

While field studies are the most reliable means of assessing the efficacy of SCMs in conjunction with high alkali cements, they take a very long time to manifest results, and thus, the use of laboratory test methods is a much attractive option. The reliability of existing test methods, however, remain in question. The limitations of which are discussed in the next section.

2.4.2 Limitations of AMBT and CPT for Assessing the Influence of Cement Alkalinity

AS 1141.60.1 (Accelerated Mortar Bar Test, AMBT) and AS 1141.60.2 (Concrete Prism Method, CPT), accelerated test methods designed to assess the susceptibility of aggregates to ASR, are also being employed to assess SCM efficacy as there are currently no Australian standards dedicated to assessing SCM efficacy in ASR mitigation.

AS 1141.60.1 (AMBT) involves immersing the mortar specimens in 1M NaOH 80 °C for 21 days and has a similar mortar preparation procedure to ASTM C1260 and ASTM C1567 but with minor difference in expansion limits. In AS 1141.60.1, the aggregate is slowly reactive if it exceeds 0.10% expansion at 10 days and reactive if it exceeds 0.30% expansion at 21 days. AS 1141.60.1 was found to be a relatively good method in classifying slowly reactive aggregates (Sirivivatnanon, Mohammadi & South 2016).

AS 1141.60.2 (CPT) involves boosting concrete alkali content to 1.25% Na_2O_{eq} and storing specimens in a high humidity sealed environment at 38 °C, which is similar to ASTM C1293. AS 1141.60.2 classifies an aggregate with expansion of less than 0.03% at 52 weeks as ‘‘non-reactive” and an aggregate with a prism expansion equal to or greater than 0.03% at 52 weeks as ‘‘potentially reactive” (Sirivivatnanon, Mohammadi & South 2016). AS 1141.60.2 makes no mention of the duration of the test when used with SCMs as well as acceptance criterion but SA HB 79:2015 recommends the adoption of the Canadian requirements (expansion of less than 0.04% at 2 years) unless

client or other local specifications provide alternatives. A summary comparing AMBT with CPT is shown in Table 2-5.

Table 2-5 AMBT (AS1141.60.1:2014) vs. CPT (1141.60.2:3014)

Category	Australian Standard	
	AS 1141.60.1:2014 (AMBT)	**AS 1141.60.2:2014 (CPT)**
Aggregate Grading	4.75 mm ≤ 2.36 mm = 10% 2.36 mm ≤ 1.18 mm = 25% 1.18 mm ≤ 0.60 mm = 25% 0.60 mm ≤ 0.30 mm = 25% 0.30 mm ≤ 0.15 mm = 15%	19.0 mm ≤ 13.2 mm = 33.33 % 13.2 mm ≤ 9.5 mm = 33.33 % 9.5 mm ≤ 4.75 mm = 33.33%
Alkalinity	No NaOH Addition in Mixing Water	add NaOH to mixing water to bring equivalent alkali content of the concrete mix to 1.25% Na_2O_{eq}
Sample Storage	immerse specimens in 1M NaOH Bath at 80 °C	store the concrete prisms in a sealed container at 38 °C and high relative humidity
Sample Size	25 mm x 25 mm x 285 mm	75 mm x 75 mm x 285 mm
Test Duration	minimum 21 days	1-2 years
Reactivity Criteria	a. 21-day expansion below a lower limit of 0.10% is non-reactive b. 10-day expansion equal or greater than the lower limit of 0.10% or 21-day expansion equal or greater than the upper limit of 0.30% to be reactive c. 10-day expansion below the lower limit of 0.10% but 21-day expansion equal to or exceeding the lower limit of 0.10% but not exceeding the upper limit of 0.30% is ‘‘slowly reactive”	a. expansion of less than 0.03% at 52 weeks is ‘‘non-reactive” b. expansion equal to or greater than 0.03% at 52 weeks is ‘‘potentially reactive”

While both test methods are generally accepted worldwide as suitable for determining dosages of SCMs required for mitigation (Thomas et al. 2006), both are in question for their ability to accurately assess the influence of cement alkalinity on ASR expansion (Lindgård et al. 2012; Thomas et al. 2007).

AMBT offers inexhaustible supply of alkali which can easily mask out the alkali contribution of the Portland cement. Hence, assessing the effect of cement alkalinity on ASR expansion using this method is difficult and conclusions appear to vary in literature (Islam et al. 2016; Li, Afshinnia & Rangaraju 2016). In an AMBT study on the influence of cement alkali content on ASR expansion that made use of reactive aggregates and three dosages of cement alkalis of 0.42, 0.84 and 1.26 % Na_2O_{eq}, the increase in expansion of mortars stored in 1M NaOH was found to be negligible with an increase in cement alkali (Islam et al. 2016). The authors pointed out however, that at lower concentrations of the soak solution (0.25M), the expansion difference due to cement alkalinity is better elucidated.

In another AMBT study on high performance cementitious mixtures (HPCM), it was reported that ASR-induced expansion increased with an increase in the alkali content of the cement. The higher the alkali content of the cement used in the HPCM mixture, the earlier the occurrence of a rapid increase in ASR induced expansion of HPCM. However, for HPCMs containing fly ash, the ASR induced expansion was minimal even up to 28 days of exposure (expansion < 0.03%), and the difference in expansion between alkali content of 0.49% and 0.88% Na_2O_{eq} was not significant. Fly ash was found effective in mitigating ASR in conjunction with high alkali content cement using AMBT (Li, Afshinnia & Rangaraju 2016).

During AMBT, the pozzolanic reactions due to presence of SCMs continuously consume the alkalis in solution, resulting to lower amount of alkali in the pore solution to react with aggregates and induce ASR (Shafaatian et al. 2013). Thus, as long as pozzolanic reactions are occurring, the concentration of alkalis in the mortar will be much lower than that of the soak solution. The lower permeability induced by the presence of additional hydration products from pozzolanic reactions also lowers the rate of influx of alkali ions into the mortar. However, this effect will eventually be overwhelmed by the continued supply of alkalis from the external solution, and thus, the effect of SCMs in AMBT is only temporary (Thomas et al. 2007).

CPT which in theory should provide a finite supply of alkali, is generally accepted as the most accurate laboratory test method worldwide for assessing SCM efficacy in ASR mitigation. However, the method was found to be prone to alkali leaching leading to inconsistencies in expansion results (Lindgård et al. 2012; Thomas et al. 2007; Yamada et al. 2014). After 52 weeks in high moisture storage, concrete prisms lost up to 25% of their initial Na_2O_{eq} content (Rivard et al. 2007). Thomas et al. also estimated that 35% of the alkalis would leach from the prisms after 1 year and reported that in the vast majority of cases, due to alkali leaching, the long-term expansion (i.e. up to 10 years) of concrete blocks under field conditions exceeded that of laboratory-stored concrete prisms from the same mixture (Thomas et al. 2006). This can underestimate the expansion, the reactivity classification of aggregates and the required SCM dosage for mitigation. Moreover, because CPT prisms are being boosted to 1.25% Na_2O_{eq} alkali content, it is difficult to use this method to determine the required amount of SCM to mitigate ASR as a function of total alkali content of the concrete (Thomas et al. 2006).

2.4.3 Efforts to Improve the Concrete Prism Test

There are several studies focused on developing test procedures that limit or eliminate alkali leaching during testing. The use of a cotton cloth wrapping saturated with a basic solution with pH = 14.2 was found to lessen alkali leaching from the concrete prisms. The effect of wrapping the prisms with cotton cloth saturated with the pH 14.2 solution is remarkable for prisms exposed to 60 °C with wrapped prisms expanding about 25% more than the corresponding unwrapped prisms after 26 and 39 weeks of exposure. For prisms exposed to 38 °C, the effect on the expansion of wrapping the prisms with cotton cloth saturated with the pH 14.2 solution is still highly positive but not statistically significant (Lindgård et al. 2013). Covering the upper two-thirds of each prism with a plastic bag was also found to reduce alkali leaching to only 10% (Einarsdottir & Hooton 2018).

Another study proposed that alkali leaching depends on water vapour-concrete interactions in the test container. Storage containers with reduced net container volume (nc)/concrete volume (c) ratio ($V_{nc}/V_{concrete}$ = 2.32; one prism per container) were found to reduce alkali leaching to just 8-10% Na_2O_{eq} (Costa, Mangialardi & Paolini 2017). However, despite current efforts, leaching remains to be a problem. Hence, the need to continuously search for more reliable test methods for assessing the influence of cement alkalinity on ASR expansion.

2.4.4 Influence of Cement Alkalinity on Microstructure and Composition of Hydrates

Potassium and sodium ions accelerate the early hydration of cement, while resulting in reduced hydration and strength at later ages (Jawed & Skalny 1978). Compressive strengths closely correlate with the total capillary porosity of the cement paste, which relates to the total volume of hydrates. NaOH lowers the total volume of hydrates, mainly the volume of ettringite. The addition of NaOH increases the pH of the pore solution which increases the solubility of ettringite, resulting in higher capillary porosity. A higher volume of hydrates can better fill the space, decrease porosity, and consequently increase strength (Mota, Matschei & Scrivener 2018).

Electron microscopy studies have suggested that the alkalis also modify the morphology of the calcium silicate hydrate gel (C-S-H) formed during hydration, leading to the formation of plate (lath)-like gel hydration products (Bentz 2006). Strength differences were however reported to be not dependent on the bulk density, chemical composition or morphology of C-S-H (Mota, Matschei & Scrivener 2018).

2.5 Effect of Increased Limestone in Cements on ASR Mitigation

Cement production produces substantial amount of carbon dioxide (CO_2) emissions which may be attributed to: calcination of the limestone, a primary raw ingredient in clinker manufacturing, and fossil fuel consumption to heat the raw materials to the temperature required to form clinker. Limestone is 44% by mass CO_2 and release of

this CO_2 during calcination together with burning of fossil fuels to heat the kiln accounts for about 60% of the CO_2 emissions produced at a cement plant (Tennis, Thomas & Weiss 2011).

GP cement is the most common commercially used cement in Australia and accounts for over 85% of the total cement market for production of concrete (Mohammadi & South 2016a). To support efforts to lower reductions in CO_2 emissions associated with the production of cement, Australian Standard AS 3972 allows the substitution of clinker in General purpose (GP) cement with minerals up to 7.5%. Although the use of pozzolans and blast-furnace slag (slag cement) are options, the use of limestone is generally preferred as it is usually available in large quantities at clinker manufacturing plants (Tennis, Thomas & Weiss 2011).

A minimum of 75% $CaCO_3$ content is required by AS 3972 for a limestone mineral to qualify as mineral addition. Limestone with $CaCO_3$ content equal to or greater than 75% and less than 80% is acceptable, provided the clay content determined by the methylene blue test (EN 933-9 test method) does not exceed 1.20%, and the total organic carbon content (EN 13639 test method) does not exceed 0.50% by mass. For limestone with $CaCO_3$ content of 80% or greater, testing for clay content and TOC is not required (Mohammadi & South 2016a; Standards Australia 2010).

Currently, there are initiatives to increase the recommended allowable mineral addition in the Australian Standard AS 3972 for the Type GP cement from 7.5 to 12% (Mohammadi & South 2016a). For more than two decades, Europe has allowed 20% and 35% limestone content for widely used CEM II types A/L and B/L, respectively

while Canada in 2008 and US in 2012 permitted higher limestone content in manufactured cement up to 15% (Mohammadi, South & Chalmers 2015).

Several studies have been performed to understand the effect of increased cement limestone addition to concrete performance but very few studies worldwide studied its effect on ASR. In fact, no comprehensive study has been performed so far in the Australian context to the author's best knowledge.

2.5.1 Influence of Cement Limestone Content on Mechanical Properties

In Australia, a comprehensive study on the effect of increasing the limestone content of cement up to 12% showed no effect on most properties of cement, mortar and concrete (Mohammadi & South 2016a). There were generally very limited performance reductions and the authors argue that were statistically insignificant and that variability in performance among the different tests was influenced more by concrete mix design and binder composition than by limestone content in the Type GP cement. Moreover, all properties of 12% limestone content cement complied with the requirements of Australian Standards (Mohammadi, South & Chalmers 2015).

In a number of full-scale plant trials in Canada, it has been demonstrated that equivalent strength can be achieved in concrete produced with Portland Limestone Cement (PLC) containing up to 15% limestone by inter-grinding the limestone with

clinker (Tennis, Thomas & Weiss 2011; Thomas et al. 2010). Moreover, limestone contents up to 15% may actually increase early-age strength as a combined result of improving particle packing, increasing the rate of cement hydration due to more nucleation sites (Bonavetti et al. 2003) and production of calcium carboaluminate from the reaction of the aluminate phases in the clinker or SCMs with $CaCO_3$ (Bonavetti, Rahhal & Irassar 2001; Tennis, Thomas & Weiss 2011; Thomas et al. 2013; Voglis et al. 2005).

Minor differences in performance between PC and 15% PLC concretes of the same cement content and water/cement (w/c) ratio (cement= Portland cement + addition) have been observed. However, a considerable decrease in strength was observed with limestone addition levels in the range of 15% to 45% (Dhir et al. 2007). This is supported by another study which showed that concrete containing up to 15% limestone gives comparable results with PC concrete but increasing the amount of limestone above 15% in the cement results in concrete with decreased compressive strength, increased carbonation depth and decreased permeability (Rajbhandari 2010).

2.5.2 Influence of Cement Limestone Content on ASR Expansion

There is very limited work on the effect of limestone addition on ASR. Some reports show that limestone addition has insignificant effect on ASR (Tennis, Thomas & Weiss 2011; Thomas et al. 2013). Other reports, however, argue that higher limestone

replacement results in lower expansion due to dilution effects. Figure 2-10 shows expansion results for the concrete prism test after 2-year storage over water at 38 °C (100 °F) and for mortar bars after 14 or 28-day immersion in a 1M NaOH solution at 80 °C (176 °F). The data show that the expansion levels for Portland cement (PC) and Portland-limestone cement (PLC) mixtures are almost identical for mixtures with the same SCM and replacement level. Mixtures with SCM exhibit profoundly lower expansion than the control mixtures, and the efficacy of cement replacement with Class F fly ash or slag cement does not appear to be significantly influenced by the presence of 12% limestone in the cement (Thomas et al. 2013).

Another study shown in Figure 2-11 suggests that inter-grinding 15% and 22% limestone in Portland cement with 25% fly ash and 40% slag results in lower expansion. Moreover, higher amount of limestone content at the same SCM replacement level further lowers the expansion. The results are attributed to the dilution of the Portland cement alkalis (Hooton, Nokken & Thomas 2007; Rajbhandari 2010). Another work which showed similar trend argues that limestone is acting as a nucleation site in the mortar bars which contributes to the densification of the microstructure (Chen & Yang 2013).

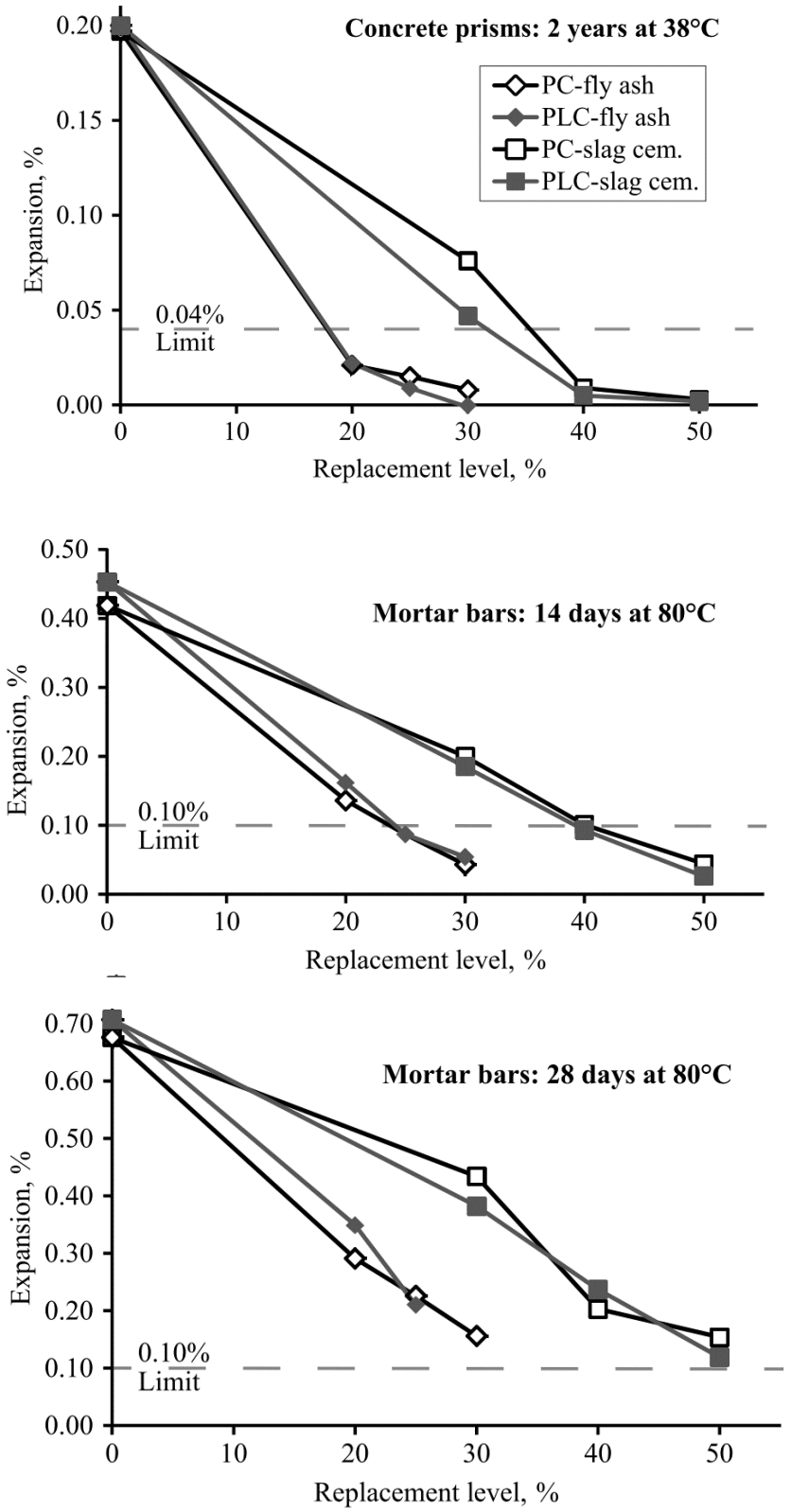

Figure 2-10 Expansion results for concrete (ASTM C1293) and mortar (ASTM C1567) produced with alkali-silica reactive aggregate and blends of PC-SCM or PLC-SCM (Thomas et al. 2013).

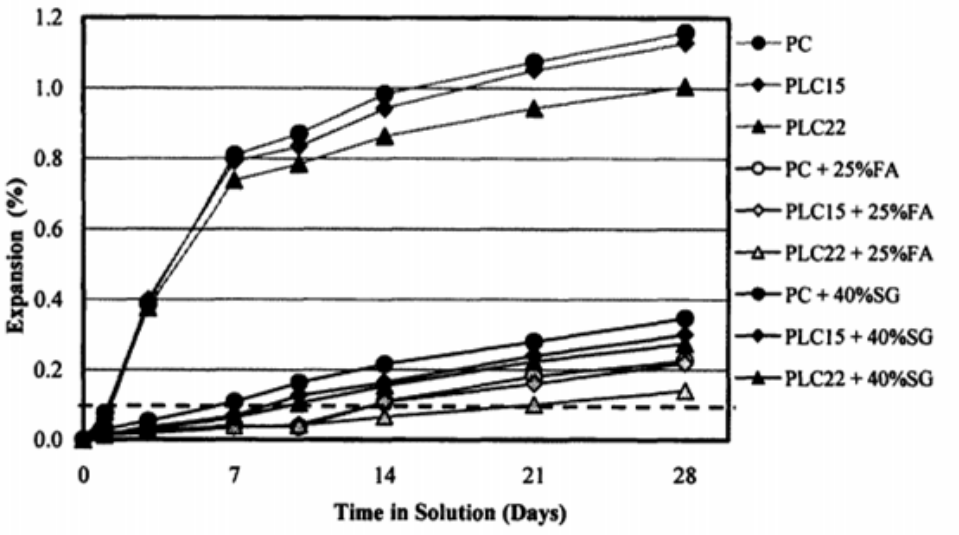

Figure 2-11 Accelerated Mortar Bar Test Results (Rajbhandari 2010)

Limited literature on the effect of limestone on ASR presents inconsistent results. Thus, the need to do further studies in order to establish the effect of increased limestone in cements on ASR.

2.5.3 Reaction Mechanisms of Limestone with Cement and SCMs

Figure 2-12 shows XRD patterns corresponding to the plain cement paste and cement pastes containing 20% limestone filler. The paste with 20% limestone shows presence of monocarboaluminate after 3 days of hydration (Bonavetti, Rahhal & Irassar 2001). The limestone portion of Portland-limestone cements reacts with the alumina phases and produces carboaluminates, which increases compressive strength by means of producing more hydrates and reducing porosity. It has been proposed that the maximum strength and minimum porosity correspond to the point where all the

available alumina is used up. Without excess alumina, the additional limestone would not react to form additional hydrates (i.e. carboaluminates), and therefore, would not increase the strength (except by filler or nucleation effects). However, if additional aluminate is provided (i.e by addition of alumina-containing SCMs such as fly ash or metakaolin), more limestone could participate in the reactions, which implies that the optimum limestone content (for optimum strength and porosity) would also increase. Hence, the addition of SCMs would allow for more limestone to be added in order to achieve the optimum strength (Ramezanianpour & Hooton 2014 ; Shannon et al. 2017). Moreover, experimental observations indicate that in the presence of limestone, monocarboaluminate is produced at the expense of monosulfoaluminate. Thermodynamic modelling showed that the stabilisation of monocarboaluminate in the presence of limestone indirectly stabilised ettringite leading to a corresponding increase of the total volume of the hydrate phase and a decrease of porosity (Lothenbach et al. 2008). The extent of this reaction is expected to increase as the fineness of the limestone increases (Bonavetti, Rahhal & Irassar 2001).

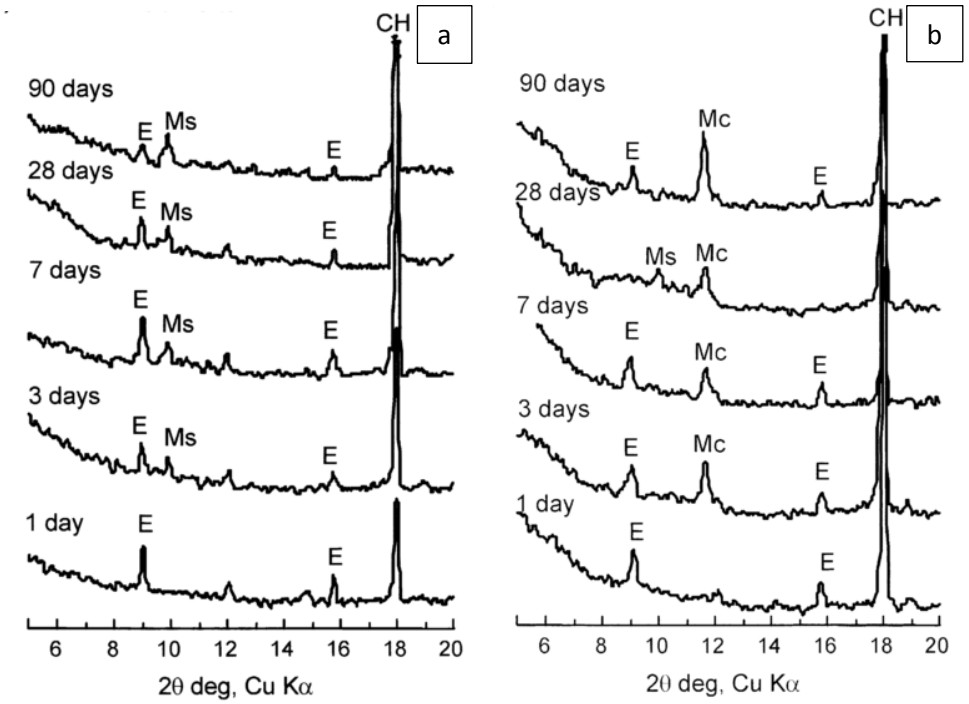

Figure 2-12 XRD patterns of a) Portland cement and b) Portland cement with 20% limestone filler where E=ettringite, Ms=mososulfate and Mc=monocarboaluminate (Bonavetti, Rahhal & Irassar 2001)

This effect is amplified for the fly ash/limestone blended cements due to the additional alumina provided by the fly ash reaction (Weerdt, Haha, et al. 2011). The fly ash blended cements have higher amount of AFm phases relative to the OPC content due to the additional alumina provided by the reaction of the fly ash and to a smaller extent due to the acceleration of the hydration of the aluminate phase of the OPC (Weerdt, Haha, et al. 2011). This synergistic effect between limestone powder and fly ash in ternary cements translates to improved mechanical properties that persist over time (Weerdt, Kjellsen, et al. 2011). The effect for slag blended cements is not as pronounced as for fly ash and metakaolin containing systems (Adu-Amankwah et al. 2017).

3 Materials and Methods

This chapter introduces the raw materials, characterization techniques used, as well as the experimental program employed to achieve the objectives of this work.

3.1 Characterization Techniques

The major characterization techniques used in this work include scanning electron microscopy energy dispersive spectroscopy (SEM EDS), X-ray Diffraction (XRD), thermogravimetric analysis (TG), inductively coupled plasma emission spectroscopy (ICP-OES), inductively coupled plasma mass spectrometry (ICP-MS) and particle size analyzer. The principle behind each equipment, as well as actual parameters used are discussed in the succeeding sections.

3.1.1 Scanning Electron Microscopy (SEM-EDS)

3.1.1.1 *Principles*

Scanning electron microscope (SEM) is a technique commonly used for high magnification imaging. It is particularly useful in characterizing the morphology and

microstructure of different materials with resolution up to nanometers. SEM uses a high energy electron beam (kiloelectron volt, kEV) to scan the surface of the sample. When the incident electrons come in contact with the sample at various depths, energetic electrons are released then collected by a detector which then results in a black and white image (Scrivener, Snellings & Lothenbach 2016).

SEM imaging can be done in two ways depending on the interest. Secondary electrons (SE) are used to better show morphology and topography while backscattered electrons (BSE) are useful for showing different phases as the material composition affects the image contrast (grey levels). Secondary electrons are low energy electrons ejected from the conduction or valence bands of the specimen atoms due to inelastic scattering when the sample gets in contact with the beam electrons. BSE, on the other hand, are high energy electrons that are reflected back or backscattered from the specimen due to elastic scattering. During BSE imaging, heavier materials yield more backscatter electrons, which produces much lighter regions in the images.

Energy-dispersive X-ray spectroscopy (EDS), which is typically coupled with SEM is used to determine the composition of materials. EDS X-ray detector measures the amount of emitted X-ray when electrons hit the sample. The emitted X-ray is characteristic of the element from which it was emitted. With EDS, the spatial resolution is limited by the interaction volume which depends on the beam energy as well as sample density. Typically, the interaction volume is around 1 to 1.5 microns for 15 kEV beam energy.

3.1.1.2 Operating Parameters

All imaging and elemental analysis of raw materials and fractured paste/mortar/concrete were performed using Zeiss Supra 55VP SEM fitted with a Bruker SDD EDS Quantax 400 system and FEI Quanta 200 with Bruker XFlash 4030 EDS detector. The microscopes were operated at 15 kV accelerating voltage and 12.5 mm working distance.

All imaging and elemental analysis of sectioned samples were carried out using FEI Quanta 200 with Bruker XFlash 4030 EDS detector. The microscopes were operated at backscattered electron (BSE) mode, 15 kV accelerating voltage and 12.5 mm working distance. To ensure consistent beam current, X-ray intensities from copper film placed on the metallic sample holder was measured before each measurement to obtain a target "system factor" by adjusting the spot size. A predefined list of elements (O, Na, Mg, Al, Si, P, S, Cl, K, Ca, Ti, Fe) was used for identification and quantification. Figure 3-1 shows the mounted specimen in the metallic sample holder for BSE imaging.

Figure 3-1 Mounted specimen for SEM-EDS analysis

3.1.1.3 Sample Preparation

The sectioned samples (paste/mortar/concrete) were first dehydrated by immersing in isopropanol for 7 days (solvent exchange process), vacuum impregnated with epoxy resin (Epotek-301) as shown in Figure 3-2 and then polished. The samples were first polished with sandpaper grade 500 and 1200 respectively until the sample surface has been fully uncovered from the resin and this is followed by automated polishing using MD-Largo Struers discs lubricated with petrol and diamond spray as a polishing agent (9µm, 3µm and 1µm particle sizes). The polishing parameters are specified in Table 3-1 and the polishing set-up is shown in Figure 3-3. After polishing, the samples were subjected to 2 minutes ultrasonic cleaning to remove polishing debris and then afterwards stored in the vacuum desiccator for at least 2 days to dry. All samples were carbon coated to prevent charging during SEM imaging.

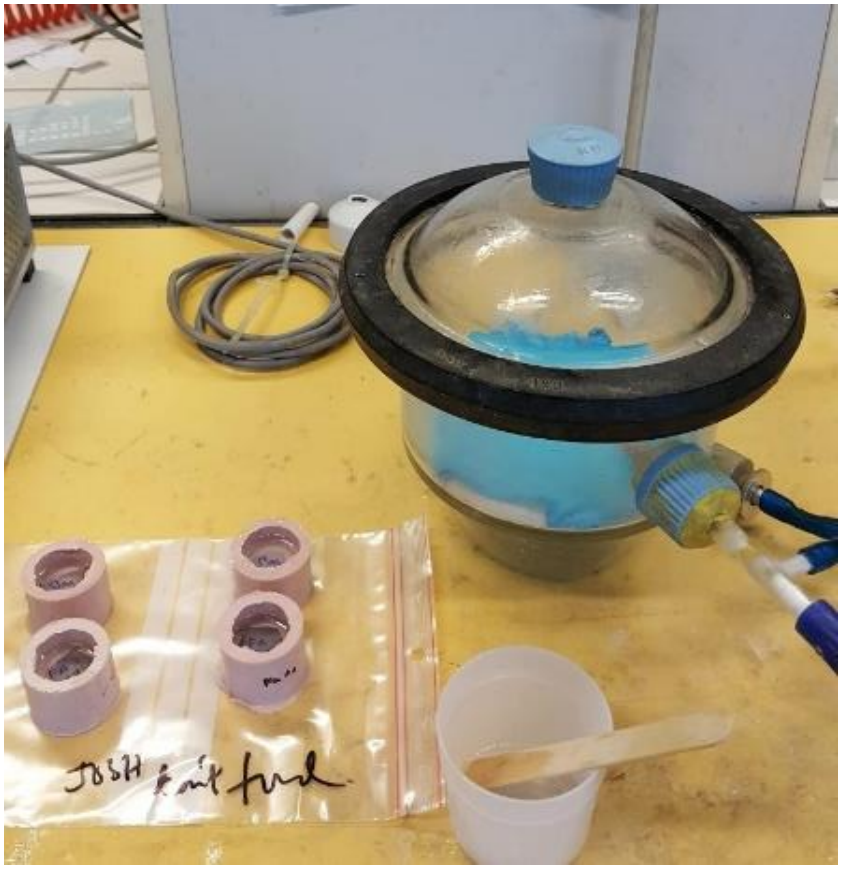

Figure 3-2 Vacuum impregnation set-up for mounting of the sectioned specimens in resin

Table 3-1 Polishing Parameters

Diamond Particle	Cement Paste	Mortar	Concrete
9 µm	30 mins, 20N	3 hours, 25N	4 hours, 25N
3 µm	2 hours, 20N	2 hours, 25N	4 hours, 40N
1 µm	3 hours, 20N	3 hours, 25N	8 hours, 40N

Figure 3-3 Sample polishing using automated polishing equipment

The fractured surface samples for SEM imaging were directly mounted on metal stubs using carbon tape and likewise coated with gold-palladium prior SEM imaging to prevent charging.

3.1.2 X-ray Diffraction (XRD)

3.1.2.1 Principles

X-ray Diffraction (XRD) is a tool primarily used to identify and characterize the crystalline phases of a material by comparing the pattern obtained with a database containing diffraction patterns of known crystalline substances. An X-ray beam of a single wavelength is used to examine polycrystalline specimens. The scattering of X-rays from atoms produces a diffraction pattern, which contains information about the atomic arrangement within the crystal. Amorphous materials like glass do not have long-range atomic order and therefore produces only broad scattering peaks (Leng 2013).

Figure 3-4 shows the Bragg-Brentano geometry where the X-ray source and the detector lies on the circumference of the measuring circle, and the sample is in the center. The average angle of incidence is θ and diffraction occurs at an angle of 2θ with respect to the incident beam. Bragg-Brentano geometry has two types of configuration: θ:θ and θ:2θ. In θ:2θ configuration, the sample is moving to vary the angle of incidence of the X-ray beam. The actual XRD setting used in this study is Bragg-Brentano θ-θ configuration (Figure 3-5) where the X-ray source and the detector are mounted on goniometer arms that rotate around a common axis located at the center of the goniometer. The sample, which is stationary, is situated at the center of the goniometer. The movement of the X-ray source and the detector are

synchronized such that they form equal angles with respect to the surface of the sample and hence, said to vary in the ratio θ:θ.

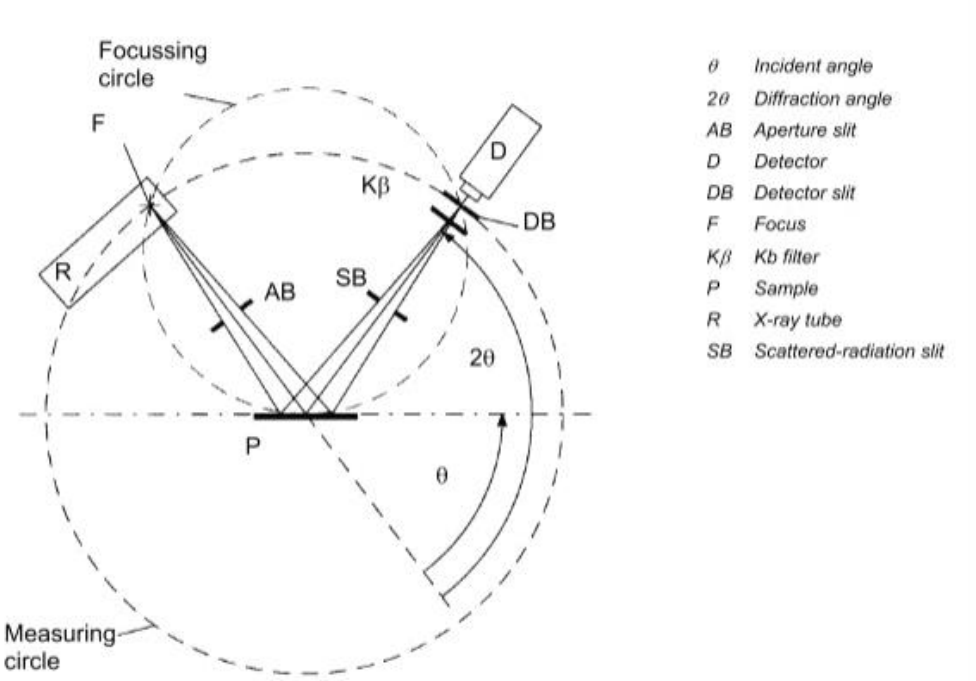

Figure 3-4 Bragg-Brentano diffraction geometry (D8 Advance/D8 Discover User Manual 2010)

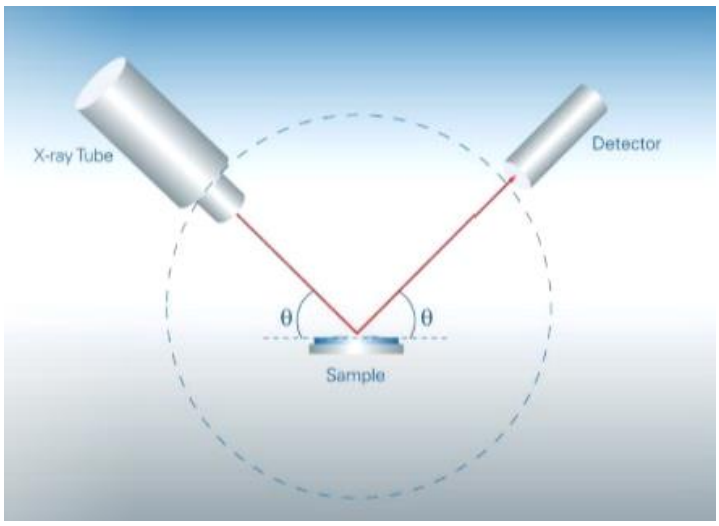

Figure 3-5 Bragg-Brentano θ:θ configuration (D8 Advance/D8 Discover User Manual 2010)

3.1.2.2 Operating Parameters and Sample Preparation

All diffraction patterns were taken using Bruker D8 Discover XRD in Bragg-Brentano mode using Cu Kα radiation (1.5418 Å). Diffraction patterns were obtained at a scan rate of 0.04 °/second. Phases were identified using DIFFRAC.EVA software and ICDD PDF 4+ database. All XRD measurements were performed using a knife edge to minimize background and scattering at low angles. Figure 3-6a shows the actual XRD set-up employed in this study.

The samples were powdered using mortar and pestle. Analysed samples are in powder form to increase the amount of crystallites in the sample. The higher the amount of crystallites in the sample, the lower is the scatter in intensities and the better is the repeatability of the analysis (Scrivener, Snellings & Lothenbach 2016).

The samples were prepared by front loading as in Figure 3-6b, ensuring to not over press the surface to prevent preferred orientation. Random orientation of crystallites is important to avoid the occurrence of preferred orientation. Preferred orientation occurs when not all crystal planes are equally exposed to X-rays, and thus, diffraction intensity can be more biased towards specific peaks. In hydrated cements, portlandite and AFm phases (alumina, ferric oxide and monosulfate phases) and ettringite crystals may undergo preferred orientation (Scrivener, Snellings & Lothenbach 2016).

XRD patterns are presented with all critical peaks labelled and in cases, “stacked” with y-offset if necessary.

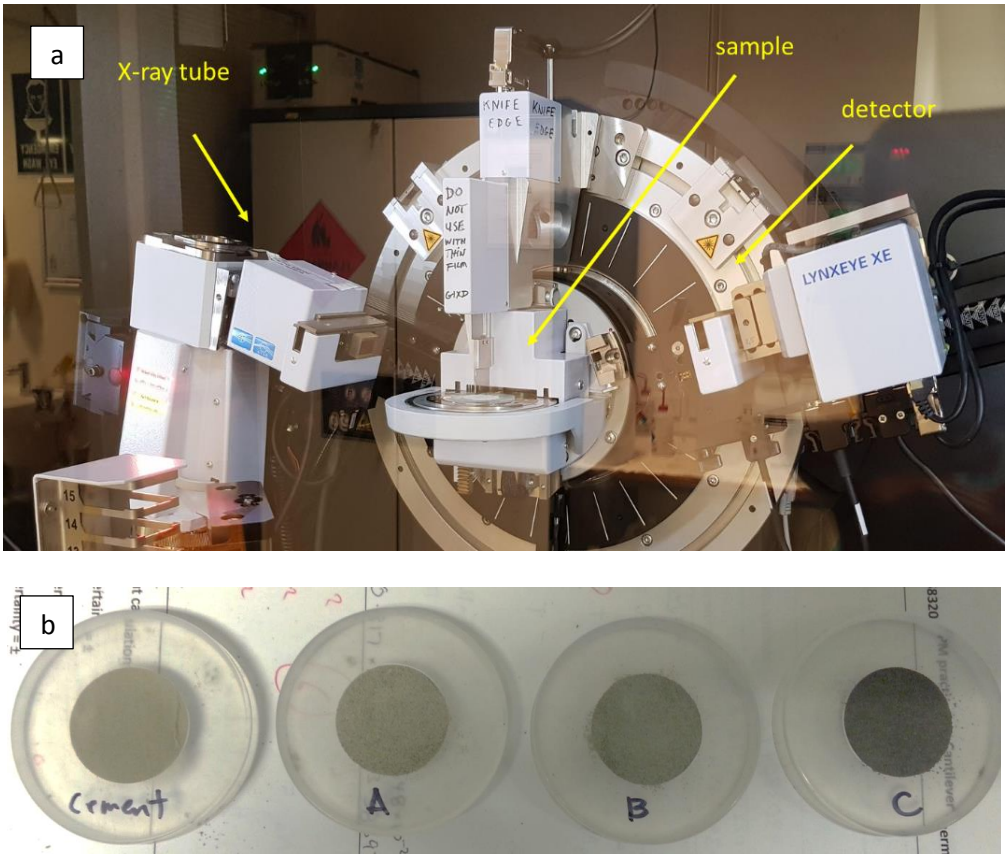

Figure 3-6 a) Actual XRD set-up (Bruker D8 Discovery XRD) showing the position of X-ray source, sample, and detector and b) front-loaded XRD samples

3.1.3 Thermogravimetric Analysis (TG)

3.1.3.1 Principles

TG monitors the change in mass of a material as a function of increasing temperature at a controlled heating rate (Ramachandran et al. 2002). Mass loss occurs as the material undergoes decomposition reactions at higher temperatures. Thus, TG is a useful tool to monitor heat stability and degradation of components.

A sample TG plot of hydrated cement paste is shown in Figure 3-7. Typical decomposition reactions that occur in hydrated cements are as follows (Alarcon-Ruiz et al. 2005):

30 – 105 °C: the evaporable water and a part of the bound water escapes

110 – 170 °C: the decomposition of gypsum (with a double endothermal reaction), the decomposition of ettringite and the loss of water from part of the carboaluminate hydrates take place

180 – 300 °C: the loss of bound water from the decomposition of the C-S-H and carboaluminate hydrates

400 – 500 °C: dehydroxylation of portlandite

700 – 900 °C: decarbonation of calcium carbonate

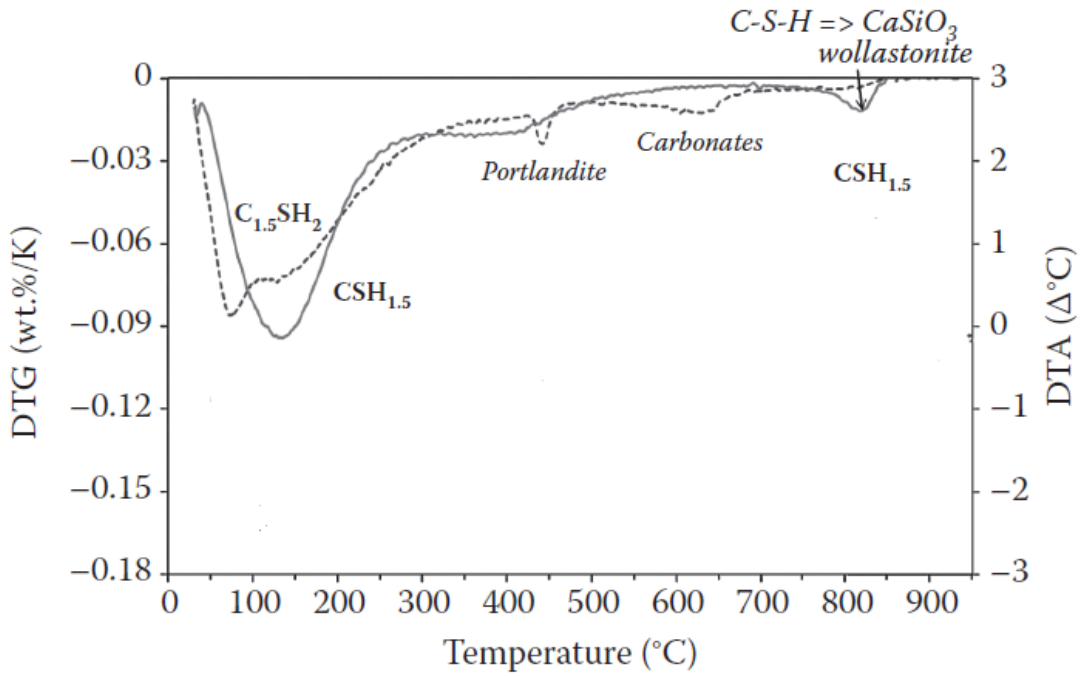

Figure 3-7 Sample TG plot of hydrated cement (Scrivener, Snellings & Lothenbach 2016)

3.1.3.2 Operating Parameters and Sample Preparation

TG curves in this study were obtained using TA Instruments SDT-Q600 Simultaneous TGA/DSC equipment. The paste specimens were ground using mortar and pestle and 50 mg sample was taken from the ground material and transferred to a platinum crucible, which was then placed inside the TG instrument. The thermal analysis was performed in a nitrogen gas atmosphere, within a temperature range from 23 °C to 1000 °C and at a heating rate of 10 °C/min.

3.1.4 Inductively Coupled Plasma Optical Emission Spectrometry (ICP-OES)

ICP-OES is a technique used to measure the concentration of elements in solution (Caruso et al. 2017). In this technique, the solution to be analysed is injected by a pump into the spray chamber through a nebulizer. Schematic diagram of a typical ICP-OES equipment is shown in Figure 3-8. Plasma, generated from ionized argon gas, is used to excite atoms from the sample. When the atoms are ionized, they jump from lower energy state to higher energy state. Upon returning to low energy position, the atoms emit photons with wavelength characteristic of their respective elements. The concentration of each element is determined based on the intensity of the emitted photons and calibration results.

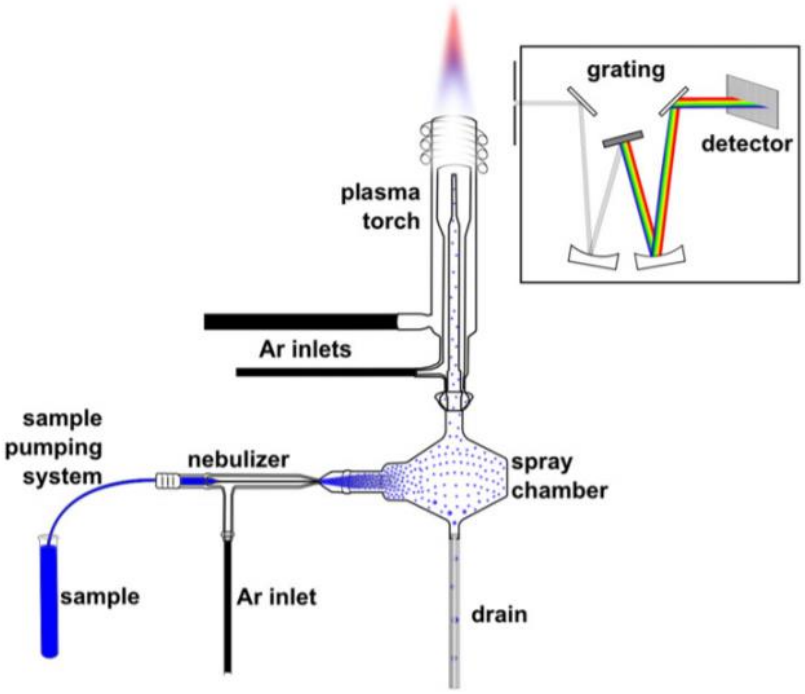

Figure 3-8 Schematic diagram of a typical ICP-OES instrument (Caruso et al. 2017)

The concentration of elements in all extracted pore solutions was determined using ICP-OES. All ICP-OES analysis in this study was conducted at the EPFL environmental engineering laboratory (outsourced). Note that all pore solution extractions were also performed in EPFL, Switzerland since UTS has no pore solution extraction device at the time the experiments were conducted. The ICP-OES instrument used was Shimadzu ICPE-9000. The quantitation range of the ICP-OES is 1 ppb (1µg/L) to 10 ppm (10 mg/L).

3.1.5 Inductively coupled plasma mass spectrometry (ICP-MS)

ICP-MS follows the same principle as ICP-OES. It uses a plasma source to ionize atomic elements. Once ionized, the ions are then sorted on account of their mass. The added advantage of the ICP-MS technique over ICP-OES is its much lower detection limits. Schematic of a typical ICP-MS equipment is shown in Figure 3-9.

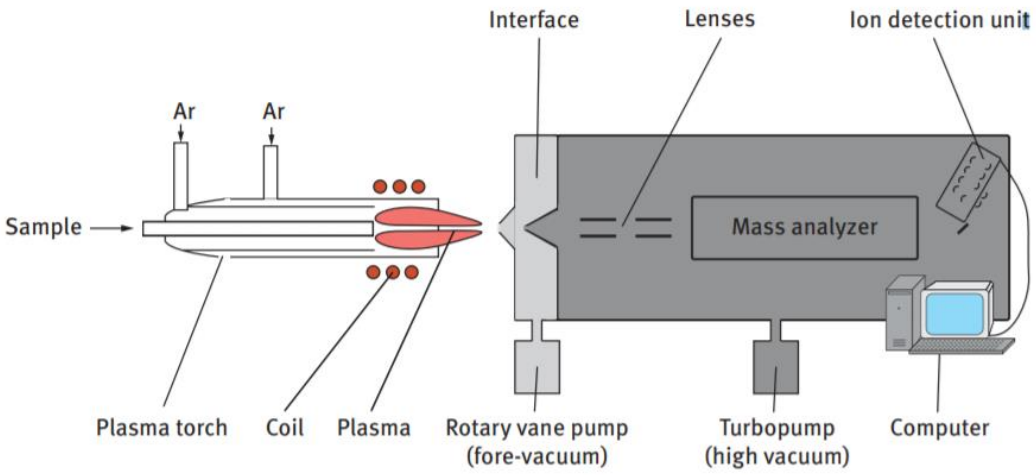

Figure 3-9 Schematic view of an ICP-MS instrument (Hu et al. 2017)

In this study, analysis of solutions from dissolution test experiments were carried out using ICP-MS. All solutions were filtered to remove any residue and diluted to 0.01M NaOH concentration before acidification with high purity HNO_3 to produce a 1 % v/v HNO_3 solution. Analysis of the solution was carried out using Agilent Technologies ICP-MS 7500 Series. Si and Al calibration standards in the range of 0.1-1 parts per million (ppm) dissolved in a consistent matrix as the samples and a control solution (reference blank) were prepared. Calibration was performed prior to running

the samples. Calibration standards were also analysed in between and after the samples to ensure accuracy of the results. The calibration standard solutions used in this study were diluted from commercial stock solutions (High-Purity Standards) of known concentration. All calibration and control solutions were freshly prepared before the measurements. In cases where measured concentrations exceed 1 ppm, the samples were further diluted to ensure that concentrations fell within the calibration curve. The quantitation range of the ICP-MS is 50 ppt (0.05 ug/L) to 1 ppm (1 mg/L).

3.1.6 X-ray Fluorescence Spectroscopy (XRF)

XRF has similar principle as EDS except it uses X-rays to excite electrons rather than electrons. Since the electron beam can be focused on a microscopic area on a sample, EDS analysis can examine chemical compositions in a microscopic scale (typically 1.5 μm interaction volume); while the XRF spectrometer is mainly used to examine overall chemical compositions in a sample (Leng 2013).

X-ray ionizes the atoms of the sample leading to the ejection of an electron from the atom. The removal of electron makes the structure unstable and therefore, the electron from higher orbital moves to the lower orbital to fill the hole. This causes the release of fluorescence radiation which corresponds to the energy difference of the two orbitals involved. Since the emitted radiation has the characteristic energy of the atoms in the sample, this enables the identification of elements present (Leng 2013). The process is illustrated in Figure 3-10.

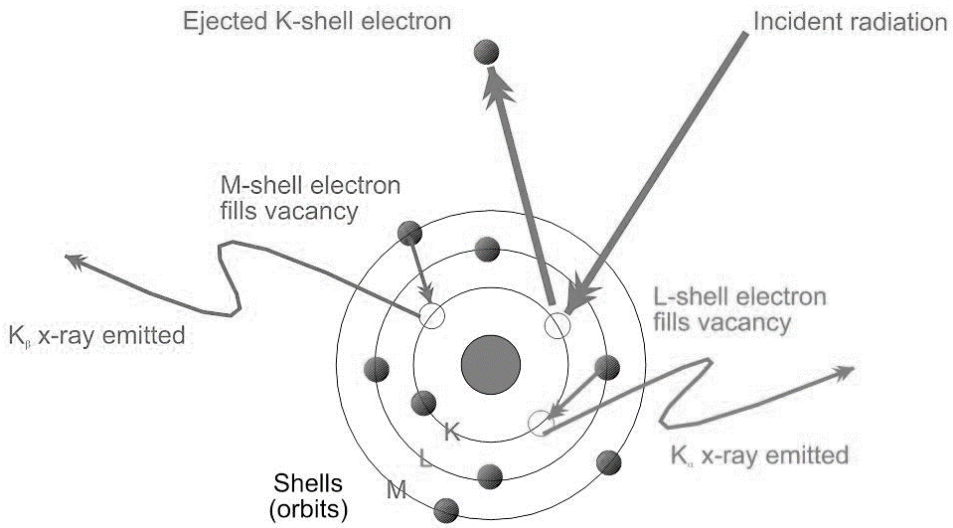

Figure 3-10 Excitation of electrons and release of X-ray fluorescence (Bruker)

All XRF analyses results reported in this study were outsourced to University of New South Wales (UNSW). The XRF equipment used was a Philips PW2400 XRF Rh end-window tube coupled with SUPERQ software. The equipment detection level is 0.01%. Certified reference materials (CRMs) supplied by Malvern Panalytical were used for calibration. For the purposes of calibration, the XRF readings of the CRMs were obtained three times (Table 3-2). These data were used to estimate the standard deviation (STDEV). The maximum STDEV calculated is 0.02%, which confirms that the measurements are repeatable. Repeat XRF analysis of cements was performed by an independent laboratory (Boral Cement) to also verify the alkali contents (in cases where the reported UNSW XRF values exceed 0.6% Na_2O_{eq}). Measured values are in close agreement.

Table 3-2 Certified reference material XRF calibration data

Element Oxide	Measured values (wt. %)			Average (%)	STDEV (%)
	Triplicate 1	Triplicate 2	Triplicate 3		
Na_2O	1.03	1.03	1.03	1.03	0.00
MgO	1.55	1.55	1.55	1.55	0.00
Al_2O_3	36.37	36.41	36.39	36.39	0.02
SiO_2	46.15	46.10	46.15	46.13	0.02
P_2O_5	0.17	0.17	0.17	0.17	0.00
SO_3	0.06	0.06	0.06	0.06	0.00
K_2O	1.70	1.70	1.70	1.70	0.00
CaO	1.21	1.21	1.21	1.21	0.00
TiO_2	0.47	0.47	0.47	0.47	0.00
Mn_3O_4	0.14	0.14	0.14	0.14	0.00
Fe_2O_3	2.66	2.66	2.66	2.66	0.00
L.O.I	8.39	8.39	8.39	8.39	0.00
Total	99.9	99.89	99.92	99.90	0.01

3.1.7 Particle Size Analysis by Laser Diffraction

Laser diffraction measures particle size distributions by measuring the angular variation in intensity of light scattered as a laser beam passes through a dispersed particulate sample. It can determine particle sizes in the range from 0.1 to 3000 mm. Moreover, a distinct advantage of laser light diffraction spectrometry is the short measurement time required, especially compared with several other non-optical methods (Teipel 2005). Optical properties of the material such as refractive index and absorption index should be known to be able to accurately determine the particle size distribution.

The particle size distribution of powder samples was measured by laser diffraction Malvern MasterSizer 2000 as shown in Figure 3-11. Samples that are prone to

hydration were measured in isopropanol, while samples that are not were measured in water. The powders were dispersed in an appropriate solvent in beakers using an ultrasonic bath.

Figure 3-11 Particle Size Analyzer Malvern Mastersizer 2000

3.2 Materials

The results of the analysis of the raw materials used in this study are reported in the succeeding sections. Raw materials include cement, SCMs, aggregates, ground limestone and alumina (Al_2O_3). This study used three types of cement (Australian low alkali GP cement with 7.5% limestone content, Australian low alkali GP cement with 0% limestone content and high alkali GP cement sourced from Germany), four types of SCMs (FA, SL, MK and SL) and three types of reactive aggregates (greywacke, dacite and rhyolite). The slag (SL) used in this study is ground granulated blast furnace slag (GGBFS).

3.2.1 Morphology (SEM-EDS)

Figure 3-12 shows representative scanning electron microscope (SEM) images of fly ash, metakaolin, slag and silica fume. Fly ash is characterized by spherical particles with a generally smooth texture (Fernandez-Jimenez & Palomo 2005; Gebregziabiher, Thomas & Peethamparan 2016). Silica fume exhibits comparable appearance to fly ash, except that is about 100 times finer (Thomas 2013). Slag and metakaolin exhibit angular appearance due to the grinding process they undergo to make them suitable for concrete use (Gebregziabiher, Thomas & Peethamparan 2016).

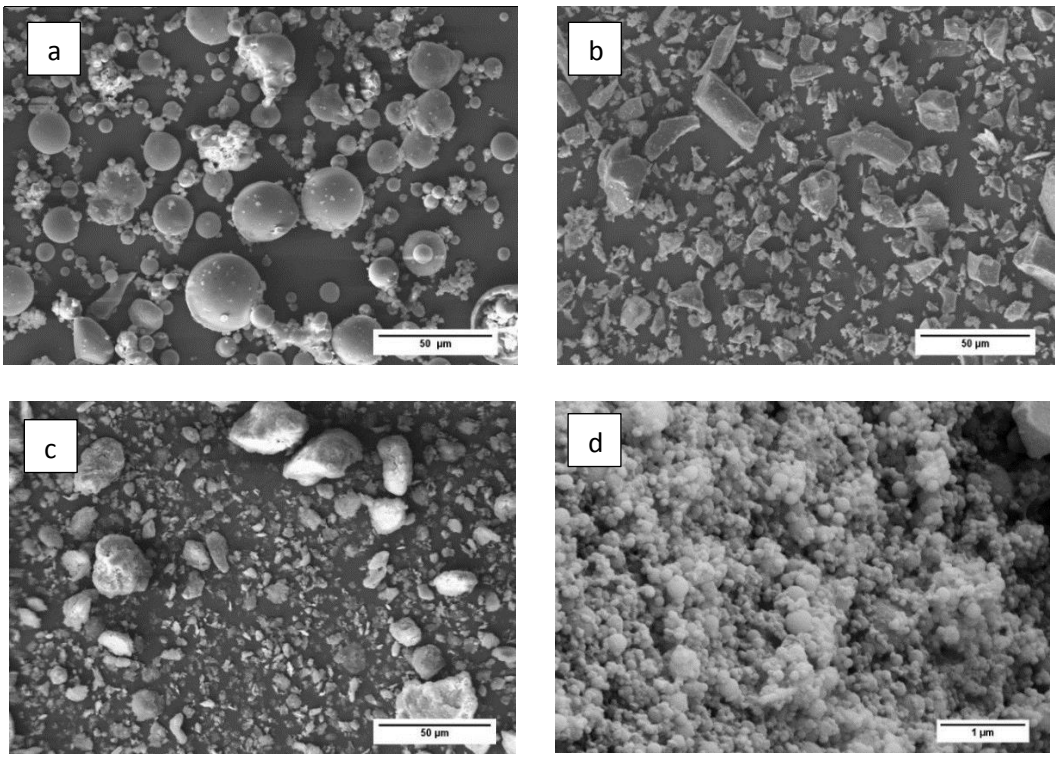

Figure 3-12 SEM images of a) fly ash , b) slag c) metakaolin and d) silica fume particles

3.2.2 Composition Analysis (XRF)

Oxide composition of cements, SCMs and aggregates utilized in the study is shown in Tables 3-3, 3-4 and 3-5 respectively. The total alkali content of the cements was conventionally calculated as equivalent sodium oxide [$\%Na_2O_{eq} = \%Na_2O + (0.658 \times \%K_2O)$]. All Australian cements are from Cement Australia and have alkali content $\leq 0.6\%$ Na_2O_{eq} while the high alkali cement (supplied by Heidelberg Germany) has alkali content of about 1% Na_2O_{eq} (Table 3-3).

Oxide composition of the SCMs in Table 3-4 shows that fly ash contains a much higher amount of silica (SiO_2) and alumina (Al_2O_3) than slag. AS/NZS 3582.1 only allows fly ash with composition of $SiO_2 + Al_2O_3 + Fe_2O_3 \geq 70\%$ to be suitable for use. Moreover, slag has a relatively high calcium content and a composition close to that of Portland cement. AS 3582.2 requires slag to have maximum 18% Al_2O_3 and maximum 15% MgO content. Both fly ash and slag conform to required specifications. Silica fume contains 91% SiO_2 and conforms to the requirement of AS/NZS 3582.3 which requires silica fume or amorphous silica to contain at least 85% silica to be suitable for use as a cementitious material in concrete, mortar and related applications. Oxide composition of the aggregates in Table 3-5 shows that all reactive aggregates used in this study have SiO_2 content > 60%.

Table 3-3 XRF Oxide Composition of the Cements and Ground Limestone

Oxide wt.%	Low Alkali Cement/ 7.5% Limestone GP Cement (Australia)	0% Limestone GP Cement (Australia)	High Alkali Cement (Germany)	Ground Limestone
SiO_2	19.67	20.36	19.3	1.30
TiO_2	0.22	0.30	0.30	0.04
Al_2O_3	4.78	5.25	5.70	0.43
Fe_2O_3	3.10	3.06	3.60	0.21
Mn_3O_4	0.12	0.05	0.03	0.02
MgO	0.91	1.35	1.60	0.36
CaO	64.18	63.55	63.6	55.11
Na_2O	0.33	0.28	0.20	0.14
K_2O	0.41	0.40	1.20	0.06
P_2O_5	0.06	0.22	0.05	0.02
SO_3	2.37	2.44	3.20	0.02
Na_2O_{eq}	0.60	0.54	0.99	
L.O.I.	4.09	2.77	1.22	42.99

Table 3-4 XRF Oxide Composition of the SCMs

Oxide wt%	Fly Ash	Slag	Metakaolin	SiO_2 Fume
SiO_2	59.21	34.12	62.5	91.46
TiO_2	1.11	0.87	1.02	0.01
Al_2O_3	28.11	14.37	32.39	0.10
Fe_2O_3	3.68	0.3	0.82	0.01
Mn_3O_4	0.11	0.36	0.01	0.02
MgO	0.53	5.31	0.67	0.70
CaO	2.48	41.59	0.07	0.24
Na_2O	0.63	0.35	0.22	0.28
K_2O	1.18	0.26	0.28	0.52
P_2O_5	0.41	0.01	0.03	0.14
SO_3	0.16	2.83	0.08	0.07
L.O.I.	1.05	0.35	1.75	5.55

Table 3-5 XRF Oxide Composition of the Reactive Aggregates

Oxide wt%	Greywacke	Dacite	Rhyolite
SiO_2	66.85	68.38	61.93
TiO_2	0.65	0.36	0.81
Al_2O_3	14.24	13.25	15.44
Fe_2O_3	3.80	3.32	5.75
Mn_3O_4	0.09	0.06	0.10
MgO	1.58	1.30	1.57
CaO	1.94	2.35	2.30
Na_2O	4.25	2.41	5.65
K_2O	3.11	3.84	2.89
P_2O_5	0.14	0.08	0.18
SO_3	0.19	<0.01	0.07
L.O.I.	2.29	4.52	4.09

3.2.3 Calcite Content in Cements and Ground Limestone

Thermogravimetric analysis (TG) was performed to verify limestone content of the cement and ground limestone used to study the effect of limestone on ASR mitigation (Chapter 6). Weight loss curves obtained using TGA are shown in Figure 3-13. The 0% limestone GP cement showed only ~0.2% mass loss at about 600-800 °C confirming the negligible amount of $CaCO_3$ present. The ground limestone, on the other hand, registered a mass loss of about 43%. The corresponding molar masses of the reactant and formed products can be expressed as:

Equation 3-1 $CaCO_{3(solid)}(100\ g/mol) \rightarrow CaO_{(solid)}(56\ g/mol) + CO_{2(gas)}(44\ g/mol)$

Thus, the weight loss of about 43% in the ground limestone confirms that it is about 98% $CaCO_3$. This is consistent with about 43% loss of ignition (LOI) in XRF results which likely corresponds to the release of carbon dioxide at higher temperatures.

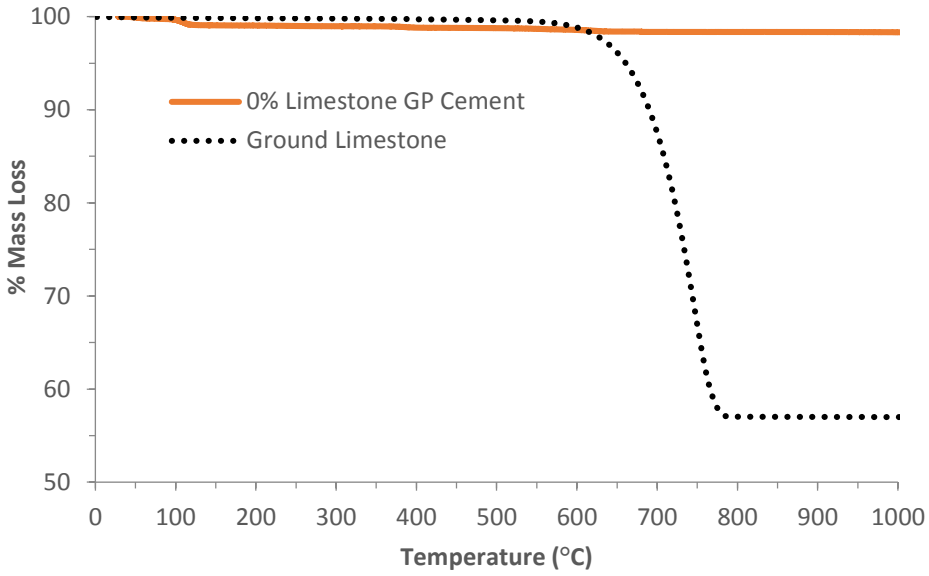

Figure 3-13 TG Curves of the 0% Limestone GP cement and ground limestone

3.2.4 Identification of Phases (XRD)

XRD patterns of the unhydrated cements in Figure 3-14 show identical peaks characteristic of expected phases: alite (C_3S), belite (C_2S), tricalcium aluminate (C_3A) and tetracalcium aluminoferrite (C_4AF). The main phases are abbreviated using cement chemist notation where C=CaO, S=SiO_2, A=Al_2O_3 and F=Fe_2O_3 (Taylor 1997).

XRD patterns of the SCMs are shown in Figure 3-15. XRD pattern of fly ash shows presence of both crystalline and amorphous glassy phase. The major crystalline peaks are quartz (silica) and mullite (aluminosilicate). The presence of an amorphous phase is indicated by a broad hump in the XRD spectrum at about 2Θ=15-30°. The XRD patterns of slag and silica fume both show absence of crystalline peaks and presence of a broad hump confirming their primarily amorphous/glassy nature (Gebregziabiher, Thomas & Peethamparan 2016). The XRD pattern of metakaolin shows presence of quartz peaks, which indicates that the metakaolin used is not purely amorphous aluminosilicate.

XRD pattern of the ground limestone in Figure 3-16 shows the crystalline phases attributed to calcite consistent with 98% $CaCO_3$ composition of the ground limestone as per TG measurements. The tiny peak of quartz detected is consistent with 1.3% of SiO_2 detected in the ground limestone from XRF measurement.

XRD patterns of the aggregates in Figure 3-17 show the presence of quartz and albite (plagioclase feldspar) phase consistent with petrographic analysis. Whereas quartz is a SiO_2 phase, albite is an aluminosilicate.

XRD pattern of the alumina in Figure 3-18 shows the presence of corundum which is a crystalline aluminium oxide (Al_2O_3) as well as θ-Al_2O_3, which is a metastable phase of alumina.

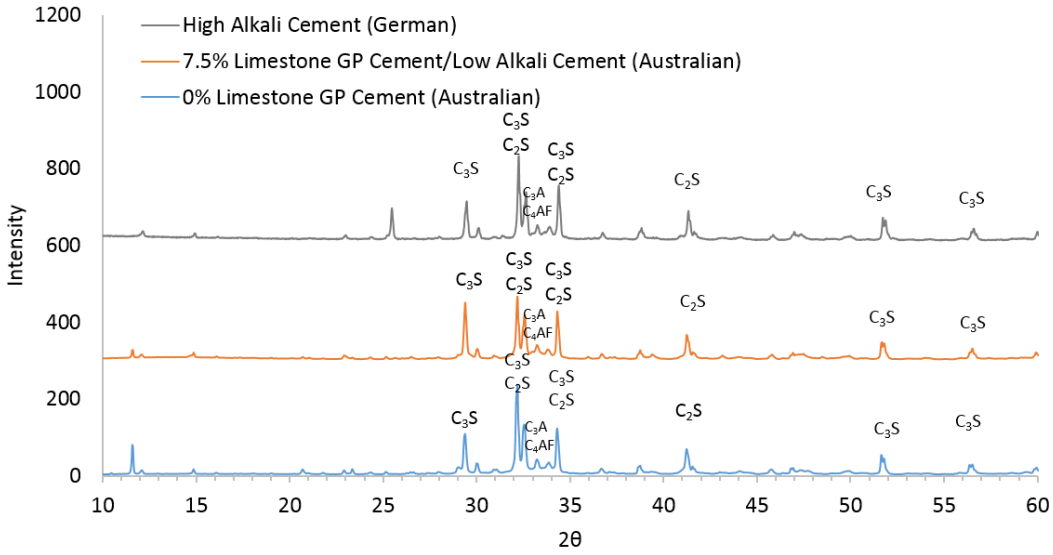

Figure 3-14 XRD patterns of cement where C_3S= Alite ($3CaO \cdot SiO_2$), C_2S=Belite ($2CaO \cdot SiO_2$), C_3A= Tricalcium aluminate ($3CaO \cdot Al_2O_3$) and C_4AF=Tetracalcium Aluminoferrite ($4CaO \cdot Al_2O_3 \cdot Fe_2O_3$)

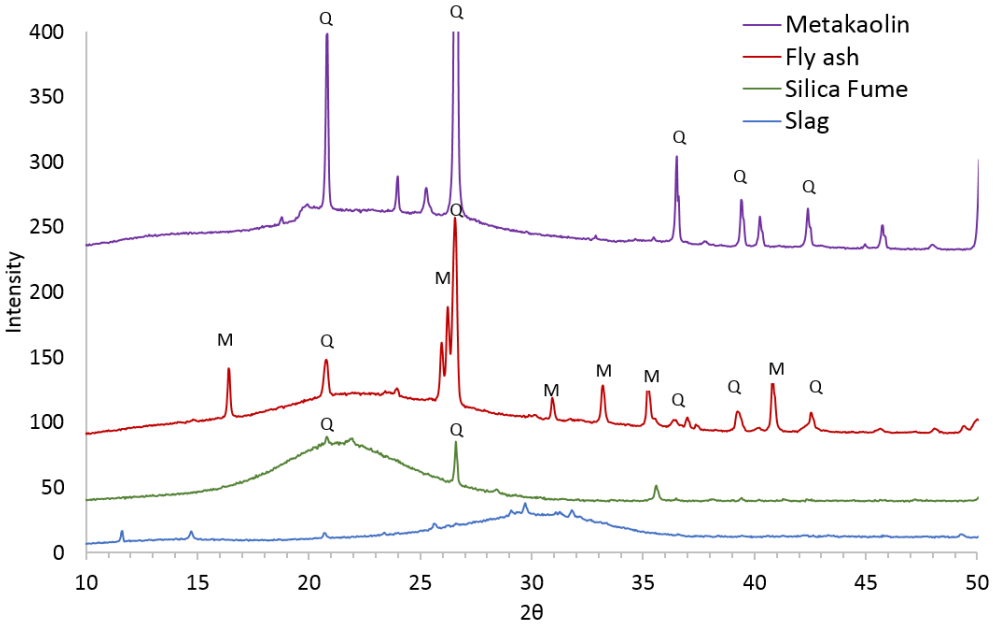

Figure 3-15 XRD patterns of raw SCMs where Q=quartz and M=mullite

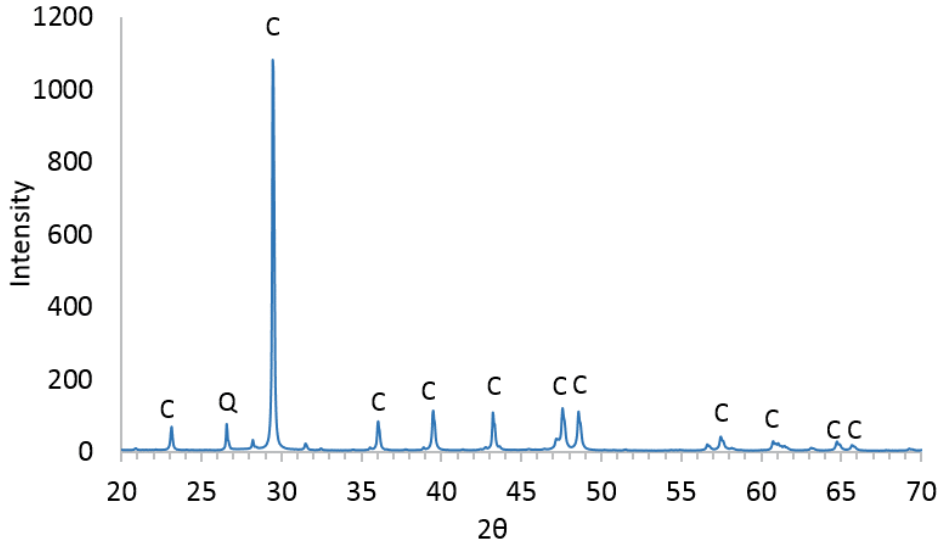

Figure 3-16 XRD pattern of ground limestone where C=calcite and Q=quartz

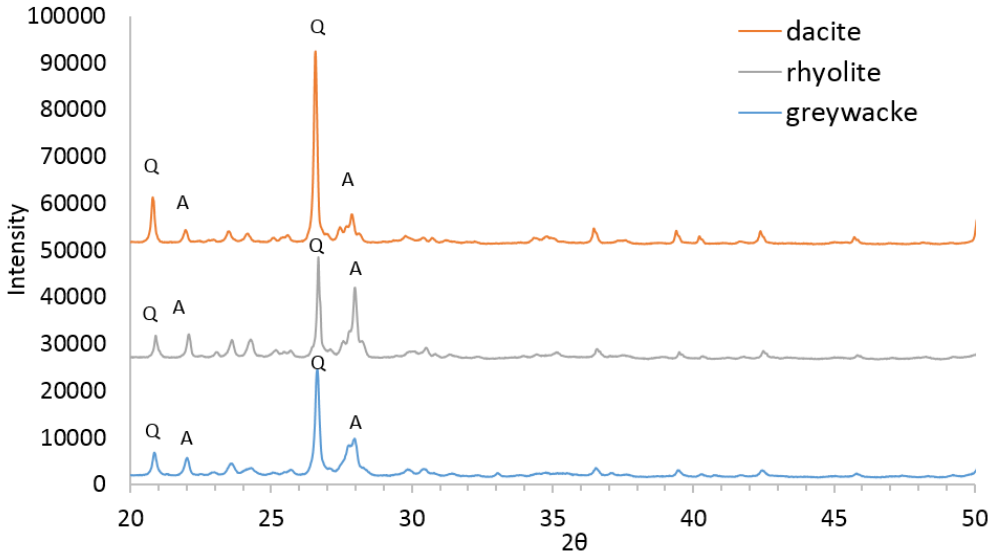

Figure 3-17 XRD patterns of raw aggregates where Q=quartz and A=albite

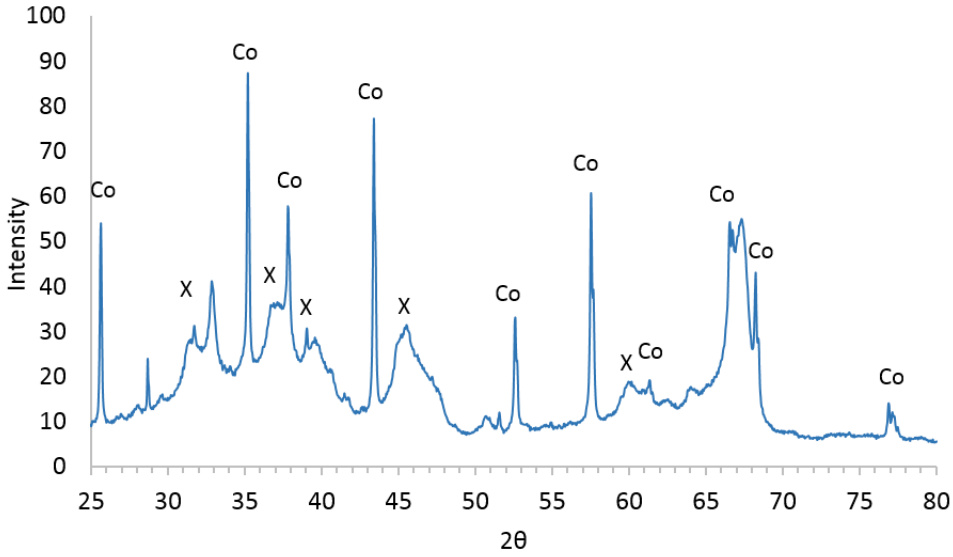

Figure 3-18 XRD pattern of alumina where Co=corundum and X=θ-Al_2O_3

3.2.5 Particle Size Analysis

Table 3-6 summarizes the results of the particle size analysis of the raw materials obtained using laser diffraction represented by D10, D50 and D90 which represent 10%, 50% and 90% of the cumulative mass. D10 refers to the diameter at which 10% of the sample's mass is comprised of particles with a diameter less than this value. The D50 is the diameter of the particle at which 50% of a sample's mass is smaller than and 50% of a sample's mass is bigger than. Likewise, D90 indicates that 90% of a sample's mass is composed of diameter less than this value. The results show that the cements used have comparable particle size with D(50) of about 15 µm. The values in the table reflect the average of five measurements. Corresponding standard deviations also shown accordingly.

Table 3-6 D(10), D(50) and D(90) of the raw materials

Raw Material	D (0.1) µm	D (0.5) µm	D (0.9) µm
Low Alkali 0% Limestone GP Cement (Australia)	3.81 ± 0.01	15.56 ± 0.03	37.69 ± 0.12
Low Alkali 7.5% Limestone GP Cement (Australia)	3.74 ± 0.01	16.11 ± 0.04	39.28 ± 0.40
High Alkali Cement (Germany)	3.81 ± 0.01	15.56 ± 0.10	37.69 ± 0.60
Slag	2.86 ± 0.03	12.26 ± 0.02	32.11 ± 0.11
Fly Ash	0.97 ± 0.02	17.12 ± 0.17	63.23 ± 1.67
Metakaolin	3.03 ± 0.01	19.52 ± 0.06	73.19 ± 0.16
Ground limestone	3.07 ± 0.18	19.66 ± 0.32	157.92 ± 5.55
Alumina	3.78 ± 0.03	20.31 ± 0.31	47.89 ± 1.27

3.2.6 Petrographic Analysis (outsourced)

Mineralogical composition of the aggregates used in the study obtained from petrographic study (outsourced) is shown in Tables 3-7 to 3-9. All aggregates contain presence of SiO_2-containing minerals quartz and feldspar consistent with high amount of SiO_2 detected from XRF (> 60%).

Table 3-7 Greywacke Mineralogical Composition

Mineral	%
Microcrystalline feldspars	37
Microcrystalline Quartz	17
Quartz	13
Epidote	8
Moderately Strained Quartz	7
Feldspar	7
Lithic clasts	5
Calcite	3
Chlorite	2
Sericite	1

Table 3-8 Dacite Mineralogical Composition

Mineral	%
Quartz	45
Feldspar	30
White mica	10
Chlorite	5
Calcite	5
Magnetite	5
Biotite	1

Table 3-9 Rhyolite Mineralogical Composition

Mineral	%
Quartz	45
Feldspar	35
Calcite	7
White mica	5
Chlorite	5
Magnetite	1

3.3 Experimental Program

This section details the experimental work undertaken to meet the objectives of this work. The experimental work is comprised of expansion tests as well as characterization studies to investigate the underlying mechanisms.

3.3.1 ASR Expansion Tests

Two types of expansion tests were carried out: accelerated mortar bar test (AMBT) and modified concrete prism test (CPT) using simulated pore solution as storage solution. AMBT was carried out in the civil engineering laboratories of UTS while the

modified CPT (Pore Solution Method) was carried out at EPFL, Switzerland. Details of both tests are discussed in succeeding chapters.

3.3.1.1 Accelerated Mortar Bar Test (AMBT)

AMBT was conducted to evaluate the effect of substituting portion of the cement with SCMs (fly ash, slag, metakaolin and silica fume), Al_2O_3 and limestone on ASR mitigation.

Mortar bars composed of: 1 part of cement to 2.25 parts of graded aggregate by mass (440 g cement per 990 g of aggregate) and water to cement ratio equal to 0.47 by mass were prepared in accordance to AS 1141.60.1. The aggregate grading requirements are shown in Table 3-10. The aggregates were crushed and sieved as necessary to obtain the required aggregate grading. In mixes where SCMs/limestone/Al_2O_3 are used, they replaced part of the cement at a nominated percentage while maintaining water to cement ratio at 0.47 by mass.

Table 3-10 AMBT aggregate grading requirements

Sieve size, mm		% by mass
Passing	Retained on	
4.75	2.36	10
2.36	1.18	25
1.18	0.60	25
0.60	0.30	25
0.30	0.15	15

For mortar specimens with ground limestone addition, the ground limestone was added to 0% limestone GP cement at 8%, 12% and 17% by mass of cement. The SCMs were

used both at recommended replacement dosages and at similar dosages to be able to comparatively assess their effect on ASR expansion. Al_2O_3 was used at a fixed dosage of 25% with three types of reactive aggregates (greywacke, dacite and rhyolite).

The mortar specimens were prepared on 25 x 25 x 285 mm moulds with a gauge length of 250 mm then cured in high humidity environment at room temperature (23 ±2 °C) for 24 hours. After, the specimens were carefully de-moulded and put in a container filled with water. The container was then placed in an oven set at 80 °C for another 24 hours to allow the specimens to further cure. After which, zero hour length measurements were obtained using a horizontal comparator prior immersing the specimens in 1M NaOH solution at 80 °C for 28 days, as shown in Figure 3-19. Succeeding expansion measurements were obtained at 1, 3, 7, 10, 14, 21, and 28 days using a comparator as shown in Figure 3-20. Three mortar bars were prepared for each mix. Therefore, each point in the AMBT plot represents the average expansion of the three mortar samples. Each point is presented with maximum +/- 8.3% error based on Section 12.2 of ASTM C1567-13, which states that the precision of the AMBT method within the same laboratory environment should not differ by more than 8.3% of the mean expansion. This value was also found to be in close agreement with the range of calculated standard deviations from the actual measured expansion data. Lines of best fit for all expansion measurement plots have been used based on the known trends and relationships reported in literature.

Figure 3-19 1M NaOH bath at 80 °C for accelerating mortar expansion (AMBT)

Figure 3-20 AMBT Specimen Expansion Measurement (horizontal comparator)

Tables 3-11 to 3-13 summarize the parameters investigated for AMBT. Total expansion incurred by the aggregate after 10 days and 21 days of NaOH immersion was used to classify its ASR potential when used in the field in accordance with AS 1141.60.1. Likewise, since Australia does not have an existing standard for assessing the efficacy of SCMs in ASR mitigation, same criteria were employed for mixes with SCMs as it is very similar to widely accepted ASTM C1267. The classification criteria are shown in Table 3-14.

Table 3-11 Effect of SCM Type and Dosage on ASR Mitigation (Chapter 4)

Factors	Variables
SCM Type and Dosage	fly ash (10%, 15%, 25%), slag (10%, 35%, 65%), metakaolin (10%, 15%, 25%), silica fume (5%, 10%, 25%)
Cement	Australian Low Alkali 7.5% Limestone GP Cement
Reactive Aggregate	greywacke

Table 3-12 Effect of Limestone on the Efficacy of SCMs in Mitigating ASR (Chapter 6)

Factors	Variables
Cement	Australian Low Alkali 0% Limestone GP Cement, +8% limestone, +12% limestone, +17% limestone
SCM Type and Dosage	fly ash (15% and 25%), slag (35% and 65%)
Reactive Aggregate	greywacke

Table 3-13 Effect of Al_2O_3 on ASR Expansion (Chapter 4)

Factors	Variables
Alternative SCM	Al_2O_3 (calcined alumina)
Replacement Level	25% for all mixes
Reactive Aggregate	greywacke, dacite, rhyolite
Cement	Australian Low Alkali 7.5% Limestone GP Cement

Table 3-14 AMBT expansion criteria

Standard	Mortar Bar Expansion in 1M NaOH (80 °C) [%]		Reactivity Classification
AS 1141.60.1	Day 10 immersion	$E < 0.1$	Non-reactive
	Day 21 immersion	$0.1 \leq E < 0.3$	Slowly reactive
		$0.3 \leq E$	Non-reactive
ASTM C1567	Day 14 immersion	$E < 0.1$	Non-reactive

3.3.1.2 Concrete Prism Test (Simulated Pore Solution)

Concrete prisms (70 x 70 x 280 mm) with cement content of 410 kg/m^3 were cast using Australian reactive aggregates, SCMs and cement. Three concrete prisms as shown in Figure 3-21 were prepared for each mix using the same type of aggregate for both fine and coarse components (0.16 µm-22.4 mm aggregate sizes) keeping the water to cement ratio at 0.46 for all mixes. To simulate a cement with 0.8% and 1% Na_2O_{eq} alkali content, the cement with original 0.6% Na_2O_{eq} (Australian cement) was boosted with 0.2% and 0.4% extra alkali by adding sodium hydroxide (NaOH) to the mixing water. The alkali was added based on the cement content and not the binder content. The SCMs were used at Australian recommended dosages for effective mitigation, 25% for fly ash and 50% for slag. Table 3-15 and Table 3-16 show summary of the concrete mixes investigated.

Figure 3-21 Casting of concrete prisms

The concrete prisms were demoulded after 24±2 hours and left to cure for 28 more days in high humidity environment, 20±2 °C before being stored in simulated pore solution at 38 °C or 60 °C. This is in contrast to one day curing in ASTM C1293.

Table 3-15 Concrete mixes stored at 38 °C

Investigated Concrete Mixes	Aggregate	SCM	Cement Na_2O_{eq} (original alkali content+NaOH)
Mix 1	rhyolite	none	0.6%
Mix 2	rhyolite	25%FA	0.6% +0.2% =0.8%
Mix 3	rhyolite	25%FA	0.6% +0.4% =1.0%
Mix 4	rhyolite	50%SL	0.6% +0.2% =0.8%
Mix 5	rhyolite	50%SL	0.6% +0.4% =1.0%
Mix 6	dacite	none	0.6%
Mix 7	dacite	25%FA	0.6% +0.2% =0.8%
Mix 8	dacite	25%FA	0.6% +0.4% =1.0%
Mix 9	dacite	50%SL	0.6% +0.2% =0.8%
Mix 10	dacite	50%SL	0.6% +0.4% =1.0%

Table 3-16 Concrete mixes stored at 60 °C

Investigated Concrete Mixes	Aggregate	SCM	Cement Na_2O_{eq} (original alkali content+NaOH)
Mix 1	rhyolite	none	0.6%
Mix 2	rhyolite	25%FA	0.6% +0.4% =1.0%
Mix 3	rhyolite	50%SL	0.6% +0.4% =1.0%
Mix 4	dacite	none	0.6%
Mix 5	dacite	25%FA	0.6% +0.4% =1.0%
Mix 6	dacite	50%SL	0.6% +0.4% =1.0%

Pastes with equivalent composition and water to cement ratio as the concrete prisms were prepared in sealed containers and cured for 28 days under high humidity environment at 20±2 °C. Additional pastes with SCMs but no alkali boosting and with

SCMs + 0.2% alkali boosting were also prepared. The pastes were then subjected to pore solution extraction at 28 days using 1500 kN force from a compression testing machine at 5 kN/s ramp rate and then holding the force for 10 minutes after, the extracted solutions filtered with 0.2 μm membrane to remove solid residues and then subjected to inductively coupled plasma atomic emission spectroscopy (ICP-OES) to determine the concentration of elements, Ca, Al, Si, S, Na and K in the pore solution. The solutions were stored in glass vials at 4 °C until testing.

The simulated pore solution used to store the concrete prisms was prepared based on the alkali content (Na and K concentration) of the paste system corresponding to the binder of the concrete at 28 days. Another set of pastes cast from the same mix as the 28 day pastes were also subjected to pore solution extraction after 6 months (168 days) in order to monitor the effect of time on the stability of the pore solution. Figure 3-22 illustrates the process of pore solution extraction.

Figure 3-22 Pore solution extraction of blended pastes using 1500 kN force from compression testing machine

Concrete expansion measurements were obtained using a vertical comparator as shown in Figure 3-23 before immersing the concrete prisms in the storage solution (zero hour expansion reference) and every 28 days to monitor expansion. For expansion measurements, the concrete prisms were taken out of the oven 1 day prior

measurement to allow to cool to room temperature as this ensures that the concretes are in similar conditions and therefore reduce measurement errors.

Each point in the expansion plot reports the average expansion of three concrete specimens. The calculated standard deviation from the expansion measurements were used to represent error. Lines of best fit for all expansion measurement plots have been used based on known trends and relationships reported in literature.

Figure 3-23 Vertical comparator for length measurements

3.3.2 Solubility of SCMs in Alkali Environment

Five grams of each type of SCM was immersed in 50 ml 1M NaOH solution and kept at 80 °C for 28 days. 2ml aliquots were pipetted from each mix at 7, 14, 21 and 28 days and filtered to remove any residue and diluted to 0.01M NaOH concentration before acidification with high purity HNO_3 to produce a 1 % v/v HNO_3 solution prior ICP-MS analysis.

The solid residues in the samples were filtered after 28 days, air-dried and subjected to SEM-EDS and XRD analysis to characterize the microstructural and phase changes that have occurred in the SCMs.

3.3.3 Effect of SCMs and Limestone on Portlandite Content

Blended pastes containing SCMs at 10%, 25% and 50% replacement by mass of cement were prepared by mixing cement (Australian OPC/low alkali cement), SCMs and water (0.46 water-to-cementitious material ratio). Similarly, blended pastes with 0%, 8%, 12% and 17% ground limestone were prepared by adding ground limestone to 0% limestone GP cement at the same 0.46 water to cement ratio.

The paste specimens were cured for one day in 90% RH 23±2 °C oven and after which stored in 1M NaOH 80 °C for 28 days. Pure cement paste was also prepared to serve as a reference. Thermogravimetric (TG) data of all samples were obtained at Day 1

and Day 28 to monitor the amount of portlandite in the paste. The measurement of portlandite content was performed with TA Instruments SDT-Q600 Simultaneous TGA/DSC equipment.

3.3.4 Effect of SCMs and Limestone on Pore Solution Alkalinity

To assess the effect of various SCMs and limestone on pore solution alkalinity, blended pastes with proportions detailed in Tables 3-17 to 3-19 were mixed at water/binder ratio of 0.46, subjected to pore solution extraction at defined extraction periods and then to ICP-OES analysis to determine concentrations of Na and K as well as other elements in solution (Ca, Al, Si and S). All blended pastes were stored at 20±2 °C environment prior pore solution extraction.

Table 3-17 Effect of SCM Type on Pore Solution Alkalinity

Cement	low alkali 7.5% limestone GP cement (Australia), high alkali cement (Germany)
SCM Type and Dosage	fly ash (15% and 25%), metakaolin (15%, 25%), silica fume (10%, 25%), slag (25%, 50%)
Extraction Periods	28 days, 168 days

Table 3-18 Effect of Cement Alkalinity on the Efficacy of SCMs in ASR Mitigation

Cement	low alkali 7.5% limestone GP cement (Australia)
SCM Type and Dosage	fly ash 25%, slag 50%
Levels of Alkali Boosting	0.2%, 0.4%
Extraction Periods	28 days, 168 days

Table 3-19 Effect of Limestone on Pore Solution Alkalinity

Cement	low alkali 7.5% limestone GP cement (Australia), high alkali cement (Germany)
Limestone Replacement Level	25%
Extractions	28 days, 168 days

Part of the extracted solution (about 1 to 2 ml) was subjected to pH measurement. The pH was measured by calibrating the equipment using 3 buffer solutions pH=4.01, pH=6.87 and pH=9.18. After which the pH was measured per solution for about 2 minutes to allow the system to equilibrate and to get comparable results. The probe was rinsed and dried with each measurement. Deionized water was used to rinse the probes to avoid cross-contamination of other ions. Figure 3-24 shows the actual pH measurement process and the buffer solutions for calibration.

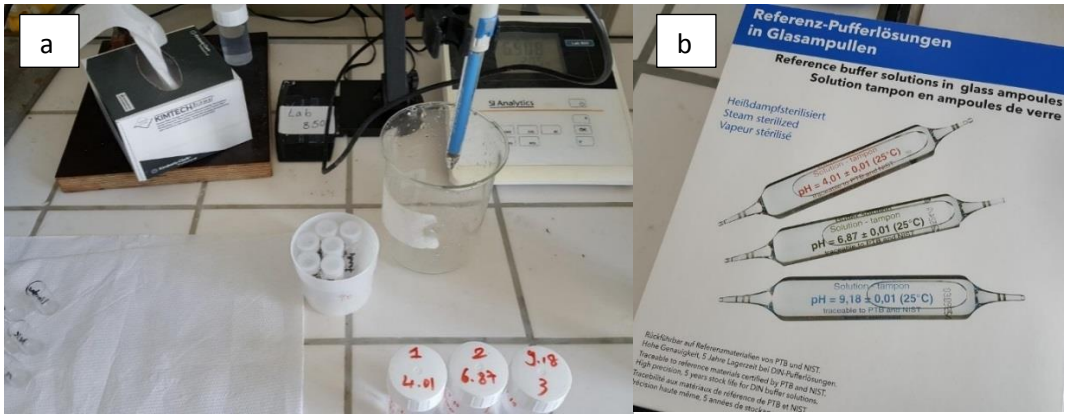

Figure 3-24 a) actual pH Measurement of the pore solutions and b) buffer solutions for calibration

3.3.5 C-S-H and ASR Gel Composition Analysis

The composition of C-S-H was measured by point EDS analysis on the hydration rims around the hydrated clinker (inner C-S-H). The analyses were carried out on 'inner C-S-H' as it is considered to be relatively homogeneous compared to the 'outer C-S-H' which is finely intermixed with other hydration products (mainly aluminates) (Gallucci, Zhang & Scrivener 2013). Minimum of 200 points were analysed per sample.

Elemental analysis and mapping of the ASR gel was also carried out to determine its composition and better illustrate the distribution of elements in the ASR gel. Mapping was carried out using similar parameters as point EDS but longer signal acquisition time of 20 minutes. Both C-S-H and ASR gel composition analysis were carried out on sectioned specimens.

4 Mechanistic Role of SCMs in ASR Mitigation

Adding supplementary cementitious materials (SCMs) to concrete mixes is widely recognized as the most practical way of mitigating alkali-silica reaction (ASR) (Thomas 2011). In the Australian context, it is recommended to add 25% fly ash or 50-65% slag in concrete mixes (Standards Australia 2015). Shayan et al. have done numerous work to qualify the effectivity of Australian SCMs in suppressing ASR in concrete (Shayan, Diggins & Ivanusec 1996a; Shayan, Diggins & Ivanusec 1996b). However, although SCMs are generally accepted as an optimal solution for ASR, the fundamental mechanisms in ASR mitigation is still not fully understood. Understanding the mechanisms by which SCMs function as well as the role of composition in their efficacy in mitigation is critical in the identification and assessment of future SCMs. Globally, there is already a foreseen scarcity in fly ash and slag due to closure of coal fired power stations and increase in steel recycling (Scrivener, John & Gartner 2016).

This chapter aims to better understand the mechanistic role of SCMs in ASR mitigation by investigating the effect of traditional SCMs such as fly ash (FA), slag (SL), metakaolin (MK) and silica fume (SF) on ASR expansion, portlandite consumption, pore solution alkalinity and Ca/Si and Al/Si ratio of the C-S-H phases. Solubility study of the SCMs was also undertaken to characterize their ability to release aluminium and silicon in solution and how these correlate with the SCMs ability to mitigate ASR. Currently, to the author's best knowledge, there is no study in literature that

systematically links ASR expansion to pozzolanicity, reduction in pore solution alkalinity, modification of the C-S-H composition, and SCM solubility in the context of the four common SCMs (FA, SL, MK and SF) both at recommended replacement levels and at equivalent replacements for better comparative assessment

4.1 Effect of SCM Type and Dosage on the Expansion of Mortar Specimens

Mortar expansion measured over a period of time is a widely used method to assess the alkali reactivity of an aggregate being examined (ASTM International 2014; Thomas et al. 2007). The higher the degree of expansion, the more reactive is the aggregate. Consequently, a decrease in expansion when SCMs are incorporated in the mix is an indication that the SCMs are effectively mitigating ASR. Accelerated mortar bar test (AMBT) based on AS 1141.60.1 was carried out to assess how the type of SCM and dosage affect the expansion of mortar specimens with a reactive aggregate. The test involves subjecting the mortar specimens to 1M NaOH at 80 °C for 28 days. AMBT was carried out using recommended replacement levels of SCMs (FA at 15% and 25%, SL at 35% and 65%, MK at 10% and 15%, and SF at 5% and 10%) and at fixed dosages to compare SCM efficacy in ASR mitigation. Greywacke, an aggregate classified as reactive both by AMBT (AS 1141.60.1) and CPT (AS 1141.60.2), was used as the reactive aggregate in all AMBT tests.

Figure 4-1 shows AMBT expansion of greywacke mortar without SCM and with different SCMs at recommended dosages. Each point in the AMBT plot represents the average expansion of three mortars. The dotted lines at 0.10% and 0.30% correspond to the limits as specified in AS 1141.60.1. The percent replacement indicates substituting part of the cement by a particular SCM. The reference mortar with no SCM confirms that greywacke is a highly reactive aggregate, exceeding both expansion limits at 10 days and 21 days. AMBT expansion results for greywacke aggregate with different SCMs at recommended replacement levels show that 10%SF has the capacity to reduce ASR expansion to below 0.10% at 10 days and 0.30% at 21 days as do 15%FA, 35%SL and 15%MK. Moreover, expansion further decreases with an increase in the amount of SCM dosage.

Expansion of greywacke mortar specimens in Figure 4-2 with 10% replacement of each SCM type allows direct comparison of the ability of each SCM to mitigate expansion of reactive greywacke aggregate. The ability of the SCMs to reduce ASR expansion is in the following order: SF>MK>FA>SL. As is expected, silica fume generates the lowest expansion and slag generates the most. Moreover, only the mortar with 10%SL exceeded 0.30% expansion at 21 days. Fly ash, metakaolin and silica fume at 10% replacement level are able to successfully reduce expansion to below 0.30% at 21 days.

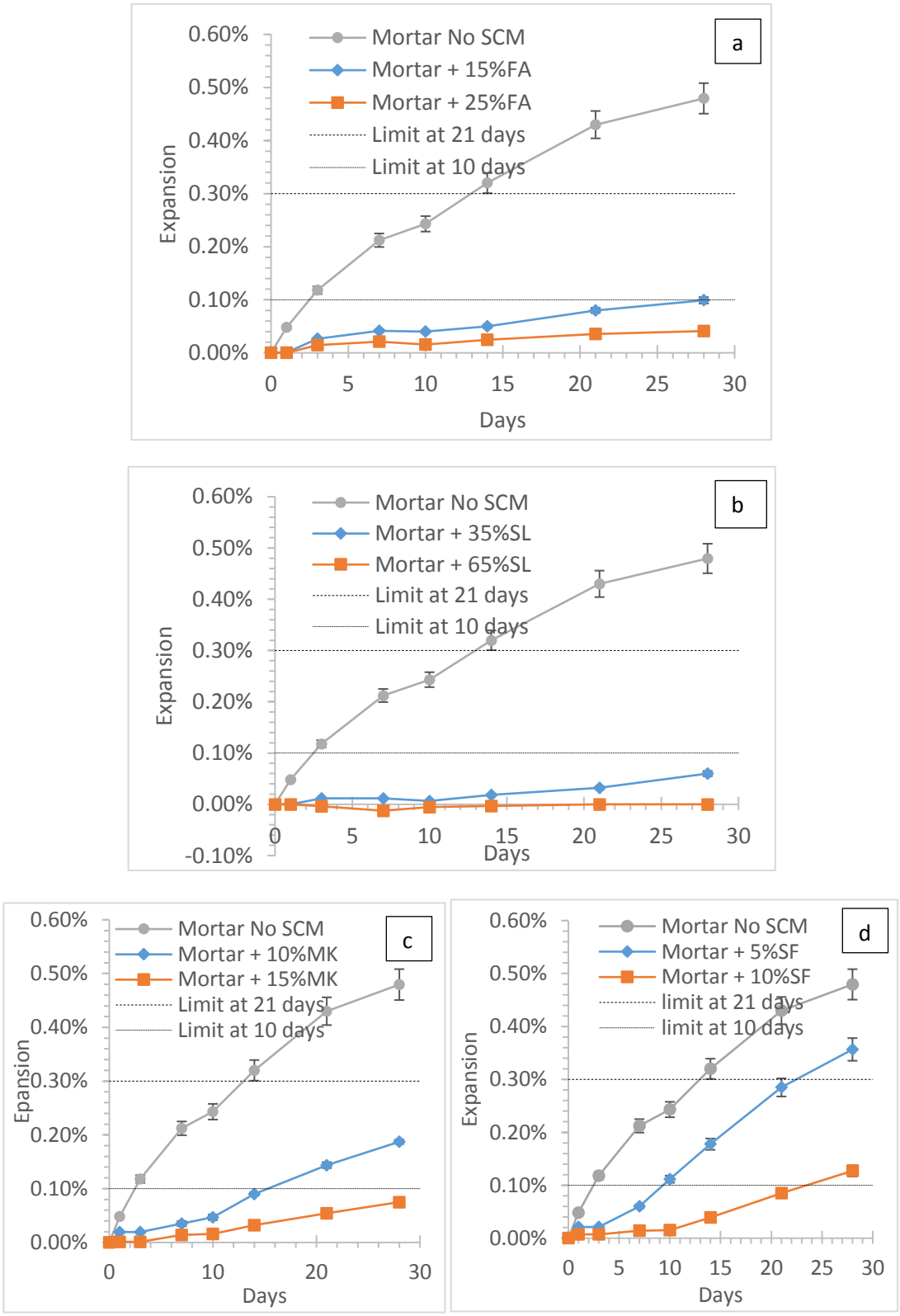

Figure 4-1 AMBT expansion of greywacke aggregate at recommended replacement levels: a) FA (15% and 25%), b) SL (35% and 65%), c) MK (10% and 15%) and d) SF (5% and 10%).

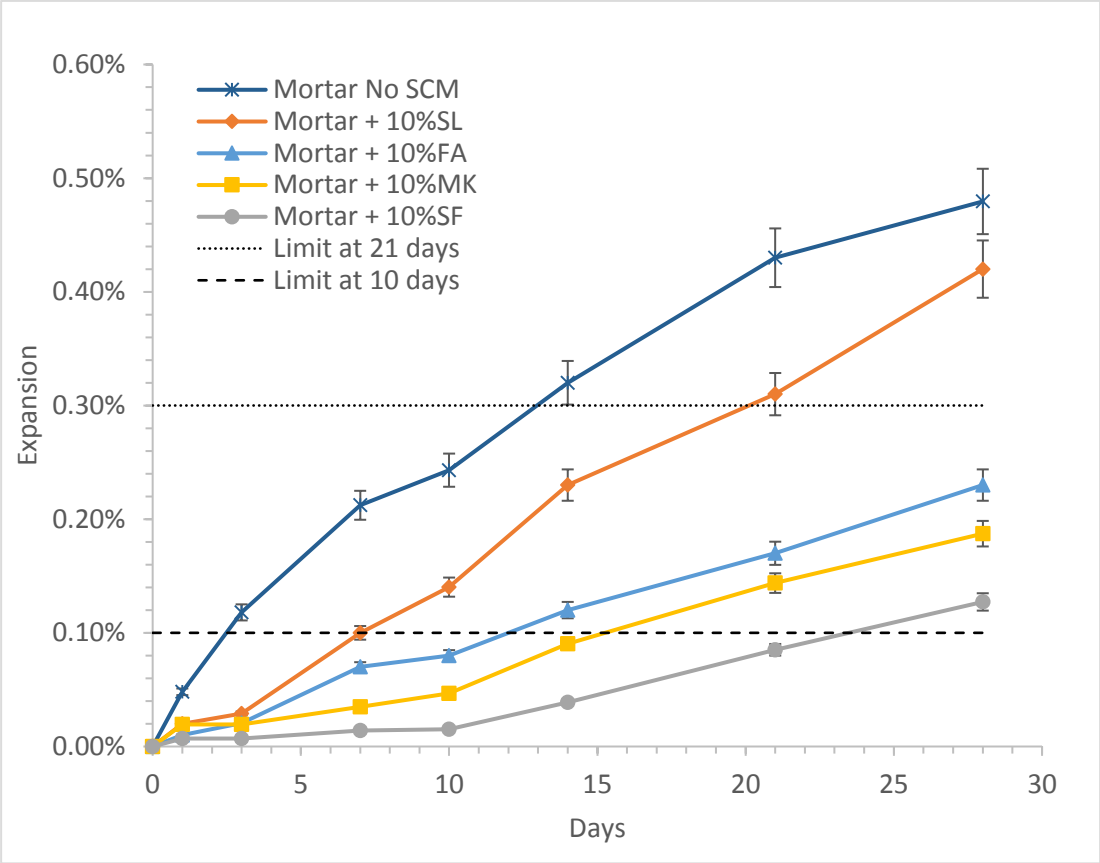

Figure 4-2 AMBT expansion of greywacke aggregate with 10% SCM replacement level.

Comparing Mortar+25%SL and Mortar+25%FA, and Mortar+15%FA and Mortar+15%MK in Figure 4-3 again shows that SL>FA and FA>MK. At 25% replacement level, still notable difference in the ability to reduce expansion can be observed for SL and FA. At 15% replacement level, MK is still more effective than FA, although the difference in expansion is minimal.

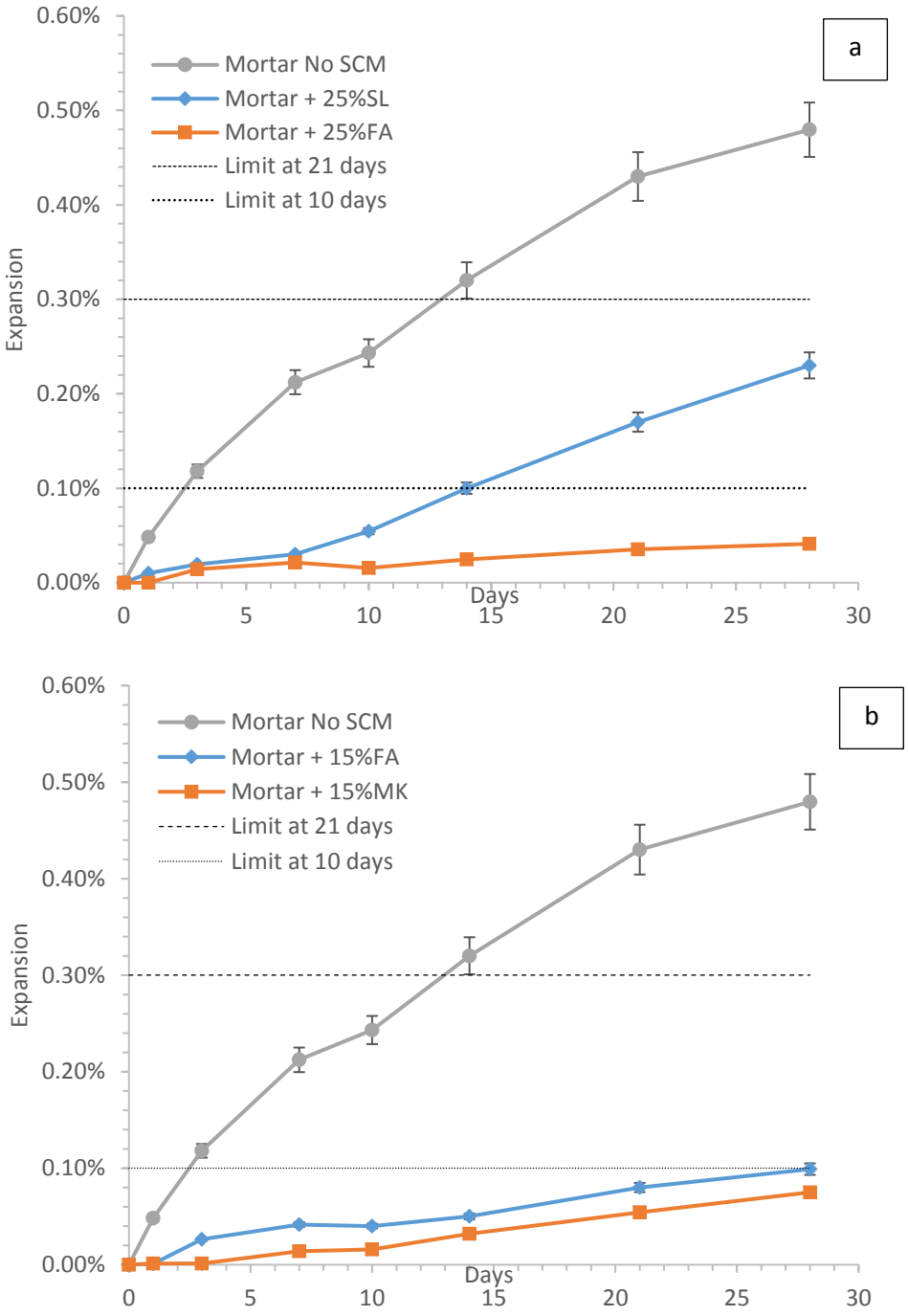

Figure 4-3 AMBT expansion of greywacke mortars showing effect of a) FA and SL at 25% replacement level and b) FA and MK at 15% replacement level.

Observed expansion is consistent with literature where silica fume is widely accepted as the best in reducing expansion due to ASR in terms of dosage requirement, closely followed by metakaolin, Class F fly ash, and then blast furnace slag (Boddy, Hooton & Thomas 2003; Durand et al. 1990; Thomas 2011). In Australia, SA HB 79:2015 provides recommended levels of SCM replacement to mitigate ASR as follows: SL at 65%, FA at 25%, MK at ≤ 15% and SF at 10% which is again consistent with the reactivity order of SCMs in ASR mitigation as observed in the AMBT expansion results: SF>MK>FA>SL.

4.2 Effect of SCM addition on mortar cracking and binder composition

The AMBT specimens were sectioned to compare the degree of cracking in mortars with and without SCMs. The effect of SCM addition on the binder phase is likewise reported. Figure 4-4 shows the SEM images of cross-sectioned greywacke mortar specimen without SCM addition post 28 days AMBT. Extensive cracking can be observed in the aggregates, which is consistent with the high degree of expansion during AMBT. The presence of ASR gel can also be clearly observed. The gel appears to originate inside the aggregate and extend towards the cement paste.

Figure 4-5 shows the low magnification SEM images of the cross-sectioned greywacke AMBT specimens with SCM additions at recommended replacement levels: mortar+65%SL, mortar+25%FA, mortar+15%MK and mortar+10%SF. All mortar specimens with SCMs show no major cracking in the aggregate or paste.

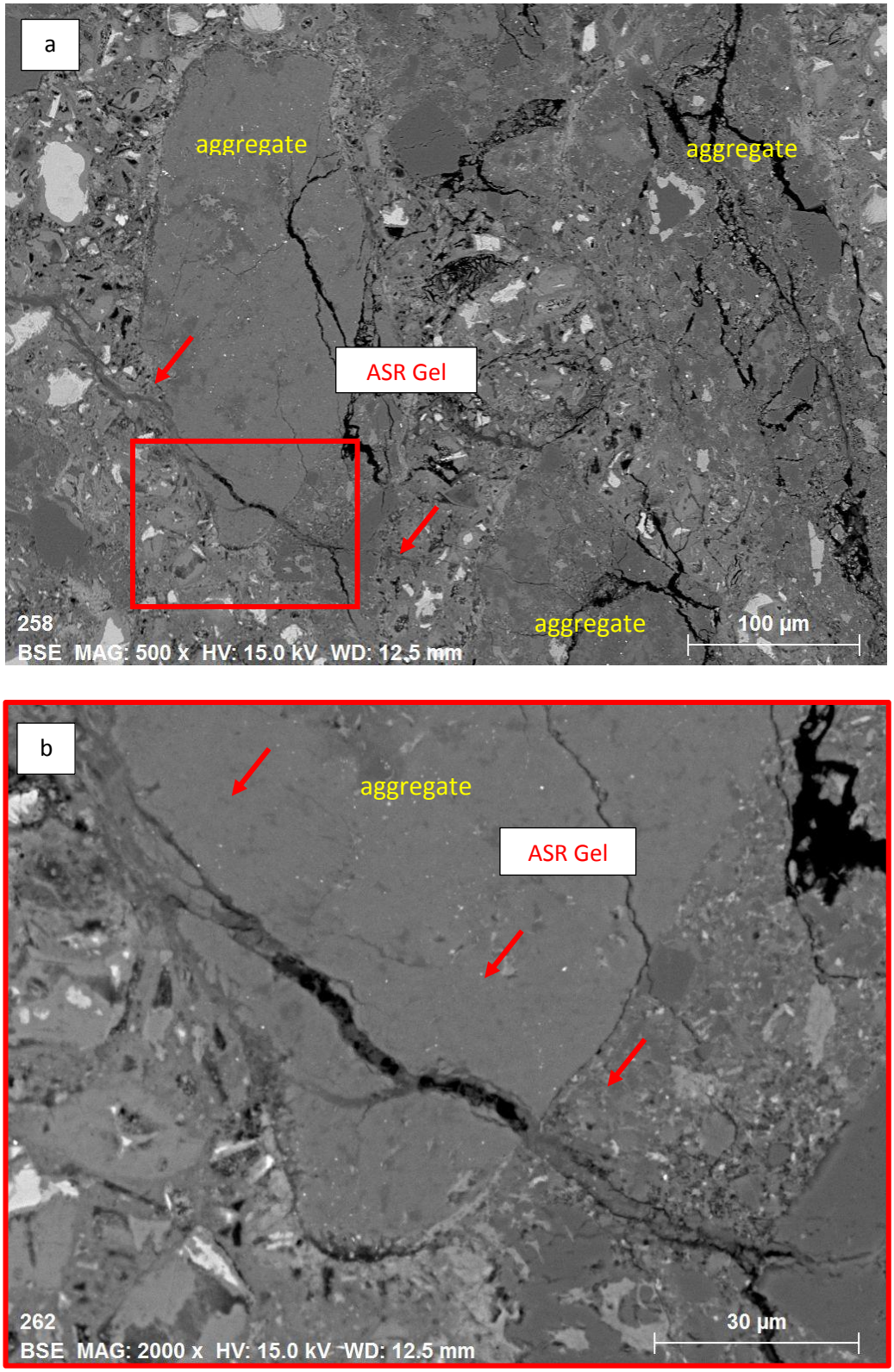

Figure 4-4 BSE SEM images of greywacke mortar without SCM showing the presence of ASR gel taken at a) 500x magnification and at higher magnification of b) 2000x

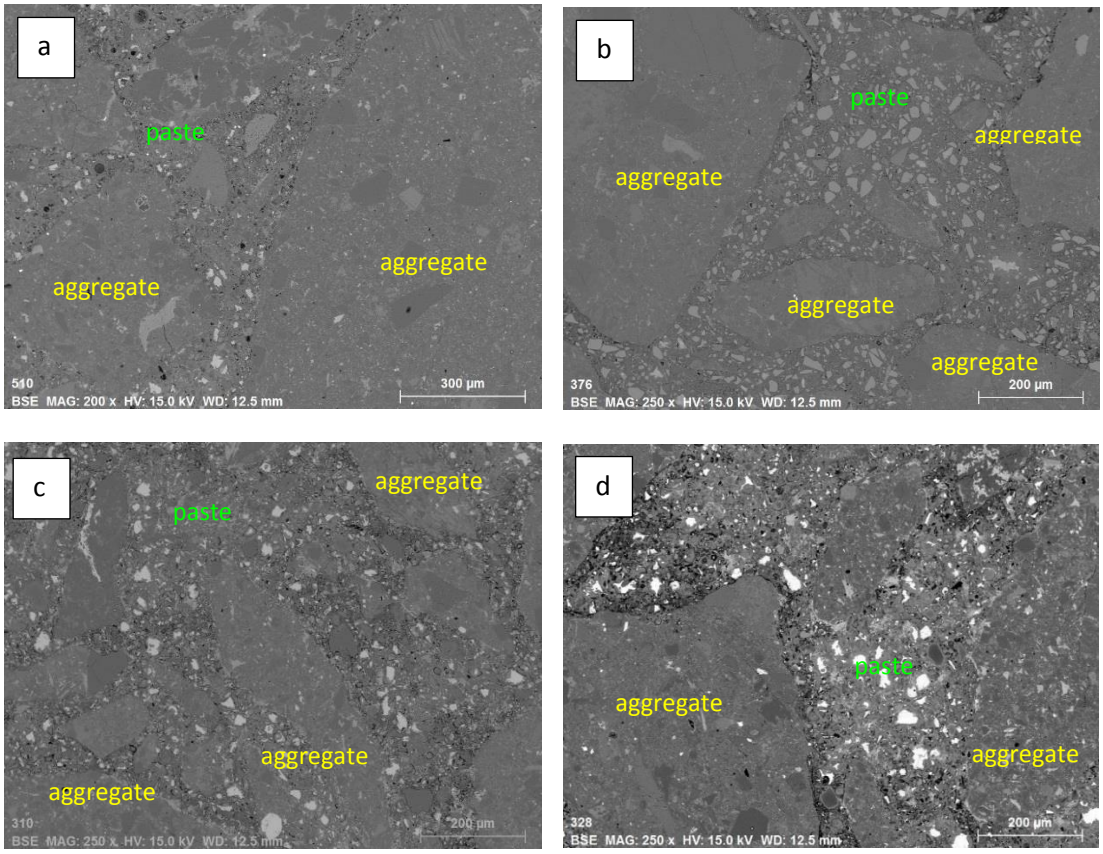

Figure 4-5 BSE SEM images of the mortars with a) 25%FA, b) 65%SL, c) 15%MK and d) 10%SF showing absence of ASR induced cracks

Figure 4-6 shows the higher magnification BSE SEM images of the sectioned mortars. Whereas the angular slag and spherical fly ash particles are still very visible, metakaolin and silica fume are hard to distinguish from the paste. This observation is likely due to higher reactivity and lesser amount of both MK and SF in the mortar (just 15% and 10% respectively compared to slag mortar which has 65% and fly ash 25%). For the same reason, very little amount of clinker can be observed in the mortar+65%SL due to high SCM replacement level (bright particles under BSE) compared to the other mortars.

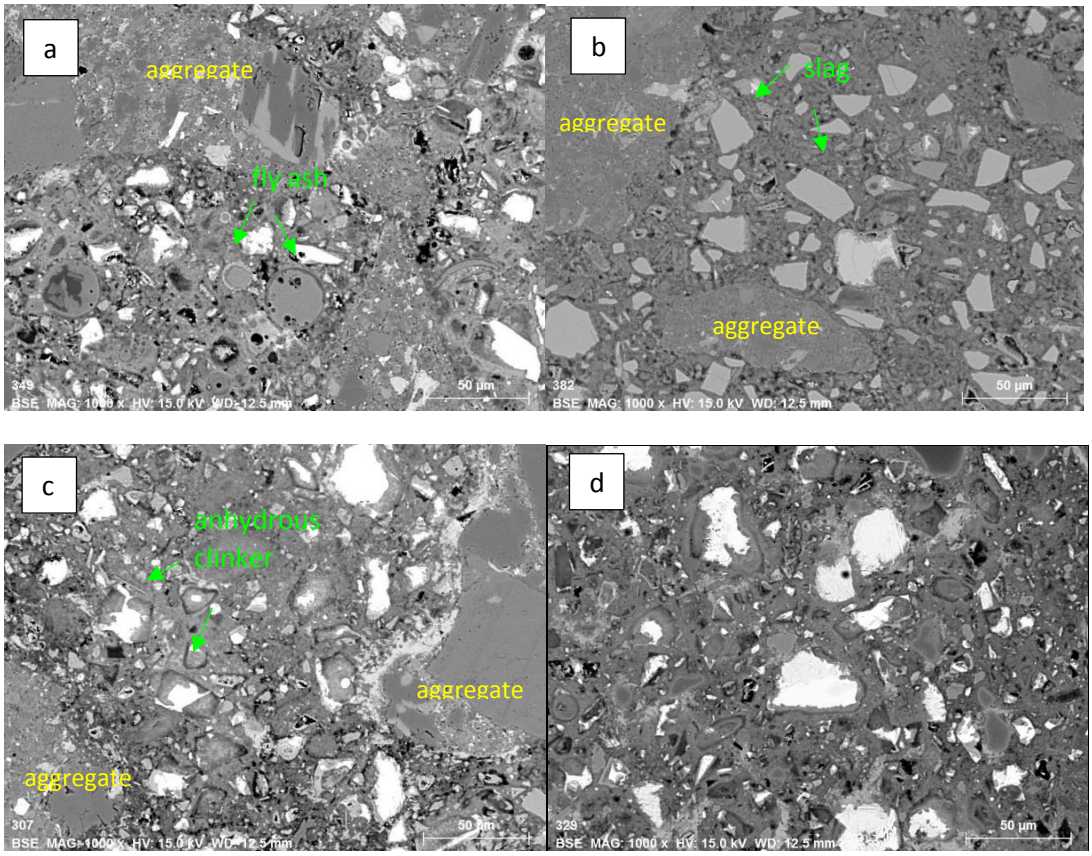

Figure 4-6 BSE SEM images of the mortars with a) 25%FA, b) 65%SL, c) 15%MK and d) 10%SF showing difference in binder composition

4.3 Effect of SCMs on C-S-H Composition

This section reports on the effect of SCMs on the Ca/Si ratio and Al/Si ratio of the C-S-H and correlates this to observed ASR expansion. The AMBT specimens with recommended replacement levels (25%FA, 65%SL, 15%MK and 10%SF) corresponding to AMBT specimens in Figure 4-1 and blended pastes with 25% SCM replacement levels also subjected to AMBT conditions were sectioned and subjected to EDS analysis to determine the effect of SCM type on C-S-H composition. The use of 25% replacement level is to be able to compare the effect of SCM at equivalent

amounts on C-S-H composition. Further, the use of blended paste is to eliminate any effect the finer aggregate particles may have on the C-S-H composition.

Figure 4-7 shows the C-S-H composition of the mortar specimens post-AMBT. Each scatter plot represents a minimum of 200 EDS points. The scatter plots show the effect of 25%FA, 65%SL, 15%MK and 10%SF on the Ca/Si and Al/Si ratio of the C-S-H. All mortars with SCM addition exhibit much higher Si/Ca (or lower Ca/Si ratio) and Al/Si ratio than mortar with no SCM. Since the formation of C-S-H is affected by the pore solution whose composition is determined by species available in the paste, when the pore solution changes, such as in the case of SCM blends, the composition of C-S-H is expected to change with respect to the dominant species in the pore solution (Rossen, Lothenbach & K.L.Scrivener 2015). Thus, the increase in Si/Ca and Al/Si ratio observed is due to the release of silicon and aluminium from SCMs into the pore solution.

The average C-S-H composition of the mortars with and without SCMs are summarized in Table 4-1. The mortar with no SCM addition has average Si/Ca ratio of 0.56, which is equivalent to Ca/Si ratio of 1.79. This C-S-H composition agrees with that reported by other studies (Chappex & Scrivener 2012a; Chappex & Scrivener 2012b; Gallucci, Zhang & Scrivener 2013). The Ca/Si in the plain cement was around 1.80-1.90 for both “inner” and “outer C-S-H” (Chappex & Scrivener 2012a). Moreover, it was reported that the Ca/Si ratio of around 1.8 remains the same regardless of age and curing temperature (Gallucci, Zhang & Scrivener 2013).

The mortars with SCMs exhibit average Si/Ca ratio from 0.62-0.66 or Ca/Si ratio of 1.51-1.61. The decrease in Ca/Si ratio of the C-S-H with SCM addition indicates that although the pore solution is dominated by calcium initially, it is enriched in silica from the SCMs over time (Chappex & Scrivener 2012a). Moreover, initially, the system has a lot of portlandite (source of soluble calcium) and therefore, Ca-rich C-S-H dominates. As the SCMs react to consume portlandite (and therefore less source of calcium available), Si-rich C-S-H forms (Rossen, Lothenbach & K.L.Scrivener 2015). Comparable Ca/Si ratio in the C-S-H suggests that at the recommended replacement levels, the SCMs are able to contribute almost equivalent amounts of silica to the pore solution and eventually into the C-S-H.

The obtained average Ca/Si ratio of mortars with SCMs also agrees with literature. Silica fume has C-S-H Si/Ca ratio of 0.66 or Ca/Si =1.50, consistent with another study which reported Ca/Si of the of about 1.40-1.50 for SF replacement levels of 10-45% (Rossen, Lothenbach & K.L.Scrivener 2015). Likewise, the obtained Si/Ca ratio of mortar+15%MK is 0.62, which is consistent with Si/Ca of 0.63 for 15%MK blended paste (Chappex & Scrivener 2012a). Ca/Si ratio of 1.58 (Si/Ca=0.63) was reported for blended pastes with 30% fly ash which also closely agrees with the current study (Girao et al. 2007).

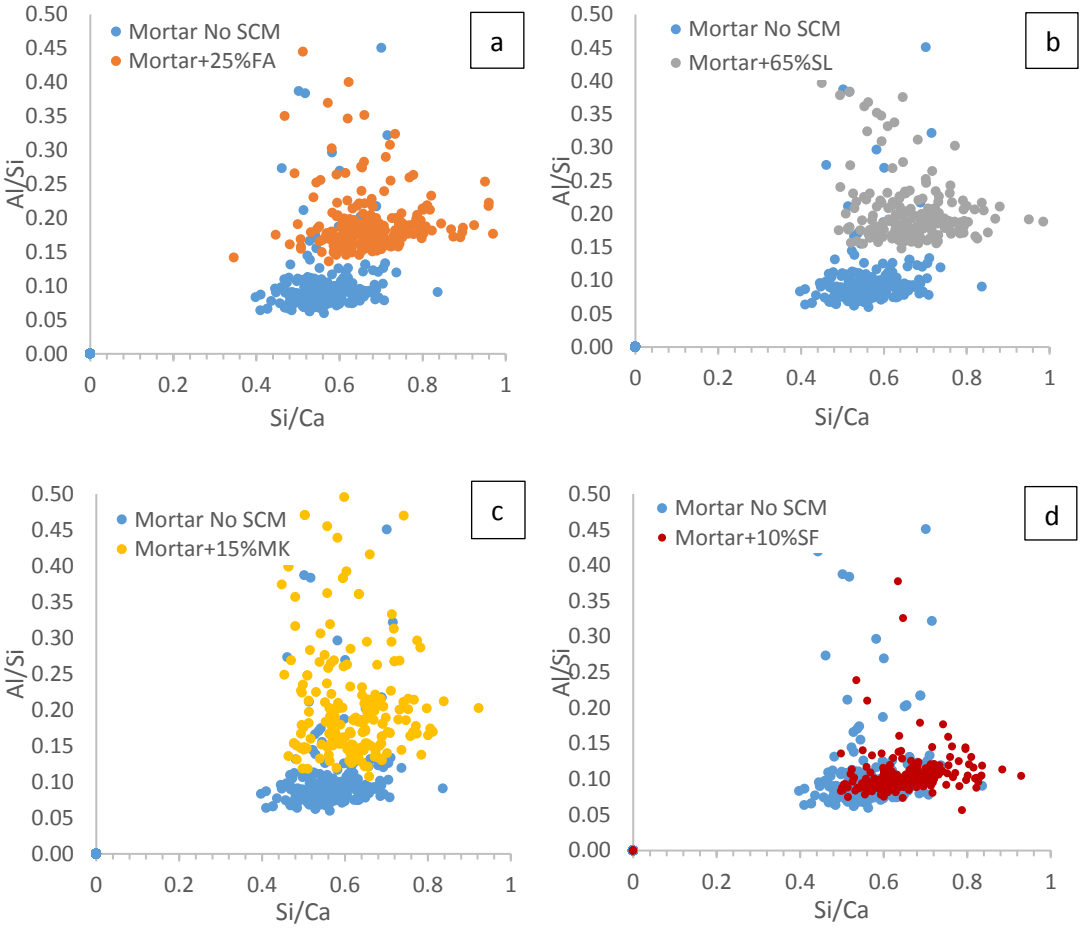

Figure 4-7 Effect of SCM addition at recommended replacement levels on C-S-H composition comparing a) mortar No SCM and Mortar+25%FA, b) mortar No SCM and mortar+65%SL, c) mortar No SCM and mortar+15%MK and d) mortar No SCM and mortar+10%SF.

Table 4-1 Average C-S-H composition of the mortar bars post-AMBT (atomic wt%)

Sample	Al/Si	Al/Ca	Si/Ca	Ca/(Si+Al)
Mortar No SCM	0.10 ± 0.03	0.05 ± 0.02	0.56 ± 0.06	1.65 ± 0.20
Mortar + 65%SL	0.21 ± 0.06	0.14 ± 0.04	0.66 ± 0.09	1.28 ± 0.17
Mortar + 25%FA	0.19 ± 0.05	0.13 ± 0.03	0.67 ± 0.10	1.27 ± 0.20
Mortar + 15%MK	0.20 ± 0.07	0.12 ± 0.04	0.62 ± 0.09	1.37 ± 0.20
Mortar + 10%SF	0.11 ± 0.03	0.07 ± 0.02	0.66 ± 0.08	1.40 ± 0.18

Calcium silicate hydrate (C-S-H) with much lower Ca/Si ratio results in higher alkali binding capacity (Thomas 2011). The capacity to bind more alkalis is due to the

increase in the amount of acidic silanol (Si-OH) sites in the C-S-H layers that are negatively charged (Duchesne & Berube 1994b; Hong & Glasser 1999). Hence, they attract alkali cations Na^+ and K^+ in the pore solution. The sorption of alkalis increases as the volume of the silanol sites increases. Both the number and acidity of the sites increase as the Ca/Si ratio of C-S-H decrease (Hong & Glasser 2002).

The mortars with 65%SL, 25%FA and 15%MK showed significant increase in Al/Si (0.19-0.21) in comparison to the mortar without SCM addition (0.10) and mortar with 10%SF (0.11). The mortars with 65%SL, 25%FA and 15%MK have comparable Al/Si ratio. This result is consistent with literature where adding aluminium-containing SCMs has increased the Al/Si of the C-S-H (Deschner et al. 2013; Taylor, Richardson & Brydson 2010). The increase in Al/Si ratio suggests aluminium uptake in the C-S-H (i.e. formation of C-A-S-H) which enhances its alkali binding capacity. When Al^{3+} substitutes for Si^{4+} in the C-S-H, the net charge is negative, and therefore alkali cation (Na^+ or K^+) is bound in order to charge balance effectively reducing the alkali concentration in the pore solution (Skibsted & Andersen 2013).

To be able to directly compare the effect of SCMs on C-S-H composition without the influence of aggregate, blended pastes with 25% SCM replacement were subjected to AMBT conditions, sectioned and analysed for C-S-H composition. The result of which is shown in Figure 4-8. Again, SCM addition increases the Si/Ca ratio of the C-S-H (i.e. lowers Ca/Si ratio). Although, in the case of slag, at this replacement level, this effect is very minimal. The role of Si in the effectivity of the SCM in ASR mitigation is again clearly illustrated in this case. At 25% replacement level, the silica fume has the greatest ability to increase Si/Ca ratio of the C-S-H while SL has the least which

supports the lower replacement required for SF to mitigate ASR in comparison to SL. Al/Si ratio also increases in all systems with MK, FA and SL. The greatest increase in Al/Si ratio is observed with OPC+25%MK. The Al/Si of the blended paste with 25%SF is almost similar to that of reference OPC. Table 4-2 lists the average C-S-H composition of the blended pastes with 25% SCM replacement.

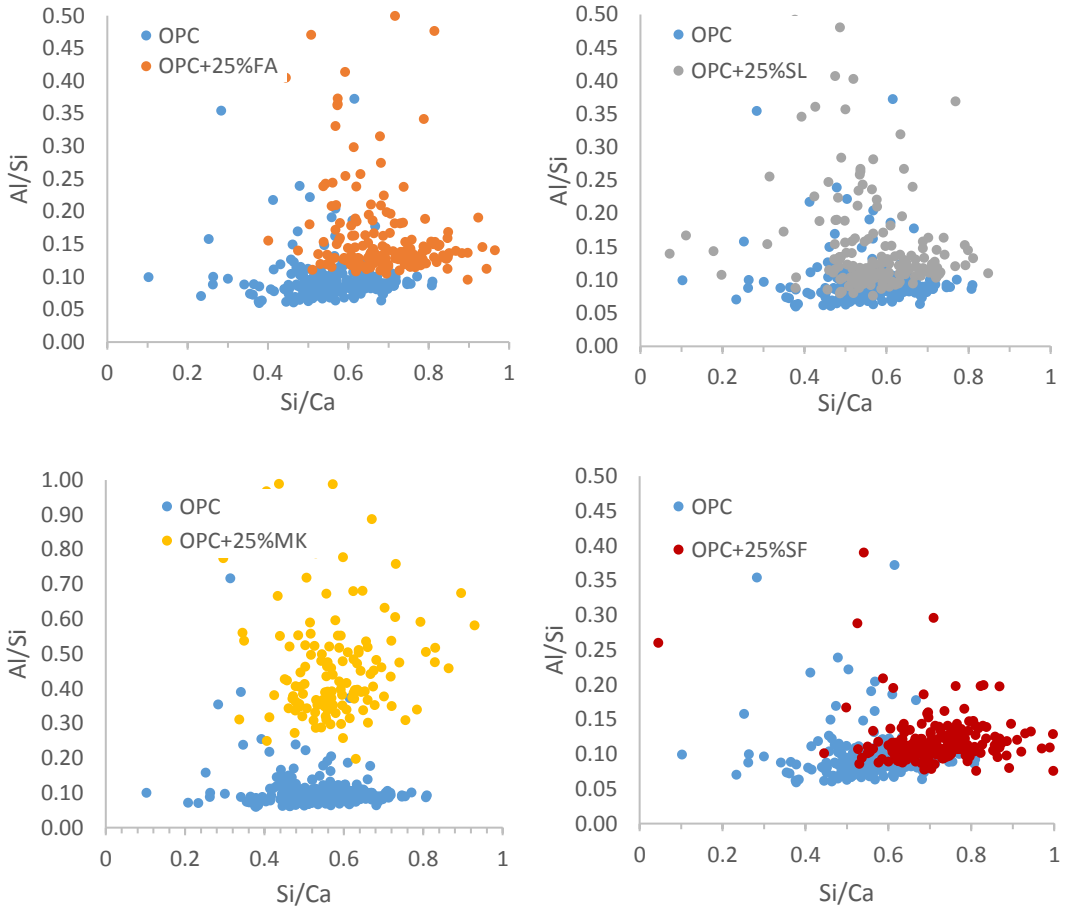

Figure 4-8 Effect of SCM addition at equivalent replacement levels of 25% on C-S-H composition

Table 4-2 Average C-S-H composition of the blended pastes post-AMBT conditions (atomic wt%)

Sample	Al/Si	Al/Ca	Si/Ca	Ca/(Si+Al)
OPC	0.09 ± 0.02	0.05 ± 0.01	0.58 ± 0.08	1.61 ± 0.22
OPC+25%SL	0.12 ± 0.04	0.07 ±0.02	0.58 ± 0.08	1.57 ± 0.22
OPC+25%FA	0.14 ± 0.03	0.10 ± 0.02	0.68 ± 0.10	1.32 ± 0.25
OPC+25%MK	0.43 ± 0.10	0.25 + 0.09	0.62 ± 0.11	1.24 ± 0.26
OPC+25%SF	0.11 ± 0.01	0.08 ± 0.02	0.72 ± 0.10	1.27 ± 0.17

4.4 Effect of SCM Type on the Availability of Alkalis

High alkalinity in the pore solution is a requirement for the dissolution of siliceous phases of the aggregates to occur (ASR begins by hydroxyl ions attacking the silicate structure). Thus, reduced pore solution alkalinity inhibits ASR (Rajabipour et al. 2015). Due to the significant role of alkalis in ASR, mitigation strategies typically involve lowering the alkali content in the concrete.

This section assesses the ability of SCMs (FA, SL, MK and SF) to bind alkalis and how these correspond to their ability to reduce expansion. In particular, this section aims to characterize the pozzolanic behaviour of the SCMs (in terms of portlandite consumption) and correlate with their ability to bind alkalis (Na and K) and reduce pH of the pore solution. Blended pastes were used in order to better illustrate the effect of SCMs without intervention from aggregates which studies report to also both adsorb

and release alkali (Berube et al. 2002; Constantiner & Diamond 2003; Thaulow, Jakobsen & Clark 1996).

4.4.1 Pozzolanic Behaviour of SCMs

The degree by which SCMs consume portlandite (CH) is known as pozzolanicity. Thermal analysis is a common tool to assess pozzolanicity of the SCMs (Scrivener, Snellings & Lothenbach 2016). The higher the CH consumption, the more pozzolanic the SCM. Thermal analysis can be used to estimate the amount of CH in the cement pastes based on mass loss in the range of CH decomposition at about 400-500 °C which corresponds to the dehydroxylation of calcium hydroxide as shown in Equation 4-1. The area under the curve at about 400-500 °C indicates the amount of CH remaining, and thus, larger area means more CH.

Equation 4-1 $Ca(OH)_{2(s)} \rightarrow CaO_{(s)} + H_2O_{(l)}$

Cement pastes with 25% SCM replacement level (fly ash, slag, metakaolin and silica fume) were immersed in 1M NaOH and 80 °C for 28 days and after which subjected to TG measurements. 25% SCM addition was chosen as it is the standard dosage of fly ash for mitigating ASR which is still the most utilized SCM for ASR mitigation in Australia (Standards Australia 2015). Moreover, the use of equivalent replacement levels is to be able to directly compare the pozzolanic behaviour of the SCMs.

TG plots of pastes exposed to 80 °C storage conditions shown as derivative of the weight loss with respect to temperature in Figure 4-9 showed reduced portlandite amount in all pastes with SCMs. The reduction in the amount of CH is a combination of cement "dilution" and pozzolanic reactions occurring in the binder system. The observed order of portlandite consumption is as follows: OPC+25%SF > OPC+25%MK > OPC+25%FA > OPC+25%SL, with silica fume being the top consumer of portlandite, and slag being the least.

The order of portlandite consumption in this study agrees well other studies that employed accelerated tests to assess pozzolanicity of SCMs (Snellings & Scrivener 2016; Suraneni & Weiss 2017). Measured reaction of various SCMs with CH in a 0.5M KOH solution at 50 °C after 240 hours showed order of portlandite consumption as follows: silica fume > calcined clay > fly ash > quartz > slag > limestone (Suraneni & Weiss 2017). Chapelle test where 1 g of SCM and 1 g of CH are reacted in a volume of 200 mL distilled water and heated to boiling temperature under continuous stirring showed SCM reactivity by portlandite consumption as follows: metakaolin > fly ash > slag (Snellings & Scrivener 2016).

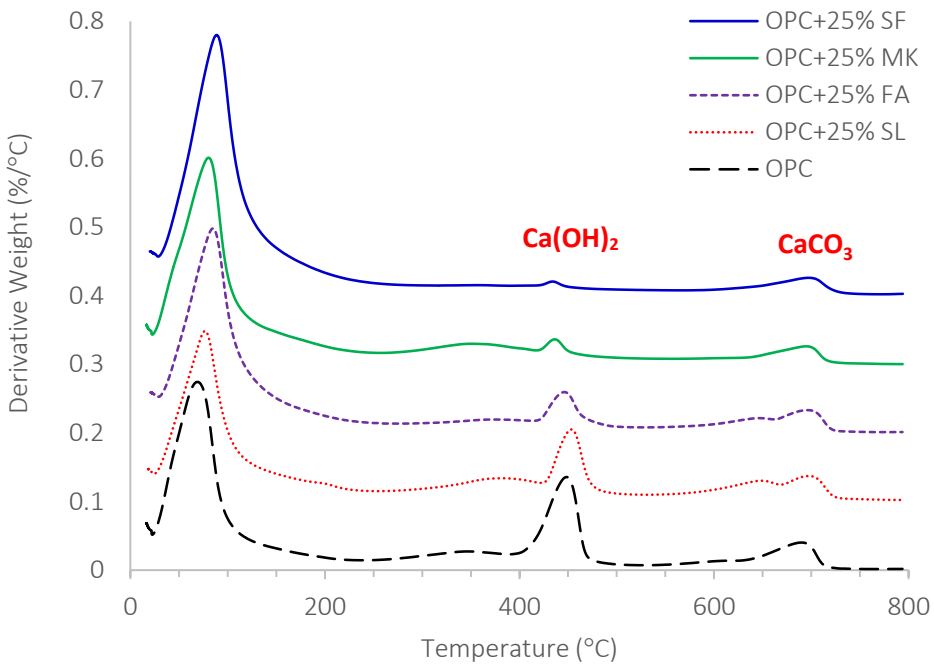

Figure 4-9 DTG plot of the hydrated cement-SCM pastes obtained after 28 days immersion in 1M NaOH 80 °C

The bar chart in Figure 4-10 shows the amount of portlandite in the blended pastes as a function of age. As the weight loss during $Ca(OH)_2$ decomposition results from loss of water, $WL_{Ca(OH)_2}$, Equation 4-2 can be used to calculate the remaining portlandite where $m_{Ca(OH)_2}$ and m_{H_2O} correspond to the molecular masses of portlandite (CH) and water respectively.

Equation 4-2 $$Ca(OH)_{2,measured} = WL_{Ca(OH)_2} x \frac{m_{Ca(OH)_2}}{m_{H_2O}} = WL_{Ca(OH)_2} x \frac{74}{18}$$

With the exception of cement and slag, portlandite was found to decrease with time on all binder systems as a function of time. Slag, having a composition close to that of Portland cement, is a latent hydraulic material and thus, capable of hydration producing portlandite in the process. The fact, however that portlandite in

OPC+25%SL is much lower than that of pure cement even after considering dilution effect confirms that slag is also consuming portlandite. Similar literatures also report portlandite consumption by slag (Escalante et al. 2001; Kolani et al. 2012; Pane & Hansen 2005; Saeki & Monteiro 2005).

Portlandite is consumed by slag hydration itself. Slag usually requires external supply of calcium during hydration to form C-S-H. The calcium demand by the slag-blended cements is supplied by the CaO of anhydrous slag particles completed by a part of the CH produced by cement hydration. To form their C-S-H, slag in blended cements can get calcium from the dissolution of CH or from the remaining calcium in the unhydrated slag (Kolani et al. 2012). Increase in the portlandite amount in OPC+25%SL after 28 days, suggests that slag "hydration" occurs faster than consumption of portlandite.

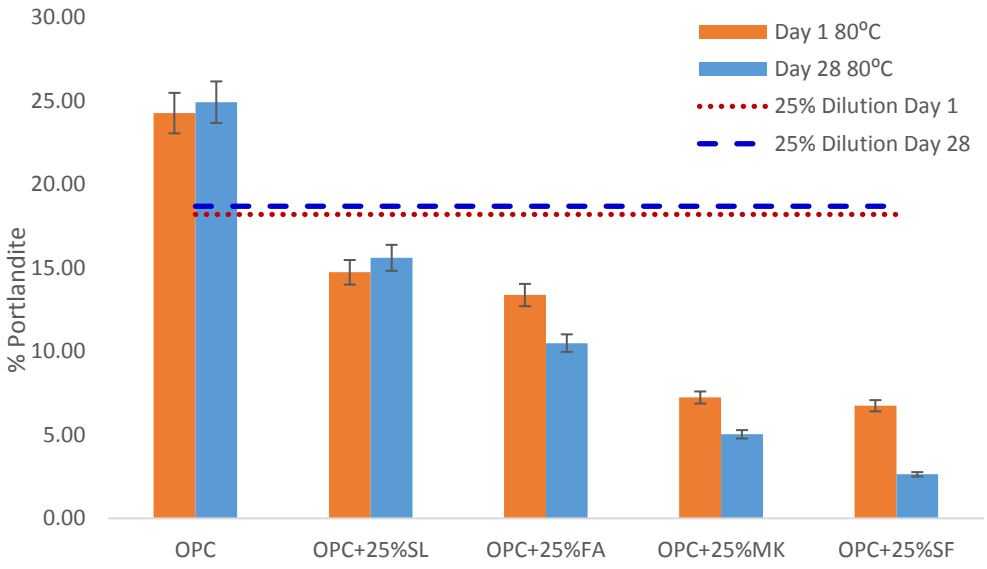

Figure 4-10 Amount of portlandite in the SCM-blended pastes after 1 day and 28 days immersion in 1M NaOH 80 °C

The portlandite amount remaining in the SCM blended pastes after immersion in 1M NaOH 80 °C for 28 days, plotted as a function of SCM amount in Figure 4-11 shows that the amount of portlandite decreases as the amount of SCM replacement increases (from 10% to 50%). The higher the SCM content, the lower the portlandite content (Duchesne & Berube 1994b). In fact, at 50% silica fume replacement, no more portlandite can be detected in the blended pastes after 28 days.

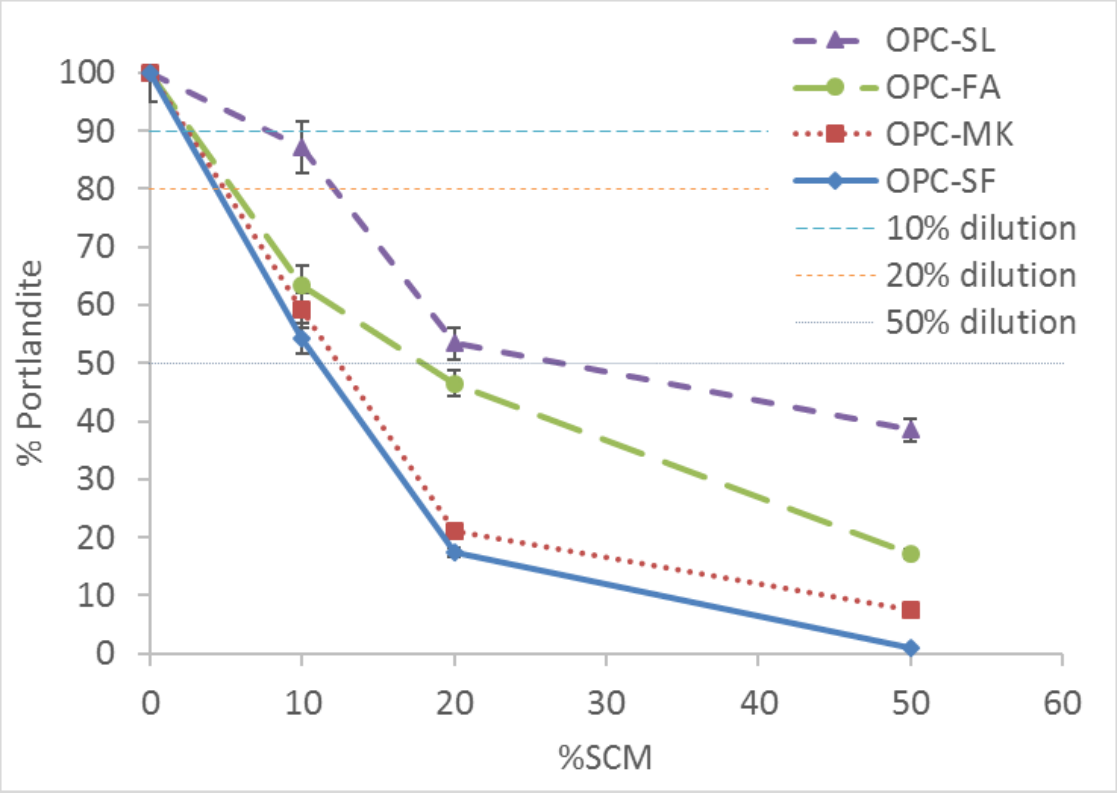

Figure 4-11 Amount of portlandite in SCM-blended pastes after 28 days immersion in 1M NaOH 80 °C

SCMs rich in soluble silica such as FA, MK and SF are pozzolanic and higher pozzolanic activity results in the formation of more hydrates with lower Ca/Si ratio that has higher alkali binding capacity (Duchesne & Berube 1994b; Hong & Glasser 1999, 2002). Lower availability of portlandite also lowers the source of soluble

calcium which is an essential constituent in the formation of ASR reaction products (Chatterji 2005; Leemann et al. 2016). With abundant alkali hydroxides and reactive silica, but no calcium, silica dissolves and remains in solution (Leemann et al. 2016; Leemann & Lura 2013; Rajabipour et al. 2015). Calcium in the pore solution also increases Ca/Si ratio thereby resulting in much lower alkali binding capacity. Higher Ca/Si results in less negatively charged silanol sites in the C-S-H that are able to bind alkali. Moreover, calcium also competes with alkali adsorption in the C-S-H. As Ca^{2+} is preferably bound than alkali Na^{+} and K^{+} in the negatively charged C-S-H, more calcium in the pore solution will decrease the amount of bound alkali in the C-S-H (L'Hôpital et al. 2016).

4.4.2 Effect of SCM Type on Pore Solution Alkalinity

Adding SCMs in concrete mixes leads to a reduction in the concentration of alkali-hydroxides in the pore solution (NaOH and KOH) (Thomas 2011). The amount of alkali metal cations sodium (Na^{+}) and potassium (K^{+}) in the pore solution is generally used as a measure of alkali concentration. Likewise, pH is also a good indicator of acidity or basicity of the solution. This section compares the ability of SCMs to reduce pore solution alkali concentration.

In order to generate a comparable assessment of the SCMs in terms of reducing alkali concentration of the pore solution, blended pastes containing 25% of each SCM type were prepared and stored in sealed containers at 98% RH 20±2 °C until the specified time for pore solution extraction (28 days and 168 days). Similar to the assessment of

pozzolanic behaviour and effect on C-S-H composition, the use of 25% replacement levels for all SCMs is to generate a better comparison of their efficacy in removing alkalis in solution. 25% is chosen with it being the standard replacement level for fly ash in ASR mitigation (Standards Australia 2015). Two types of cements were used. Low alkali cement which has 0.6% Na_2O_{eq} and high alkali cement which has 1% Na_2O_{eq}. The use of 20±2 °C (normal temperature conditions) instead of higher temperatures employed in accelerated tests is to ensure that enough solution will be available in the paste during extraction (i.e. to not dry out the solution). At these conditions, only ~5 ml was extracted at 28 days and even much less at 168 days. Sufficient solution is required both for pH measurements and ICP-OES analysis.

Extracted solutions of blended pastes (for low alkali and high alkali cement) at 28 days with equivalent SCM replacement level (25%) in Figure 4-12 shows much lower alkali concentration in all pastes with SCMs as expected. The reduction of total alkali (Na and K) as a function of SCM regardless of the type of cement occurs in the following order: OPC+25%SF> OPC+25%MK> OPC+25%FA> OPC+25%SL. Since 25% SCM replacement does not have an identical effect on the pore solution alkali concentration, this indicates that the effect of SCM addition is more than just cement dilution. Silica fume consumes the most alkali with very little remaining after 28 days. Also, it is notable that K is present in greater concentrations in the pore solution suggesting that Na is more bound in the hydrates.

The trend observed is consistent with other studies where fly ash reduces more alkali than slag (Canham, Page & Nixon 1987) and with silica fume with greater ability to reduce alkali than metakaolin (Chappex & Scrivener 2012a). It was reported that the

addition of 15% silica fume is able to reduce as much as 80% of total alkali in the pore solution (Durand et al. 1990) while increasing the dosage to up to 20% silica fume removed almost all the alkali ions in solution (Rasheeduzzafar & Hussain 1991).

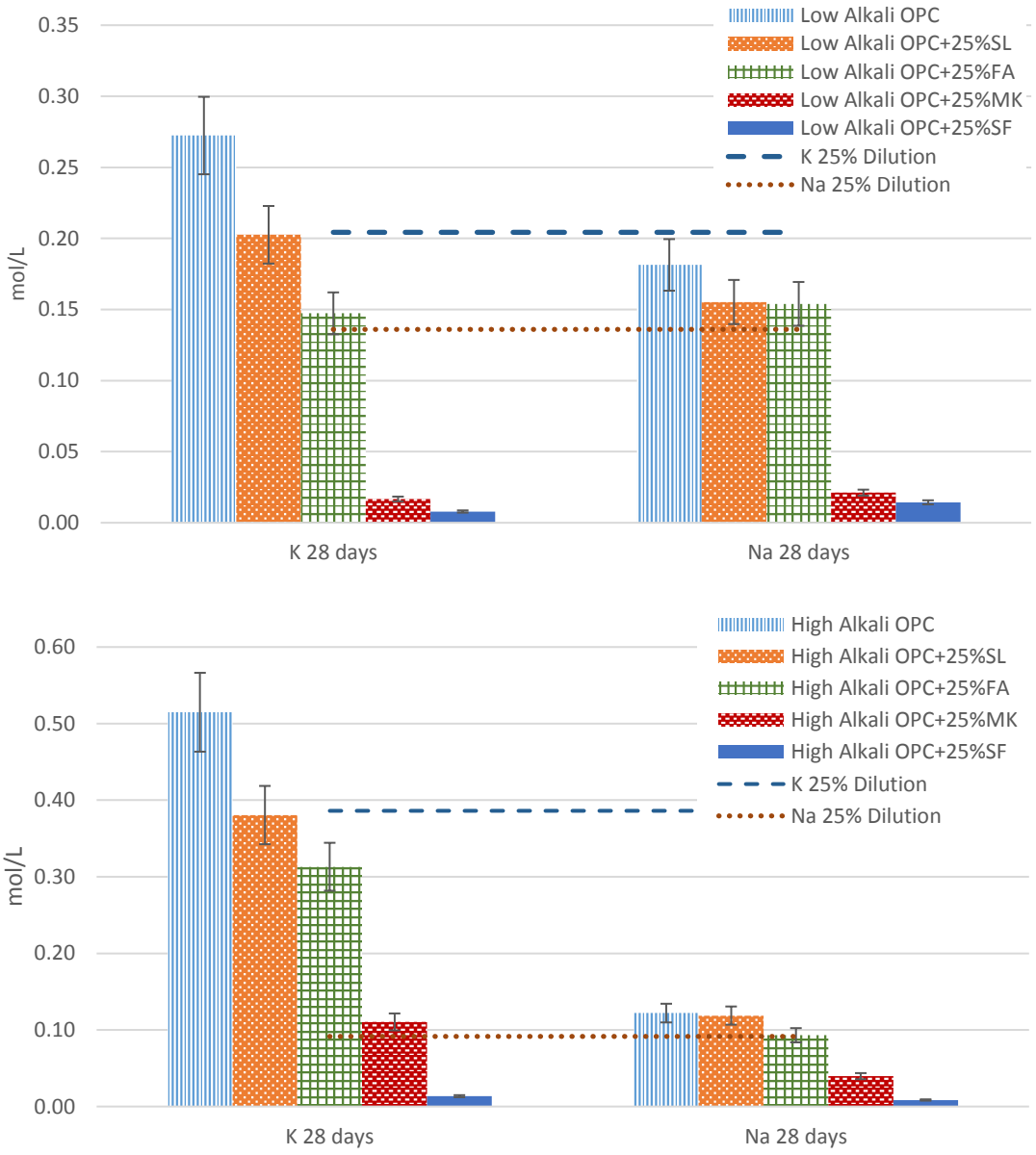

Figure 4-12 Effect of the type of SCM on pore solution for 2 types of cements after 28 days hydration

A similar trend was also observed for pore solutions extracted after 168 days (6 months) as shown in Figure 4-13. The K+Na of the reference OPC is between 0.45 to 0.50 mol/L (28 days to 168 days). OPC+25%SF lowers the alkali and hydroxide concentrations in the pore solution significantly with 95% reduction in total alkalis (Na+K) after 28 days and up to 97% after 168 days as shown in Table 4-3.

The strong pozzolanic reaction associated with higher amount of reactive silica in SF increases the amount of C-S-H formed with lower Ca/ Si ratio that are able to take up more alkalis. It has been reported that at very high SF replacement levels, portlandite is completely consumed, low Ca/Si C-S-H is present and more alkalis are bound (Vollpracht et al. 2016). Moreover, from Table 4-3, further decrease in alkali concentration with time is clearly observed. This indicates that the process of alkali binding is continuous with time as the SCM reacts in the paste.

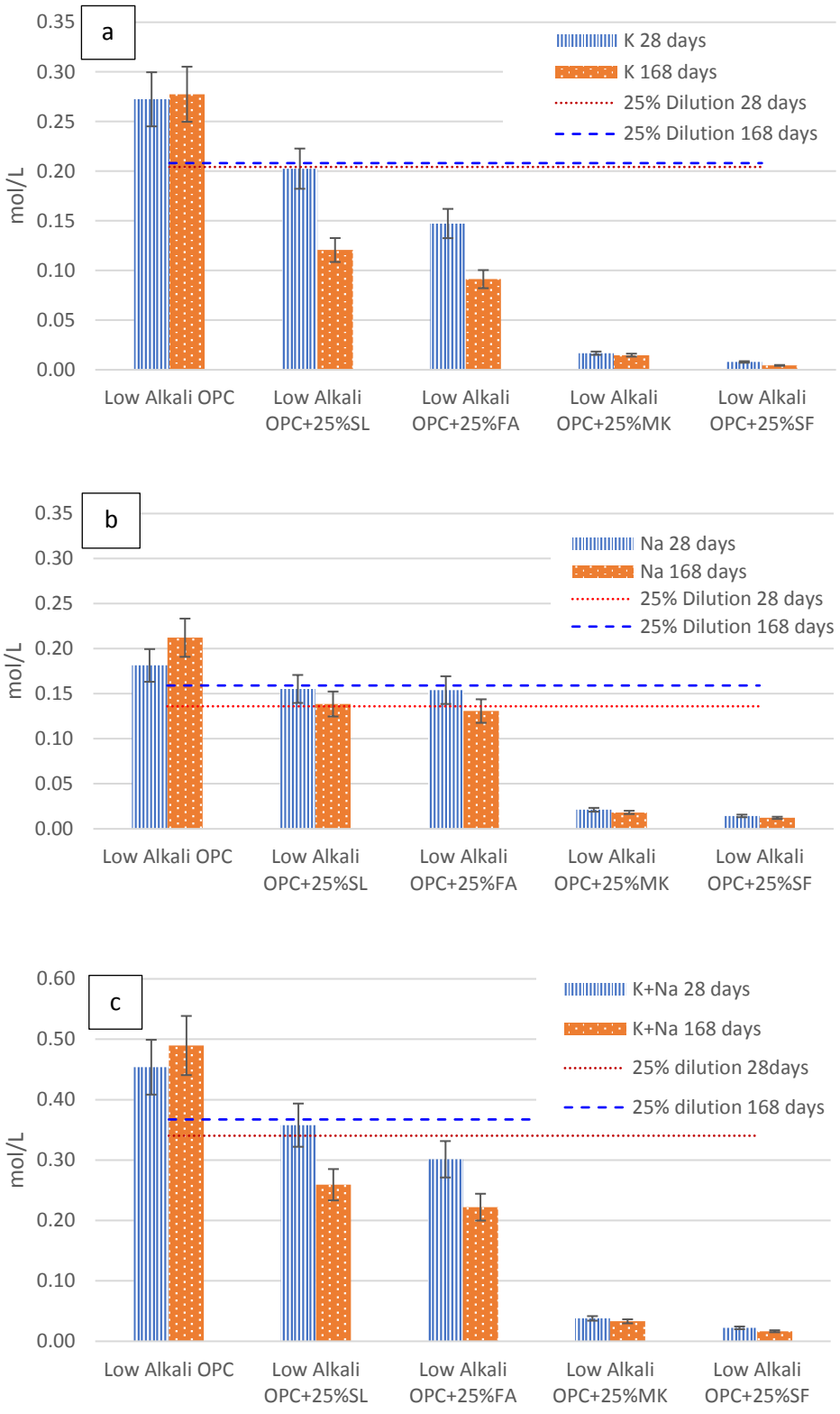

Figure 4-13 Effect of SCM Type on the concentration of alkalis in the pore solution at 28 days (1 month) and 168 days (6 months) a) potassium (K) b) sodium (Na) and c) total alkali concentration (K+Na)

Table 4-3 Alkali (Na+K) remaining in blended pastes at 25% SCM replacement

Blended Pastes	K+Na 28 days	K+Na 168 days
Low Alkali OPC+25%SL	78.9% ± 7.9%	52.9% ± 5.3%
Low Alkali OPC+25%FA	66.4% ± 6.6%	45.3% ± 4.5%
Low Alkali OPC+25%MK	8.4% ± 0.1%	6.7% ± 0.1%
Low Alkali OPC+25%SF	4.9% ± 0.1%	3.4% ± 0.1%

Likewise, a similar trend was observed in the pH of the pore solutions obtained at 28 days and 168 days. The pH of the solutions was measured for 2 minutes each to give the solution sufficient time to stabilize and to allow direct comparison of values. Figure 4-14 shows that pH decreases as a function of time (i.e. lower pH at 168 days compared to 28 days) consistent with increasing percentage of SCM reacted in the system. The decrease of pH with time is related to the increase in the amount of reacted SCM. More SCM reacted, produces more C-S-H with lower Ca/Si ratio, resulting in more bound alkalis (Vollpracht et al. 2016). Moreover, for both 28 days and 168 days, consistent trend of decreasing pH was observed as follows: OPC only> OPC+25% SL > OPC+25%FA > OPC+25%MK > OPC+25%SF. Slag is consistently the most basic and silica fume the least.

The effect of SCM type on the concentration of alkalis and pH correlates with pozzolanic behaviour as well as the recommended replacement levels for effective ASR mitigation. The higher the pozzolanicity, the higher the ability to reduce pore solution alkalinity, the lower the dosage requirement for effective ASR mitigation. High calcium fly ash and slag are the least effective SCMs for lowering pore solution alkalinity while silica fume and metakaolin are the most effective (Thomas 2011).

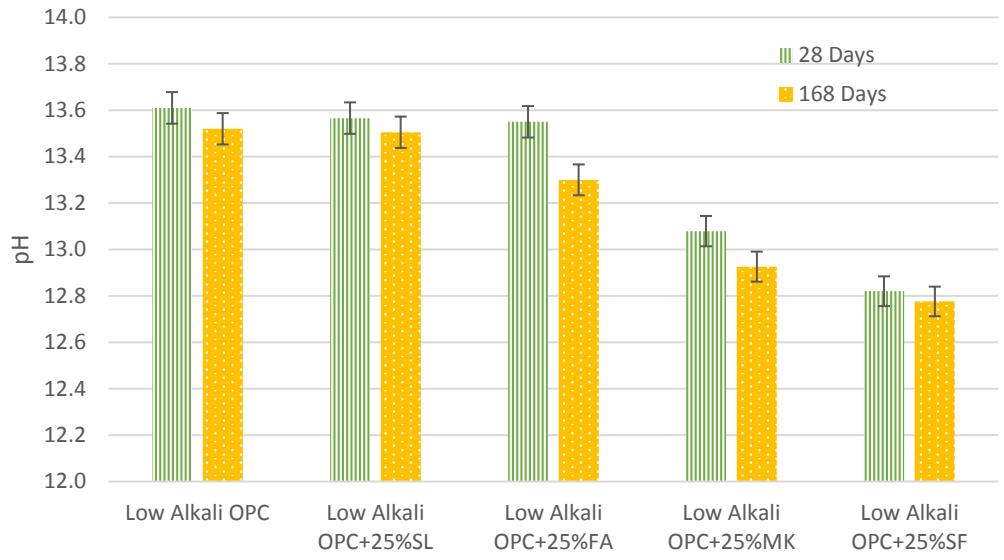

Figure 4-14 pH Measurements of the pore solutions at 28 days (1 month) and 168 days (6 months)

The C-S-H structure is composed of alternating layers of calcium oxide and silicate tetrahedral. Alkalis are bound into C-S-H mainly at acidic silanol sites, Si–OH, which increases as the Ca/Si ratio of the C-S-H decreases (Hong & Glasser 2002). Presence of SCMs lowers Ca/Si ratio, and the more reactive silica available from the SCM, the lower the Ca/Si ratio of the C-S-H. Hence, silica fume which is almost entirely amorphous silica, generates the lowest Ca/Si ratio and therefore able to bind the most alkali. This effect was found to be consistent regardless of initial alkali content of cement (low alkali and high alkali).

The observed effect of SCM type on the pH of the pore solution is consistent even for high alkali cements. Figure 4-15 shows a comparison of pH measurements for low alkali and high alkali cement at 28 days. The high alkali cement has higher pH than the low alkali cement for all blended pastes but essentially exhibits the same trend for

efficacy of SCMs in lowering pH: OPC+25%SF > OPC+25%MK > OPC+25%FA > OPC+25%SL.

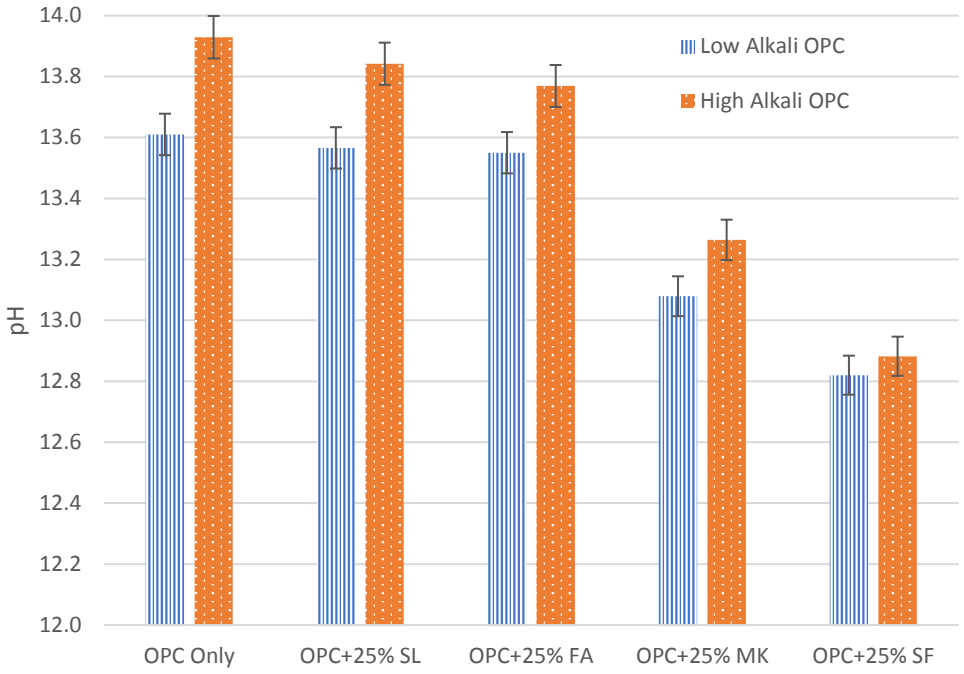

Figure 4-15 pH measurements comparison for low alkali cements and high alkali cement at 28 days

The effect of SCM addition on pore solution alkali concentration of blended pastes was also evaluated using recommended replacement levels of SCMs (25%FA, 50%SL, 15%MK and 10%SF) to determine how much percentage of alkalis are consumed at standard SCM additions. At this replacement levels, Figure 4-16 shows that 10%SF has the greatest efficacy to remove alkali in the pore solution. Table 4-4 shows that 10%SF removes 86% of Na+K in just 28 days. 10%SF is followed by 15%MK, 50%SL and 25%FA in efficacy to remove alkalis. 15%MK removing 67% total alkalis Na+K, 50%SL removing 48% and 25%FA removing 34%.

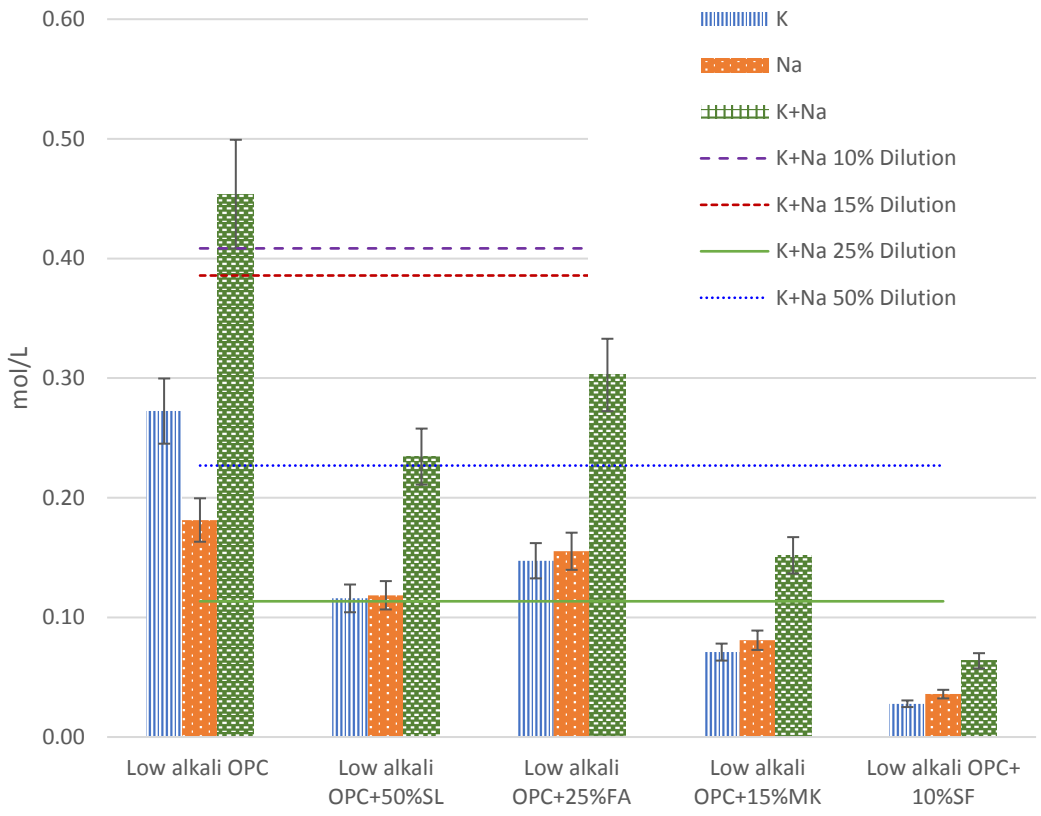

Figure 4-16 Effect of SCM at recommended replacement levels on pore solution alkali concentration at 28 days

Table 4-4 Alkali (Na+K) remaining in the blended pastes after 28 days at recommended SCM replacement levels

Blended Pastes	**K+Na 28 days**
Low Alkali OPC+50%SL	51.6% ± 5.2%
Low Alkali OPC+25%FA	66.4% ± 6.6%
Low Alkali OPC+15%MK	33.5% ± 3.4%
Low Alkali OPC+10%SF	14.0% ± 1.4%

4.5 Effect of AMBT Conditions on the Microstructure

Blended pastes with 25% replacement levels of SCMs were subjected to AMBT conditions and the fractured surfaces were subjected to SEM analysis to characterize the effect of testing conditions on the microstructure. Likewise, XRD was performed on powdered blended pastes to characterize the change in phase composition. XRD results in Figure 4-17 shows the effect AMBT conditions on hydrated cement, which is loss of ettringites and even monocarboaluminates (Deschner et al. 2013; Scrivener & Taylor 1993; Taylor, Famy & Scrivener 2001).

SEM images of the blended pastes in Figures 4-18 to 4-21 likewise confirm the disappearance of ettringites (needle-like structures) post 28 days exposure to 1M NaOH 80 °C. Ettringite is intrinsically unstable in cement pastes above 70 °C (Taylor, Famy & Scrivener 2001) (Scrivener & Taylor 1993). Ettringite and other AFm phases (aluminate ferrite monosulfate) were also destabilised in fly ash blended pastes at temperatures above 80 °C (Deschner et al. 2013). Dissolution of the ettringite and AFm phases during AMBT does not affect the efficacy of the SCMs in ASR mitigation as observed in Figure 4-1, 4-2 and 4-3. This is probably because, whereas, higher temperature destroys ettringites and AFm phases, it accelerates the SCM reactions leading to more C-S-H phases and denser microstructure.

It has been reported that the mortars with fly ash after 3 days submersion in 1M NaOH bath exhibit higher tensile and compressive strength than control mortars. Higher

strength delays the formation of cracks which can promote immediate access of the NaOH solution to the interior of the specimen (Shafaatian et al. 2013). The high early-age strength is attributed to increased rate of pozzolanic reactions due to higher temperature and alkalinity. Under normal curing conditions, SCMs also increase strength, but this takes a longer time because of much slower pozzolanic reactions (Juenger & Siddique 2015).

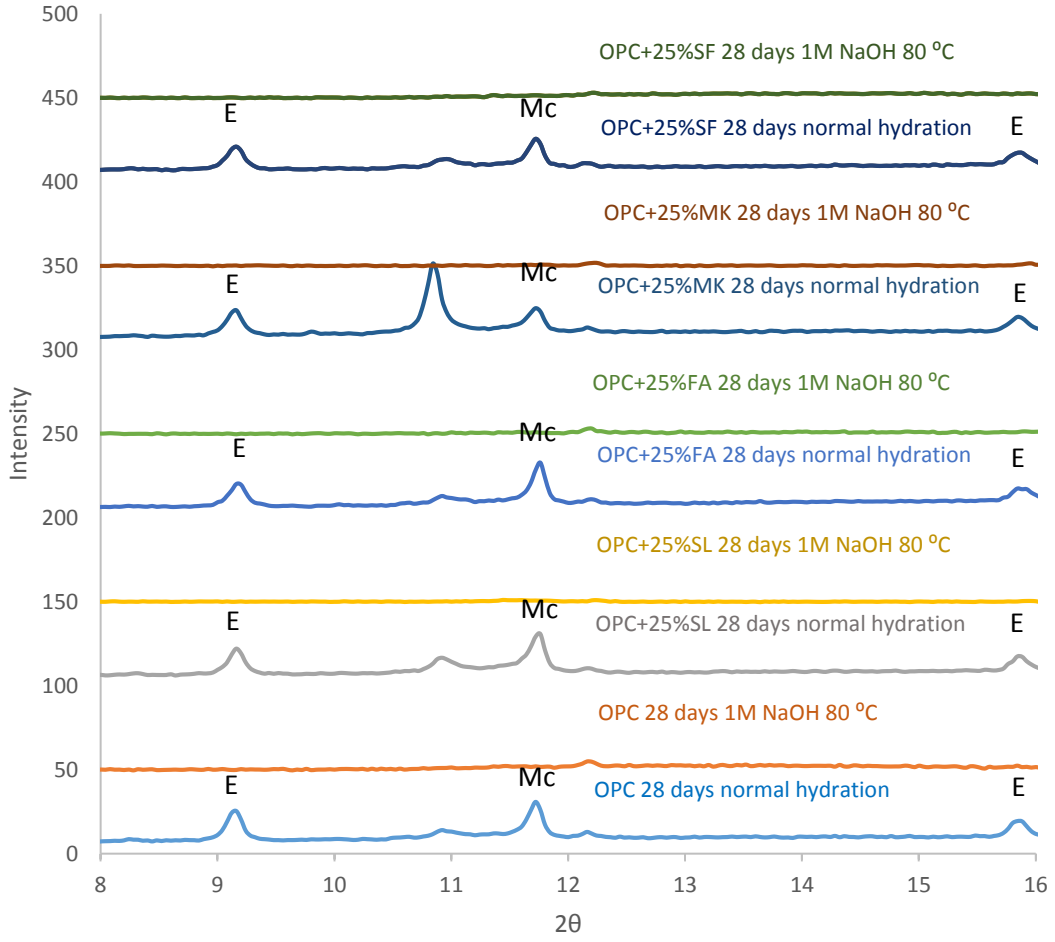

Figure 4-17 XRD patterns of the blended pastes subjected to 28 days normal hydration and 28 days 1M NaOH 80 °C.

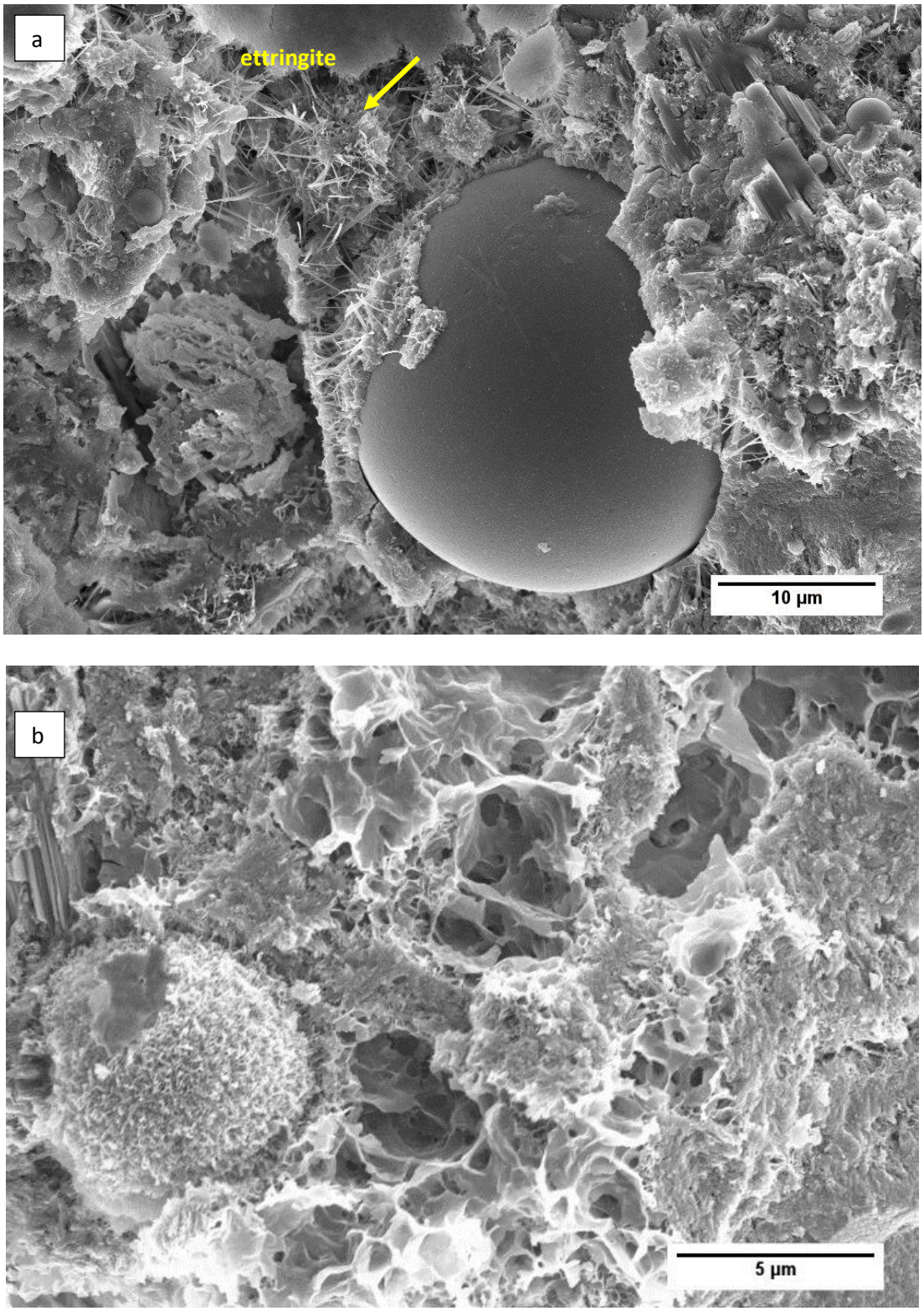

Figure 4-18 SEM images of OPC+25%FA at a) 28 days normal hydration and b) after exposure to 1M NaOH 80 °C for 28 days

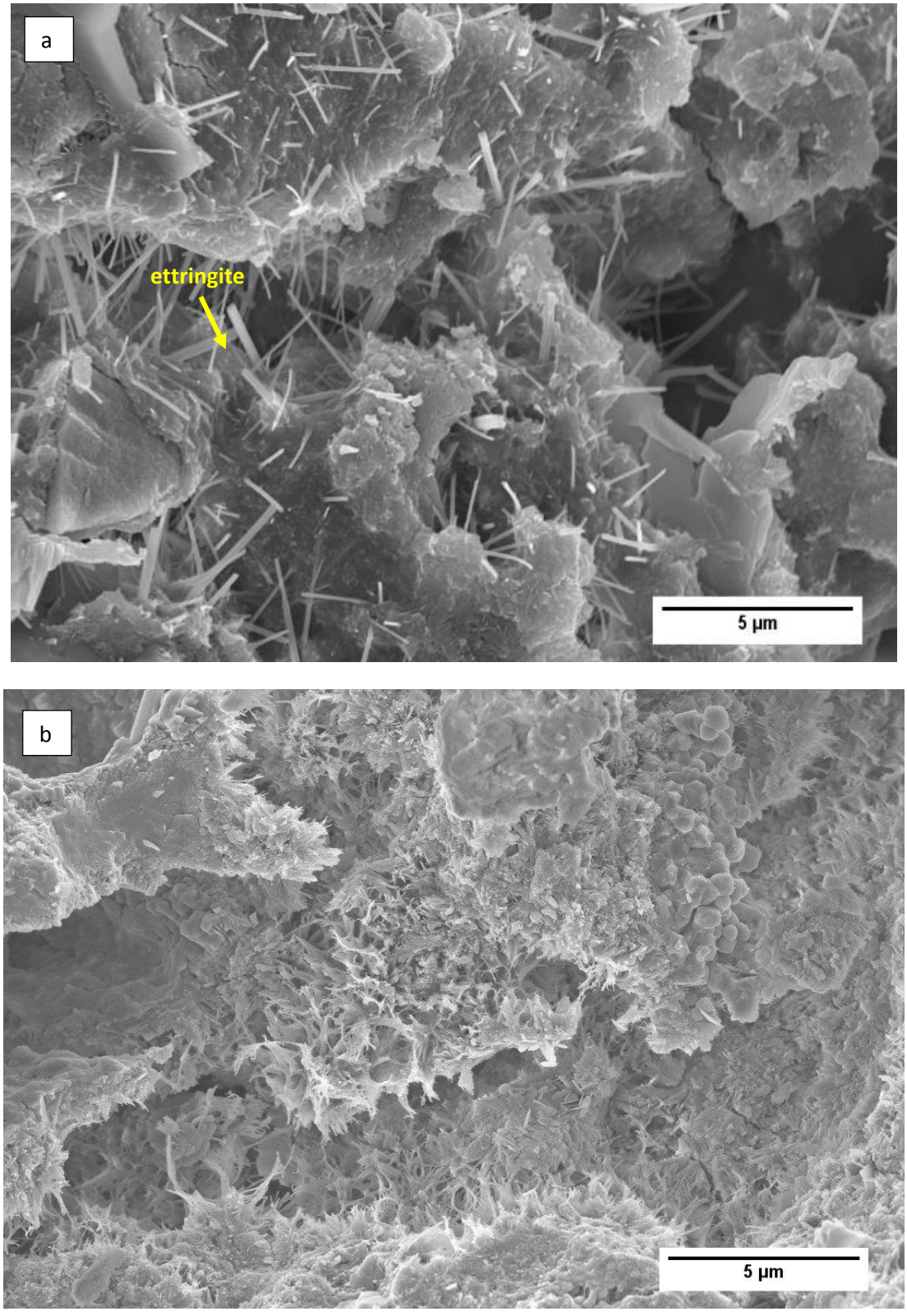

Figure 4-19 SEM images of OPC+25%SL at a) 28 days normal hydration and b) after exposure to 1M NaOH 80 °C for 28 days

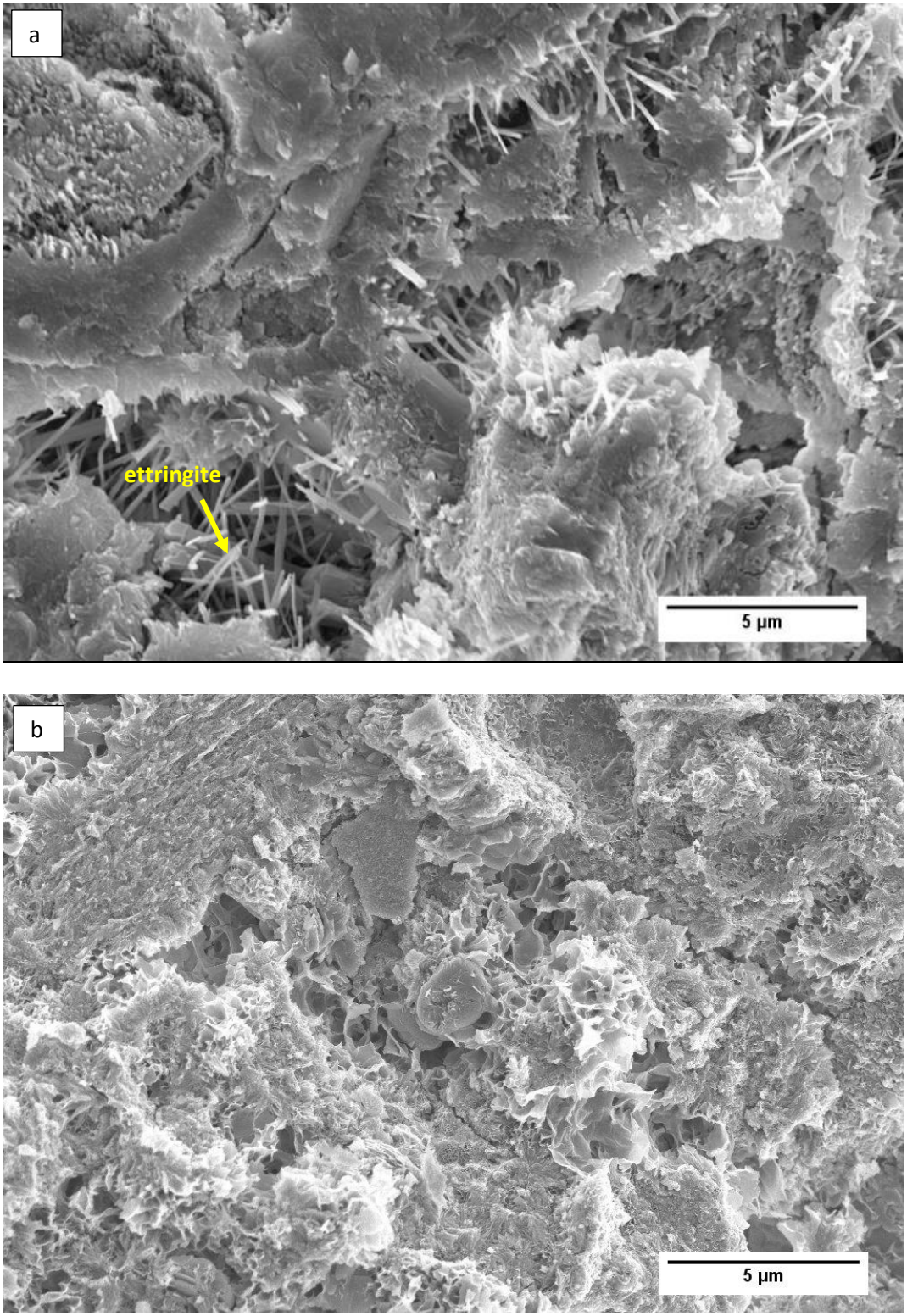

Figure 4-20 SEM images of OPC+25%MK at a) 28 days normal hydration and b) after exposure to 1M NaOH 80 °C for 28 days

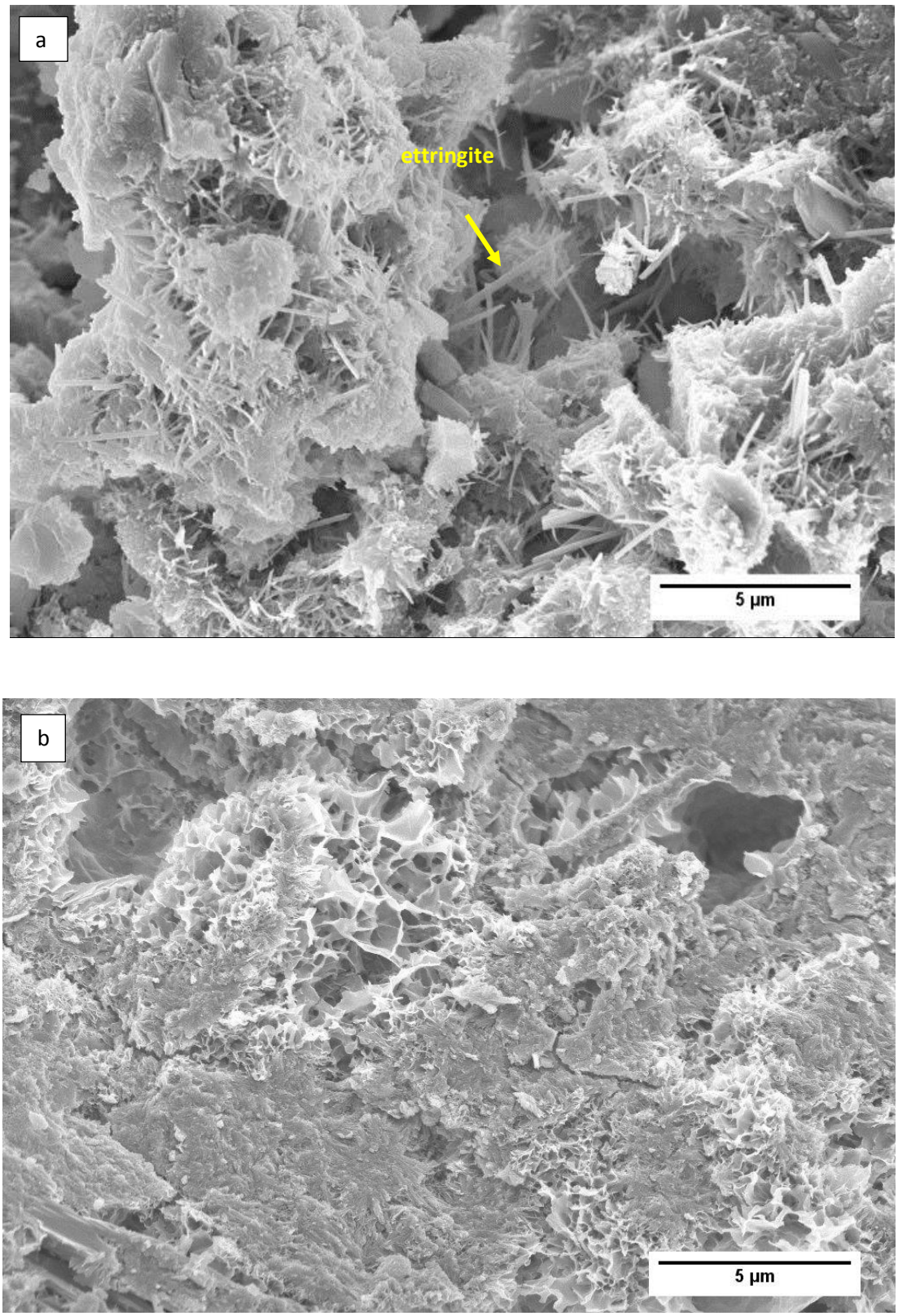

Figure 4-21 SEM images of OPC+25%SF at a) 28 days normal hydration and b) after exposure to 1M NaOH 80 °C for 28 days

4.6 The Role of Silicon and Aluminium in ASR Mitigation

SCM efficacy in ASR mitigation is reported to be related to its active silica and alumina content (Chappex & Scrivener 2012b; Gebregziabiher, Thomas & Peethamparan 2016; Scholz, Hübert & Hünger 2016; Shehata & Thomas 2000; Snellings & Scrivener 2016). The higher amount of reactive silica is correlated to increased pozzolanic products that have much higher alkali binding capacity. Therefore, as discussed in previous sections, higher amount of reactive silica from SCMs results in better ASR mitigating properties. Several studies have also reported on the beneficial role of aluminium in ASR mitigation (Berube & Duchesne 1993; Bickmore et al. 2006; Brykov & Anisimova 2013; Chappex & Scrivener 2012b; Chappex & Scrivener 2013; Feng, Jia & Hu 2013; Hay & Ostertag 2019; Hong & Glasser 2002). The mechanisms by which aluminium mitigates ASR however still remains controversial.

This section compares the amount of silicon (Si) and aluminium (Al) released by SCMs under AMBT conditions, the interaction of the dissolved SCM species in the system (i.e. formation of reaction products) and how these all correlate to explain the differences in SCM dosage requirements for effective mitigation.

4.6.1 Release of silicon and aluminium from SCMs in alkaline solution

Five grams of each SCM type (FA, SL, MK and SF) was immersed in 1M NaOH 80 °C for 28 days and the concentration of release Si and Al in solution was measured by ICP-OES at 7, 14, 21 and 28 days. Figures 4-22 and 4-23 show the amount of Si and Al the SCMs released in solution under AMBT conditions. The measured concentrations of Si and Al in solution represent instantaneous concentrations of these species on extraction of the aliquot of supernatant fluid. From Figure 4-22, the highest concentration of dissolved Si is observed for silica fume, followed by metakaolin, fly ash and then slag consistent with that reported in another study (Panagiotopoulou et al. 2007). The amount of Si in solution for fly ash, metakaolin and slag increases significantly with respect to time. Highest concentration of Si is observed for the silica fume as there is a significant availability of free silica, it is amorphous and therefore reactive. Moreover, SF used in this study only has 0.10% Al_2O_3 and 0.24% CaO as per XRF analysis, and therefore it can be assumed that there are not much other ions present which can promote precipitation of the Si in solution. Slag, on the other hand, has very little (almost none) free Si available in solution. The absence of Si in solution for slag implies that all available silica is bound in the products. The products formed in the dissolution reactions are discussed in the next section. The amount of available Si in solution measured for all SCMs correlates well with the dosage requirements for effective ASR mitigation (that is, silica fume with the least and slag with the most), the degree of pozzolanicity as well as alkali binding capacity.

SCMs with high proportion of reactive SiO_2 content such as SF, MK and FA, therefore have significant potential in mitigating ASR. Indeed, silica fume which is almost entirely amorphous silica generally requires lowest replacement level among the SCMs at 5-10%, while slag which is a calcium-rich SCM requires the highest dosage to mitigate, normally > 50% (Duchesne & Berube 1994a; Duchesne & Berube 2001; Hobbs 1986; Rasheeduzzafar & Hussain 1991). Fly ash and metakaolin releases considerable amount of Si and thus requires intermediate amounts (15-25%) for effective ASR mitigation (Standards Australia 2015).

Aluminium concentration in solution as reported in Figure 4-23 is in the following order: MK>FA>SL>SF. That is, metakaolin with the highest amount of aluminium in solution followed by fly ash and slag with almost equivalent amounts. This is consistent with another dissolution study of aluminosilicate materials in alkali media (NaOH and KOH at 2M, 5M, and 10M concentrations), where, metakaolin consistently registers the highest amount of Al in solution followed by fly ash, then slag (Panagiotopoulou et al. 2007). No presence of aluminium in solution was detected for silica fume, consistent with negligible amount of Al_2O_3 (just 0.1%) in the XRF oxide analysis. Moreover, it is notable that the aluminium concentration in solution decreases as a function of time, suggesting that they precipitate in solution to form other phases.

The release of aluminium from FA, MK and SL under AMBT conditions is also consistent with increased Al/Si ratio in the C-S-H composition of mortars/pastes with FA, MK and SL. The increase in Al/Si ratio suggests aluminium uptake in the C-S-H forming C-A-S-H. When Al^{3+} substitutes for Si^{4+}, this results in a net negative charge

and thus alkali cation (Na^+ or K^+) is bound in the process leading to further decrease in pore solution alkali concentration.

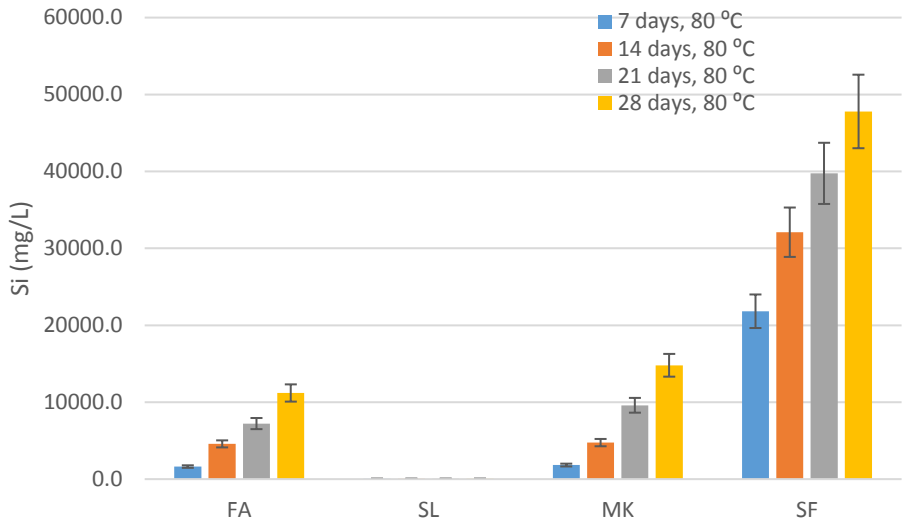

Figure 4-22 Measured concentration of silicon (Si) after 7, 14, 21 and 28 days in 1M NaOH at 80 °C

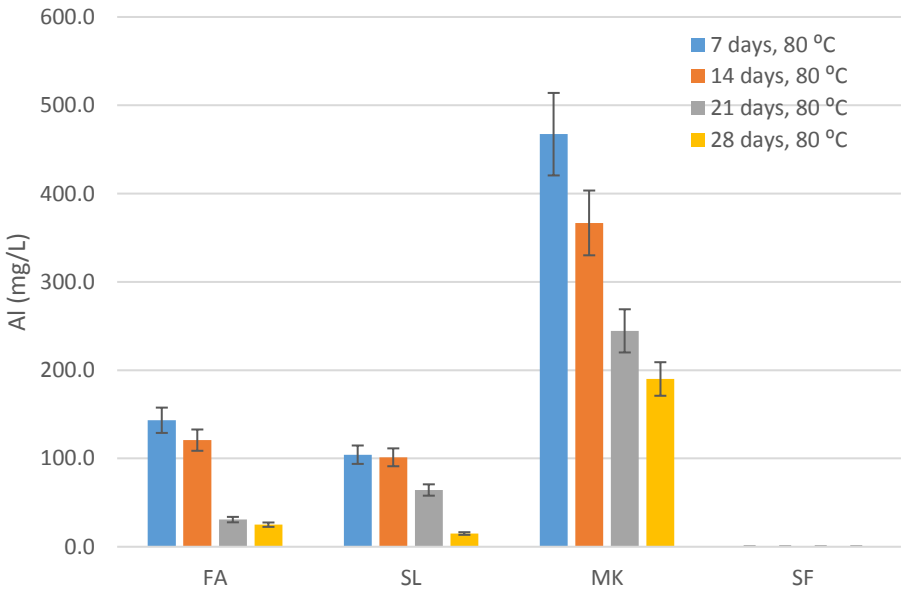

Figure 4-23 Measure concentration of aluminium (Al) after 7, 14, 21 and 28 days in 1M NaOH 80 °C

4.6.2 Formation of Aluminosilicates and Alkali Binding

This section reports on the observed changes in microstructure, as well as the formation of aluminosilicates in the SCMs after being subjected to AMBT conditions. Note that the concentrations measured in the preceding section do not take into account those consumed by the reaction products. At a highly alkaline environment, the OH^- ions hydrolyze the glassy phase of the SCMs releasing silicate and aluminate species into solution. When supersaturation occurs, aluminosilicate hydrates precipitate. Hence, the concentrations measured in Figures 4-22 and 4-23 correspond to instantaneous concentrations in a metastable matrix (i.e. whatever amount is excess from precipitation reactions) (Newlands et al. 2017).

The reaction products were filtered, dried and subjected to SEM analysis to characterize the changes in microstructure that have occurred. Figure 4-24 shows SEM images of unreacted fly ash and fly ash after immersion in 1M NaOH for 28 days at 80 °C. The unreacted fly ash is characterized by spherical particles with a generally smooth texture consistent with literature (Figure 4-24a and b) (Fernandez-Jimenez & Palomo 2005; Gebregziabiher, Thomas & Peethamparan 2016). After 28 days in 1M NaOH solution at 80 °C, fleurette-like crystalline structures are observed to be co-existing with some remaining unreacted spheres (Figure 4-24c to d) indicating a significant degree of reaction with the development of a new phase.

XRD pattern of fly ash before alkali immersion in Figure 4-25 shows presence of both crystalline and amorphous phases. The major crystalline peaks in the unreacted fly ash were identified as quartz and mullite. The presence of an amorphous phase is indicated

by a broad ‘halo’ in the XRD spectrum centred on 22° 2θ. After 28 days immersion in 1M NaOH at 80 °C, the formation of peaks attributed to N-A-S-H (zeolite, N-Na_2O, A-Al_2O_3, S-SiO_2, H-H_2O) coupled with a further decrease in the intensity of the amorphous halo is observed. The quartz and mullite phases initially present before alkali immersion remain apparently unmodified after 28 days alkali immersion indicating that the primary reactant to this point is the amorphous aluminosilicate phase present.

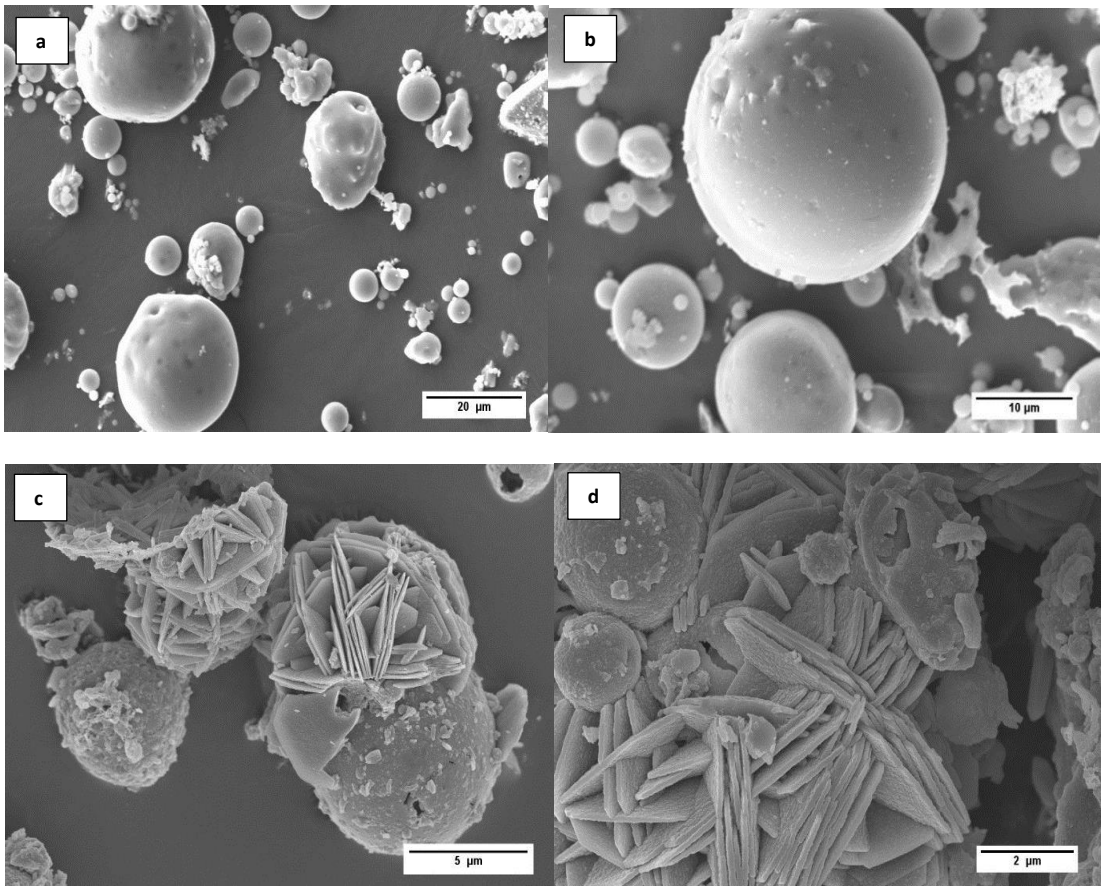

Figure 4-24 SEM images of the unreacted fly ash (a and b), and fly ash after 28 days immersion in 1M NaOH at 80 °C (c and d)

The differences observed in the morphology in the SEM micrographs and in the XRD patterns, shows alkali activation of fly ash at 1M NaOH 80 °C. At 80 °C, zeolite, a crystalline product is produced. This is consistent with reported mechanisms of the alkaline activation of fly ash where an X-ray amorphous aluminosilicate gel, a ‘‘zeolite precursor’’ is reported to be initially produced, while at elevated temperature crystalline zeolite phases are observed (Fernandez-Jimenez, Torre, et al. 2006). The two-step process is referred to as the ‘‘zeolitisation’’ process. The significantly elevated temperature provides the necessary reaction environment for the formation of crystalline aluminosilicates and, hence, the zeolitisation process is completed resulting in the observation of the N-A-S-H phase in the XRD (Criado et al. 2007; Fernandez-Jimenez & Palomo 2005; Fernandez-Jimenez, Palomo, et al. 2006; Fernandez-Jimenez, Torre, et al. 2006; Palomo, Grutzeck & Blanco 1999). For both steps of the zeolitisation process, the amorphous phases act as the source of the silicate and aluminate ions as the crystalline phases (mullite and quartz) present in the fly ash typically remain unreactive (Criado et al. 2007; Fernandez-Jimenez, Torre, et al. 2006).

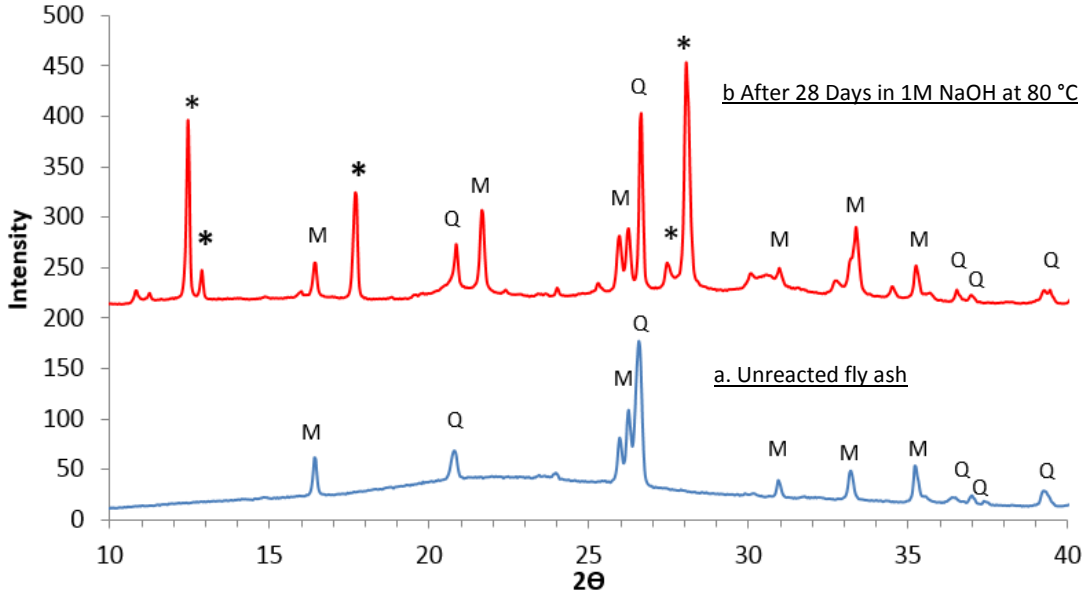

Figure 4-25 XRD patterns of the a) unreacted fly ash and b) fly ash after 28 days immersion in 1M NaOH 80 °C where Q=quartz, M=mullite and *=sodium aluminium silicate hydrate (N-A-S-H)

Figure 4-26 shows the microstructural changes in metakaolin when immersed in 1M NaOH 80 °C showing the formation of cubic crystals comparable to those reported by Zhang et al. (Zhang, MacKenzie & Brown 2009). XRD results in Figure 4-27 confirmed the cubic crystals to be N-A-S-H (type A zeolite, $Na_{96}Al_{96}Si_{96}O_{384}.216H_2O$) which is consistent with the phases reported for the reaction of metakaolinite with NaOH at elevated temperature (Madani et al. 1990).

In a similar stepwise process as that observed with the reaction of fly ash, alkaline attack on metakaolin induces the release of silicate and aluminate species in solution which polycondense to form, initially an amorphous aluminosilicate gel which, once formed, converts to the type A zeolite by a structural rearrangement without further change in composition (Zhang, MacKenzie & Brown 2009). The EDS map in Figure

4-28 show presence of sodium (Na), aluminium (Al) and silicon (Si) in the cubic crystals consistent with the observed formation of N-A-S-H.

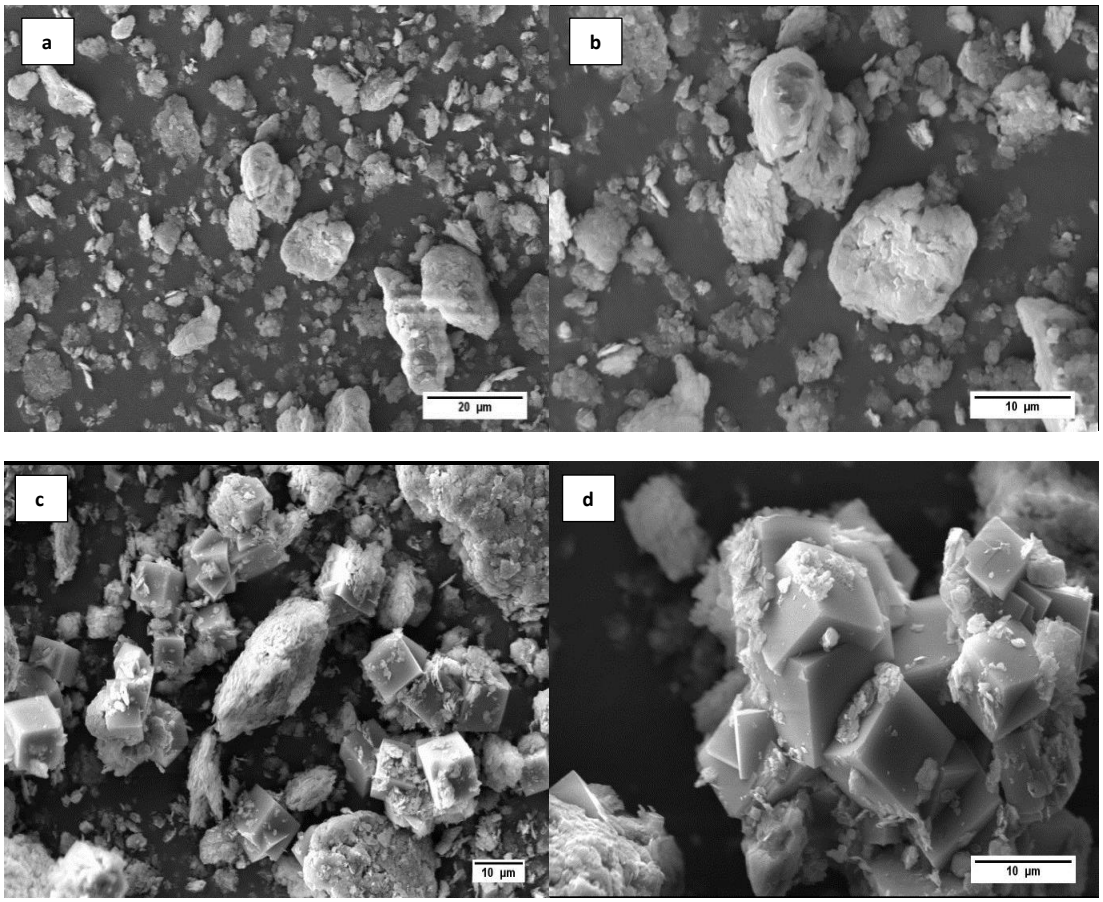

Figure 4-26 SEM images of unreacted metakaolin (a and b) and metakaolin after 28 days immersion in 1M NaOH at 80 °C (c and d)

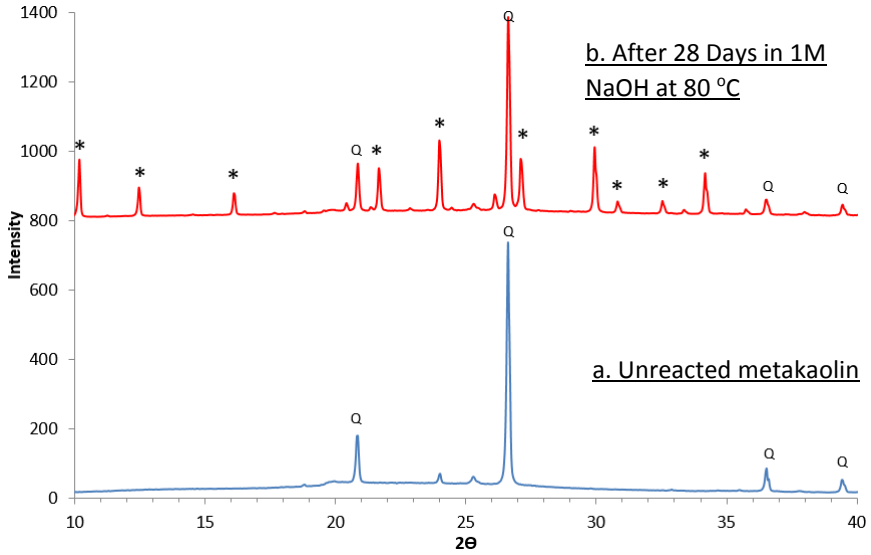

Figure 4-27 XRD pattern of the a) unreacted metakaolin and b) metakaolin after 28 days immersion in 1M NaOH 80 °C where Q=quartz and *=zeolite (N-A-S-H, sodium aluminosilicate hydrate)

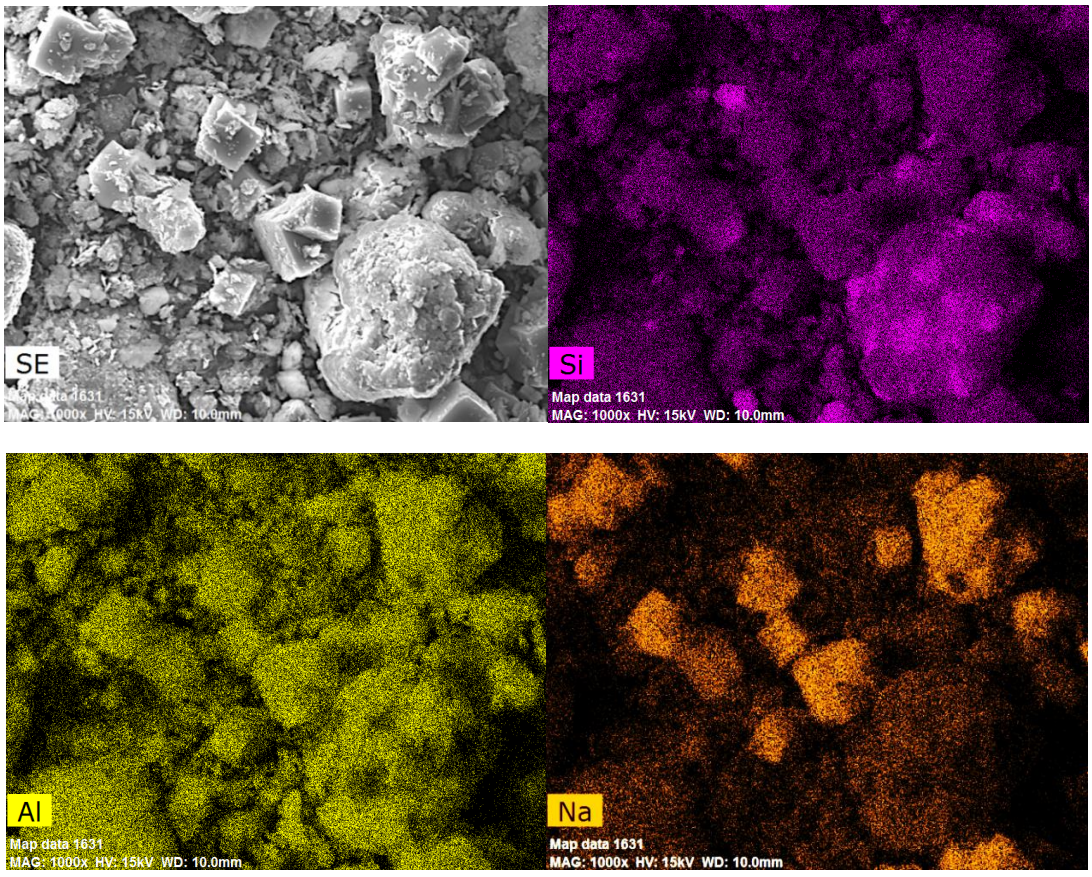

Figure 4-28 EDS mapping of metakaolin immersed in 1M NaOH 80 °C for 28 days

Figure 4-29 shows SEM images of slag before and after 28 days immersion 1M NaOH 80 °C. Unreacted slag (Figure 4-29a and b) exhibits angular appearance due to the grinding process and the brittle nature of the glass (Gebregziabiher, Thomas & Peethamparan 2016). The XRD pattern of unreacted slag in Figure 4-30 shows presence of a broad halo centred around 30° 2θ confirming its primarily amorphous/glassy nature (Gebregziabiher, Thomas & Peethamparan 2016). In general, blast furnace slag may be described as $CaO\text{-}SiO_2\text{-}Al_2O_3\text{-}MgO$ glass (Ye & Radlińska 2016).

A change in slag microstructure has been observed (Figure 4-29c and d) confirming the occurrence of dissolution and formation of a new phase. Development of a platelike microstructure is evident at 80 °C. The change in morphology is supported by the formation of a crystalline phase identified as katoite $(Ca_3Al_2SiO_4)(OH)_8$, a form of calcium aluminosilicate hydrate (C-A-S-H) as shown in Figure 4-30.

In a similar fashion to fly ash and metakaolin, slag undergoes dissolution in alkali releasing calcium, aluminium and silicon ions, however, the products formed from the dissolution of slag are calcium-based (C-A-S-H) rather than sodium-based (N-A-S-H) aluminosilicates suggesting that the precipitation of calcium aluminosilicates is more favourable. The precipitation of calcium aluminosilicates also allows the sodium ions to be retained in solution which, in a cement or concrete context, is effectively a regeneration of the alkalis to the pore solution (Rajabipour et al. 2015).

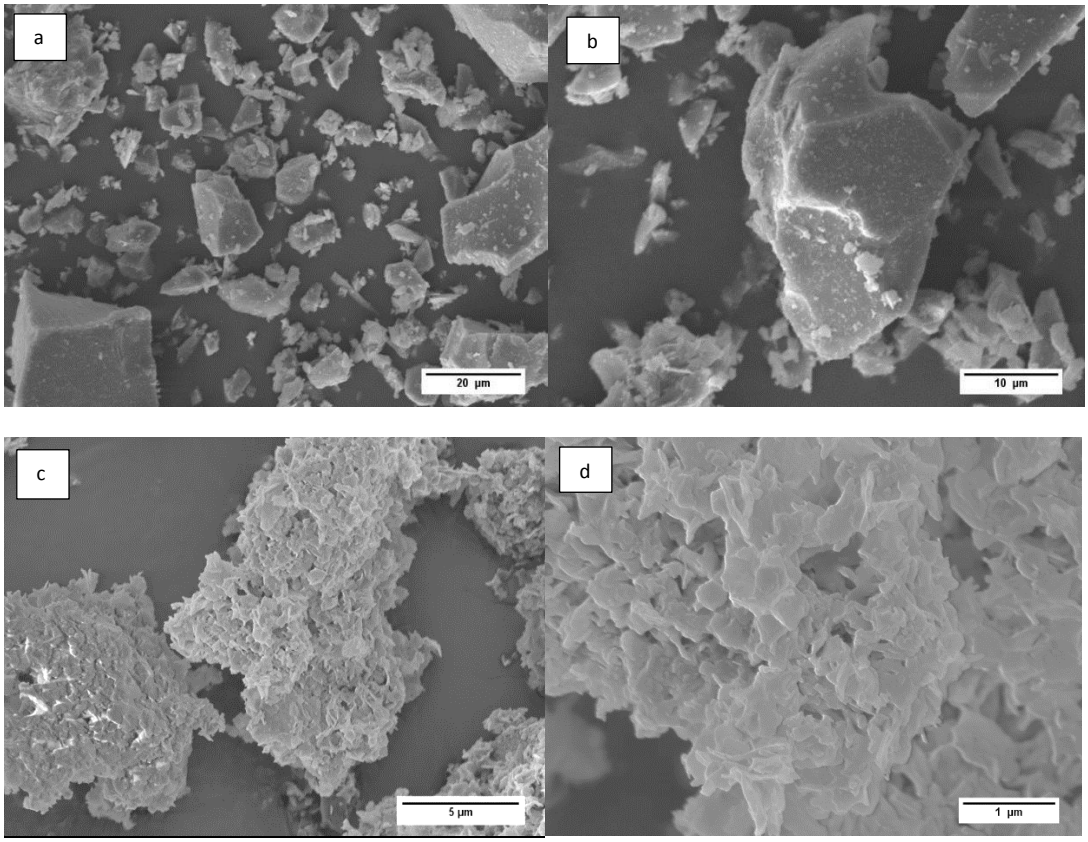

Figure 4-29 SEM images of unreacted slag (a and b), and slag after 28 days immersion in 1M NaOH at 80 °C (c and d)

The alkali activation of slag results in the dissolution of silicate and aluminate ions and importantly calcium ions which aid the precipitation of C-S-H and C-A-S-H phases (Li, Sun & Li 2010). The proportion and type of each phase produced is strongly dependent on the composition of the slag (Tanzer, Buchwald & Stephan 2015). Under the conditions used in this work, katoite was the major crystalline C-A-S-H phase produced.

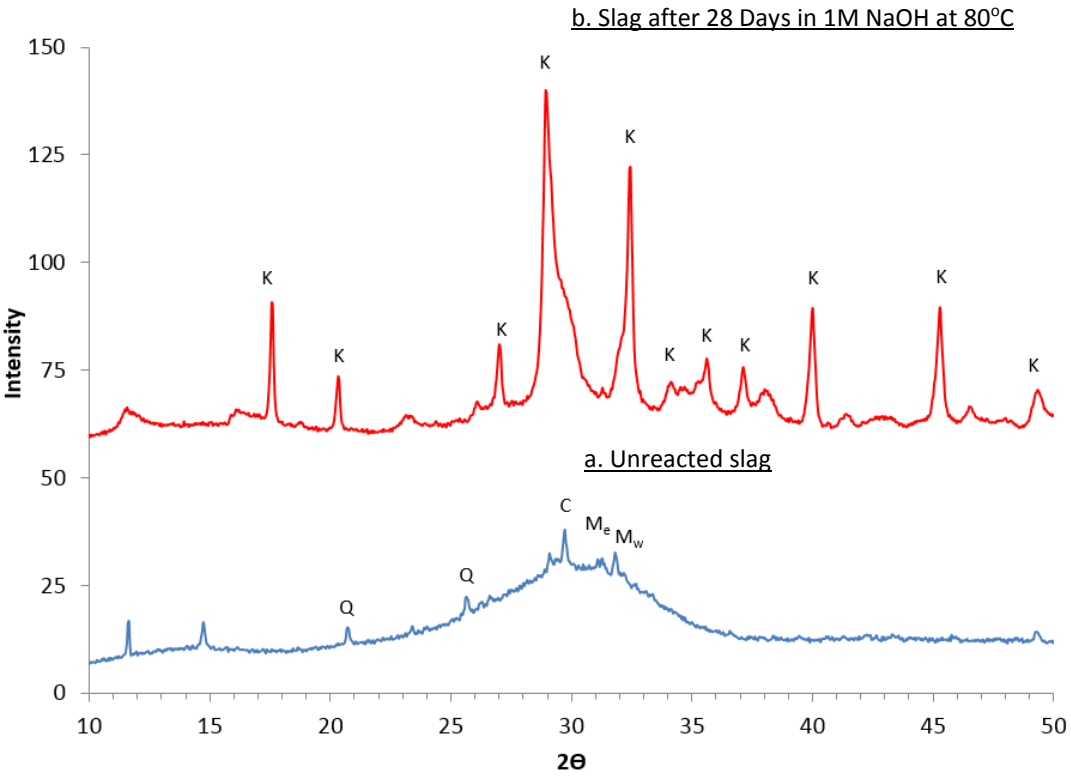

Figure 4-30 XRD pattern of the a) unreacted slag and b) slag after 28 days immersion in 1M NaOH at 80 °C where Mw=Merwinite, Me=Melilite, C=calcite, Q=quartz and K= katoite $(Ca_3Al_2SiO_4)(OH)_8$

The SEM images of unreacted silica fume are shown in Figure 4-31a showing the typical spherical particles in the submicron range (Thomas 2013). After 28 days immersion in alkali at 80 °C, the formation of spherical rosette morphology is observed (Figure 4-31b to d). The rosettes have a diameter of circa 5 microns, which is significantly greater in size than the original spherical particles of the unreacted silica fume indicating a significant degree of reaction.

The XRD pattern of unreacted silica fume in Figure 4-32 shows a broad diffraction peak (halo) centred on 22° 2θ confirming its amorphous nature. Quartz is also observed

in the diffraction pattern indicated by the sharp peak at 26.6° 2θ. The features observed in the diffraction pattern of the unreacted silica fume remain largely unchanged after alkali immersion and no crystalline products are observed. A halo centred on 13° 2θ is, however, developed which suggests that an amorphous gel, which has an increased average spacing between silica tetrahedra, is produced. The lack of the development of a crystalline phase may be due to the lack of an aluminium source for the precipitation of an aluminosilicate product as is observed for fly ash, metakaolin and blast furnace slag. Additionally, as sodium silicate is soluble in alkaline media, it is also likely that a "water glass" is present.

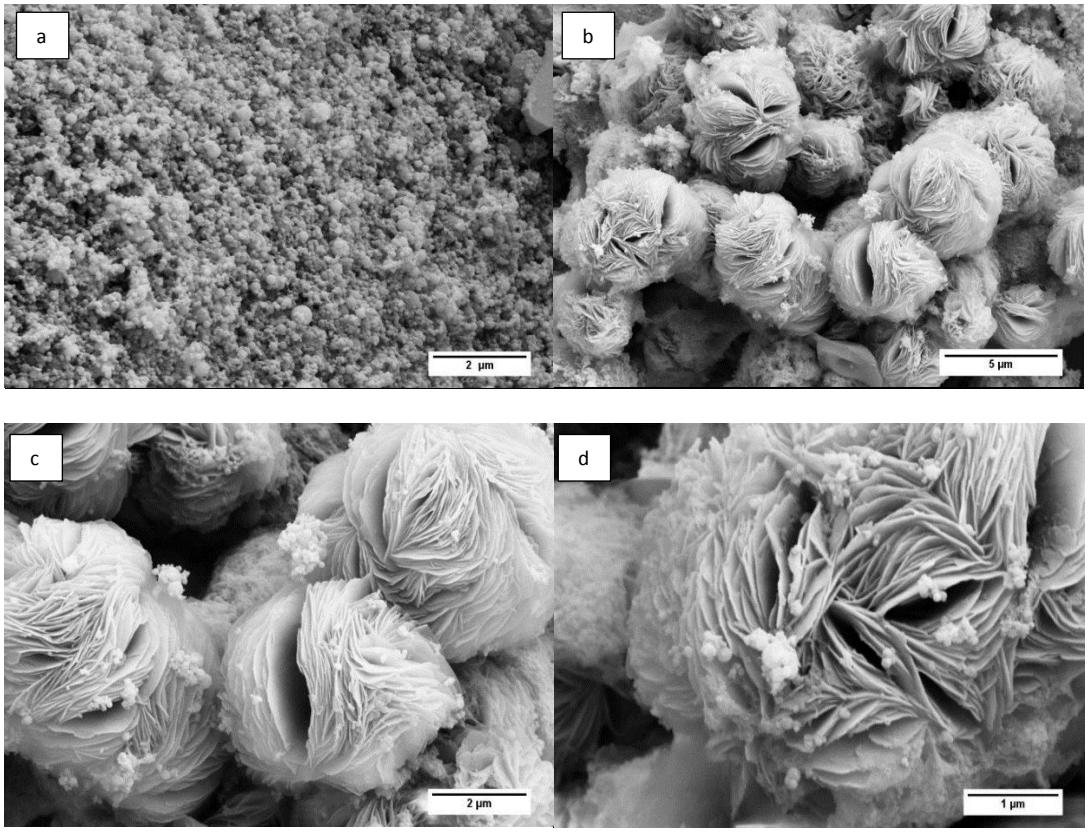

Figure 4-31 SEM images of unreacted silica fume (a) and silica fume after 28 days immersion in 1M NaOH at 80 °C (b, c and d)

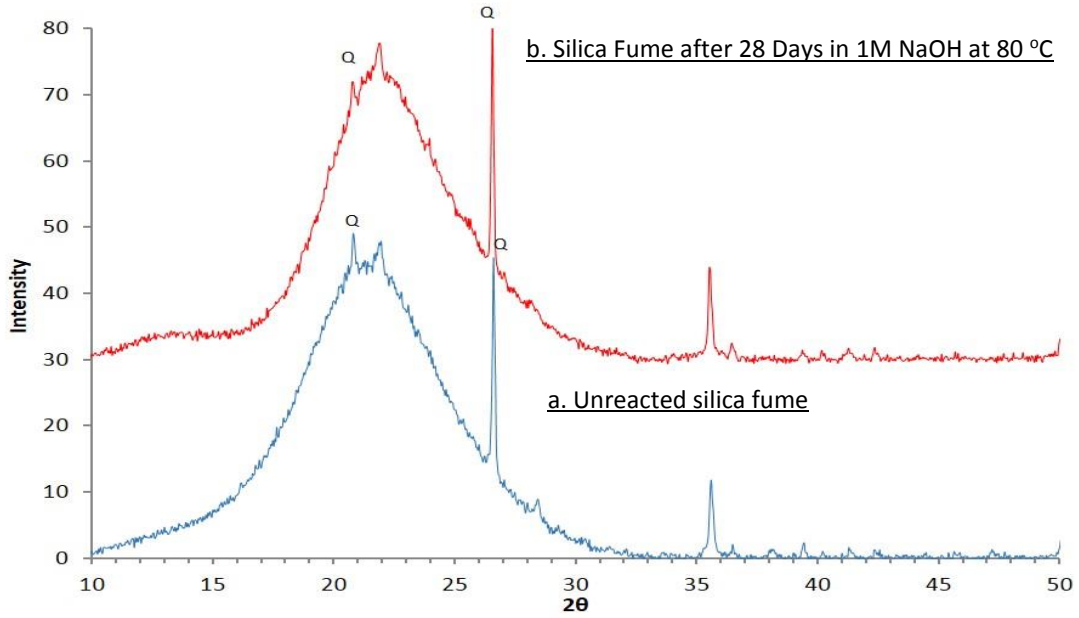

Figure 4-32 XRD pattern of the a) unreacted silica fume and b) silica fume after 28 days immersion in 1M NaOH 80 °C where Q=quartz

The aluminium-containing SCMs showed formation of aluminosilicate hydrates after being exposed to AMBT conditions. FA and MK showed formation of N-A-S-H (sodium aluminosilicate hydrate) while slag showed formation of C-A-S-H (calcium aluminosilicate hydrate). The SCMs can be taken as representative of systems rich in Si (SF), rich in Si and Al (FA and MK), rich in Si, Al and Ca (slag). Under alkali environment, in this case 1M NaOH, the SCMs dissolve and form reaction products. If aluminium is present, it can bind silicon forming aluminosilicates, thus reducing the free Si in solution (Hünger 2007). The aluminosilicates are negatively charged in basic environment and therefore attracts a cation to charge balance. Thus, Na^{+} and Ca^{2+} compete in the process where Ca^{2+} is more preferentially absorbed. Thus, FA and MK form N-A-S-H while slag forms C-A-S-H since it is saturated with calcium. This indicates that in systems with higher calcium contents, less alkalis are bound since calcium competes with the alkali (L'Hôpital et al. 2016).

The mechanism of the formation of aluminosilicates is consistent with another study which reported that aluminium can react with silica from aggregates to form an aluminosilicate layer on the silica surface, which could protect the substrate silica against further attack of hydroxyl ions (Chappex & Scrivener 2012b; Sang, Jakubik & Barkatt 1994).

4.6.3 Effect of Al_2O_3 Addition on AMBT Expansion

Since there is no SCM with pure Al_2O_3 composition, to examine the effect of Al_2O_3 on expansion, 25% of the cement was replaced with Al_2O_3 in AMBT specimens where three reactive aggregates (greywacke, rhyolite and dacite) were evaluated.

Figure 4-33 shows that replacing part of cement with 25% Al_2O_3 results in a reduction in expansion for all aggregates. All mortars with 25% Al_2O_3 exhibit expansion lower than 0.30% at 21 days. This result agrees with recent reports where the use of Al_2O_3, $Al(OH)_3$, and even aluminium pieces and powder as cement substitute can successfully mitigate ASR (Brykov & Anisimova 2013; Feng, Jia & Hu 2013; Hay & Ostertag 2019).

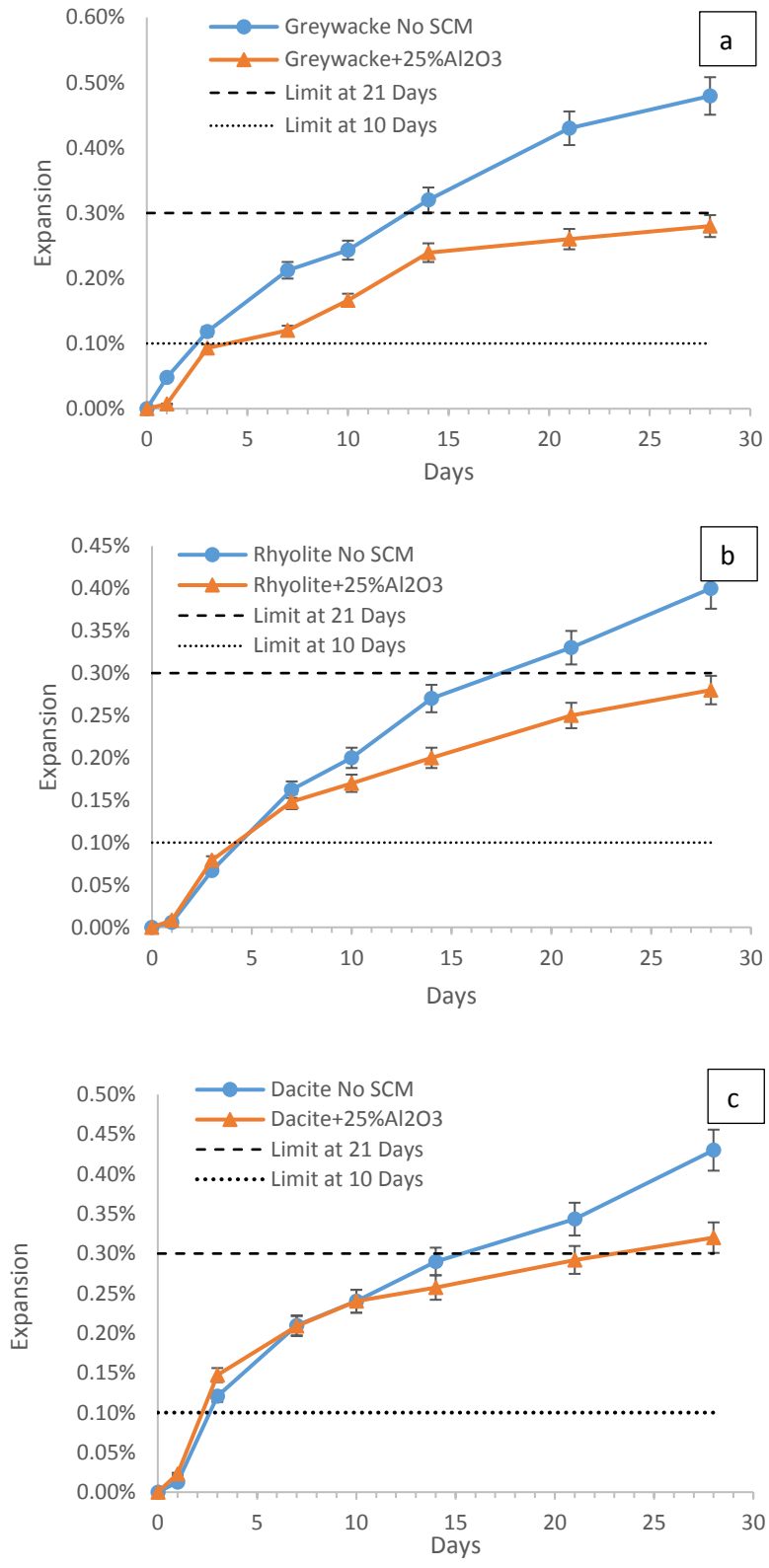

Figure 4-33 Effect of 25% Al_2O_3 cement substitution on ASR expansion of a) greywacke, b) rhyolite and c) dacite aggregates.

4.7 Summary of Findings

In order to better understand the mechanistic role of SCMs in ASR mitigation and why the efficacy of SCMs vary as a function of SCM type, this chapter investigated the effect of traditional SCMs (FA, SL, MK and SF) on ASR expansion, pozzolanic behaviour, pore solution alkalinity, and composition of the C-S-H phases. The ability of the SCMs to release Si and Al in solution, as well as the potential of pure Al_2O_3 to mitigate ASR expansion was also investigated.

Below summarizes the important findings from this chapter.

1. AMBT expansion results show that the required dosage for SCMs to mitigate ASR expansion increases as follows: silica fume (5-10%), metakaolin (10-15%), fly ash (15-25%) and slag (35-65%). Likewise, at equivalent replacement levels of 10%, the efficacy of SCMs to reduce expansion due to ASR is in the following order: SF>MK>FA>SL. The results agree with literature and recommended replacement levels of SCMs where silica fume requires the least and slag requires the most amount to mitigate ASR.

2. Sectioned mortar specimens post-AMBT show extensive cracking in the mortar without SCM and almost no cracks in all mortars with SCMs at recommended replacement levels (25%FA, 65%SL, 15%MK and 10%SF) consistent with negligible expansion observed. ASR gel was observed in the mortar without SCM.

3. C-S-H composition of mortar specimens post-AMBT was analysed. All mortars with SCMs at recommended replacement levels (10%SF, 15%MK, 25%FA and 65%SL) showed much lower Ca/Si ratio than the mortar without SCM. C-S-H with much lower Ca/Si ratio has a higher alkali binding capacity. The Al/Si ratio of the C-S-H increased in mortars with fly ash, metakaolin and slag. The increase in Al/Si ratio suggests aluminium uptake in the C-S-H (i.e. formation of C-A-S-H), resulting in a net negative charge and consequent alkali binding. Aluminium uptake in the C-S-H, therefore, enhances alkali uptake in the C-S-H.

4. C-S-H composition of blended pastes with 25% SCM (FA, SL, MK and SF) subjected to AMBT conditions was also analysed for comparative analysis. The use of blended pastes allows analysis of a pure system with no influence of aggregates. Results show that 25%SF blended paste has the lowest Ca/Si ratio among the four blends and OPC+25%SL with the highest Ca/Si ratio. Al/Si ratio of the blend with 25%SF is similar to OPC. All pastes with aluminium-containing SCMs (FA, MK and SL) has much higher Al/Si ratio than reference plain OPC paste.

5. Cement pastes and SCM blended pastes with various SCM replacement levels were subjected to TG measurements after 28 days exposure to AMBT conditions to characterize the degree of consumption of portlandite. All pastes with SCMs showed much lower portlandite content than reference cement paste. At equivalent replacement dosage, the order of portlandite consumption is as follows: SF>MK>FA>SL. Silica fume being almost entirely amorphous silica and very fine is the most pozzolanic. Slag, a latent hydraulic material, was also observed to consume

a small amount of portlandite. Slag takes extra calcium from sparingly soluble portlandite during hydration.

6. Cement pastes and SCM blended pastes with 25% SCM replacement and at recommended replacement levels (25%FA, 50%FA, 15%MK and 10%SF) were subjected to pore solution extraction after 28 days and 168 days curing at normal hydration conditions.

All pastes with SCMs showed much lower pore solution alkali concentration (Na+K) than the reference cement paste. For the blended pastes with 25% SCM, reduction in total alkali (Na and K) and reduction in pH occurs in the following trend at 28 days and at 168 days: SF>MK>FA>SL. Silica fume, in fact, with very little Na+K remaining in the pore solution (only 4.9%) after just 28 days. The varying levels of alkali content in the blended pastes with SCMs show that the effect of SCM on pore solution is more than just dilution. For blended pastes with SCMs at recommended replacement levels, 10%SF was still observed to be the best in reducing pore solution alkalinity (86% alkali reduction after 28 days), followed by 25%FA, 15%MK and 65%SL. The alkali concentration in the pore solution of the blended pastes at 168 days is much lower than that at 28 days. The decrease in alkali content with time suggests continuous alkali binding in the pastes with SCMs as they react in the system.

7. SCMs (FA, SL, MK and SF) were immersed in 1M NaOH 80 °C for 28 days to determine concentration of soluble silicon and aluminium from the SCMs. The ability of SCMs to release Si is as follows: SF>MK>FA>SL, which correlates well with the dosage required to reduce expansion, pozzolanic behaviour and ability to reduce alkali

in solution. The higher amount of Si enhances the pozzolanic reactions which results in increased alkali adsorption in the C-S-H. Slag has almost no free Si in solution and thus has the lowest reduction in portlandite and pore solution alkalinity. Metakaolin released the highest amount of aluminium in solution followed by fly ash and slag. No aluminium was detected in the SF solution.

8. The solid residues post SCM dissolution test were characterized. Microstructure and phase studies confirm formation of aluminosilicate hydrates in all SCMs with the exception of silica fume. This indicates that the presence of aluminium can precipitate silicon. This results in the formation of aluminosilicates that are highly stable under alkali attack and consequent reduction of free Si in solution. The lack of development of a crystalline phase in silica fume was attributed to the lack of calcium or aluminate ions in solution to promote the precipitation of a crystalline aluminosilicate hydrates. Fly ash and metakaolin both formed sodium aluminosilicates, whereas, slag formed calcium aluminosilicates. This shows competitive reaction between Na^+ and Ca^{2+}, where the latter is always preferentially adsorbed. The dissolution of the SCMs and observed formation of reaction products can also be taken as a representative of systems that are: 1) rich in silica without aluminium and calcium (silica fume), 2) rich in both silica and aluminium (fly ash and metakaolin) and 3) rich in silica, aluminium and calcium (slag). Under these conditions, as observed, if aluminium is present, it will bind silicon and take either alkali cations (Na^+ or K^+) or divalent cation Ca^{2+} as a form of charge compensation. If solution is saturated with calcium, Ca^{2+} is bound instead of alkali. Therefore, the presence of calcium lowers the amount of bound alkali.

9. AMBT was carried out by substituting cement with 25% Al_2O_3. The mortars containing reactive aggregates all showed considerable reduction in expansion, confirming that aluminium presents a potential to mitigate ASR.

5 Pore Solution Method for Assessing the Efficacy of SCMs in Mitigating ASR in Cements of Higher Alkali Contents

Complementary to the use of SCMs, Australian standards impose a strict limit of 0.6% Na_2O_{eq} (sodium oxide equivalent=Na_2O + 0.658 K_2O) on cement alkali content in order to mitigate ASR. This low alkali limit results in tremendous amount of raw materials (limestone in particular) to be unsuitable for cement production. Since the ability of SCMs to mitigate ASR has long been established, both by accelerated test methods and field exposure studies (Boddy, Hooton & Thomas 2003; Duchesne & Berube 2001; Durand et al. 1990; Hobbs 1986; Ramlochan, Thomas & Gruber 2000; Rasheeduzzafar & Hussain 1991; Shehata & Thomas 2000; Thomas 2011; Thomas et al. 2011), there is then a question as to whether a strict cement alkali limit is still necessary when SCMs are already incorporated in the concrete mix. Increasing the cement alkali limit offers potential not only to reduce costs associated with cement production but also conserve environmental resources.

Standard laboratory test methods such as accelerated mortar bar test (AMBT) and concrete prism test (CPT) are typically employed to assess SCM efficacy in the short term. However, despite worldwide popularity, with several countries having their own version of the tests, AMBT and CPT are both questionable with respect to their ability to assess the effect of cement alkalinity on ASR expansion (Sirivivatnanon, Mohammadi & South 2016; Thomas et al. 2006). For ASR testing, Australia uses its

own version of these accelerated tests, AS 1141.60.1 (AMBT) and AS 1141.60.2 (CPT) which are very similar to well-known ASTM C1260 and ASTM C1293, respectively.

In the AMBT there is an inexhaustible supply of alkalis from the storage solution of 1M NaOH and high temperature of 80 °C. As a consequence, this test has been shown incapable of detecting expansion differences in mortars of varying cement alkali contents (Islam et al. 2016). CPT, which is generally accepted as the more reliable test method due to the lower temperature of 38 °C and fixed supply of alkali, is prone to alkali leaching. The reported leaching of alkali in concrete prisms for 1 year ranges from 25-35% (Rivard et al. 2007; Thomas et al. 2006) and even goes as high as 45% for a 2-year test period (Einarsdottir & Hooton 2018). This results in an underestimation of expansion and consequently, may indicate lower dosage of SCMs than required for effective mitigation in the field (Lindgård et al. 2012; Thomas et al. 2006; Thomas et al. 2007; Yamada et al. 2014); hence, the many efforts to prevent leaching and improve reliability of the CPT which, to date, remain unresolved (Costa, Mangialardi & Paolini 2017; Einarsdottir & Hooton 2018; Lindgård et al. 2013). Field studies, which are considered to be the most reliable, take very long time and require not only commitment but also abundant resources. For this reason, most countries, including Australia, do not have field exposure sites at present.

Due to the limitations of existing ASR test methods, this study uses an alternative method to assess the effect of cement alkalinity on the ability of SCMs to mitigate ASR. The test method, developed by the Laboratory of Construction Materials (LMC) at EPFL (Chappex et al. 2016), makes use of simulated pore solutions to assess the

efficacy of SCMs to mitigate ASR addressing the leaching issues in CPT and eliminating aggressive test conditions in AMBT (high temperature and excessive supply of alkalis). By studying the expansion of highly reactive aggregates in combination with SCMs (fly ash and slag) using the simulated pore solution method, the aim of this study is to determine if the SCMs at recommended dosages will work to mitigate ASR when used in conjunction with cement which has effective equivalent alkali content of 1% Na_2O_{eq}. In addition, this chapter also investigates the effect of SCM addition on calcium silicate hydrate (C-S-H) composition, alkali uptake in the C-S-H and ASR gel composition.

5.1 Extracted Pore Solution from Blended Pastes

Pastes with equivalent composition and water to cement ratio as the concrete prisms were prepared in sealed containers and cured for 28 days in a high humidity environment at 20±2 °C. Pastes with SCMs but no alkali boosting and with SCMs + 0.2% alkali boosting were also prepared. The pastes were then subjected to pore solution extraction at 28 days using 1500 kN force from a compression testing machine, the extracted solutions filtered with 0.2 µm membrane to remove solid residues and then analysed by inductively coupled plasma optical emission spectroscopy (ICP-OES) to determine the concentration of elements, calcium (Ca), aluminium (Al), silicon (Si), sodium (Na) and potassium (K) in the pore solution.

Figures 5-1 and 5-2 show the concentration of Al, Ca, K, Na, Si in the extracted pore solution at 28 days. The reported concentrations are in agreement with other studies that despite the alkalis being a very small percentage of the cement, they dominate the pore solution (Thomas 2011; Vollpracht et al. 2016; Weerdt, Haha, et al. 2011). Whereas, K concentration ranges from 0.10 to 0.27 mol/L and Na from 0.12 to 0.32 mol/L, other elements Ca, Al, and Si all have concentration lower than 0.003 mol/L. As the concentration of other elements are minor, only the alkali contents were considered for the simulated pore solution. Adding SCMs, in this case 25% fly ash or 50% slag, lowers the pore solution alkali concentration (Na^+ and K^+). 50% slag notably lowers the alkali concentration more than 25% fly ash. The effect of alkali boosting (by NaOH addition) can also be observed with Na concentration increasing with increasing level of boosting (from 0.2% to 0.4%). It is also worth noting from Figure 5-2 that aluminium in the pore solution increases with SCM addition, with 50% slag blended pastes demonstrating much higher aluminium contents in the pore solution than 25% fly ash blended pastes.

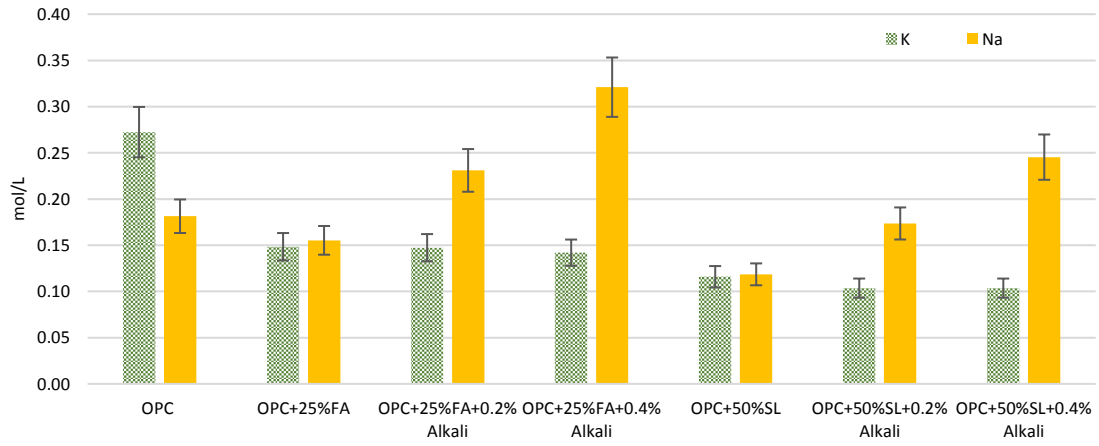

Figure 5-1 Concentration of sodium (Na) and potassium (K) in the pore solution at 28 days

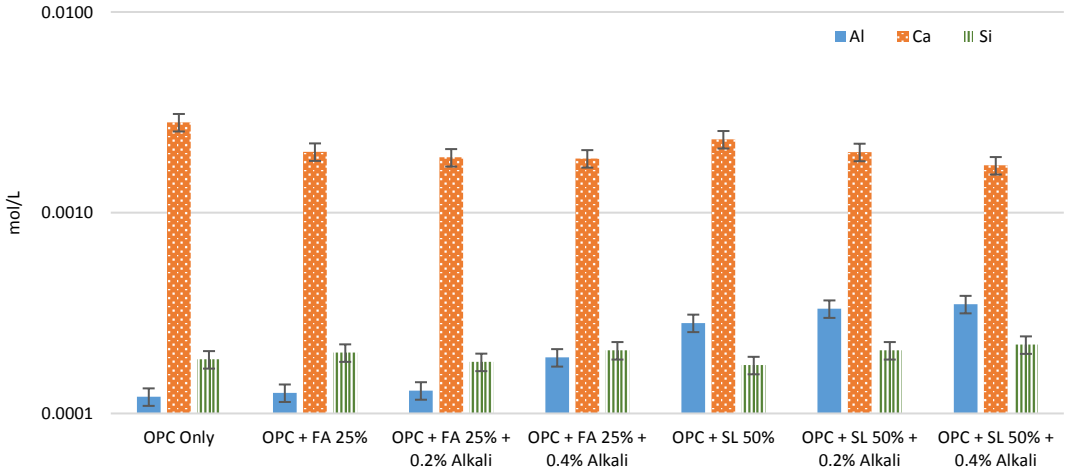

Figure 5-2 Plot of log of the concentration of aluminium (Al), calcium (Ca) and silicon (Si) in the pore solution at 28 days

Figure 5-3 shows the effect of age on the pore solution alkali concentration. For OPC, a slight increase in the concentration of both alkali cations from 28 days to 168 days can be observed. The increase in the concentration of Na and K in OPC with time has been reported in several studies (Lothenbach et al. 2008; Vollpracht et al. 2016; Weerdt, Haha, et al. 2011). The alkali concentration increases with time as alkalis continue to be released during the hydration of clinkers and as the volume of the liquid phase decreases (Lothenbach et al. 2008). For the pastes with SCMs, in general, a slight decrease in alkali concentration was observed from 28 days to 168 days. Although, taking into account the measurement error, the pore solution appears to be considerably stable after 28 days. The slight decrease observed can be attributed to SCM reactions and alkali binding in the hydration products (Thomas 2011).

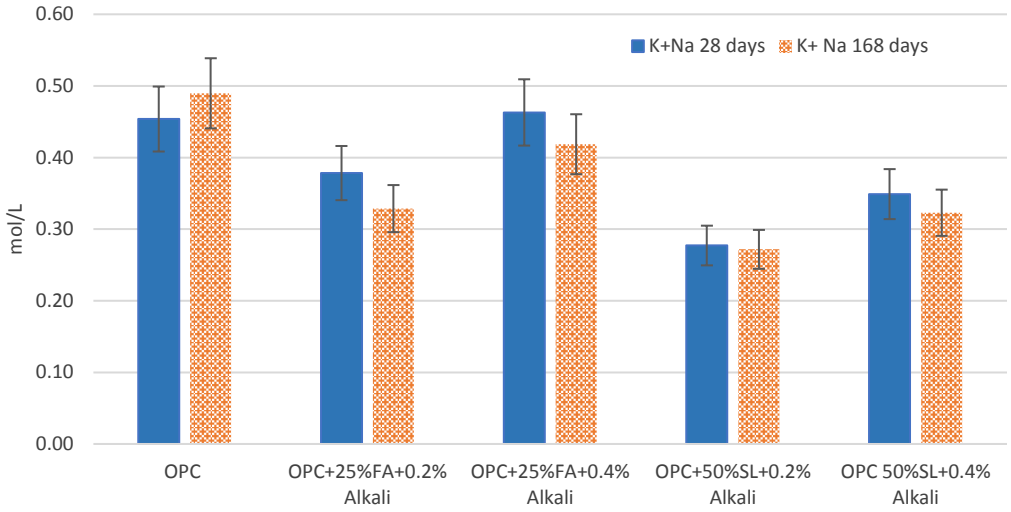

Figure 5-3 Effect of age on total alkali concentration in the pore solution

5.2 ASR Expansion of Concrete Prisms

Figure 5-4 shows the expansion data of prisms stored in simulated pore solution at 60 °C up to 12 months. Each point in the plot is an average of three expansion measurements. The error bars represent the standard deviation of the measurements. The simulated pore solution used to store the concrete prisms was prepared based on the alkali content (Na and K concentration) of the paste system corresponding to the binder of the concrete at 28 days. The results show that whereas the prisms with no SCMs have considerably expanded (both dacite and rhyolite aggregates), the prisms with SCMs (25% fly ash or 50% slag) even with cement boosted with 0.4% extra alkali (1% effective Na_2O_{eq}), do not show significant expansion. Therefore, the results demonstrate that the SCMs can mitigate even with cements of higher alkali contents.

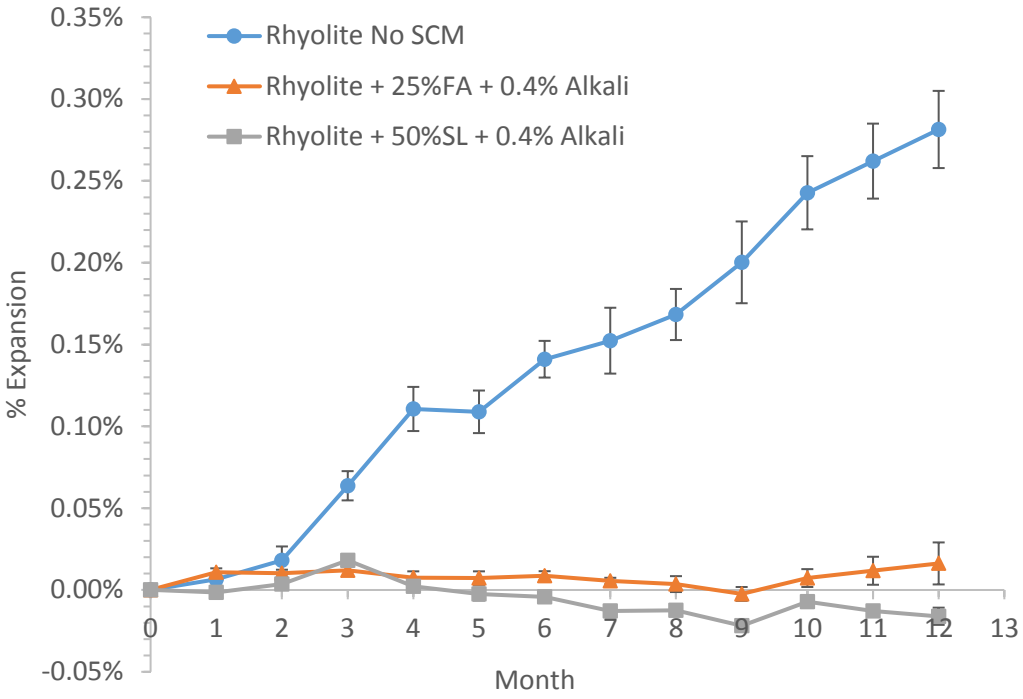

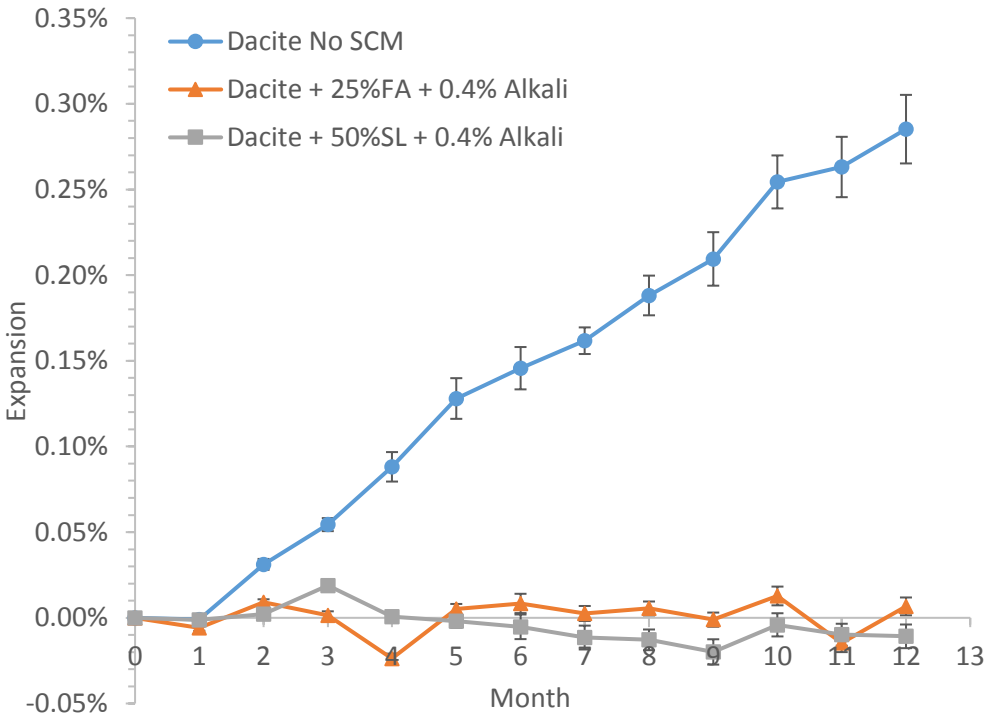

Figure 5-4 ASR expansion of rhyolite and dacite concretes stored at 60 ℃.

The expansion results are consistent with some field studies that confirmed the effectivity of SCMs when used in conjunction with high alkali cement (Hooton et al. 2013; Thomas et al. 2006; Thomas 1996; Thomas et al. 2011). The Lower Notch Dam in Ontario Canada made use of highly reactive greywacke-argillite coarse aggregates and high alkali cement (1.08% Na_2O_{eq}) in combination with 20% to 30% low CaO fly ash and showed no indications of ASR damage after more than 30 years of service (Thomas et al. 2006; Thomas 1996). Fly ash used at replacement levels of 25% and 40% is sufficient to inhibit both expansion and cracking in concrete blocks containing alkali-silica reactive aggregates, and high alkali cement (K_2O= 1.10%, Na_2O= 0.43%) on an outdoor exposure site in England for a period of up to 18 years (Thomas et al. 2011). Moreover, 50% slag used in concrete made with high-alkali cement (> 0.8%) and reactive Spratt aggregate also showed no sign of ASR or cracking after 20 years. Equivalent concrete with high alkali cement but no SCM cracked after 5 years (Hooton et al. 2013).

Figure 5-5 shows the expansion data of the dacite concretes stored at 38 °C up to 12 months. The concrete with no SCM shows high degree of expansion whereas no expansion can be observed for concrete mixes with SCMs similar to that observed for the 60 °C specimens. As is expected, lower temperature of 38 °C resulted in much lower expansion rate than 60 °C concrete prisms. Although the expansion results observed at both temperatures are in agreement, more time is needed (at least 2 years) to generate more conclusive results.

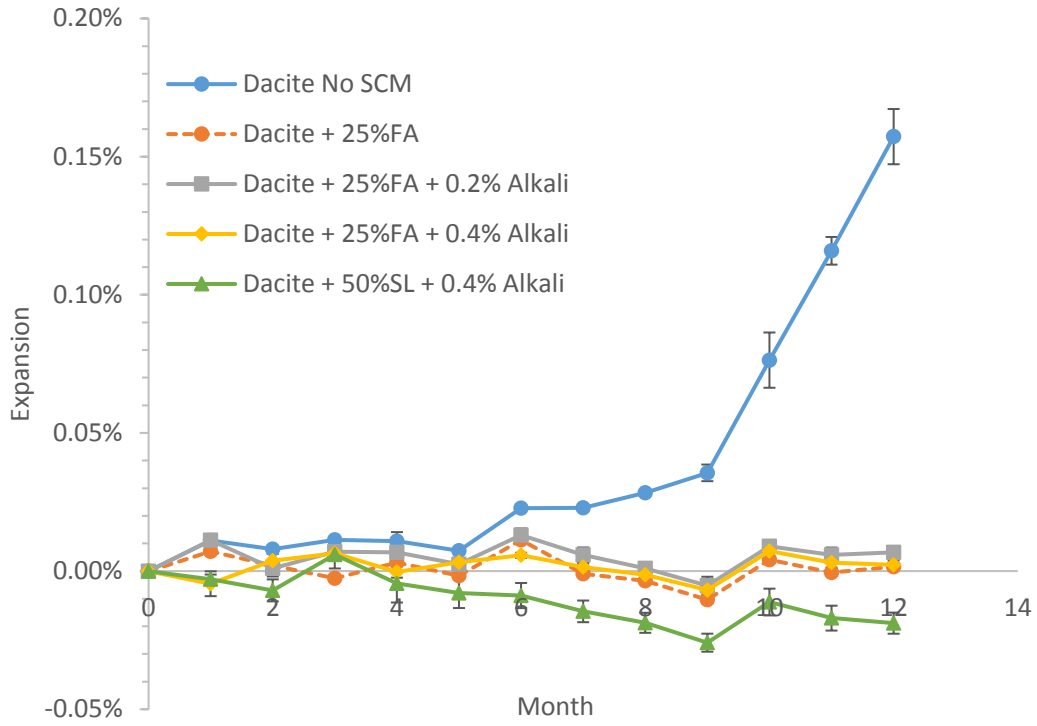

Figure 5-5 Expansion data of dacite concrete prisms stored at 38 ℃.

5.3 Morphology and Composition of the ASR Products

The 60 °C concrete specimens were sectioned to analyse the ASR products. Extensive cracking was observed in concrete specimens with no SCMs as can be seen from Figures 5-6 and 5-8. The ASR gel appears to originate from the interior of the aggregate extending towards the cement paste. The appearance and location of the gel are consistent with that reported in literature (Andreas Leemann 2017; Fernandes 2009; Leemann & Lothenbach 2008). Some cracks were found to not contain ASR gel and instead prominent black areas were observed. As all samples were subjected to

vacuum impregnation, the black areas are due to resin. Resin which is carbon-based material will emit no signal and therefore appear dark under backscattered electron (BSE) imaging. This indicates then that not all cracks are filled with ASR gel, and that some of the cracks observed may be a result of ASR gel expansion somewhere else (Andreas Leemann 2017; Fernandes 2009).

The EDS map of the ASR gel within an aggregate in Figures 5-7 and 5-9 show the presence of high amounts of calcium and alkali (Na and K) in the ASR gels. The high concentration of calcium (Ca) observed is consistent with the ASR gel being alkali calcium silicate hydrate (Andreas Leemann 2017; Fernandes 2009; Leemann et al. 2016; Leemann & Lothenbach 2008; Rajabipour et al. 2015). Some studies argue that the presence of calcium in the ASR gel is needed to facilitate cracking in concrete (Leemann et al. 2016; Leemann & Lura 2013). Essentially, calcium is able to precipitate the dissolved silicate species in solution. Moreover, since calcium is a cross-linking agent, it is able to increase stiffness of the gel which is critical for it to be able to exert stress (Leemann & Lura 2013). The actual role of calcium, however, is still not fully understood. Although higher calcium contents in the ASR gel reportedly results in higher stiffness (Leemann & Lura 2013), as the ASR gel becomes more rigid, it also decreases its swelling potential (Juenger & Ostertag 2004; Rajabipour et al. 2015).

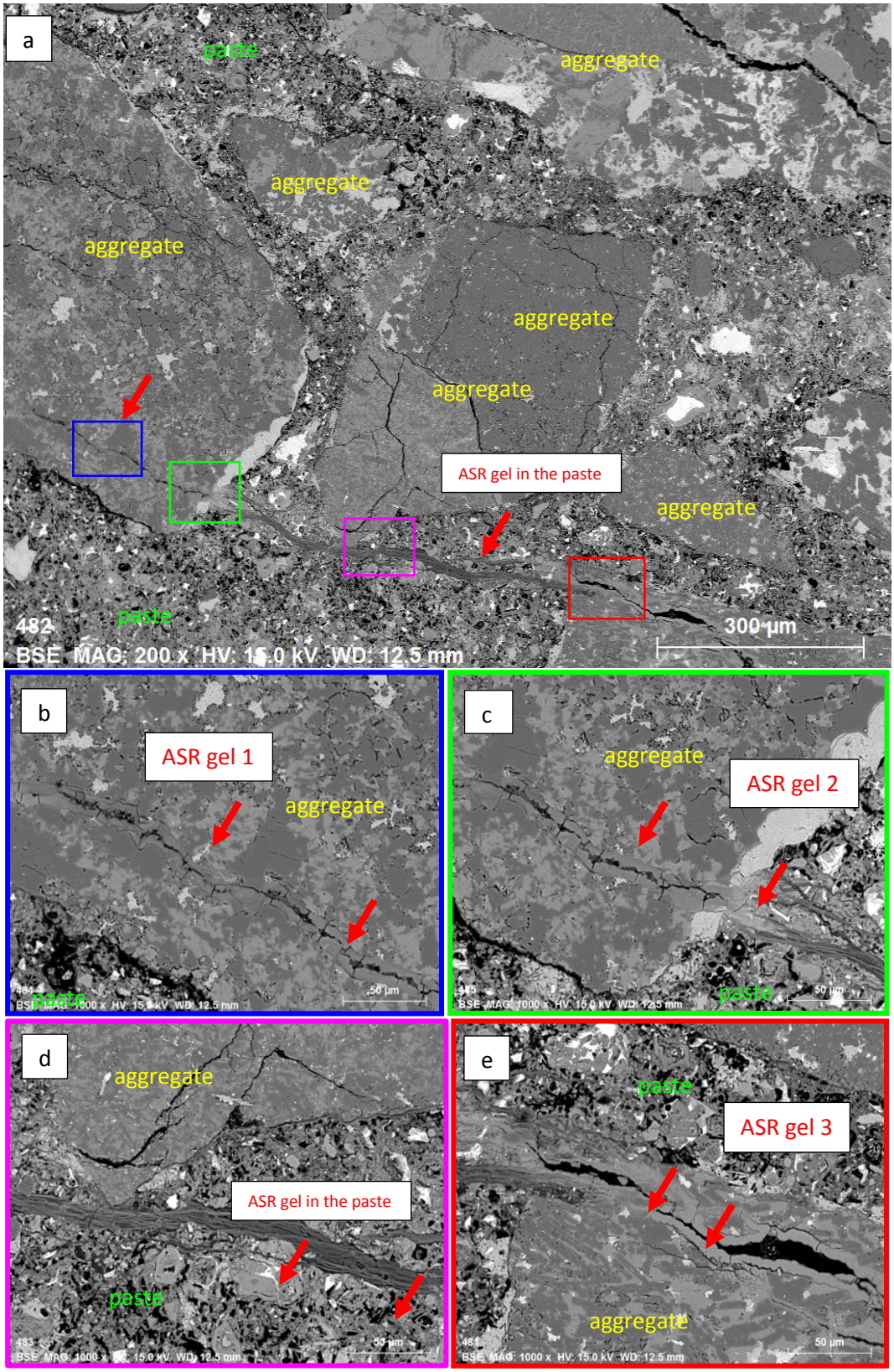

Figure 5-6 ASR gel found in Rhyolite concrete without SCM a) taken at 200x magnification and b,c, d and e) at higher magnification of 1000x

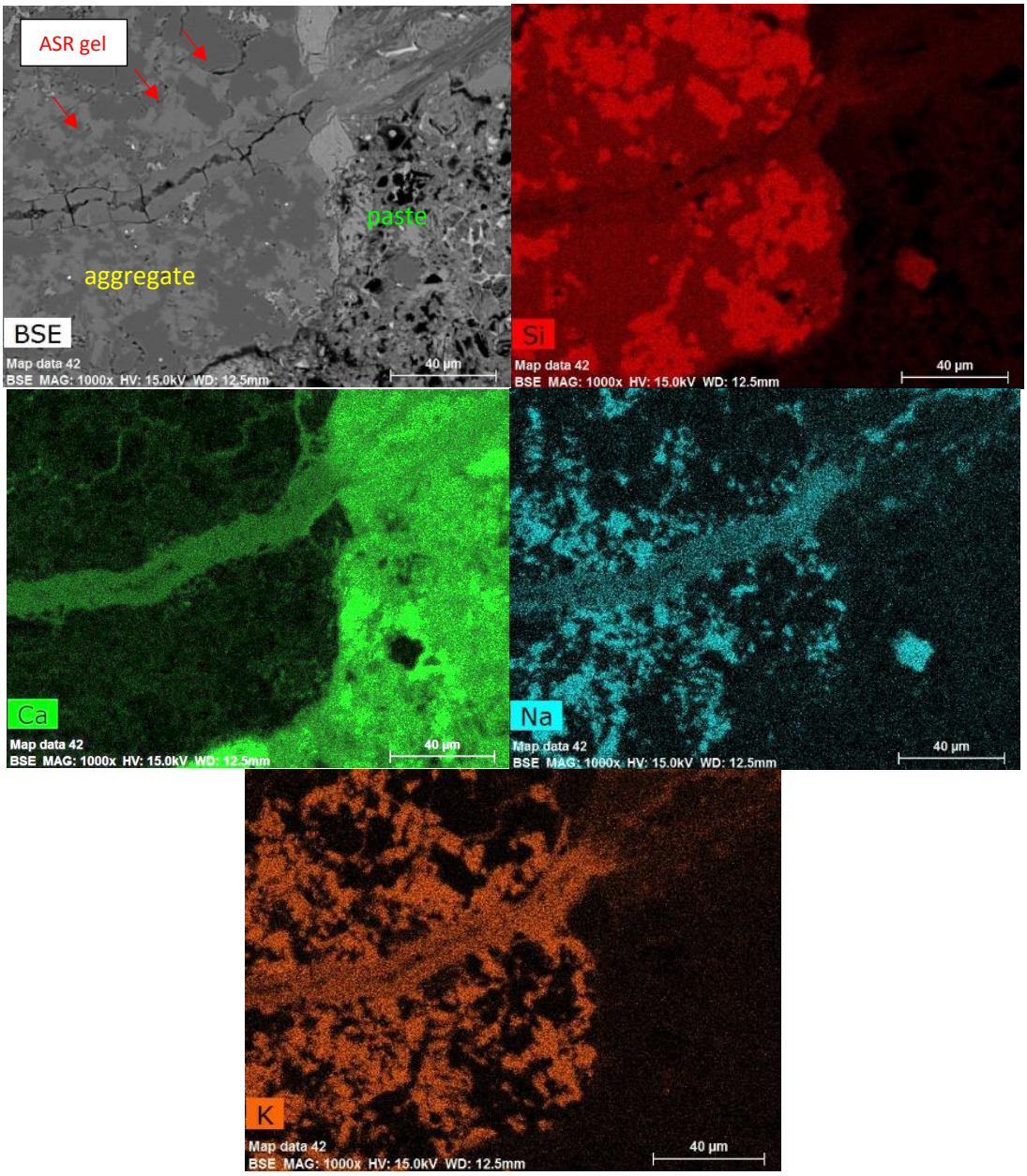

Figure 5-7 EDS map of the ASR Gel within an aggregate in Rhyolite concrete without SCM confirming high concentration of Si, Ca, Na and K in the gel

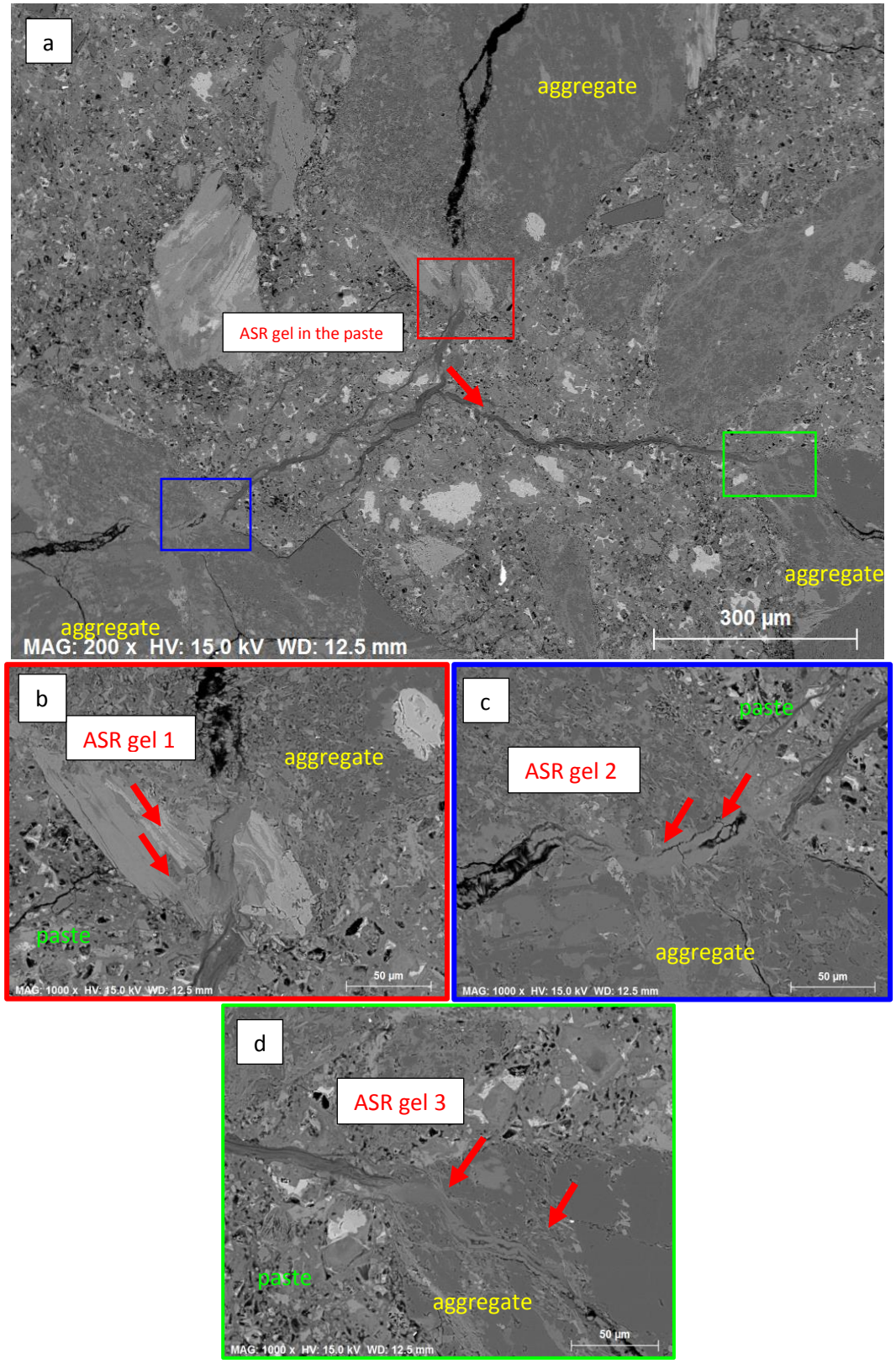

Figure 5-8 ASR gel found in Dacite concrete without SCM a) taken at 200x magnification and b,c and d) at higher magnification of 1000x

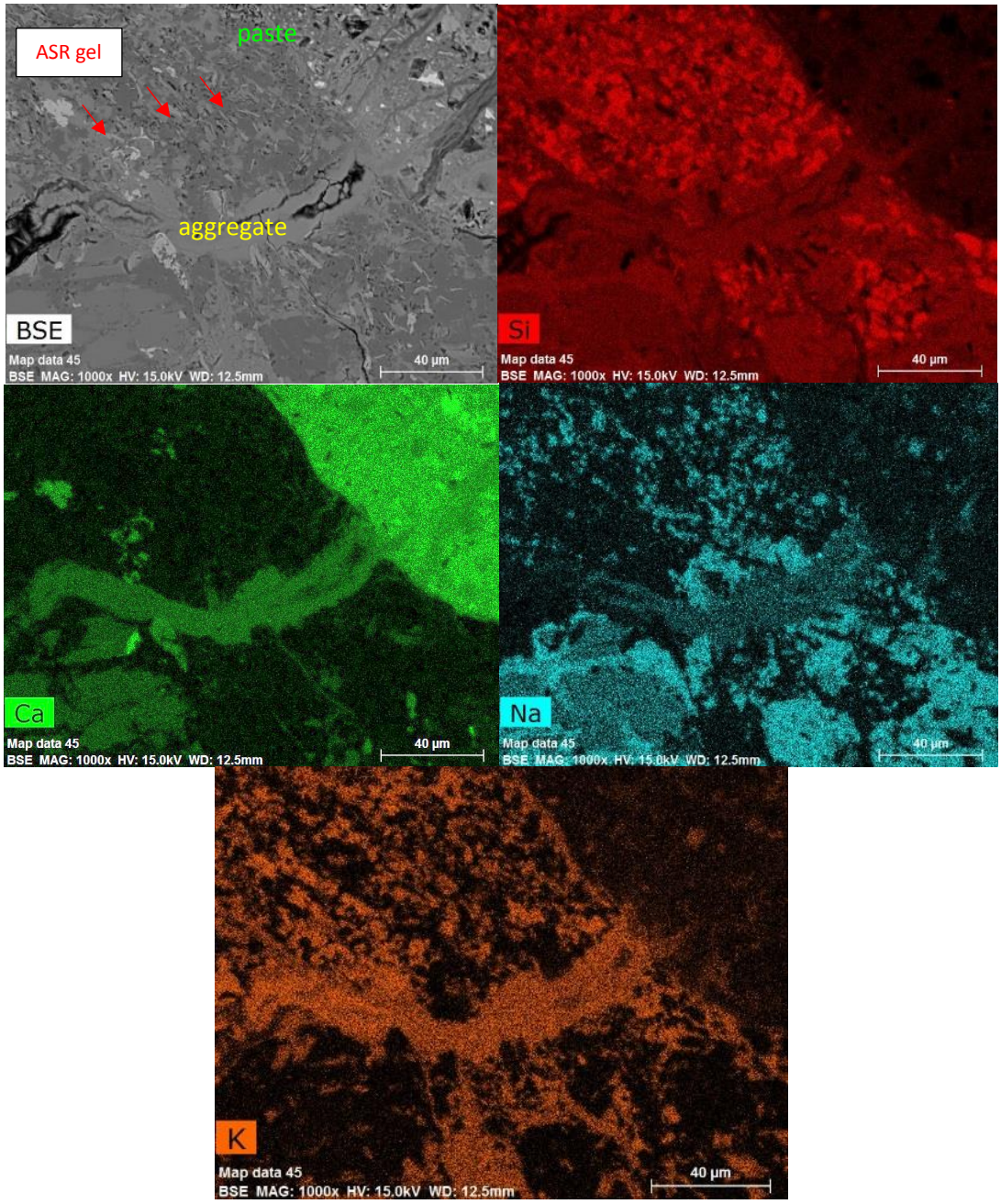

Figure 5-9 EDS map of the ASR gel within an aggregate in Dacite concrete without SCM confirming high concentration of Si, Ca, Na and K in the gel

Table 5-1 shows the elemental composition of the ASR gel in concrete without SCM depicted in Figures 5-6 and 5-8. Each reported value corresponds to an average of 10-15 EDS points. The Ca/Si ratio (0.29-0.32) and (Na+K)/Si ratio (0.30-0.37) of the

ASR gel found within the aggregate agrees with that reported in other studies (Andreas Leemann 2017; Leemann et al. 2016; Leemann & Merz 2013; Thaulow, Jakobsen & Clark 1996). No significant difference was noted in the composition of the ASR gel from both types of aggregates. Although, the gel traversing along the cement paste was found to have higher Ca/Si ratio of 1.26 and lower Na+K/Si of 0.11. Several other studies have also reported that ASR gel composition varies as a function of its location in the concrete. In general, the silicon content of the gel decreases and calcium content increases as it moves closer in contact with the cement paste (Bleszynski & Thomas 1998; Fernandes 2009; Scrivener & Monteiro 1994; Shia et al. 2019; Thaulow, Jakobsen & Clark 1996). Leeman et al. reported that the change in composition of the ASR products extruding further into the cement paste is significant. Within a few tens of micrometres, the Ca/Si-ratio increases up to 1.3 which is similar to what was observed in this study (Andreas Leemann 2017). Bleyszynski et al. likewise reported the Ca/Si ratio to be approximately 1.0 or slightly greater at the interface and to decrease to about 0.25 towards the center of the reacted particle away from the interface (Bleszynski & Thomas 1998).

The Ca/Si ratio of the ASR gel found in the cement paste is very close to typical C-S-H (Chappex & Scrivener 2012a; Chappex & Scrivener 2012b; Gallucci, Zhang & Scrivener 2013; Scrivener & Monteiro 1994; Thaulow, Jakobsen & Clark 1996). The change in composition occurs because the calcium ions are preferentially adsorbed by the gel over alkali ions. Since the calcium ions replace the alkali in the ASR gel, a much lower alkali content in the ASR gel with increasing calcium content is expected (Leemann et al. 2011). This is consistent with earlier studies which cited lower alkali contents in the ASR gel located in the cement paste area (Andreas Leemann 2017;

Scrivener & Monteiro 1994). This also agrees with observations in the current study where the high alkali concentration terminates close to the aggregate edge and does not extend towards the paste (Figures 5-7 and 5-9 EDS maps). Thus, it can be inferred that Ca content of the ASR gel is a result of a reaction between the gel and paste, and therefore a function of the location of the gel and time available for reaction (Scrivener & Monteiro 1994; Thaulow, Jakobsen & Clark 1996).

In the concrete with SCMs it was also possible to find, very occasionally deposits of gel despite having no significant expansion (Figure 5-10). The cracking observed for concrete with SCMs was also very little compared to concrete prisms without SCM. Moreover, the crack width was much narrower, with thicknesses typically of maximum 5μm in contrast to the veins of about 20 μm in concrete with no SCMs (Figures 5-6 and 5-8). The EDS maps of the gels in Figures 5-11 and 5-12 show that the main constituents of ASR gel in concrete with SCMs are also Si, Ca, K and Na.

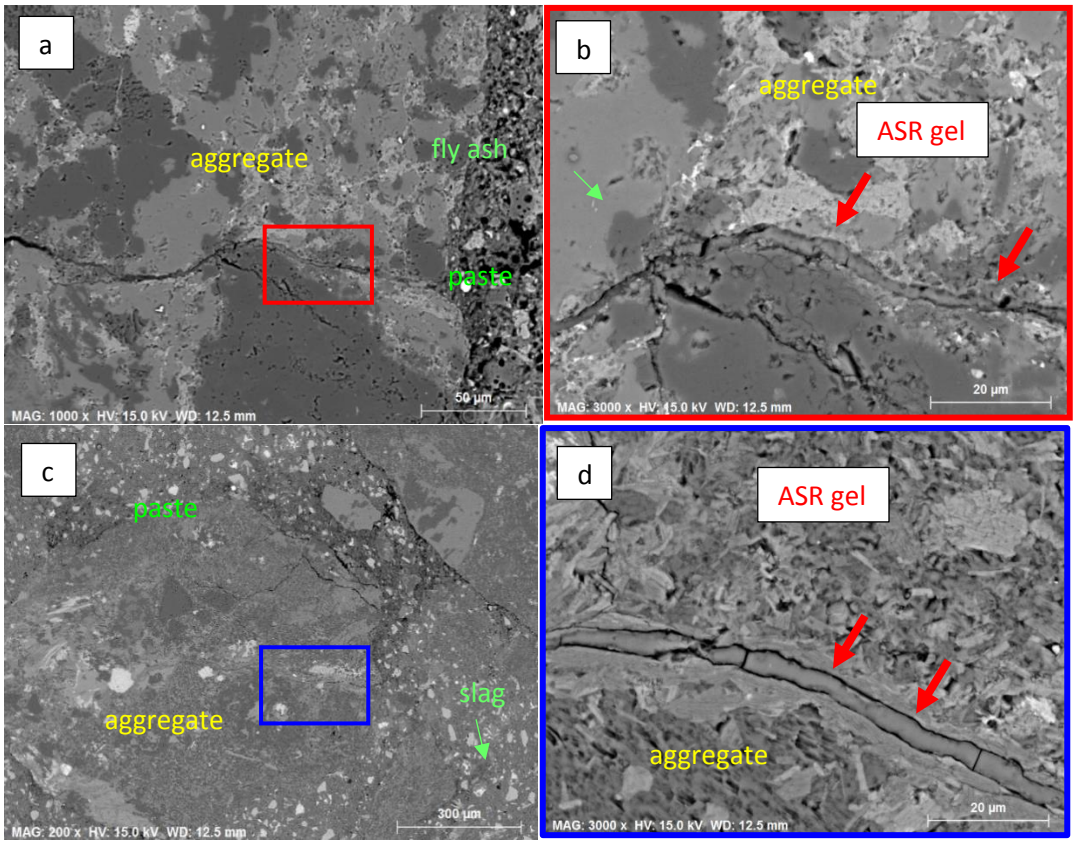

Figure 5-10 ASR gel observed in concrete with SCMs a, b) Rhyolite + 25% FA + 0.4% Alkali and c, d) Dacite + 50% SL + 0.4% Alkali

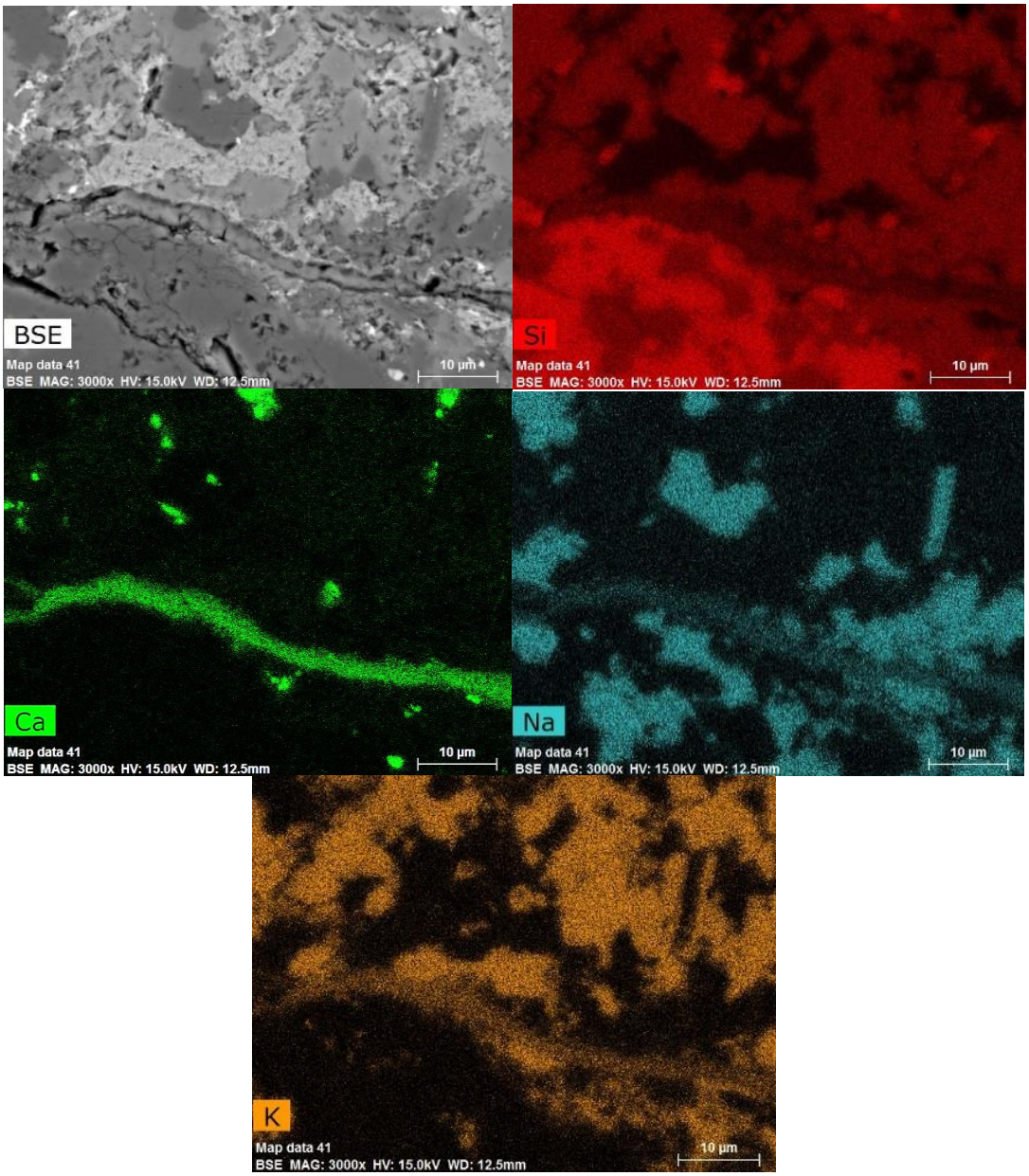

Figure 5-11 EDS map of the gel within an aggregate in Rhyolite concrete with 25% fly ash and 0.4% alkali boosting confirming high concentration of Si, Ca, Na and K in the gel

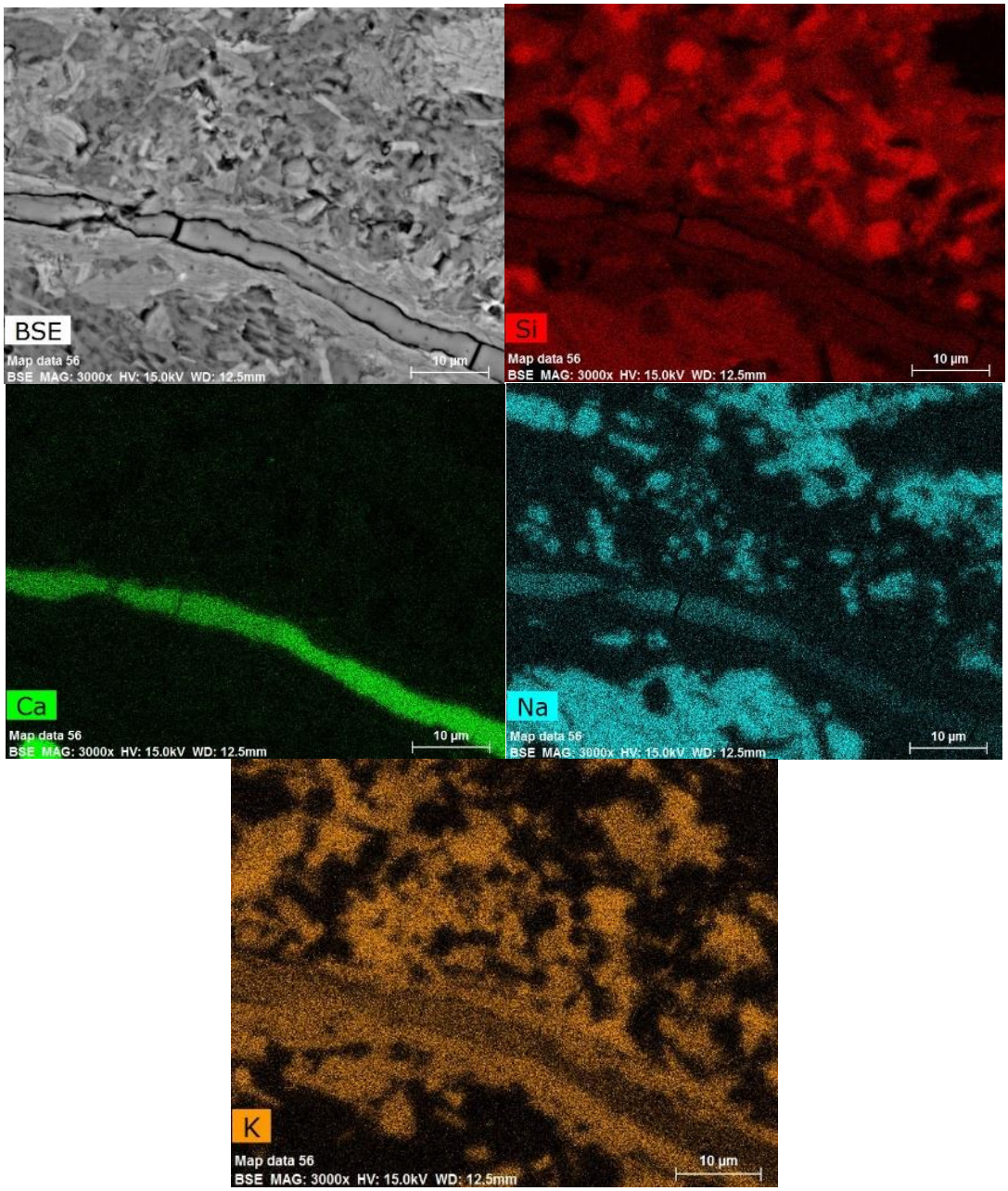

Figure 5-12 EDS map of ASR gel within an aggregate in Dacite concrete with 50% slag and 0.4% alkali boosting confirming high concentration of Si, Ca, Na and K in the gel

Table 5-2 shows the composition of ASR gel found in concrete with SCMs normalized without oxygen. At least 2 ASR gel was considered per system to better illustrate the trend. The gel compositions are plotted in the CaO, SiO_2, $(Na+K)_2O$ system in Figure

5-13. Silicon is the main component of the gel, with low contents of potassium and sodium (Fernandes, Noronha & Teles 2007). For these elements, the compositions of the ASR gel are very similar for concrete with and without SCMs, but in the complete analyses (Tables 5-1 and 5-2), it can be seen that much higher aluminium was detected in the ASR gel found in concrete with SCMs. This observation agrees with a recent study which reported higher amounts of aluminium (Al) in the ASR gels found in geopolymer mixtures (fly and slag geopolymers) compared to that in plain OPC mortar (Mahanama et al. 2019). In this study, the gels were also observed to be present even when there was little or no indication of expansion.

The aluminium in the ASR gel potentially plays a role in ASR mitigation, although its clear role at this point is still unknown. Its notable presence in the gel may be a consequence of increased concentration of aluminium in the pore solution due to the presence of SCMs. Several studies have reported on the role of aluminium in ASR mitigation. Aluminium is proposed to suppress ASR by inhibiting dissolution of reactive silica (Bickmore et al. 2006; Chappex & Scrivener 2012b; Chappex & Scrivener 2013). Aluminium adsorbs into the silicate framework, forming the negatively charged aluminosilicate surface sites that repel OH^- ions and thus making them highly stable in alkali environment (Chappex & Scrivener 2012b). It was reported that $Al(OH)_4^-$ depressed the dissolution rate of quartz and this is due $Al(OH)_4^-$ and Na^+ co-adsorbing on silanol sites and passivating the surrounding quartz surface (Bickmore et al. 2006). The reductions in alkalinity also remain stable when alumina-bearing SCMs such as fly ash and slag are used, possibly due to the formation of C-A-S-H which is reported to better retain alkalis than C-S-H (Lothenbach, Scrivener & Hooton 2011b). When Al substitutes for Si in the C-S-H, this creates a

charge deficit, which is charge balanced by the incorporation of a monovalent cation such as Na^+ or K^+ (Skibsted & Andersen 2013). This, in turn, results in better binding of the alkalis.

Table 5-1 EDS composition of the ASR gel in concrete without SCM

ASR Gel Location		Elements (atomic wt%)							
		Ca	**Si**	**Al**	**Na**	**K**	**Na+K**	**Ca/Si**	**(Na+K)/Si**
Rhyolite No SCM	ASR Gel 1	18.03 ± 1.14	61.87 ± 0.94	1.32 ± 0.20	7.27 ± 0.32	11.51 ± 0.73	18.78 ± 0.79	0.29 ± 0.06	0.30 ± 0.04
	ASR Gel 2	19.53 ± 0.76	60.96 ± 0.59	1.04 ±0.27	6.60 ± 0.21	11.88 ± 0.54	18.48 ± 0.50	0.32 ± 0.04	0.30 ± 0.03
	ASR Gel 3	19.21 ± 0.79	60.60 ± 0.62	1.20 ±0.13	6.82 ± 0.25	12.17 ± 0.55	18.99 ± 0.53	0.32 ± 0.04	0.31 ± 0.03
	ASR Gel in the paste	50.79 ± 1.84	40.28 ± 0.83	4.63 ± 0.17	3.03 ± 0.47	1.27 ± 0.29	4.30 ± 0.74	1.26 ± 0.17	0.11 ± 0.04
Dacite No SCM	ASR Gel 1	18.03 ± 0.97	59.04 ± 1.01	1.14 ± 0.19	8.50 ± 0.53	13.29 ± 0.72	21.79 ± 1.08	0.31 ± 0.05	0.37 ± 0.06
	ASR Gel 2	17.92 ± 1.00	60.51 ± 1.56	0.99 ± 1.87	1.43 ± 0.62	19.15 ± 0.81	20.58 ± 0.74	0.30 ± 0.04	0.34 ± 0.04
	ASR Gel 3	18.87 ± 2.06	59.04 ± 0.83	1.06 ± 0.82	7.95 ± 0.44	13.08 ± 0.36	21.03 ± 0.74	0.32 ± 0.16	0.36 ± 0.05

Table 5-2 EDS composition of the ASR gel in Concrete with SCM

ASR Gel Location		Elemental Analysis (atomic wt%)							
		Ca	Si	Al	Na	K	Na+K	Ca/Si	(Na+K)/Si
Rhyolite + 25% FA + 0.4% Alkali	ASR Gel 1	16.18 ± 0.76	57.14 ± 0.89	6.06 ± 0.44	10.21 ± 0.72	10.40 ± 0.72	20.61 ± 0.73	0.28 ± 0.04	0.36 ± 0.05
	ASR Gel 2	18.11 ± 1.51	58.83 ± 0.97	4.92 ± 0.39	8.77 ± 0.47	9.37 ± 0.77	18.14 ± 0.58	0.31 ± 0.09	0.31 ± 0.04
Rhyolite + 50%SL + 0.4% Alkali	ASR Gel 1	21.87 ± 0.75	54.05 ± 0.66	6.89 ± 0.12	8.12 ± 0.05	9.07 ± 0.66	17.19 ± 0.72	0.40 ± 0.05	0.32 ± 0.04
	ASR Gel 2	27.54 ± 1.76	56.31 ± 0.84	3.91 ± 1.17	5.94 ± 0.35	6.30 ± 1.05	12.24 ± 1.10	0.49 ± 0.08	0.22 ± 0.06
Dacite + 25%FA + 0.4% Alkali	ASR Gel 1	20.45 ± 1.32	60.00 ± 0.85	4.13 ± 0.94	4.53 ± 0.15	10.88 ± 0.59	15.42 ± 0.60	0.34 ± 0.06	0.26 ± 0.02
	ASR Gel 2	19.12 ± 0.91	61.61 ± 1.14	3.87 ± 1.52	3.88 ± 0.35	11.52 ± 0.61	15.40 ± 0.59	0.31 ± 0.04	0.25 ± 0.03
Dacite + 50%SL + 0.4% Alkali	ASR Gel 1	21.82 ± 0.85	57.98 ± 0.91	3.87 ± 0.54	7.16 ± 0.23	9.17 ± 0.69	16.33 ± 0.71	0.38 ± 0.05	0.28 ± 0.04
	ASR Gel 2	24.62 ± 1.46	56.56 ± 1.09	3.27 ± 0.58	7.98 ± 0.70	7.57 ± 0.51	15.55 ± 1.08	0.44 ± 0.09	0.27 ± 0.04

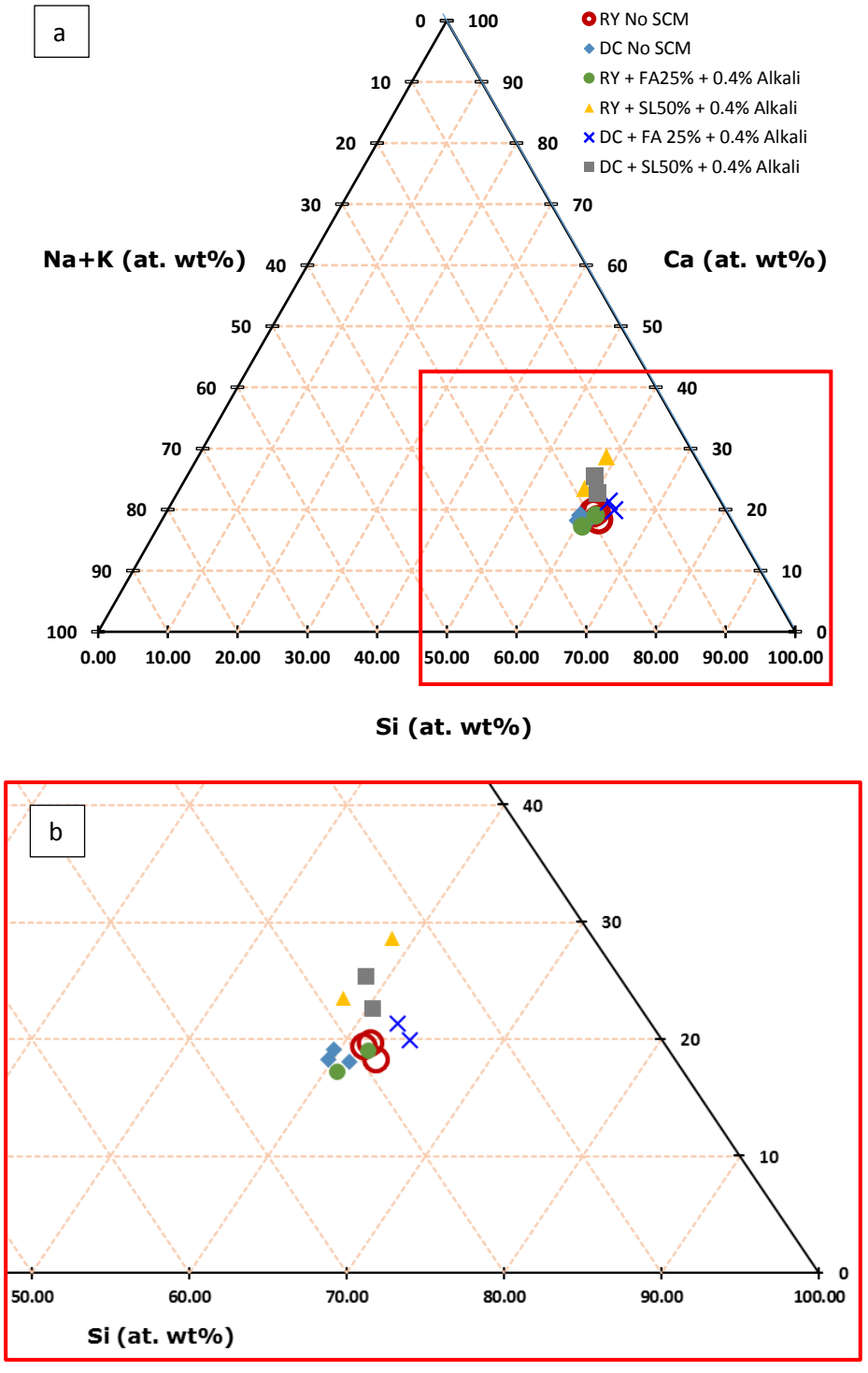

Figure 5-13 Ternary diagram showing ASR gel composition shown in a) full and in b) reduced area to show spread of data

5.4 Effect of SCM Type on C-S-H Composition and Alkali Uptake

Figure 5-14 shows the effect of SCM addition on the C-S-H composition. EDS scatter plots show that the concrete with SCMs (regardless of aggregate type) exhibit higher Si/Ca and Al/Si ratios than concrete with no SCMs. This result is consistent with studies of fly ash and slag blended pastes which reported increase in Si/Ca and Al/Si ratio with increasing SCM replacement levels (Deschner et al. 2013; Lothenbach, Scrivener & Hooton 2011a; Taylor, Richardson & Brydson 2010).

The addition of 25% fly ash and 50% slag results in almost equivalent Si/Ca ratio. However, the 50%SL concrete showed higher Al/Si ratios that the 25%FA concrete. This observation is consistent with slightly elevated concentrations of aluminium in the pore solution of 50% slag than 25% fly ash blended pastes reported in Fig. 3. Due to the ASR mitigating effects of aluminium (Bickmore et al. 2006; Chappex & Scrivener 2012b; Chappex & Scrivener 2013), the higher Al/Si ratio in 50% slag concrete therefore suggests that its effect on ASR mitigation may be more in the long term than 25% fly ash concrete.

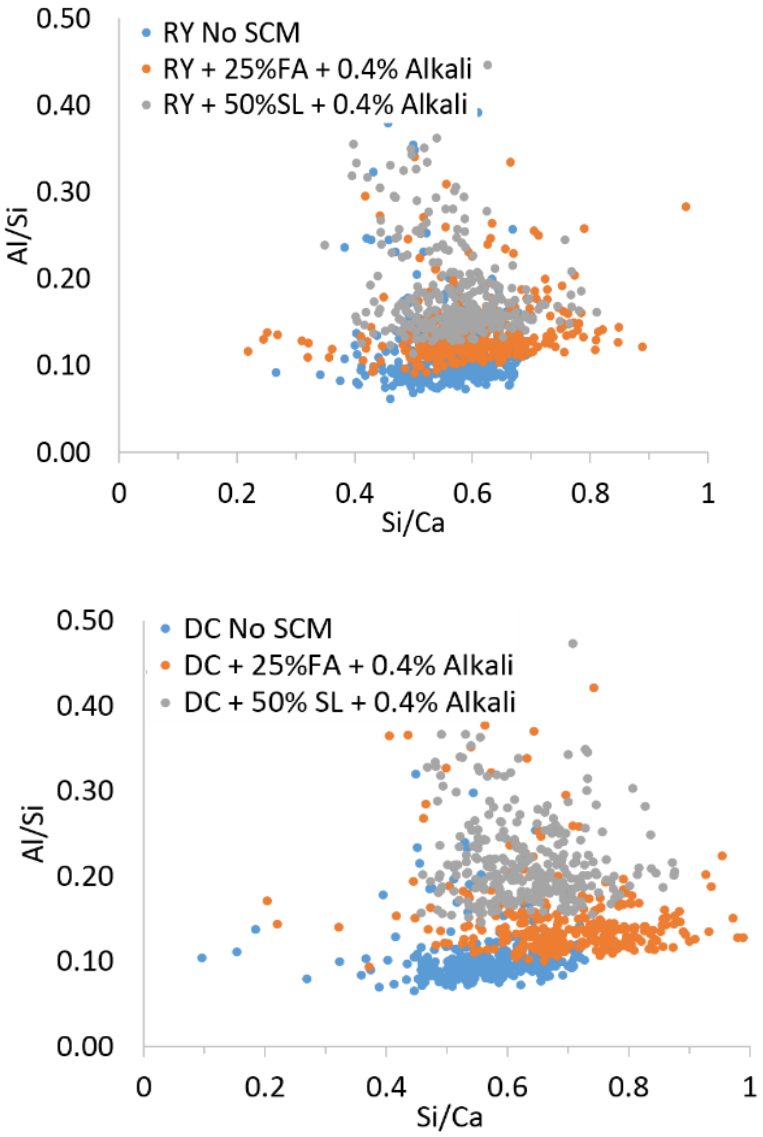

Figure 5-14 Effect of fly ash and slag addition on the Al/Si and Si/Ca of the C-S-H

The modification of C-S-H composition with SCM addition affects the alkali uptake as shown in Figures 5-15 and 5-16. The plots clearly demonstrate that SCM addition increases the amount of alkali (Na+K) in the C-S-H. C-S-H phases with higher Si/Ca ratio have higher alkali binding capacity (Duchesne & Berube 1994b; Hong & Glasser 1999; L'Hôpital et al. 2016). There is no notable difference in the alkali uptake of concrete with 25% fly ash or 50% slag, and this is possibly due to their comparable Si/Ca ratio.

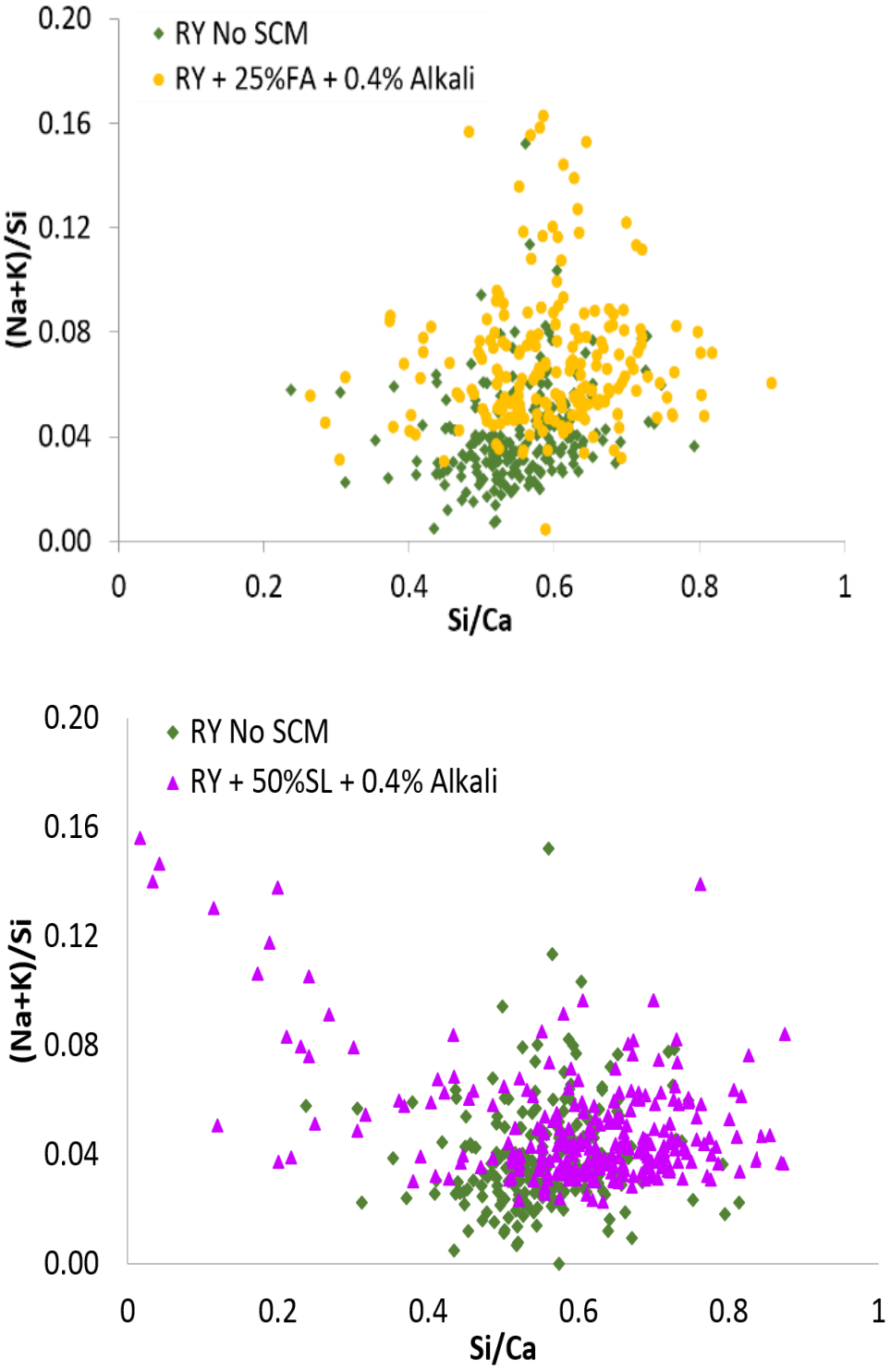

Figure 5-15 Effect of SCM addition on the alkali uptake in the C-S-H for Rhyolite concrete

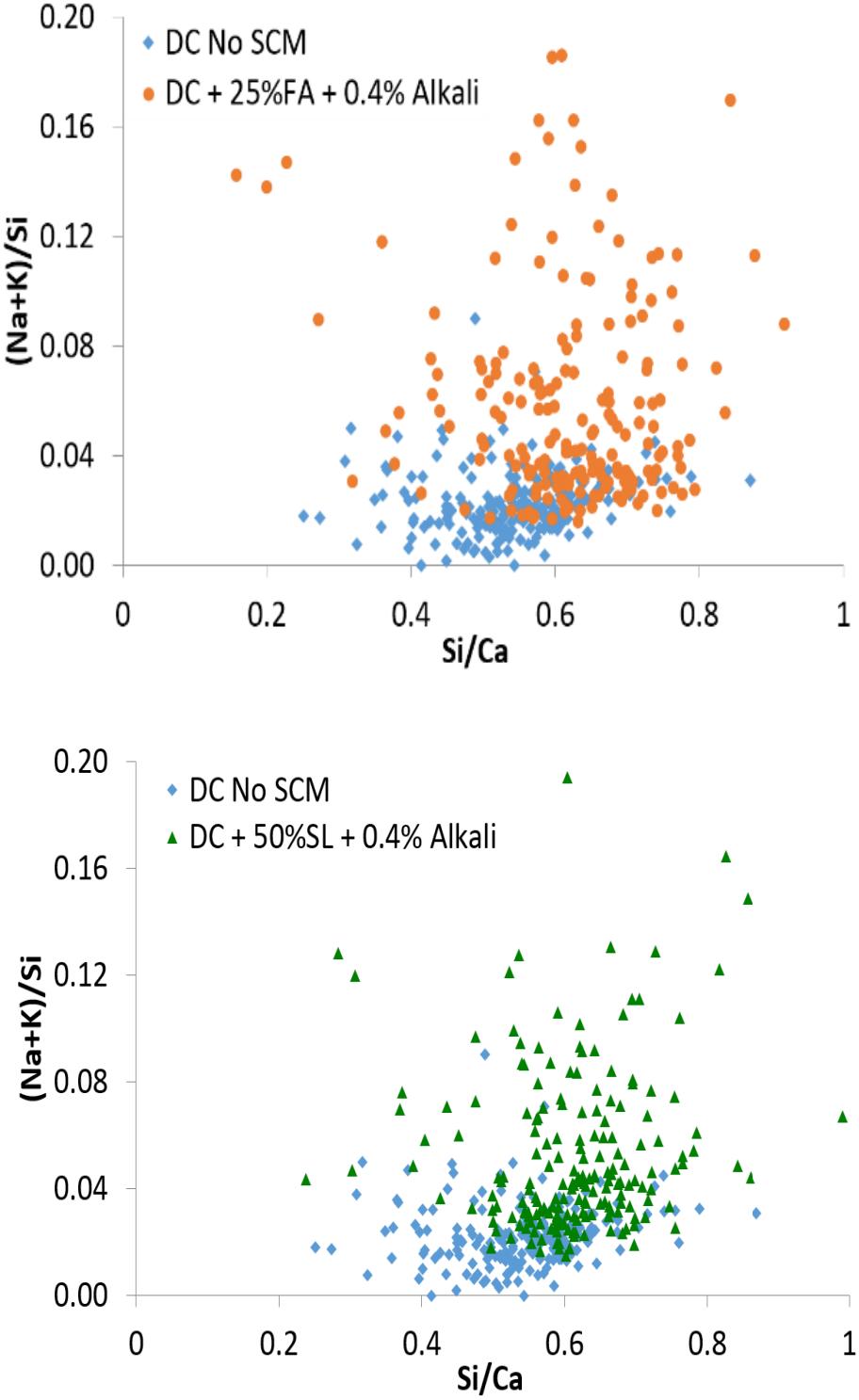

Figure 5-16 Effect of fly ash addition on the alkali uptake in the C-S-H for Dacite Concrete

5.5 Summary of Findings

This study investigated the ability of Australian SCMs to mitigate ASR at recommended dosages when the effective cement alkali content is raised to 1% Na_2O_{eq} from original alkali content of 0.6% Na_2O_{eq}. To avoid excessive alkali associated with AMBT, and leaching in CPT, simulated pore solution prepared based on the pore solution alkali concentration at 28 days was used as a storage solution.

Significant findings are as follows:

1. The expansion results show that, whereas, the concretes with no SCM have significant expansion after 12 months at 60 °C and at 38 °C, the concrete mixes with SCMs (either 25% fly ash or 50% slag) have no expansion. Results therefore suggest that Australian recommended SCM dosages are sufficient to mitigate ASR even with cement alkali content of 1% Na_2O_{eq}.

2. SEM images show extensive cracking in the concrete without SCM. ASR gel was also observed in extensive quantity. The gel seems to originate from aggregate interior and extends towards the cement paste. The concrete with SCMs, although it did not manifest expansion, also showed the presence of small amounts of ASR gel in thin cracks.

3. The composition of the ASR gel inside an aggregate in concretes with no SCM are comparable regardless of type of aggregate and agrees to that reported in other studies.

The ASR gel composition is about 60% Si, 20% Ca and 20% Na+K. The Na and K contents are almost equivalent.

4. The ASR gel in concrete with SCMs appears to have higher aluminium contents than concrete with no SCMs. The presence of aluminium in the gel is likely a consequence of increased aluminium in the pore solution. The effect of aluminium on gel properties remains to be further investigated.

5. ASR gel in the paste has higher calcium content than ASR gel inside an aggregate, and this is likely due to access to calcium in the pore solution. The composition of the gel in the paste is, in fact, comparable to that of C-S-H.

6. The C-S-H composition was observed to shift with SCM addition (fly ash or slag) towards increasing Si/Ca and Al/Si ratio. Alkali uptake in the C-S-H increased with SCM addition. Increase in alkali uptake results in lower pore solution alkali concentration.

6 Influence of Limestone on the Efficacy of SCMs in ASR Mitigation

Cement production results in substantial amount of carbon dioxide (CO_2) emissions. Calcination of limestone in order to produce cement clinker accounts for about 60% of CO_2 emissions at a cement plant (Scrivener, John & Gartner 2016). The CO_2 emissions result from the release of CO_2 from $CaCO_3$ as well as from burning of fossil fuels to heat the kiln. Addition of supplementary cementitious materials (SCMs), such as in the case of blended cements, has the potential to reduce the economic and environmental impact of cement-based construction materials. Most commonly used SCMs, fly ash and slag, are however industrial by-products and increasingly becoming scarce resources (Scrivener, John & Gartner 2016). Thus, the need to explore alternative materials for blending into cement.

Limestone is an abundant natural resource and its addition to cement offers a potential route to reducing the CO_2 emissions associated with cement production through partial substitution. General Purpose (GP) cement is the most common commercially used cement in Australia and accounts for over 85% of the total cement market for production of concrete (Mohammadi & South 2016a). The current allowable mineral addition in the Australian Standard AS 3972 for Type GP cement is 7.5%. Due to the potential environmental benefits of increased limestone addition, there is a drive to increase limestone content in Australian GP cement from 7.5% to 12% (Mohammadi & South 2016a). Whereas, the effect of limestone on various properties of concrete has been widely investigated (Lollini, Redaelli & Bertolini 2014; Mohammadi &

South 2016b; Schmidt et al. 2009; Tsivilis et al. 2000; Tsivilis et al. 2003), its effect on alkali-silica reaction (ASR) and on the efficacy of SCMs in mitigating ASR is still not fully understood.

The available literature on the effect of limestone addition on ASR is limited and in disagreement. Limestone has been reported to have either no effect on ASR acting as an inert diluent (Tennis, Thomas & Weiss 2011; Thomas et al. 2013) or to aid in ASR mitigation (Hooton, Nokken & Thomas 2007; Rajbhandari 2010). At the extreme, limestone has been reported to mitigate ASR more effectively than Class F fly ash (Turk, Kina & Bagdiken 2017), while synergistic effects of limestone with fly ash have also been recently reported to result in better ASR mitigating properties (Wang, Wu & Mei 2019), although, in the latter case the elevated SiO_2 content of the limestone powder (15.71%) is likely to have played a role in mitigation. Purity of the limestone used is, therefore, critical in ensuring that mitigation observed in laboratory studies is due to the limestone itself and not other constituents. The Australian standard, for instance, requires only 75% $CaCO_3$ content in minerals to meet the criteria as suitable limestone mineral addition (AS 3972).

The reported ability of limestone to mitigate ASR is largely attributed to cement dilution (Hooton, Nokken & Thomas 2007; Rajbhandari 2010), to limestone providing additional sites for nucleation resulting in microstructural densification, and to the formation of monocarboaluminates when limestone is present in cement (Chen & Yang 2013). Calcite ($CaCO_3$) present in limestone reacts with aluminate phases in the cement to form monocarboaluminates resulting in a more dense microstructure and an increase in compressive strength (Bonavetti et al. 2003; Bonavetti, Rahhal & Irassar

2001; Tennis, Thomas & Weiss 2011; Thomas et al. 2013; Voglis et al. 2005). The reaction is limited, however, by the amount of alumina available to react with calcite and above a certain replacement level, excess limestone (calcite) may result in degradation of concrete properties (Ramezanianpour & Hooton 2014; Scrivener et al. 2018).

This chapter investigates the effect of limestone on ASR expansion by accelerated mortar bar test (AMBT). The effect of limestone on portlandite amount, pore solution alkalinity and composition of the C-S-H were also investigated and correlated with expansion results. The effect of AMBT conditions on the microstructure of limestone-blended pastes is also reported.

6.1 Effect of Limestone on ASR Expansion

The ground limestone used in this work is of 98% calcite ($CaCO_3$) content as confirmed by XRF and TG results in Chapter 3. Series of AMBT tests based on AS 1141.60.1 using reactive greywacke aggregates were carried out to assess the effect of limestone on ASR expansion for mortars with and without SCMs (fly ash and slag). The ground limestone was added to GP cement with 0% limestone at increments of 8%, 12% and 17%. Fly ash and slag were substituted at levels typically used for ASR mitigation (Standards Australia 2015). The absence of calcite in the 0% limestone GP cement was also verified by TG.

AMBT expansion results in Figure 6-1a of mortars with no SCMs show identical behaviour (i.e. similar expansion rate) suggesting that limestone in the binder up to 17% has no influence on ASR. A similar behaviour can also be observed in the mortar with SCMs. Figure 6-1b and 1c, which contain 25% fly ash and 65% slag respectively, show negligible expansion regardless of limestone content which indicates that the SCMs are effectively mitigating ASR. The addition of limestone up to 17% appears to have no influence on the mitigating action of the SCMs. Note that each point in the AMBT plot represents the average expansion of three mortars. The error bars are however too small to be visible in the AMBT plots with the exception of Figure 6-1a.

Another set of AMBT runs in Figure 6-2 and Figure 6-3 shows the effect of increasing fly ash and slag replacement levels on mortar expansion of greywacke AMBT specimens when the level of limestone in cement is constant. Similarly, the error bars are also too small to be visible in the plots. The results show that regardless of the levels of limestone in the samples, a minimum replacement level of 15% for fly ash and 35% for slag is sufficient to mitigate ASR expansion and the expansion was observed to further reduce as the SCM content increases. Thus, up to 17% cement limestone content, the SCMs are fully effective in suppressing ASR.

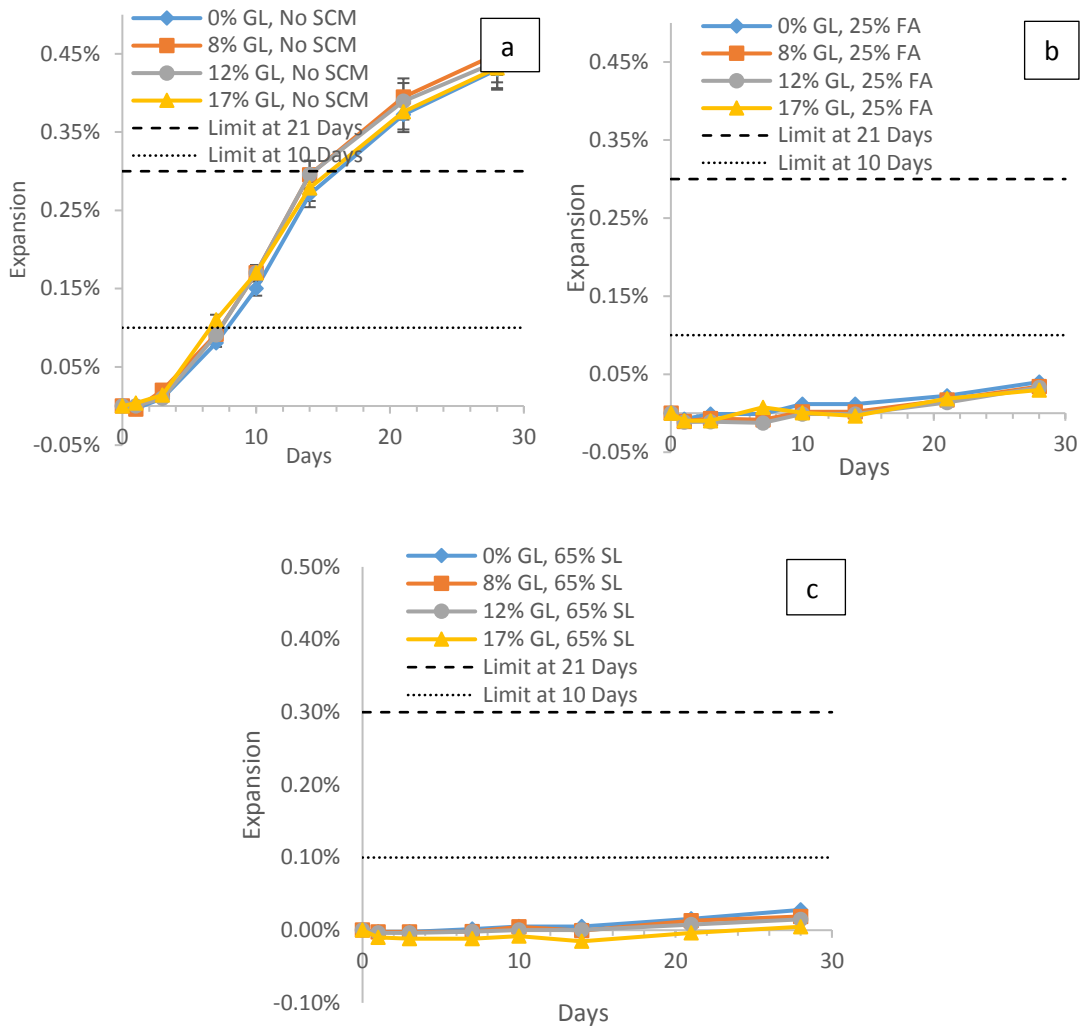

Figure 6-1 AMBT expansion results showing effect of increasing limestone content in cement on ASR expansion: a) No SCM, b) 25% FA and c) 65% SL.

The expansion data presented in this work agrees with the work of Thomas et al. (Thomas et al. 2013) which showed that the expansion levels for Portland cement (PC) and Portland-limestone cement mixtures (PLC, 12% limestone addition) are almost identical for mixtures with the same SCM and replacement level and that the efficacy of cement replacement with Class F fly ash or slag cement does not appear to be influenced by the presence of 12% limestone in the cement.

The observed identical degree of expansion with increasing limestone content in mortars without SCMs suggests that limestone ($CaCO_3$) does not aggravate ASR. From the expansion results, it is also clear that limestone possesses no ASR mitigating properties like SCMs. Adding SCMs (25%FA or 65% SL) reduced the expansion to negligible levels independently of the limestone content. The ability of SCMs to mitigate the effect of the 1M NaOH solution is likely due to the products formed by SCM reactions resulting to microstructure densification and lower permeability, thereby retarding alkali ingress (Shafaatian et al. 2013). The high alkali and high temperature present during AMBT accelerate the reactions. SCM addition also modifies the calcium silicate hydrate (C-S-H) composition resulting to enhanced alkali binding capacity (Duchesne & Berube 1994b; Durand et al. 1990; Gebregziabiher, Thomas & Peethamparan 2016; Hong & Glasser 1999; Kim, Olek & Jeong 2015). The decrease in the effective alkali concentration inside the mortar reduces the potential for ASR. Further, aluminium present in SCMs such as fly ash and slag is also proposed to suppress ASR by inhibiting the dissolution of reactive silica in aggregates (Bickmore et al. 2006; Chappex & Scrivener 2012b; Chappex & Scrivener 2013).

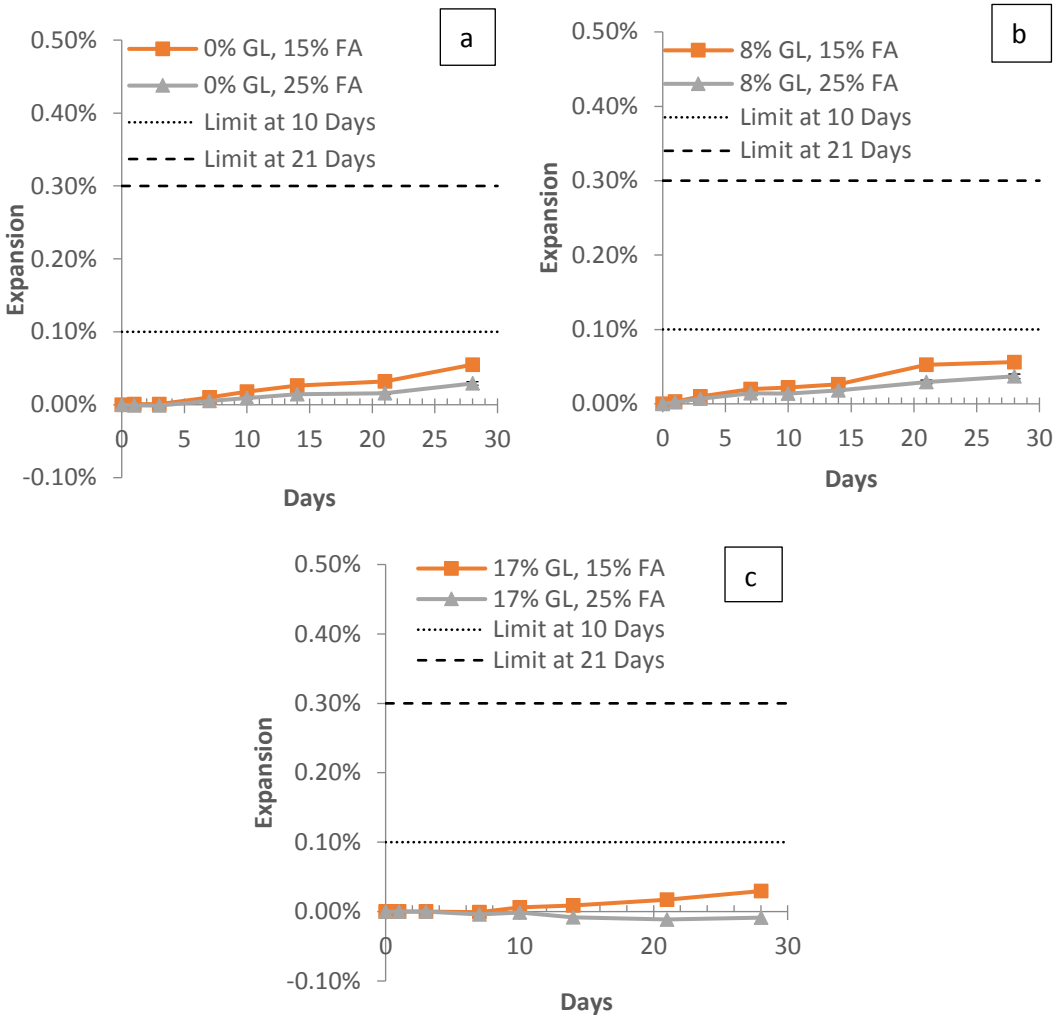

Figure 6-2 Effect of increasing fly ash replacement levels on mortar expansion of Greywacke AMBT specimens at a fixed level of limestone in cement: A) 0% limestone, B) 8% limestone and C) 17% limestone.

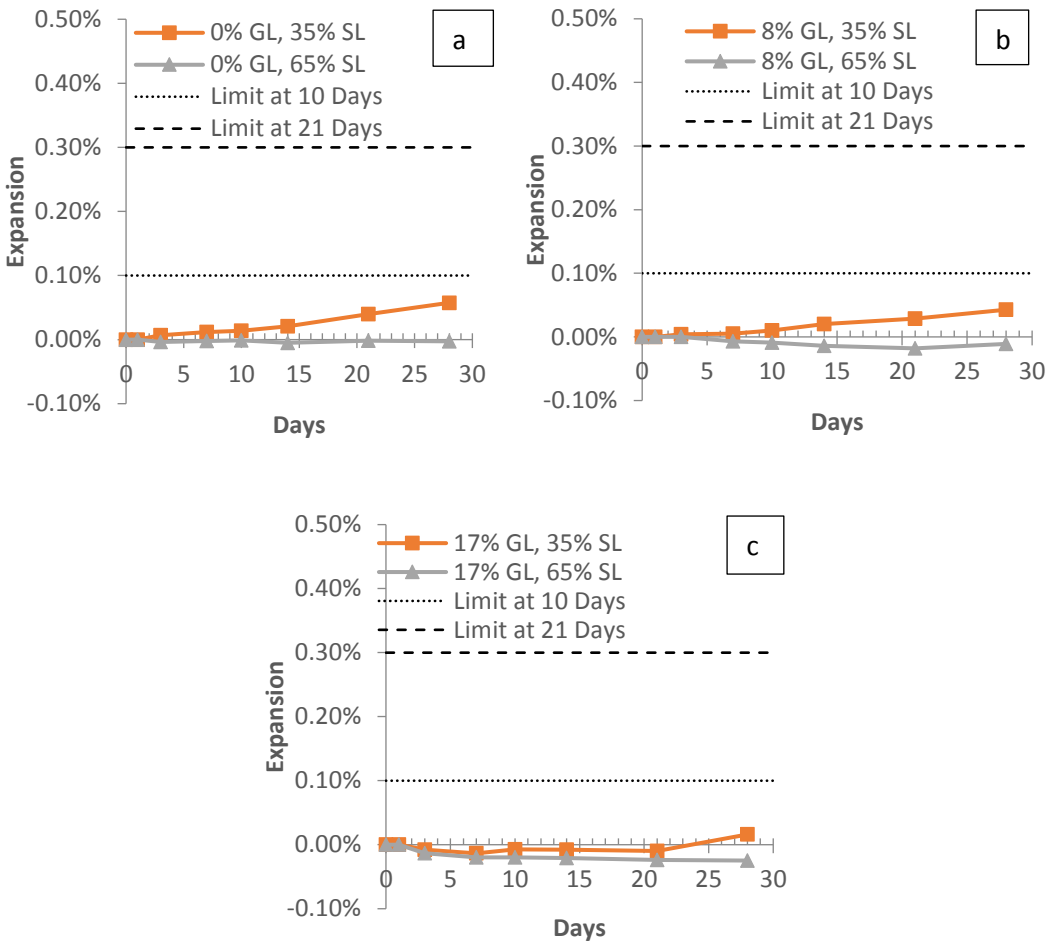

Figure 6-3 Effect of increasing slag replacement levels on mortar expansion of Greywacke AMBT specimens at a fixed level of limestone in cement: A) 0% limestone, B) 8% limestone and C) 17% limestone.

Limestone also reportedly densifies microstructure due to the formation of monocarboaluminates (Bonavetti, Rahhal & Irassar 2001; Chen & Yang 2013). The expansion results however suggest that it does not appear to contribute to ASR mitigation under the test conditions. Likewise, the dilution effect induced by limestone substitution is not apparent from the expansion results.

6.2 Characterization of the Mortar Specimens Post AMBT (ASR Gel and C-S-H Composition)

Figures 6-4 and 6-5 show the SEM images of cross-sectioned greywacke mortar specimens without SCM addition post 28 days AMBT (0%GL, 8%GL, 12%GL and 17%GL). Extensive cracking can be observed in all mortars, which is consistent with the high degree of expansion during AMBT. High magnification image of the ASR gel in the mortar with 12%GL but No SCM shown in Figure 6-6 appears similar to the ASR product reported by Leeman et al. (Andreas Leemann 2017). The gel is sandwiched between an aggregate that appears to have cracked and fully separated.

Table 6-1 corresponding to EDS point locations in Figure 6-6 shows that the ASR gel contains a significant amount of calcium (Ca), silicon (Si), and sodium (Na). Si concentration in the ASR gel dominates at ~64%, with notable concentrations of Ca at ~17% and Na ~17%. Negligible amount of potassium (~1%) detected is consistent with other ASR gel studies in AMBT specimens (Gavrilenko et al. 2007; Shafaatian et al. 2013). In contrast, ASR gel in concretes typically contains almost equivalent contents of Na and K (Andreas Leemann 2017; Leemann et al. 2016; Leemann & Merz 2013; Thaulow, Jakobsen & Clark 1996). The obtained average Ca/Si ratio and (Na+K)/Si ratio of the ASR gel is 0.26 and 0.29 respectively, which closely agrees to that reported in other studies (Andreas Leemann 2017; Leemann et al. 2016; Leemann & Merz 2013; Thaulow, Jakobsen & Clark 1996).

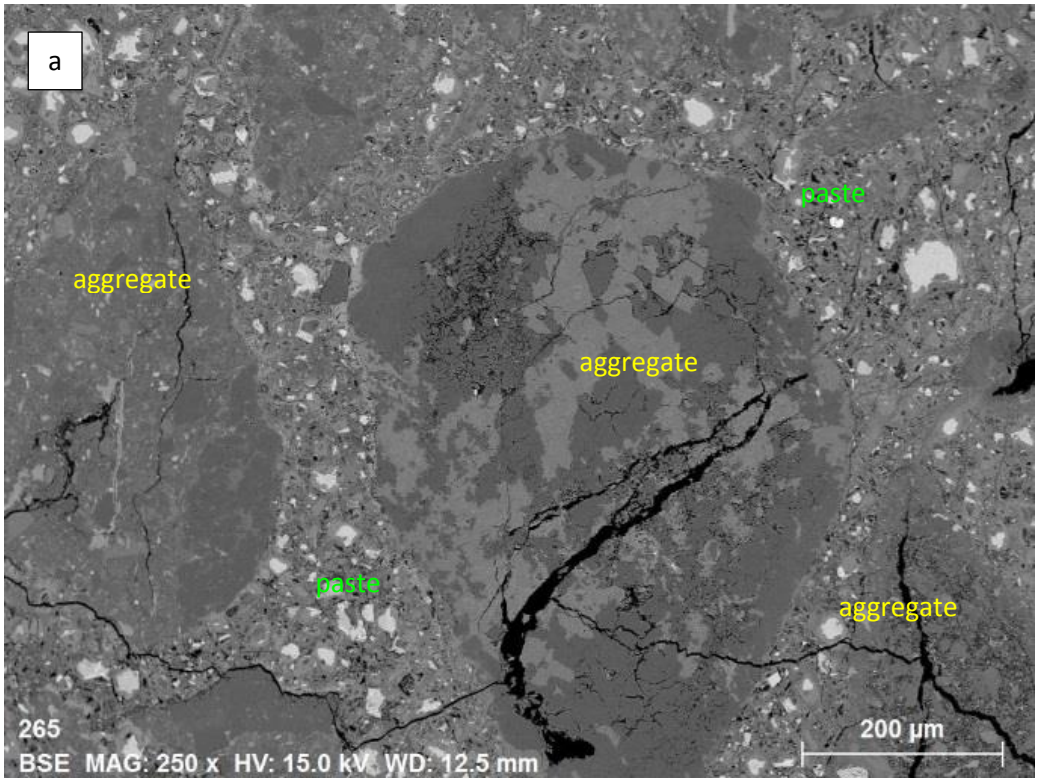

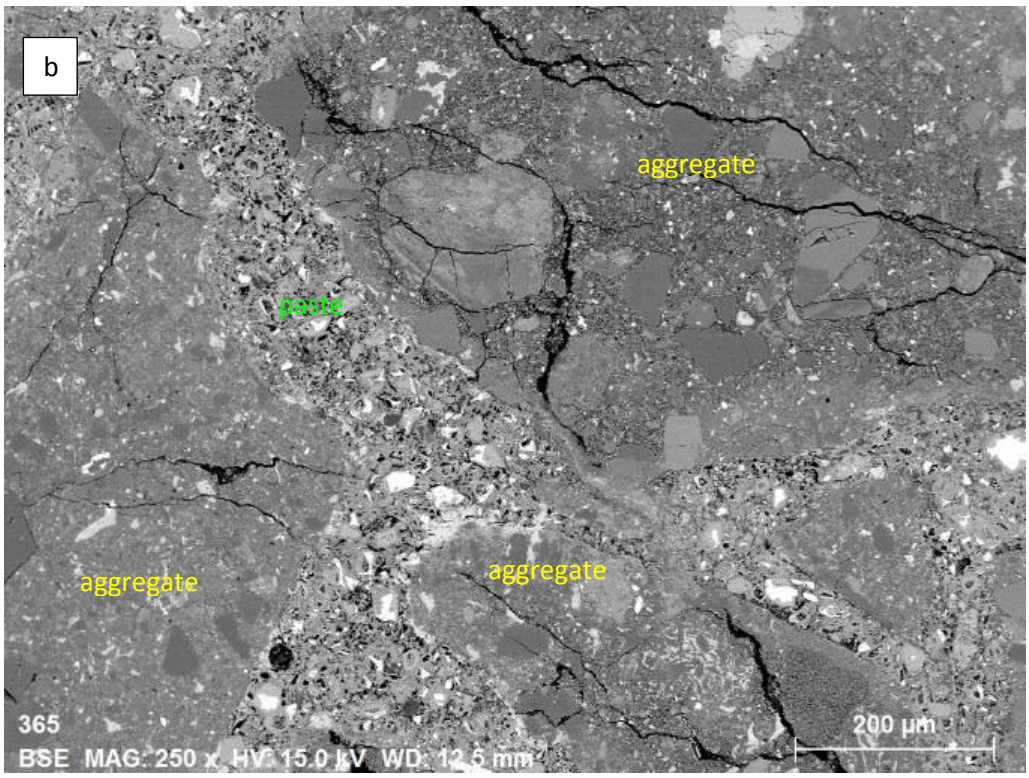

Figure 6-4 Greywacke mortar without SCM addition a) 0%GL, b) 8%GL showing extensive cracking

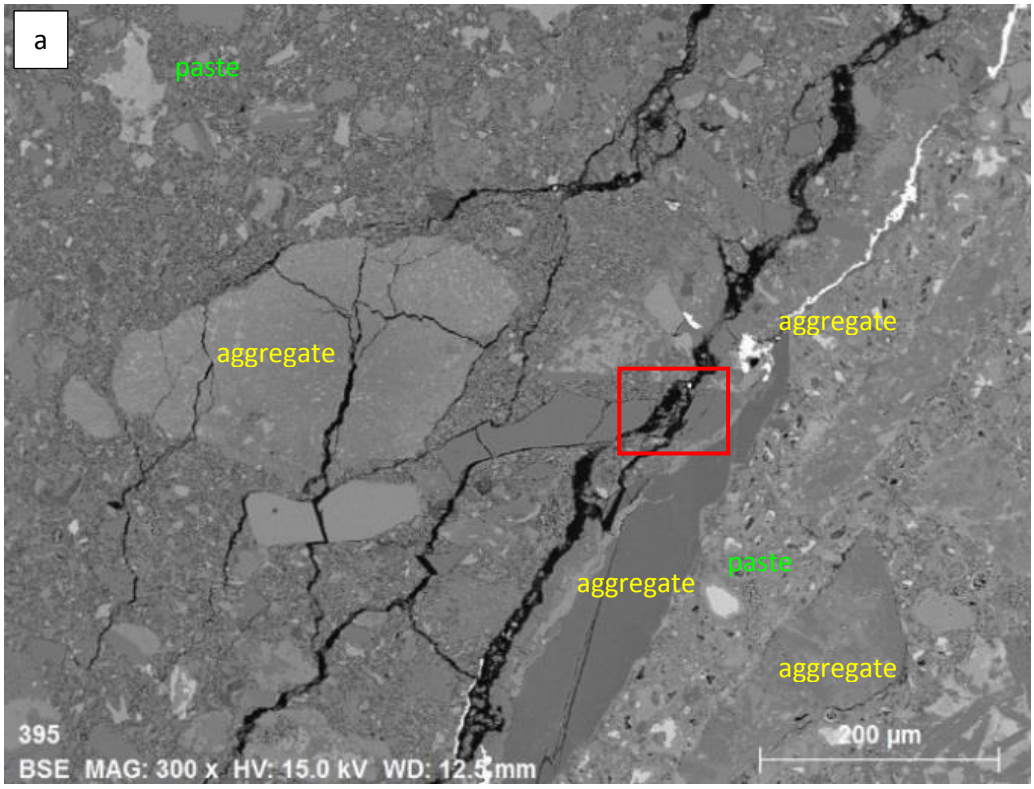

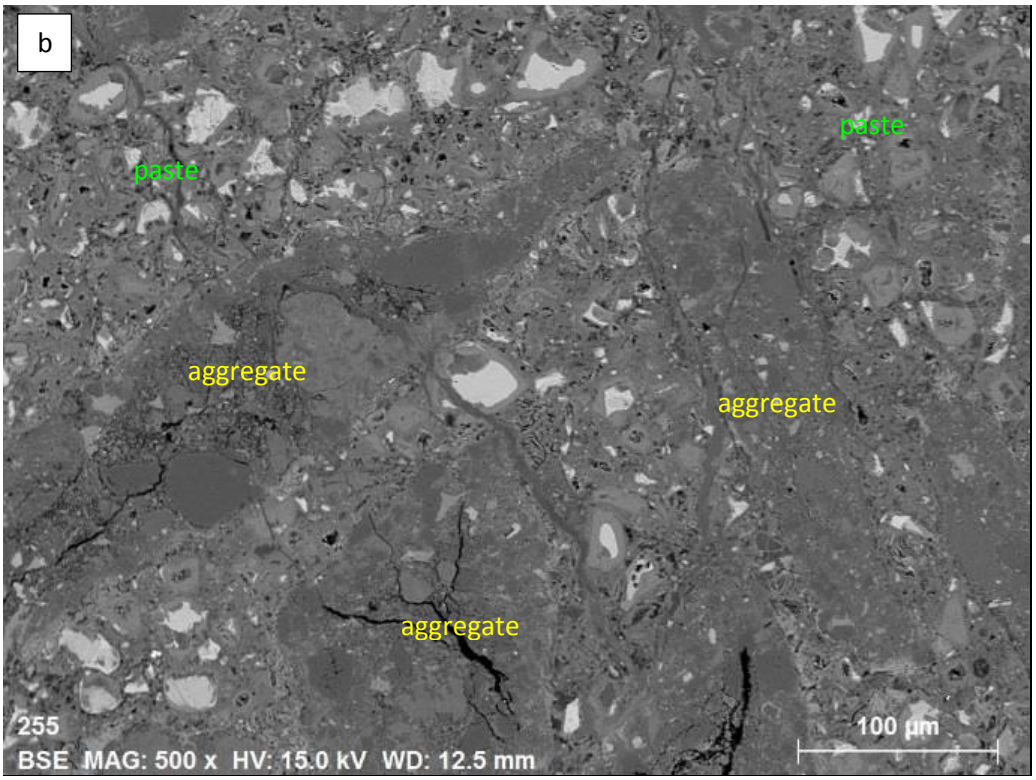

Figure 6-5 Greywacke mortar without SCM addition a) 12% GL, b) 17%GL showing extensive cracking

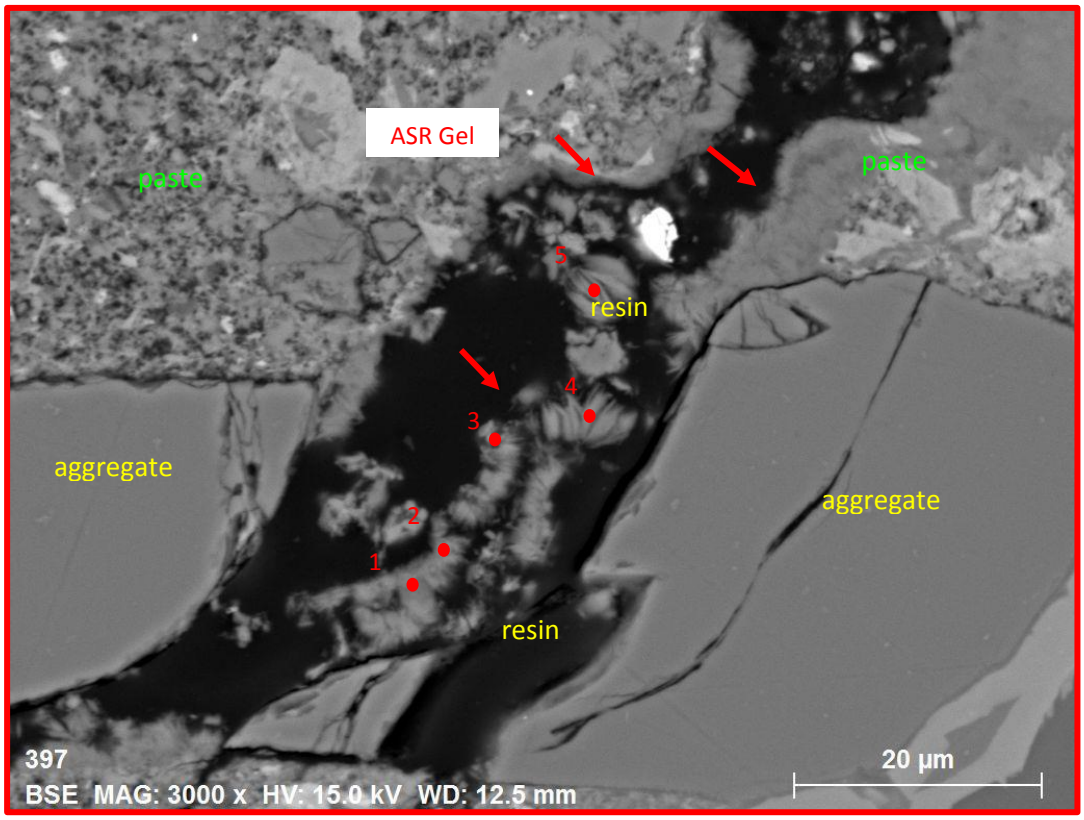

Figure 6-6 Higher magnification SEM image of ASR gel in 12% GL mortar (EDS points corresponding to Table 6-1 labelled accordingly)

Table 6-1 Elemental Analysis of the ASR Gel (normalized without oxygen)

EDS Location	atomic weight%								
	Ca	Al	Si	Na	K	Na+K	Ca/Si	(Na+K)/Si	Total
ASR Gel Pt 1	14.59	1.20	65.27	18.48	0.45	18.93	0.22	0.29	100.00
ASR Gel Pt 2	19.29	0.70	61.46	17.41	1.13	18.55	0.31	0.30	100.00
ASR Gel Pt 3	18.88	0.79	62.86	16.19	1.28	17.47	0.30	0.28	100.00
ASR Gel Pt 4	14.95	1.77	62.84	19.30	1.14	20.44	0.24	0.33	100.00
ASR Gel Pt 5	16.87	1.55	66.63	13.30	1.65	14.95	0.25	0.22	100.00
Average	16.92	1.20	63.81	16.94	1.13	18.07	0.27	0.28	100.00
STDEV	2.17	0.47	2.09	2.34	0.43	2.04	0.04	0.04	0.00

The negligible concentration of potassium (K) in the gel indicates that the 1M NaOH storage solution is masking the available potassium in the mortar pore solution consistent with the study of Golmakani and Hooton which reported that AMBT mortar bar pore solutions showed mainly sodium, with hardly any potassium (Golmakani &

Hooton 2019). Therefore, identical levels of expansion observed with increasing limestone substitution in mortars without SCMs suggests that since the 1M NaOH solution dominates the pore solution, AMBT is likely not a suitable method to assess cement dilution which is an expected effect of limestone substitution.

Figures 6-7 and 6-9 show the low magnification SEM images of the cross-sectioned greywacke AMBT specimens with SCM additions at recommended replacement levels: 0%GL + 25%FA, 0%GL + 65%SL, 17%GL +25%FA and 17%GL+65%SL. All mortar specimens show no major cracking in the aggregate or paste. Minor cracks observed are likely due to the cutting process.

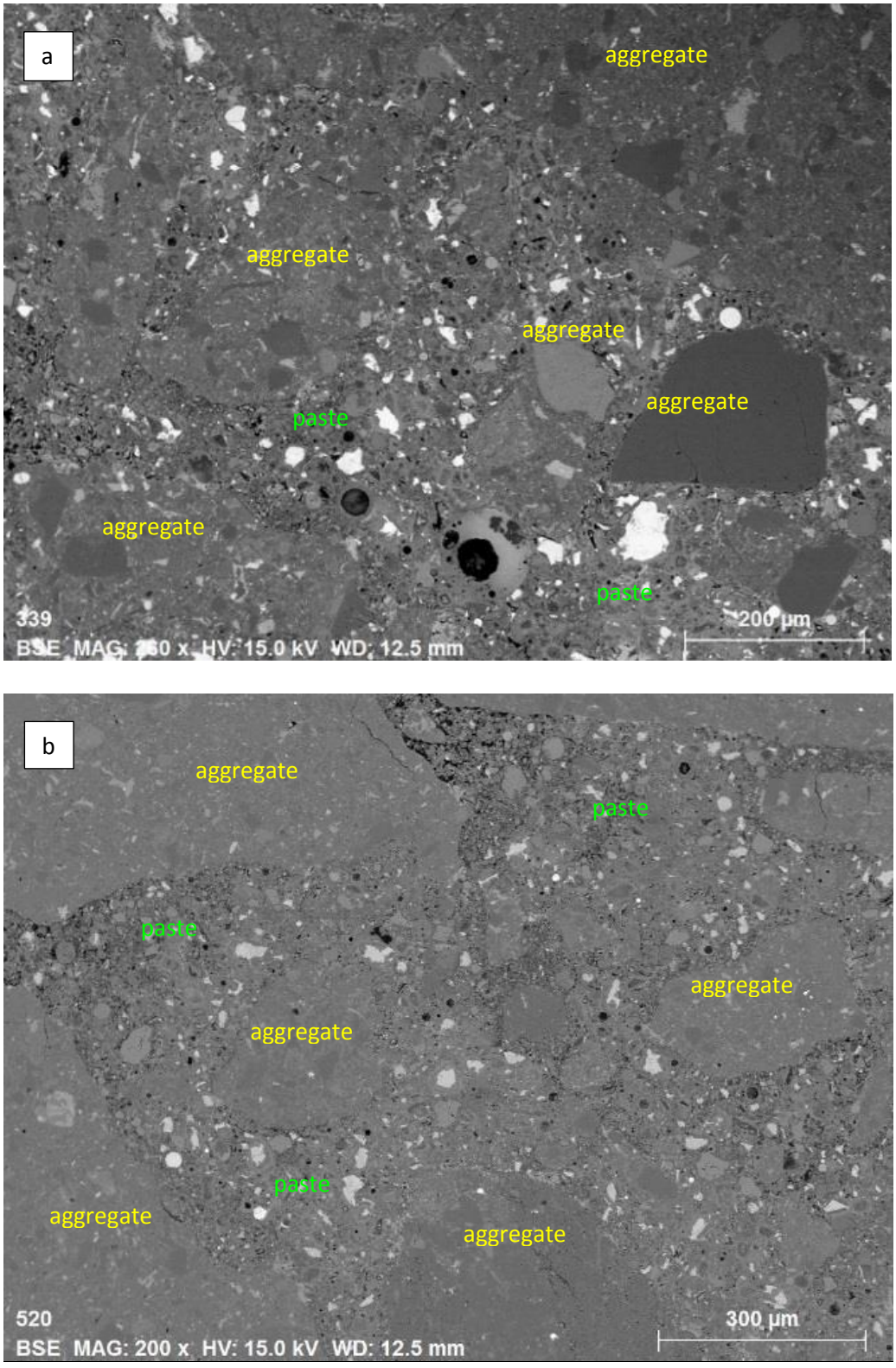

Figure 6-7 SEM images of the mortars with SCMs a) 0%GL+ 25%FA and b) 17%GL +25%FA

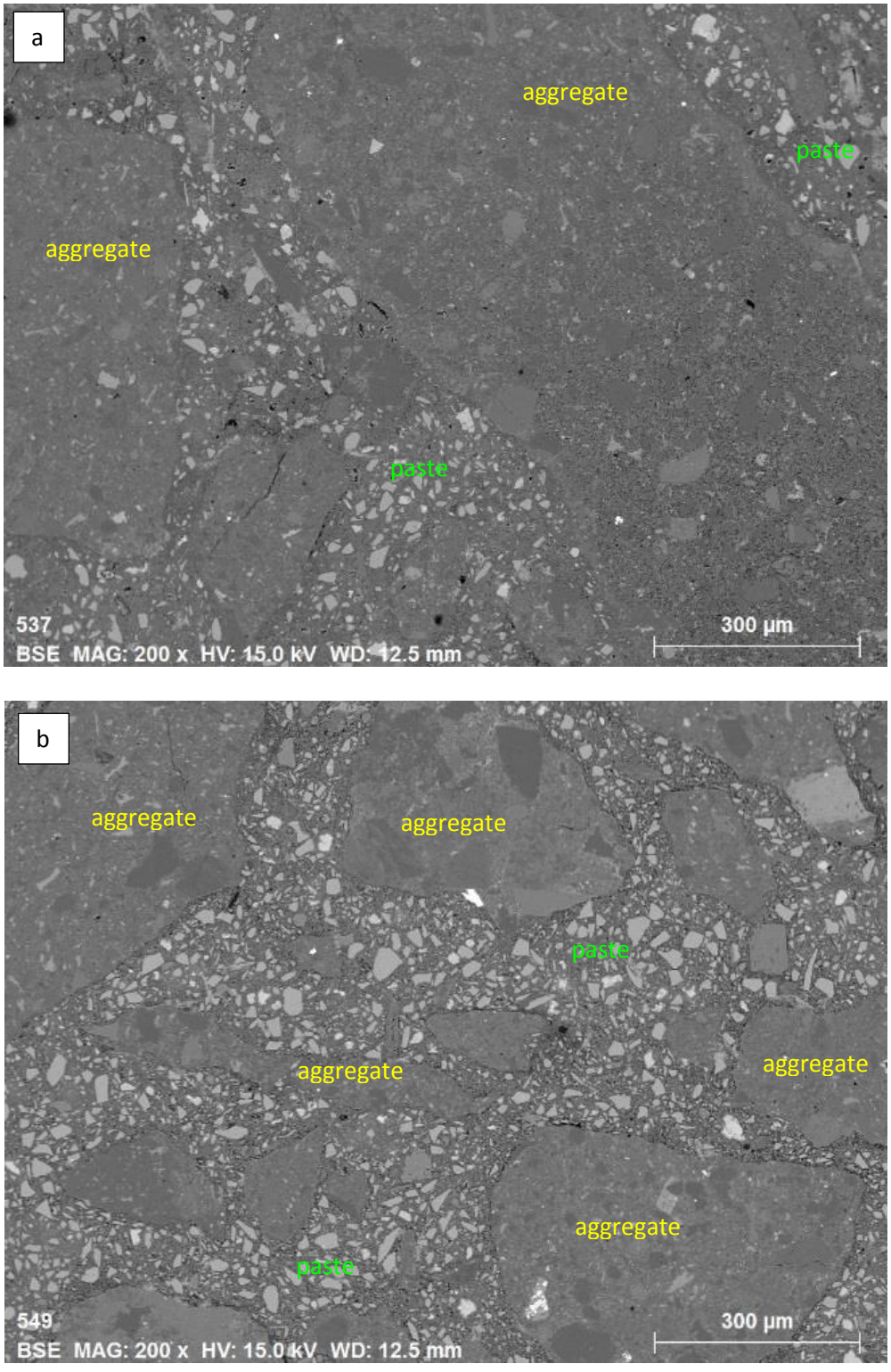

Figure 6-8 SEM images of the mortars with SCMs a) 0%GL+65%SL and b) 17%GL+65%SL

Some of the mortar specimens were subjected to SEM-EDS analysis post-AMBT to investigate the effect of limestone addition on C-S-H composition. Mortars without limestone (0%GL) and with maximum limestone content (17%GL) were chosen to better illustrate the effect of limestone. The EDS scatter plots in Figure 6-9 show that the Si/Ca and Al/Si ratio of the C-S-H is comparable in mortars without SCMs for both 0%GL and 17%GL. This agrees with another study where there was no observed significant change in the C-S-H Al/Si ratio with increasing limestone content (Adu-Amankwah et al. 2017). De Weerdt et al. likewise reported that the Ca/Si ratio and Al/Si ratio of OPC and OPC-limestone blended pastes are similar and constant over time (Weerdt, Haha, et al. 2011).

Adding 25%FA or 65%SL increases the Si/Ca and Al/Si ratio of the C-S-H. However, for the same amount of SCM, the effect on C-S-H composition is comparable regardless of limestone content in the binder. The results clearly demonstrate that although the SCMs affect the C-S-H composition, it remains the same regardless of the amount of limestone present. The modification in C-S-H composition when SCMs are present is linked to increased alkali binding capacity in the C-S-H (Chappex & Scrivener 2012a; Hong & Glasser 2002; L'Hôpital et al. 2016). Since C-S-H composition affects the ability to adsorb alkali (i.e. higher Si/Ca ratio, higher ability to bind alkali), identical C-S-H composition for 0%GL and 17%GL mortars (without SCM or with SCM but same type and dosage) suggest that limestone content has no effect on the alkali binding capacity of the C-S-H.

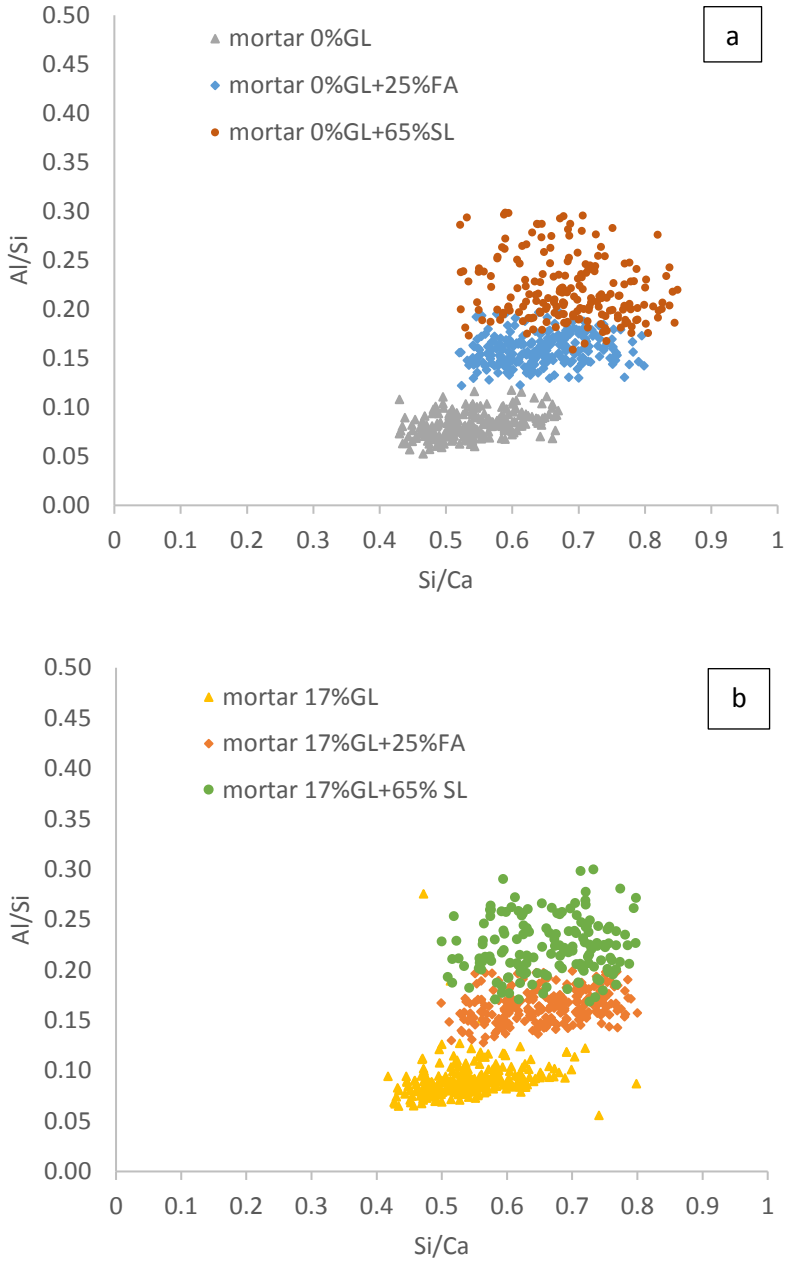

Figure 6-9 Effect of limestone content on Si/Ca and Al/Si ratio for mortars with a) 0%GL and b) 17%GL

Table 6-2 summarizes the effect of limestone addition on the composition of the C-S-H. The reported C-S-H composition corresponds to the average of the EDS points in Figure 6-9. The results clearly demonstrate that although the SCMs affect the C-S-H

composition, the composition remains the same even if the limestone content is increased.

Table 6-2 Average C-S-H composition of limestone blended mortars (atomic wt%)

Sample	Al/Si	Al/Ca	Si/Ca	Ca/(Si+Al)
Mortar 0% GL	0.08 ± 0.01	0.04 ± 0.01	0.54 ± 0.06	1.73 ± 0.19
Mortar 17%GL	0.09 ± 0.02	0.05 ± 0.01	0.54 ± 0.07	1.72 ± 0.21
Mortar 0%GL + 25%FA	0.16 ± 0.02	0.10 ± 0.02	0.64 ± 0.06	1.36 ± 0.14
Mortar 17%GL + 25%FA	0.16 ± 0.02	0.11 ± 0.02	0.66 ± 0.07	1.32 ± 0.15
Mortar 0%GL + 65%SL	0.22 ± 0.03	0.15 ± 0.02	0.69 ± 0.08	1.21 ± 0.14
Mortar 17%GL + 65%SL	0.22 ± 0.03	0.15 ± 0.03	0.66 ± 0.07	1.25 ± 0.15

6.3 Effect on Increasing Limestone on Portlandite

Thermogravimetric analysis was used to determine the amount of portlandite in blended pastes after 28 days immersion in 1M NaOH 80 °C (AMBT conditions). Calcite content was also measured to determine the limestone content in the blended pastes. The blended pastes have identical cement:limestone ratio as the AMBT specimens and were immersed in alkali after 1 day curing. The use of pastes is to isolate any effect the aggregates may have on portlandite content.

Figure 6-10 shows calcite content in the paste increasing as a function of limestone addition. The area under the curve 600-750 °C represents limestone ($CaCO_3$) decomposition to CaO (calcium oxide) and CO_2 (carbon dioxide) and therefore bigger area translates to more calcite present in the hydrate. Plain OPC is confirmed to have no calcite content.

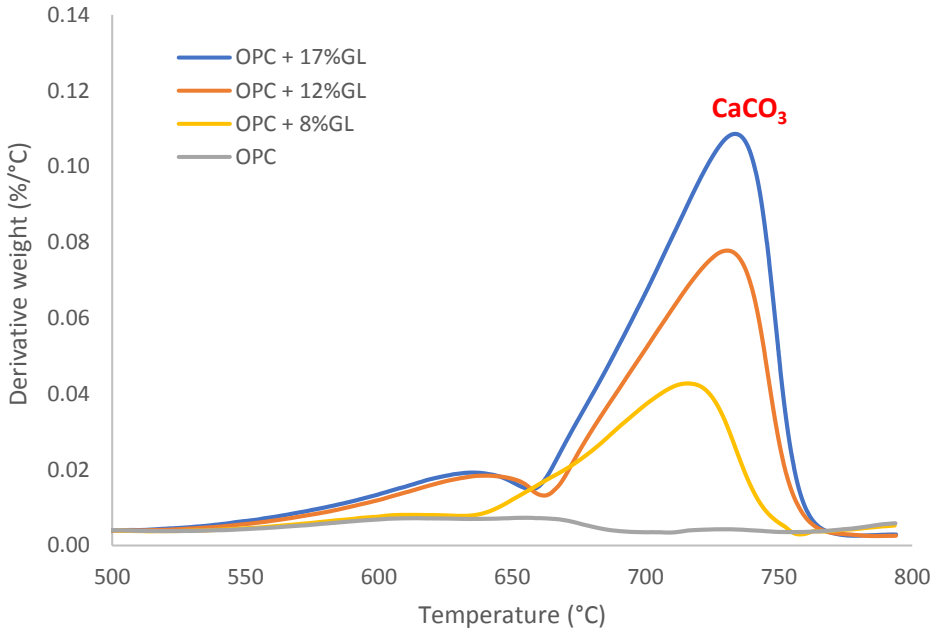

Figure 6-10 TG curves showing the increasing calcite content on the OPC-GL blended pastes with increasing limestone addition (1 day curing, before alkali immersion)

TG curve in Figure 6-11 show lower area under the curve 400 to 500 °C (CH decomposition temperature) as limestone content increases. This confirms that replacing part of the cement with limestone reduces the amount of portlandite proportional to the substitution amount. As more ground limestone is added, lower cement is available to hydrate which results in lower amount of portlandite generated.

The decrease in the amount of portlandite with increasing limestone addition is consistent with that reported in literature (Adu-Amankwah et al. 2017; Voglis et al. 2005; Weerdt, Haha, et al. 2011). Moreover, the increase in portlandite amount with respect to time (Figure 6-12) also confirms that the limestone used has no pozzolanic components consistent with it being 98% $CaCO_3$. Pozzolans react with portlandite to produce C-S-H consuming it in the process forming C-S-H of lower Ca/Si ratio. Thus, this result is consistent with the absence of change in C-S-H composition as a function of increasing limestone content discussed in the previous section. The values reported in Table 6-3 confirms that the effect of limestone on portlandite is only because of cement dilution.

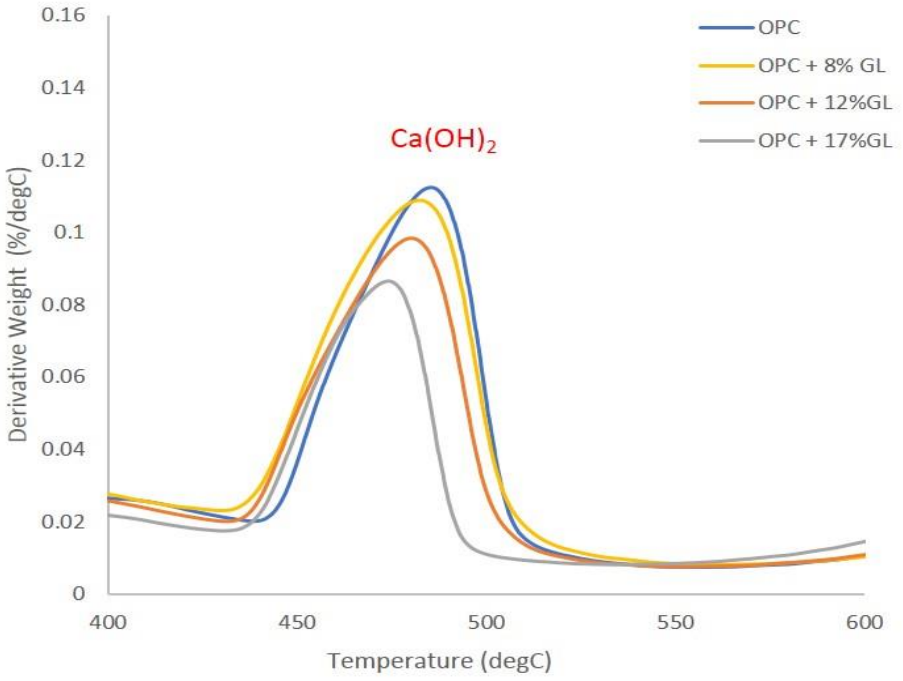

Figure 6-11 TG curves of the OPC-GL pastes after 28 days immersion in 1M NaOH 80 °C showing the effect of limestone on the amount of portlandite

The decrease in the amount of portlandite has beneficial effects on ASR mitigation. Portlandite is a soluble calcium source. Presence of calcium in the pore solution increases Ca/Si ratio, thereby resulting in much lower alkali binding capacity. Higher Ca/Si results in less negatively charged silanol sites in the C-S-H that are able to bind alkali. Moreover, calcium also competes with alkali adsorption in the C-S-H. As Ca^{2+} is preferably bound than alkali Na^{+} and K^{+} in the negatively charged C-S-H, more calcium in the pore solution will decrease the amount of bound alkali in the C-S-H (L'Hôpital et al. 2016).

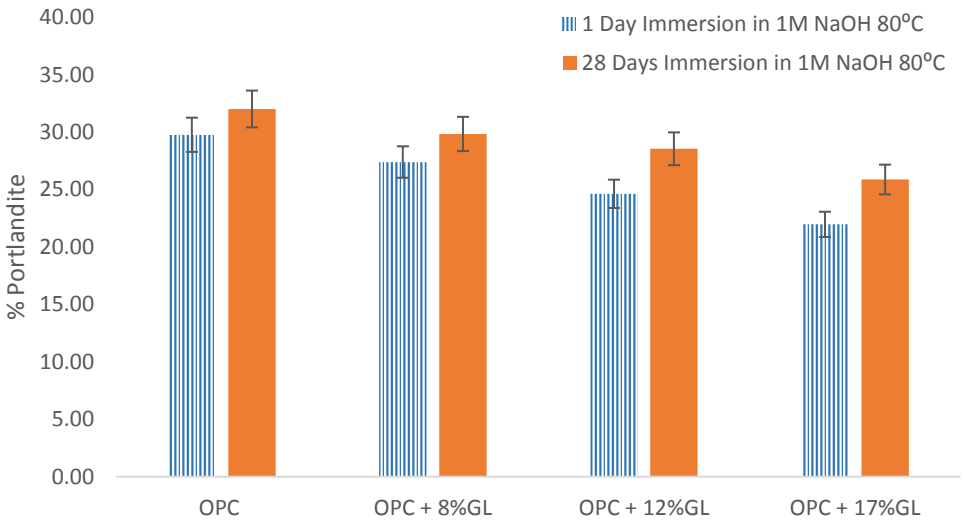

Figure 6-12 Effect of time of immersion in 1M NaOH 80 °C on portlandite content

Table 6-3 Effect of limestone on portlandite (dilution vs. actual values measured)

Portlandite	**8% Limestone**		**12% Limestone**		**17% Limestone**	
	Day 1 (%)	Day 28 (%)	Day 1 (%)	Day 28	Day 1	Day 28
Expected dilution effect	27.38	29.45	26.19	28.17	24.70	26.57
Actual values measured	27.39 ± 1.37	29.84 ± 1.49	24.63 ± 1.23	28.55 ± 1.43	21.97 ± 1.10	25.87 ± 1.29

6.4 Formation of Monocarboaluminates and its Dissolution under AMBT Conditions

The ASR mitigating effects of limestone is often attributed to the formation of additional hydrates, monocarboaluminates. The limestone portion of Portland-limestone cements reacts with the aluminate phases and produces carboaluminates, resulting to more hydrates and subsequent reduction in porosity (Bonavetti et al. 2003; Bonavetti, Rahhal & Irassar 2001; Tennis, Thomas & Weiss 2011; Thomas et al. 2013; Voglis et al. 2005). This section investigates the formation of monocarboaluminates in blended pastes with limestone and the effect of AMBT conditions on monocarboaluminates and ettringites. Blended pastes with increasing limestone contents (0 to 17%) were subjected to normal hydration conditions as well as AMBT conditions for 28 days (1M NaOH 80 °C). The changes in phases, as well as microstructure, were characterized by XRD and SEM.

XRD patterns reported Figure 6-13 confirm formation of monocarboaluminates in all blended pastes with limestone under normal hydration conditions. The excess of carbonate ions in cement paste produced the transformation of monosulfoaluminate to monocarboaluminate. In fact, no peak for monosulfate was observed at $2\theta=10°$. The sulfate liberated during the carbonate substitution reaction promotes re-precipitation of ettringite (Bonavetti, Rahhal & Irassar 2001). Moreover, the formation of monocarboaluminates is an indication that calcite is getting consumed in the reactions and not an inert diluent (Adu-Amankwah et al. 2017).

In OPC-GL blended pastes that were exposed to AMBT conditions for 28 days, both ettringite and monocarboaluminate peaks disappear which indicate that both phases are unstable under these conditions (Figure 6-14). XRD pattern of monocarboaluminates remained unchanged at temperatures ≤ 70 °C, confirming its stability but decomposes at temperatures ≥ 90 °C (Matschei, Lothenbach & Glasser 2007). Another work even reported that the amount of both ettringite and monocarboaluminate started to decrease in Portland-Limestone cements at 40 °C (Lothenbach et al. 2007). This observation is in agreement with what was observed in Chapter 4.

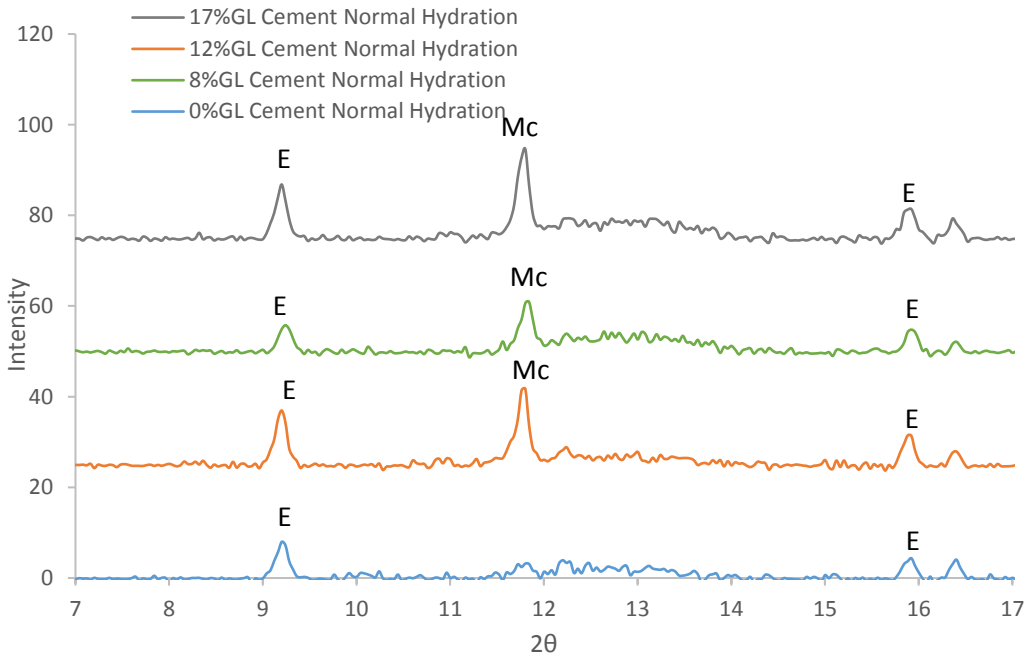

Figure 6-13 XRD patterns of the limestone blended pastes subjected to normal hydration conditions showing the formation of monocarboaluminates (Mc) as well as presence of ettringite (E).

SEM images confirm the observations from XRD. Figures 6-15a and 6-16a show SEM images of the fly ash and slag limestone blended pastes after 28 days hydration

showing presence of ettringites as characterized by needle-like morphology. Ettringite forms in as early as 3 days of cement hydration which later on slowly converts to monosulfate, which is a more stable phase (Taylor, Famy & Scrivener 2001). SEM images of blended pastes post 28 days exposure to 1M NaOH 80 °C in Figure 6-15b and 6-16b however show absence of ettringites. Ettringite is intrinsically unstable in cement pastes above 70 °C (Taylor, Famy & Scrivener 2001). Ettringite stability decreases with increasing pH and/or temperature (Scrivener & Taylor 1993; Shimada & Young 2004).

XRD and SEM results confirm that AMBT conditions facilitate dissolution of ettringites and monocarboaluminates. This suggests that during AMBT, both phases do not contribute to microstructure densification.

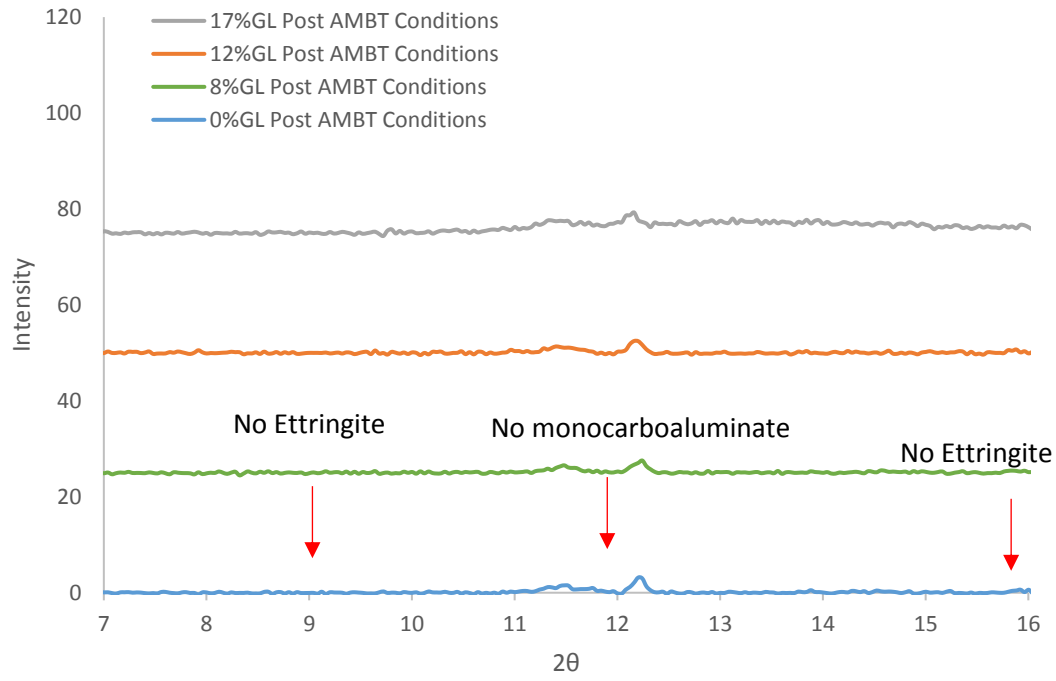

Figure 6-14 XRD patterns of the limestone blended pastes post 28 days exposure to AMBT conditions showing absence of ettringite and monocarboaluminates.

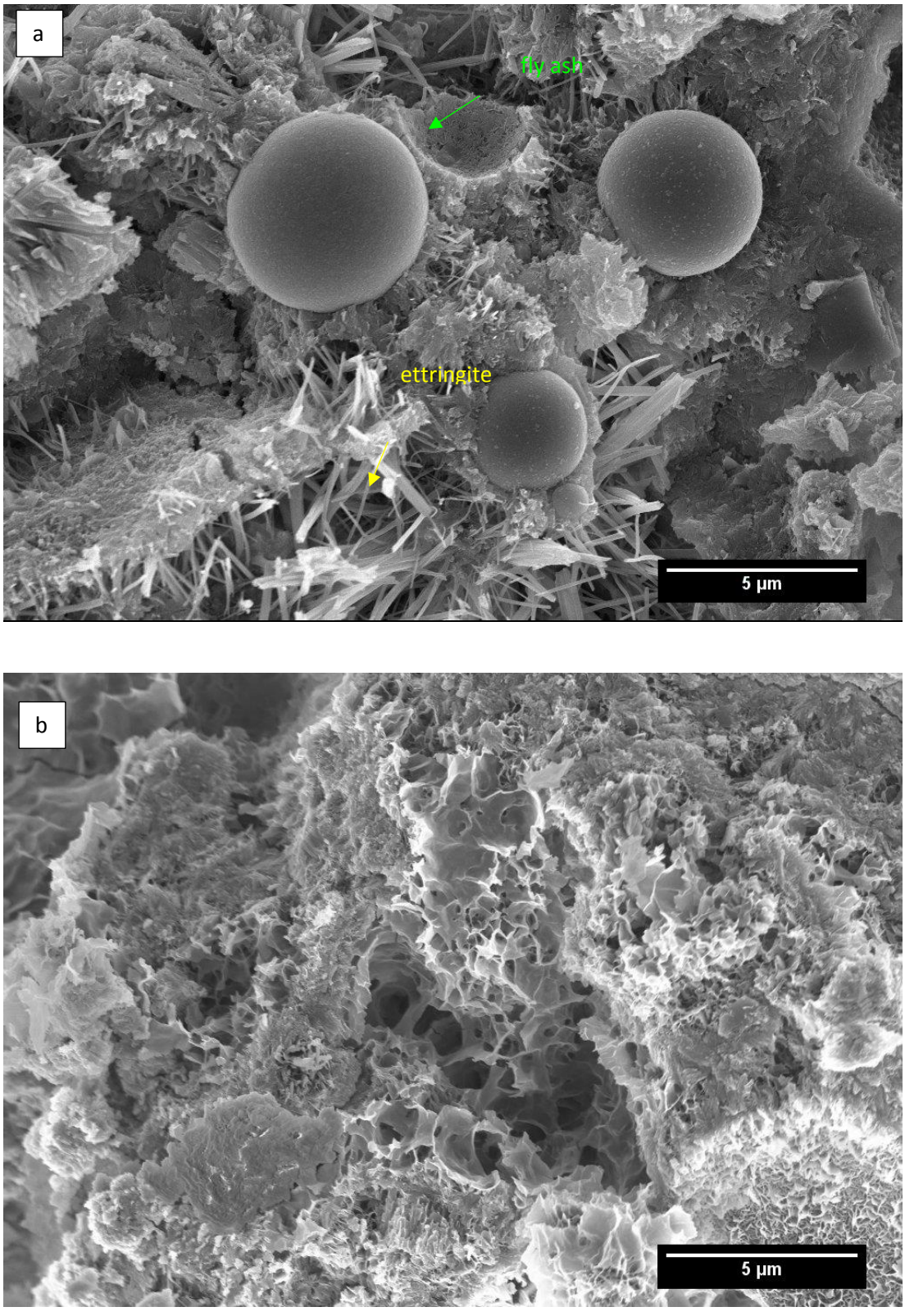

Figure 6-15 Fractured surface SEM images of 8%GL+15% FA after 28 days

a) normal hydration b) exposure to AMBT conditions

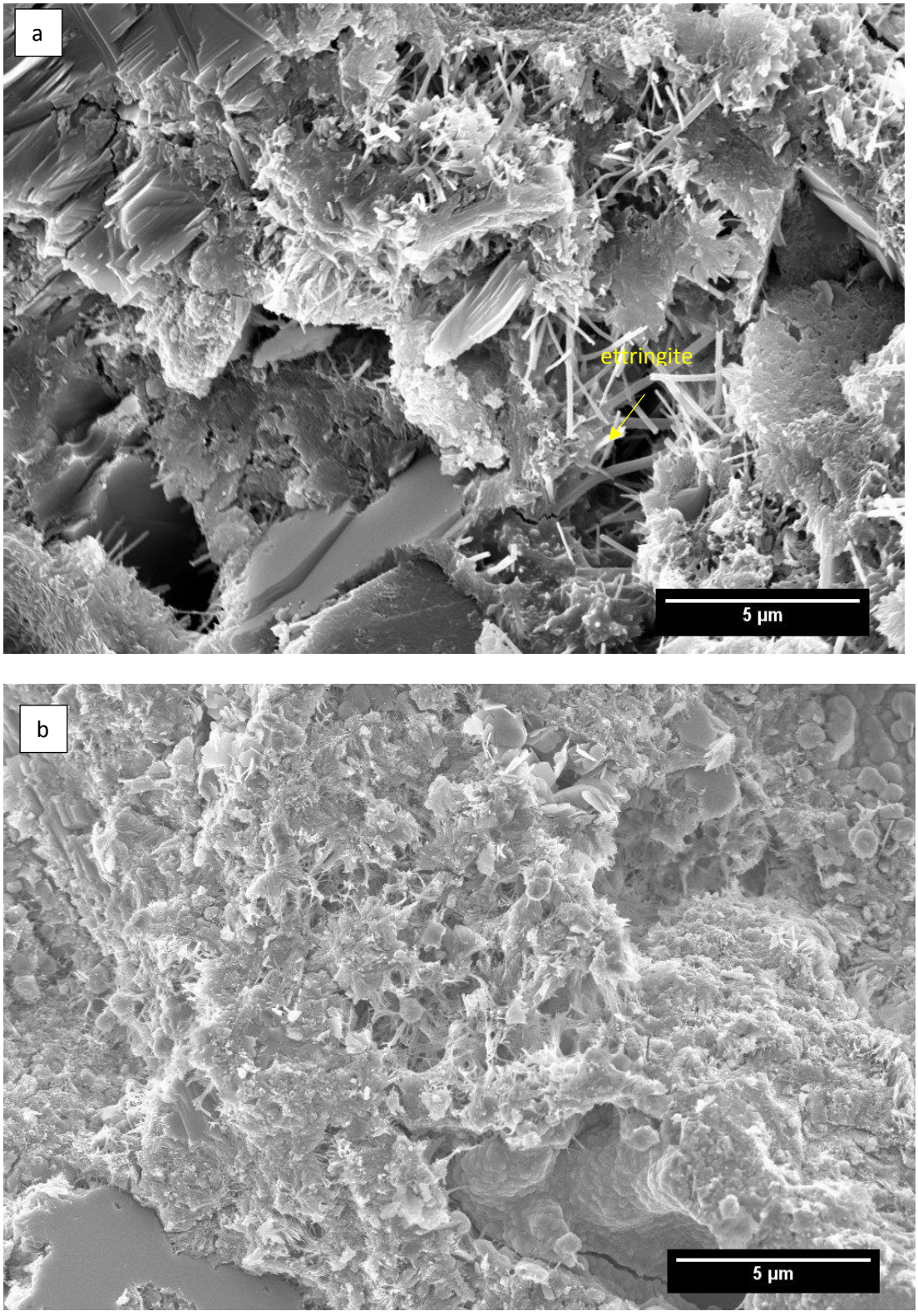

Figure 6-16 Fractured surface SEM images of 8%GL+35% SL after 28 days a) normal hydration b) exposure to AMBT conditions

6.5 Effect of Limestone Content on Pore Solution Alkalinity

This section investigates the effect of limestone on pore solution alkalinity. Pastes with and without 25% limestone substitution were cured at 20±2 °C high humidity and later on subjected pore solution extraction at 28 days (1 month) and at 168 days (6 months). Two types of cements were used, low alkali (0.6% Na_2O_{eq}) and high alkali (1% Na_2O_{eq}). The extracted solutions were subjected to ICP-OES and pH measurements to determine concentration of alkalis (Na+K) and the alkalinity of the pore solution respectively. The pH measurements were conducted on undiluted solution. Each pH measurement was for 2 minutes to allow the solution to stabilize and to generate comparable readings. For ICP-OES, all solutions were acidified with nitric acid prior analysis to prevent precipitation. 25% limestone substitution was chosen to allow comparison with other SCMs like fly ash which is normally used at 25% standard replacement level. Moreover, doing limestone substitution at various amounts was not possible as the pore solution extractions were done in another laboratory (EPFL Switzerland) and thus, access is limited.

Figure 6-17 shows alkali concentration in blended pastes with and without 25% limestone content substitution clearly demonstrating alkali dilution induced by 25% limestone substitution. The same trend can be observed regardless of type of cement (low alkali and high alkali content). Low alkali OPC has 0.6% Na_2O_{eq} and high alkali OPC has 1% Na_2O_{eq}. The decrease in the concentration of alkali cations with limestone

substitution is consistent with that reported in another study where 50% limestone substitution resulted to 50% reduction in Na and K concentration (Schöler et al. 2017).

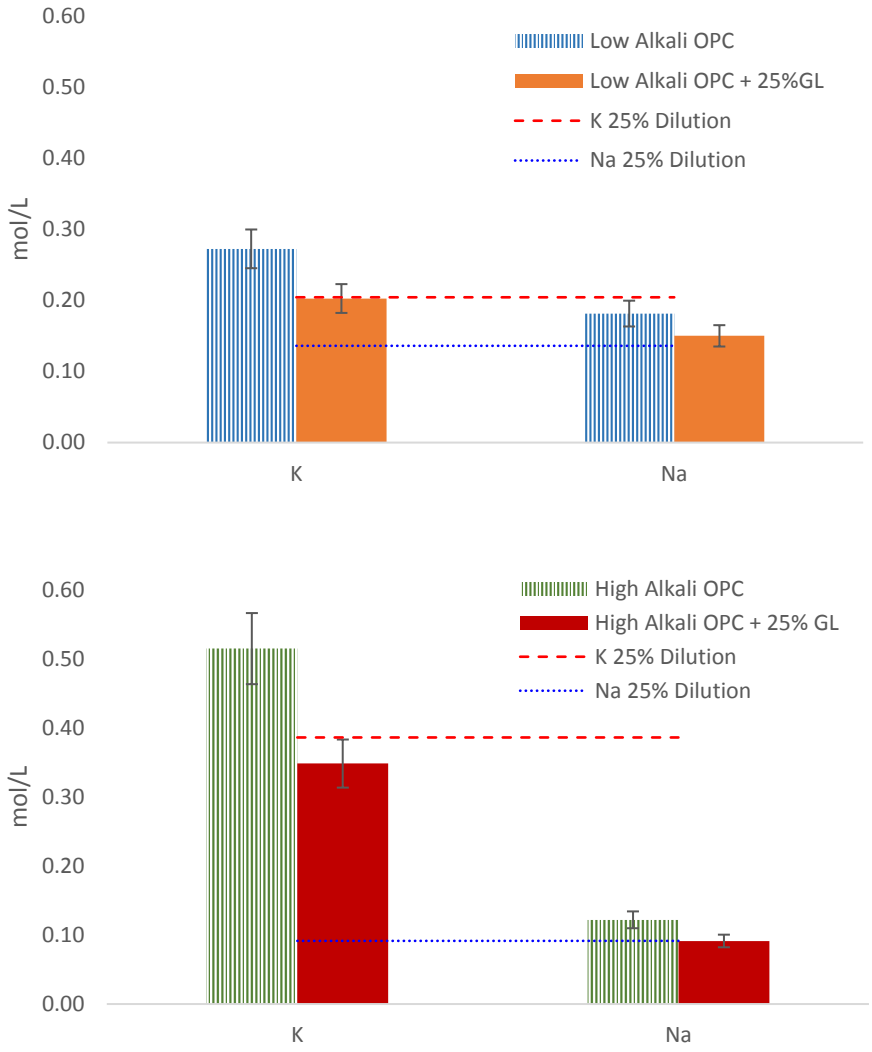

Figure 6-17 Concentration of alkali cations (Na and K) in blended pastes with 25% limestone content at 28 days

Figure 6-18 shows that the alkali concentration measured after 168 days follows the same trend as the 28-day. This indicates that limestone only dilutes cement and therefore has no capacity to continuously bind alkalis unlike SCMs which showed

decrease in alkali concentration as a function of time. Moreover, a slight increase in the concentration of alkalis from 28 days to 168 days can be observed. The increase in the concentration of Na and K with time in OPC and OPC limestone blends with time was reported in several studies (Lothenbach et al. 2008; Vollpracht et al. 2016; Weerdt, Haha, et al. 2011). Although part of the alkalis is bound in the C-S-H, the alkali concentration increases with time as alkalis continue to be released during the hydration of clinkers and as the volume of the liquid phase present decreases (Lothenbach et al. 2008).

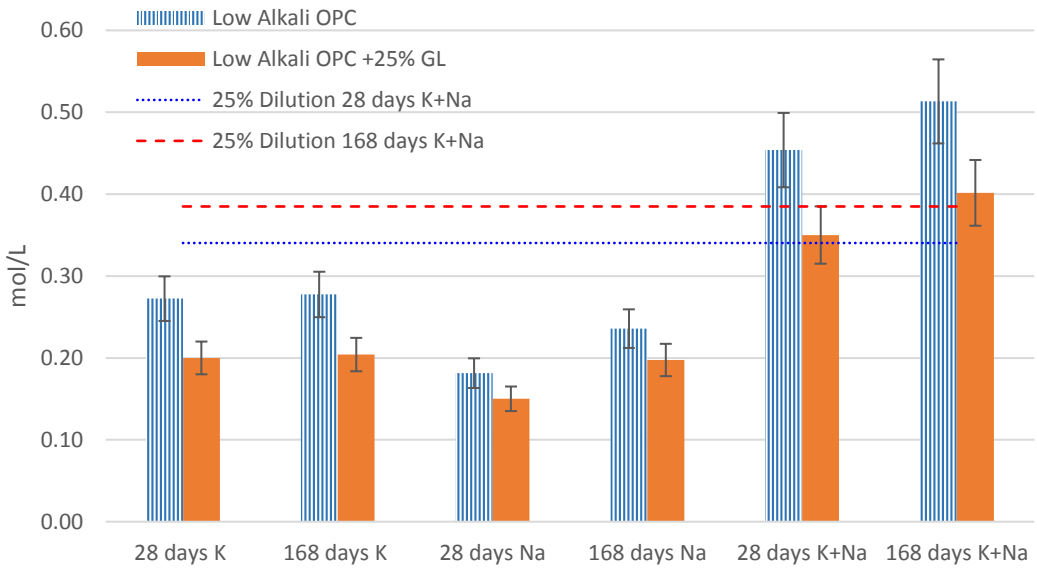

Figure 6-18 Effect of time on the concentration of potassium (K) and sodium (Na) in the pore solution

The data in Figure 6-19 likewise show a similar trend although the observed decrease in pH is minimal. 25% limestone substitution was observed to slightly lower the pH of blended pastes regardless of the initial cement alkali content, which is in agreement with the reported decrease in the concentration of Na and K. A slight pH increase with

respect to time is also notable in Figure 6-20. The increase of alkalis with time leads to an increase in pH (Lothenbach et al. 2008). The changes observed in pH are however minimal and this is possibly due to the carbonate buffer resulting from limestone addition (calcium carbonate) (Matschei & Glasser 2010).

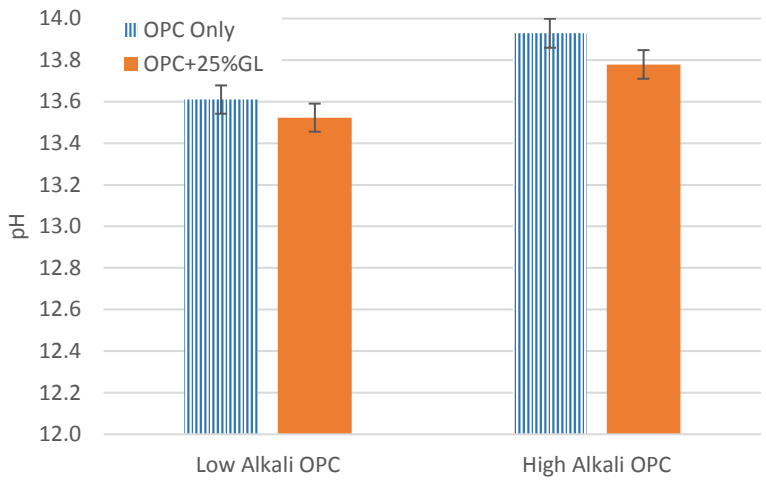

Figure 6-19 Effect of limestone substitution on pH as a function of type of cement

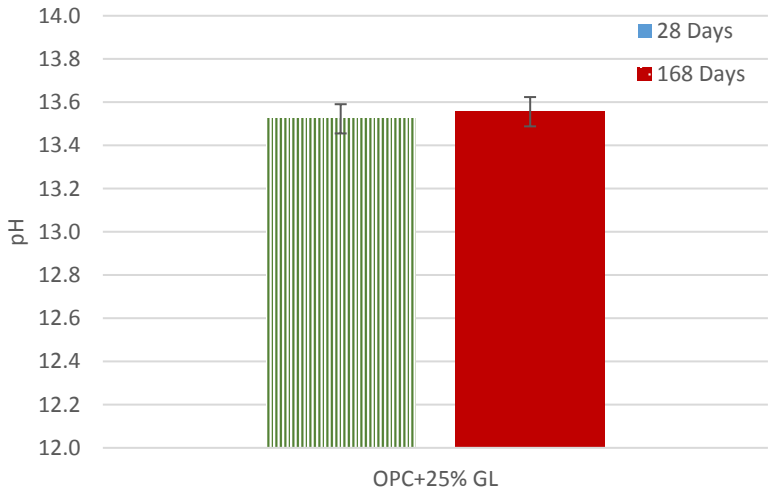

Figure 6-20 Effect of time on the pH of pastes with limestone

The alkali concentration (Na+K) and pH both decrease when part of cement is replaced by limestone. The amount of decrease is consistent with cement dilution. However, as AMBT did not detect any difference in ASR expansion as a function of limestone content, this suggests that the effect of cement dilution is beyond the capacity of the test method.

6.6 Summary of Findings

This chapter evaluates the effect of increasing amount of limestone mineral addition in cements on alkali-silica reaction (ASR) using accelerated mortar bar test (AMBT). Mortars with and without SCMs were prepared by substituting portion of 0% limestone GP cement with increasing amounts of limestone (0%, 8%, 12% and 17%). Mortar specimens post-AMBT, as well as blended pastes with equivalent limestone substitution levels as the mortars were characterized to better understand the AMBT expansion results. Likewise, the effect of limestone on portlandite content and pore solution alkalinity was investigated.

Significant findings are as follows:

1. AMBT expansion results show that limestone content up to 17% has no detrimental effect on the ability of SCMs to mitigate ASR. Fly ash (15% and 25%) and slag (35% and 65%) at recommended replacement levels both showed sufficient capacity to mitigate ASR regardless of limestone content in the binder.

2. Mortars without SCMs showed presence of extensive cracking due to ASR regardless of amount of limestone present consistent with observed high rate of expansion during AMBT. The mortars with SCMs regardless of limestone content showed either absence of cracks or very minimal cracking which is likely due to the sectioning process.

3. The ASR gel observed in the mortar without SCM is primarily composed of silicon (60%), calcium (20%) and sodium (20%). The negligible presence of potassium (about 1%) in the ASR gel indicates that the 1M NaOH storage solution dominates the pore solution of the mortar.

4. Limestone substitution resulted in lower portlandite amount and pore solution alkalinity. The decrease observed is proportional to the amount of cement substituted and does not further decrease with time. Thus, limestone only dilutes the cement and has no pozzolanic properties consistent with its 98% $CaCO_3$ content.

5. Increasing the amount of limestone (up to 17%) does not modify the composition of the C-S-H.

6. Monocarboaluminates was observed in limestone blended pastes under normal hydration conditions. However, SEM images and XRD plots confirm that monocarboaluminate and ettringite disappear post exposure to AMBT conditions.

7 Conclusions

This chapter summarizes the conclusions from Chapters 4, 5 and 6 and addresses the overall objective of the thesis which is to investigate the mechanisms by which SCMs mitigate ASR in order to be able to provide basis for identifying potential alternatives. Chapter 4 investigated the mechanistic role of SCMs in ASR mitigation, while Chapter 5 and Chapter 6 explored the effect of binder components, cement alkali content and limestone mineral addition on the efficacy of SCMs in ASR mitigation.

In order to address the defined objectives, a combination of accelerated expansion tests (AMBT and CPT using pore solution method) and various material characterization techniques were employed (SEM-EDS, XRD, TG, ICP-OES, etc.). ASR expansion tests were carried out using traditional SCMs (FA, SL, MK and SF) at various replacement levels in systems with prescribed and increased levels of alkali and limestone. The expansion behaviour was correlated with the effect of SCMs on microstructure and phase development and on the concentration of alkalis (Na and K) in the pore solution as well as to the ability of SCMs to release silicon and aluminium in solution.

The results show that SCMs at recommended dosages (15% and 25%FA, 35% and 65% SL, 10% and 15%MK and 5% and 10%SF) work effectively to mitigate ASR expansion even in cements with effective alkali content of 1% Na_2O_{eq}. The efficacy of SCMs in reducing ASR expansion is related to their ability to release silicon and aluminium in solution, consume portlandite, reduce pore solution alkali concentration

and modify calcium silicate hydrate (C-S-H) composition. Thus, siliceous materials, aluminosilicates and even pure aluminium present a potential to mitigate ASR.

Additional limestone (98% $CaCO_3$) in cement up to 17% does not aggravate ASR and has no detrimental effect on the efficacy of SCMs in mitigating ASR. Sections 7.1, 7.2 and 7.3 detail the conclusions of each chapter.

7.1 The mechanistic role of SCMs in ASR mitigation (Chapter 4)

This chapter investigated the mechanisms behind SCM mitigation by comparing four SCMs (FA, SL, MK and SF) in terms of ability to reduce ASR expansion, consume portlandite, reduce pore solution alkali concentration, modify C-S-H composition and release silicon and aluminium in solution. A separate AMBT test where Al_2O_3 was used as a cement substitute was also carried out in order to investigate the ability of aluminium to mitigate ASR.

The results show that the efficacy of SCMs in ASR mitigation is primarily related to their ability to release silicon and aluminium in solution, consume portlandite, reduce pore solution alkali concentration and modify C-S-H composition. Thus, any material that contains high amount of soluble silica and alumina is a potential SCM. The presence of calcium lowers the efficacy of SCMs in ASR mitigation.

At equivalent replacement levels, silica fume being the most pozzolanic demonstrates highest alkali binding capacity among the SCMs and therefore requires the lowest dosage to mitigate ASR. On the other hand, slag with the least capacity to consume portlandite and lowest ability to reduce alkali in the pore solution, requires the most to mitigate. Thus, pozzolanicity and the ability to reduce pore solution alkali concentration can be used as measures to assess the efficacy of SCMs in ASR mitigation.

7.1.1 Pozzolanic behaviour and alkali binding capacity of the SCMs

The results of this study show that the ability of SCMs to reduce ASR expansion is consistent with their ability to consume portlandite and reduce pore solution alkalinity. Pozzolanic reactions result in the: 1) consumption of portlandite which is a soluble calcium source, 2) formation of C-S-H phases that has higher alkali binding capacity, and 3) microstructure densification retarding alkali ingress.

The pozzolanic behaviour of the SCMs at equivalent replacement levels is in the following order: SF>MK>FA>SL. The observed efficacy of SF is because it is amorphous and very fine and therefore highly pozzolanic. Fly ash and metakaolin also have high content of soluble silica and thus, exhibit high degree of pozzolanicity. Slag, on the other hand, is a latent hydraulic material and therefore hydrates with water like cement. Minimal slag consumption of portlandite can be attributed to slag hydration reactions. Slag is calcium deficient and takes some calcium from portlandite to

compensate. As is expected from the trend in pozzolanic behaviour, analysis of the C-S-H of mortars with SCMs showed lower Ca/Si ratio compared to reference mortar with no SCM. At equivalent SCM replacement levels of 25%, SF addition generated the lowest Ca/Si ratio.

Consumption of portlandite lowers the amount of soluble calcium which is an essential constituent in the formation of ASR products. The presence of calcium helps to precipitate the alkali silicate and form the ASR gel product, alkali calcium silicate hydrate (Na(K)-Ca-SiO_2-H_2O). Higher calcium in the pore solution also results in C-S-H with much higher Ca/Si ratio that has a much lower alkali binding capacity. Moreover, calcium competes with alkali adsorption in the C-S-H. As Ca^{2+} is preferably bound than alkalis (Na^+ and K^+) in the negatively charged C-S-H, more calcium in the pore solution will decrease the amount of bound alkali in the C-S-H.

The pore solution alkali concentration (Na+K) of blended pastes with SCMs was at all times lower than reference OPC. The reduction in alkali concentration varies depending on the type of SCM and follows the same trend as pozzolanic behaviour: SF>MK>FA>SL. At 28 days, whereas the total alkali in OPC+25%SL was reduced only proportional to substitution amount, the total alkali in OPC+25%SF was reduced by 95%. The same trend was observed even at recommended replacement levels. Whereas OPC+50%SL reduced the alkali concentration by 50% after 28 days, OPC+10%SF was able to reduce it by 86%. Silica fume consistent with its high amorphous silica content is the most pozzolanic and therefore most efficient in reducing the pore solution alkali concentration. Blended pastes containing SCMs with

high amount of soluble silica, such as FA and MK, also showed high reduction in pore solution alkali concentration.

Further reduction of alkalis was observed at 168 days for all pastes with SCMs. The decrease in pore solution alkali concentration with time as well as the variation in the capacity of various SCMs to reduce pore solution alkalinity indicates that alkali binding is an ongoing process occurring as a consequence of SCM reactions. Thus, the effect of SCMs on the pore solution is more than just cement dilution.

7.1.2 The role of silicon and aluminium in ASR mitigation

Dissolution experiments where raw SCMs were immersed in 1M NaOH 80 °C showed that the ability of SCMs to release silicon (Si) occurs in the following order: SF>MK>FA>SL. The ability of the SCMs to release Si in solution is consistent with the efficacy of SCMs to reduce ASR expansion, consume portlandite, reduce pore solution alkali concentration and decrease Ca/Si ratio of the C-S-H. Higher amount of "silica" translates to more reactant available to react with portlandite to form C-S-H that not only densifies the microstructure, but also has much lower Ca/Si ratio which has higher alkali binding capacity. This suggests that the ability of SCMs to release silicon in solution is the biggest contributor to its efficacy in ASR mitigation. Thus, any material containing high amount of soluble silica is a suitable SCM to mitigate ASR.

In order to investigate the effect of aluminium on ASR expansion, 25% Al_2O_3 was used to substitute cement in mortar specimens. Results show reduction in expansion in all mortar specimens with Al_2O_3 (lower than 0.3% after 21 days). Thus, aluminium also presents a potential to mitigate ASR. Results of this study also show that aluminium can precipitate silicon reducing the concentration of free silicon in solution and forming aluminosilicates in the process. Aluminosilicates in solution are negatively charged and therefore to charge balance, they bind a cation in the process (either Ca^{2+}, Na^{+} or K^{+}). The binding of alkali cations reduces the concentration of alkali in the pore solution. Further, the higher C-S-H Al/Si ratio in mortars with aluminium-containing SCMs (FA, MK and SL) suggests aluminium uptake in the C-S-H. The aluminium uptake results in the formation of calcium aluminosilicate hydrate (C-A-S-H) which has a net negative charge. As a form of charge compensation, its binds an alkali cation. Thus, the presence of aluminium in the pore solution increases the alkali binding capacity of the C-S-H.

7.1.3 Pozzolanic C-S-H vs. ASR Gel C-S-H

The SCMs and aggregate both contain silica that in turn, make them prone to hydroxyl attack and consequent formation of reaction products. Whereas the SCMs form secondary C-S-H, the reactive silica phases from aggregates form ASR gel which is also C-S-H but with much higher alkali and much lower calcium content. This suggests that whereas both aggregates and SCMs contain silica phases and both react with alkali, the products formed are completely different, and this is due to the accessibility

of calcium. The ASR gel that forms inside an aggregate has Ca/Si ~0.30 which is different from C-S-H of the paste which has Ca/Si ratio >1 (in systems with and without SCMs, Ca/Si ratio is just higher when SCMs are present).

Since the SCMs are in close proximity to portlandite (soluble source of calcium), pozzolanic reactions dominate, forming C-S-H with much higher calcium contents. Moreover, as the paste is porous and the SCMs are very fine and evenly dispersed in the cement matrix, the formation of the pozzolanic products does not result to extra pressure as they fill the empty spaces in the paste. In fact, the formation of secondary C-S-H results in microstructure densification and improved durability properties.

The case for ASR gels forming within an aggregate, which appear to be the most deleterious based from observations in this study, is opposite that for SCMs. Since the dissolved silica inside the aggregate is negatively charged, they adsorb the readily available free alkalis Na^+ and K^+ leading to the formation of alkali calcium silicate hydrate gel that has much higher volume than the original space occupied by the dissolved silica. Note that alkalis dominate the pore solution despite being a tiny component of the cement. As the gel forms inside the aggregate, with no other place to move, the pressure builds up, and ends up cracking the concrete. Moreover, since the ASR gel is inside the aggregate, its access to calcium remains limited, resulting for it to have much lower Ca/Si ratio than typical C-S-H, thereby increasing its swelling potential. The swelling potential is related to gel stiffness. Higher calcium in the ASR gel results in higher stiffness and therefore, lower potential to swell. In addition, the resulting ASR gel containing higher alkali and much lower Ca/Si ratio is loosely structured and can imbibe water easily, causing expansion.

The ASR gel composition varies depending on its location. The Ca/Si ratio of the ASR gel within the aggregate is about 0.3, while ASR gel in the cement paste has higher Ca/Si ratio of 1.3 which is similar to the composition of a typical C-S-H formed from hydration. The increase in calcium content in the ASR gel is because of its proximity to the paste. Thus, whereas, calcium is necessary to precipitate ASR gel, as calcium is a known cross-linking agent, higher calcium contents, in fact, makes the gel more rigid and less prone to swelling. Consequently, no cracks originating from ASR gels in close proximity with the cement paste were observed.

7.2 The ability of SCMs to mitigate ASR in cements of higher alkali contents and their effect on ASR Gel composition (Chapter 5)

This study investigated the ability of SCMs to mitigate ASR when used in conjunction with cements with effective alkali content of 1% Na_2O_{eq} using simulated pore solution method. In this method, the concrete specimens were kept in a storage solution with alkali concentration based on extracted pore solution at 28 days hydration. Concrete specimens without SCMs showed high degree of expansion. On the other hand, both 38 °C and 60 °C concrete specimens with SCMs showed absence of expansion up to 12 months which clearly demonstrate that 25%FA and 50%SL are both effective in preventing ASR. Therefore, SCMs at recommended dosages can mitigate ASR even if cement alkali contents were raised up to 1% Na_2O_{eq}.

The presence of ASR gel was observed in concrete prisms with and without SCM. Concrete specimens with no SCM, however, demonstrate more extensive cracking and much higher amount of ASR gel. The ASR gel in the concrete with SCMs are contained in thinner cracks (less than 5 microns) and very less in quantity.

The ASR gel regardless of aggregate type bears a similar signature. The ASR gel is typically located inside an aggregate and exits through the cement paste (same signature as AMBT specimens). The normalized composition of the gel inside an aggregate (that is, removing oxygen), is about 60% silicon (Si), 20% calcium (Ca) and 20% sodium+potassium (Na+K). The ASR products found in concrete with SCMs were found to have higher aluminium contents which is likely due to increased levels of aluminium in the pore solution when SCMs are present. The actual effect of aluminium on ASR gel properties, however, remains to be investigated.

The Si/Ca and Al/Si ratio of the C-S-H in the concrete specimens increased with both 25%FA and 50%SL addition (consistent with the AMBT results). The alkali uptake in the C-S-H increased with SCM addition regardless of aggregate type. Thus, SCM addition enhances the alkali binding capacity of the C-S-H.

7.3 The influence of limestone on the efficacy of SCMs in ASR mitigation and the suitability of AMBT for assessing the effect of alkali dilution (Chapter 6)

This study used AMBT to investigate the influence of limestone on the efficacy of SCMs to mitigate ASR. AMBT expansion results show that limestone content up to 17% has no detrimental effect on the ability of SCMs to mitigate ASR. 25%FA and 65%SL both showed sufficient capacity to mitigate ASR regardless of limestone content in the binder. Mortars without SCMs show high degree of expansion at similar expansion rate regardless of limestone content which indicates that limestone does not aggravate ASR. Likewise, as the expansion results were not affected by the presence of limestone, it appears that limestone does not actively mitigate ASR like SCMs.

Portlandite and pore solution alkali concentration were observed to decrease proportional to the amount of substitution, which is an expected outcome of cement limestone substitution. No significant decrease in total pore solution alkali concentration (Na+K) was observed with time which suggests that limestone has no capability to bind alkalis, unlike SCMs. These observations are in agreement with the absence of change in C-S-H composition with limestone addition. The increase in Si/Ca and Al/Si ratio of the C-S-H that occurs when SCMs are present results in better alkali uptake. Limestone addition, therefore, does not increase the alkali binding capacity of the C-S-H.

Although limestone does not actively reduce pore solution alkali concentration, as shown in the results, it can reduce the total alkali concentration since it replaces part of the cement. The expected effect of reduction in pore solution alkalinity is a decrease in ASR expansion. This, however, did not manifest in the expansion results which suggests that AMBT is not a suitable method to assess the effect of alkali dilution, an expected effect of cement limestone substitution, due to the high concentrations of alkali available from the bath. The mortar specimens are saturated with the 1M NaOH storage solution as confirmed by the high dominance of sodium (Na) and negligible presence of potassium (K) in the ASR gel. Note that ASR gel in concrete specimens has an equivalent content of Na and K. Further, although monocarboaluminates were observed in ambient cured limestone cement pastes, their absence in pastes cured under AMBT conditions (1M NaOH and 80 °C) indicate that these phases are unstable under these conditions and therefore do not contribute to microstructure densification. Thus, the influence of monocarboaluminates on ASR mitigation is not possible to assess by the AMBT method.

8 Recommendations for Future Work

A number of future research areas, currently beyond the scope of this study, are suggested.

- It is recommended to evaluate alternative supplementary cementitious materials and correlate the mitigation mechanisms with traditional SCMs (as discussed in Chapter 4). Potential alternative SCMs include materials rich in silica and alumina such as reactive aggregate powders, calcined clays and ashes from agricultural by-products. Likewise, it will also be interesting to use pozzolanic behaviour and the ability to reduce pore solution alkali concentration in identifying potential SCMs for ASR mitigation.

- It will be beneficial to use the pore solution method to test aggregates with available field data as this will help establish test limits which the method still currently does not have.

- Using the pore solution method, it is also interesting to investigate the effect of potassium boosting to increase the alkali content of Australian cements. The concrete specimens in this study used only sodium to boost the cement alkali content and there remains a question as to whether the effect of sodium and potassium (both present in cement) on ASR is similar.

- In order to investigate the effect of alkali dilution due to increased levels of limestone substitution, as well as the presence of monocarboaluminates on ASR expansion, it is recommended to use other test methods which have a fixed alkali supply and a much lower storage temperature (lower than 50 °C). The use of limestone minerals with various calcite contents and impurities is also recommended to determine the effect of limestone purity on ASR expansion.

References

Adu-Amankwah, S., Zajac, M., Stabler, C., Lothenbach, B. & Black, L. 2017, 'Influence of limestone on the hydration of ternary slag cements', *Cement and Concrete Research* vol. 100, pp. 96-109.

Alarcon-Ruiz, L., Platret, G., Massieu, E. & Ehrlacher, A. 2005, 'The use of thermal analysis in assessing the effect of temperature on a cement paste', *Cement and Concrete Research* vol. 35, pp. 609–13.

Andreas Leemann, T.K., Isabel Fernandes, Maarten A. T. M. Broekmans 2017, 'Raman microscopy of alkali-silica reaction (ASR) products formed in concrete', *Cement and Concrete Research*, vol. 102, pp. 41–7.

ASTM International 2014, *Standard Test Method for Potential Alkali Reactivity of Aggregates (Mortar-Bar Method)*, ASTM C1260, West Conshohocken, United States.

ASTM International 2015, *Standard Specification for Coal Fly Ash and Raw or Calcined Natural Pozzolan for Use in Concrete*, ASTM C618 West Conshohocken, United States.

ATIC SP43 Cementitious Material for Concrete 2017, Australian Technical Infrastructure Committee

Australia.

Beaudoin, J. & Odler, I. 2003, 'Hydration, Setting, and Hardening of Portland Cement', in P. Hewlett (ed.), *Lea's Chemistry of Cement and Concrete*, Fourth edition edn, Elsevier Science and Technology.

Bentz, D.P. 2006, 'Influence of alkalis on porosity percolation in hydrating cement pastes', *Cement & Concrete Composites*, vol. 28, pp. 427–31.

Berube, M.-A., Duchesne, J., Dorion, J.F. & Rivest, M. 2002, 'Laboratory assessment of alkali contribution by aggregates to concrete and application to concrete structures affected by alkali–silica reactivity', *Cement and Concrete Research*, vol. 32, pp. 1215–27.

Berube, M.A. & Duchesne, J. 1993, 'Does silica fume merely postpone expansion due to alkali-aggregate reactivity?', *Construction and Building Materials* vol. 7, no. 3, pp. 137-43.

Bickmore, B.R., Nagy, K.L., Gray, A.K. & Brinkerhoff, A.R. 2006, 'The effect of $Al(OH)_4^-$ on the dissolution rate of quartz', *Geochimica et Cosmochimica Acta* vol. 70, pp. 290–305.

Bleszynski, R. & Thomas, M. 1998, 'Microstructural Studies of Alkali-Silica Reaction in Fly Ash Concrete Immersed in Alkaline Solutions', *Advanced Cement Based Materials*, vol. 7, pp. 66–78.

Boddy, A.M., Hooton, R.D. & Thomas, M.D.A. 2003, 'The effect of the silica content of silica fume on its ability to control alkali–silica reaction', *Cement and Concrete Research*, vol. 33, pp. 1263–8.

Bonavetti, V., Donza, H., Menendez, G., Cabrera, O. & Irassar, E.F. 2003, 'Limestone filler cement in low w/c concrete: A rational use of energy', *Cement and Concrete Research* vol. 33 pp. 865–71.

Bonavetti, V., Rahhal, V. & Irassar, E. 2001, 'Studies on the carboaluminate formation in limestone-filler blended cements', *Cement and Concrete Research*, vol. 31, pp. 853-9.

Bruker, 'Handheld XRF: How it works', viewed September 1, 2019, <https://www.bruker.com/products/x-ray-diffraction-and-elemental-analysis/handheld-xrf/how-xrf-works.html>.

Brykov, A. & Anisimova, A. 2013, 'Efficacy of Aluminum Hydroxides as Inhibitors of Alkali-Silica Reactions', *Materials Sciences and Applications*, vol. 4, pp. 1-6.

Burke, P.J., Best, R. & Jotzo, F. 2018, *Closures of coal-fired power stations in Australia:Local unemployment effects*, Crawford School of Public Policy, The Australian National University.

Canham, I., Page, C.L. & Nixon, P.J. 1987, 'Aspects of the Pore Solution Chemistry of Blended Cements Related to the Control of Alkali-Silica Reaction', *Cement and Concrete Research*, vol. 17, pp. 839-44.

Caruso, F., Mantellato, S., Palacios, M. & Flatt, R.J. 2017, 'ICP-OES method for the characterization of cement pore solutions and their modification by polycarboxylate-based superplasticizers', *Cement and Concrete Research*, vol. 91, pp. 52–60.

Chappex, T. & Scrivener, K. 2012a, 'Alkali fixation of C–S–H in blended cement pastes and its relation to alkali silica reaction', *Cement and Concrete Research* vol. 42, pp. 1049–54.

Chappex, T. & Scrivener, K. 2012b, 'The influence of aluminium on the dissolution of amorphous silica and its relation to alkali silica reaction', *Cement and Concrete Research*, vol. 42, pp. 1645–9.

Chappex, T. & Scrivener, K. 2013, 'The Effect of Aluminum in Solution on the Dissolution of Amorphous Silica and its Relation to Cementitious Systems', *Journal of American Ceramic Society*, vol. 96, no. 2, pp. 592-7.

Chappex, T., Sofia, L., Dunant, C. & Scrivener, K. 2016, 'A Robust Testing Protocol for the Assessment of ASR Reactivity of Concrete', *15th International*

Conference on Alkali Aggregate Reaction in Concrete (ICAAR), São Paulo Brazil.

Chatterji, S. 2005, 'Chemistry of alkali–silica reaction and testing of aggregates', *Cement & Concrete Composites*, vol. 27, pp. 788–95.

Chen, C.-T. & Yang, W.-C. 2013, 'Mitigation of Alkali-Silica Reaction in Mortar with Limestone Addition and Carbonation', paper presented to the *Third International Conference on Sustainable Construction Materials and Technologies*, Japan.

Constantiner, D. & Diamond, S. 2003, 'Alkali release from feldspars into pore solutions', *Cement and Concrete Research* vol. 33, pp. 549–54.

Costa, U., Mangialardi, T. & Paolini, A.E. 2017, 'Minimizing alkali leaching in the concrete prism expansion test at 38ºC', *Construction and Building Materials* vol. 146, pp. 547–54.

Criado, M., Fernández-Jiménez, A., Torre, A.G.d.l., Aranda, M.A.G. & Palomo, A. 2007, 'An XRD study of the effect of the SiO_2/Na_2O ratio on the alkali activation of fly ash', *Cement and Concrete Research* vol. 37, pp. 671–9.

D8 Advance/D8 Discover User Manual 2010, Bruker AXS GmbH, Germany.

Deschner, F., Lothenbach, B., Winnefeld, F. & Neubauer, J. 2013, 'Effect of temperature on the hydration of Portland cement blended with siliceous fly ash', *Cement and Concrete Research* vol. 52, pp. 169-81.

Dhir, R.K., Limbachiya, M.C., McCarthy, M.J. & Chaipanich, A. 2007, 'Evaluation of Portland limestone cements for use in concrete construction', *Materials and Structures* pp. 459-73.

Drolet, C., Duchesne, J. & Fournier, B. 2017, 'Effect of alkali release by aggregates on alkali-silica reaction', *Construction and Building Materials* vol. 157, pp. 263–76.

Duana, P., Shui, Z., Chena, W. & Shen, C. 2013, 'Effects of metakaolin, silica fume and slag on pore structure, interfacial transition zone and compressive strength of concrete', *Construction and Building Materials* vol. 44, pp. 1-6.

Duchesne, J. & Berube, M.-A. 1994a, 'The Effectiveness of Supplementary Cementing Materials in Suppressing Expansion Due to ASR: Another Look at the Reaction Mechanisms Part 1: Concrete Expansion and Portlandite Depletion', *Cement and Concrete Research*, vol. 24, pp. 73-82.

Duchesne, J. & Berube, M.-A. 2001, 'Long-term effectiveness of supplementary cementing materials against alkali–silica reaction', *Cement and Concrete Research* vol. 31, pp. 1057–63.

Duchesne, J. & Berube, M.A. 1994b, 'The Effectiveness of Supplementary Cementing Materials in Suppressing Expansion Due to ASR: Another Look at the Reaction Mechanisms Part 2: Pore Solution Chemistry', *Cement and Concrete Research*, vol. 24, no. 2, pp. 221-30.

Durand, B., Berard, J., Roux, R. & Soles, J. 1990, 'Alkali-Silica Reaction: The Relation Between Pore Solution Characteristics and Expansion Test Results', *Cement and Concrete Research*, vol. 20, pp. 419-28.

Durdziński, P.T., Dunant, C.F., Haha, M.B. & Scrivener, K.L. 2015, 'A new quantification method based on SEM-EDS to assess fly ash composition and study the reaction of its individual components in hydrating cement paste', *Cement and Concrete Research* vol. 73, pp. 111–22.

ECRC 2017, *Environment and Communications References Committee-Retirement of coal fired power stations*, <https://www.aph.gov.au/Parliamentary_Business/Committees/Senate/Environment_and_Communications/Coal_fired_power_stations/Final_Report>.

Einarsdottir, S.U. & Hooton, R.D. 2018, 'Modifications to ASTM C1293 that Allow Testing of Low Alkali Binder Systems', *ACI Materials Journal*, vol. 115, no. 5.

Escalante, J.I., Gómez, L.Y., Johal, K.K., Mendoza, G., Mancha, H. & Méndez, J. 2001, 'Reactivity of blast-furnace slag in Portland cement blends hydrated under different conditions', *Cement and Concrete Research*, vol. 31, no. 10, pp. 1403-9.

Fabbri, B., Gualtieri, S. & Leonardi, C. 2013, 'Modifications induced by the thermal treatment of kaolin and determination of reactivity of metakaolin', *Applied Clay Science* vol. 73, pp. 2–10.

Feng, X., Jia, Y. & Hu, C. 2013, 'Effect of Admixtures Rich in Aluminium on Expansion due to Alkali-Silica Reaction', *Applied Mechanics and Materials* vol. 268-270, pp. 806-10.

Fernandes, I. 2009, 'Composition of alkali–silica reaction products at different locations within concrete structures', *Materials Characterization*, vol. 60, pp. 655-68.

Fernandes, I., Noronha, F. & Teles, M. 2007, 'Examination of the concrete from an old Portuguese dam: Texture and composition of alkali–silica gel', *Materials Characterization*, vol. 58, pp. 1160–70.

Fernandez-Jimenez, A. & Palomo, A. 2005, 'Composition and microstructure of alkali activated fly ash binder: Effect of the activator', *Cement and Concrete Research* vol. 35, pp. 1984 – 92.

Fernandez-Jimenez, A., Palomo, A., Sobrados, I. & Sanz, J. 2006, 'The role played by the reactive alumina content in the alkaline activation of fly ashes', *Microporous and Mesoporous Materials* vol. 91, pp. 111–9.

Fernandez-Jimenez, A., Torre, A.G.d.l., Palomo, A., Alonso, M.M. & Aranda, M.A.G. 2006, 'Quantitative determination of phases in the alkaline activation of fly ash. Part II: Degree of reaction', *Fuel* vol. 85, pp. 1960–9.

Gallucci, E., Zhang, X. & Scrivener, K.L. 2013, 'Effect of temperature on the microstructure of calcium silicate hydrate (C-S-H)', *Cement and Concrete Research* vol. 53, pp. 185–95.

Gavrilenko, E., Amo, D.G.d., Perez, B.C. & Garcia, E.G. 2007, 'Comparison of ASR-gels in concretes against accelerated mortar bar test samples', *Magazine of Concrete Research*, vol. 59, no. 7, pp. 483–94.

Gebregziabiher, B.S., Thomas, R.J. & Peethamparan, S. 2016, 'Temperature and activator effect on early-age reaction kinetics of alkali-activated slag binders', *Construction and Building Materials*, vol. 113, pp. 783-93.

Girao, A.V., Richardson, I.G., Porteneuve, C.B. & Brydson, R.M.D. 2007, 'Morphology and nanostructure C–S–H in white Portland cement–fly ash hydrated at 85°C', *Advances in Applied Ceramics*, vol. 106.

Glasser, L.D. & Kataoka, N. 1981, 'The Chemistry of Alkali-Aggregate Reaction', *Cement and Concrete Research*, vol. 11, pp. 1-9.

Golmakani, F. & Hooton, R.D. 2019, 'Impact of pore solution concentration on the accelerated mortar bar alkali-silica reactivity test', *Cement and Concrete Research*, vol. 121, pp. 72-80.

Hay, R. & Ostertag, C.P. 2019, 'On utilization and mechanisms of waste aluminium in mitigating alkali-silica reaction (ASR) in concrete', *Journal of Cleaner Production* vol. 212, pp. 864-79.

Hobbs, D.W. 1986, 'Deleterious expansion of concrete due to alkali-silica reaction: influence of pfa and slag', *Magazine of Concrete Research* vol. 38, pp. 191-205.

Hong, S.-Y. & Glasser, F.P. 1999, 'Alkali binding in cement pastes Part I. The C-S-H phase', *Cement and Concrete Research*, vol. 29, pp. 1893–903.

Hong, S.-Y. & Glasser, F.P. 2002, 'Alkali sorption by C-S-H and C-A-S-H gels Part II. Role of alumina', *Cement and Concrete Research*, vol. 32, pp. 1101–11.

Hooton, D., Rogers, C., MacDonald, C.A. & Ramlochan, T. 2013, 'Twenty-Year Field Evaluation of Alkali-Silica Reaction Mitigation', *ACI MATERIALS JOURNAL*, pp. 539-48.

Hooton, R.D., Nokken, M. & Thomas, M.D.A. 2007, 'Portland-Limestone Cement: State of the Art Report and Gap Analysis For CSA A 3000', *University of Toronto*.

Hu, B., Bertau, M., Jakubowski, N., Meinhardt, J., Meyer, F.M., Niederstraßer, J., Schramm, R., Sindern, S., Stosch, H.-G. & Golloch, A. 2017, *Handbook of Rare Earth Elements : Analytics*, De Gruyter, Inc., Germany.

Hünger, K.-J. 2007, 'The contribution of quartz and the role of aluminum for understanding the AAR with greywacke', *Cement and Concrete Research* vol. 37, pp. 1193–205.

Islam, M.S., Alam, M.S., Ghafoori, N. & Sadiq, R. 2016, 'Role of Solution Concentration, cement alkali and test duration on expansion of accelerated mortar bar test', *Materials and Structures*, vol. 49, pp. 1955-65.

Jawed, I. & Skalny, J. 1978, 'Alkalis in Cement: A Review', *Cement and Concrete Research*, vol. 8, pp. 37-52.

Johnson, S. & Chau, K. 2019, 'More U.S. coal-fired power plants are decommissioning as retirements continue', *Today in Energy*, <https://www.eia.gov/todayinenergy/detail.php?id=40212>.

Juenger, M.C.G. & Ostertag, C.P. 2004, 'Alkali–silica reactivity of large silica fume-derived particles', *Cement and Concrete Research* vol. 34, pp. 1389–402.

Juenger, M.C.G. & Siddique, R. 2015, 'Recent advances in understanding the role of supplementary cementitious materials in concrete', *Cement and Concrete Research* vol. 78, pp. 71–80.

Kim, T., Olek, J. & Jeong, H. 2015, 'Alkali–silica reaction: Kinetics of chemistry of pore solution and calcium hydroxide content in cementitious system', *Cement and Concrete Research*, vol. 71, pp. 36–45.

Kolani, B., Buffo-Lacarrière, L., Sellier, A., Escadeillas, G., Boutillon, L. & Linger, L. 2012, 'Hydration of slag-blended cements', *Cement & Concrete Composites 34* vol. 34, pp. 1009–18.

L'Hôpital, E., Lothenbach, B., Scrivener, K. & D.A.Kulik 2016, 'Alkali uptake in calcium alumina silicate hydrate (C-A-S-H)', *Cement and Concrete Research* vol. 85, pp. 122–36.

Leemann, A., Katayama, T., Fernandes, I. & Broekmans, M.A.T.M. 2016, 'Types of alkali–aggregate reactions and the products formed', *Construction Materials*, vol. 169, pp. 128-35.

Leemann, A. & Lothenbach, B. 2008, 'The influence of potassium–sodium ratio in cement on concrete expansion due to alkali-aggregate reaction', *Cement and Concrete Research*, vol. 38, pp. 1162–8.

Leemann, A. & Lura, P. 2013, 'E-modulus of the alkali–silica-reaction product determined by micro-indentation', *Construction and Building Materials* vol. 44, pp. 221–7.

Leemann, A. & Merz, C. 2013, 'An attempt to validate the ultra-accelerated microbar and the concrete performance test with the degree of AAR-induced damage observed in concrete structures', *Cement and Concrete Research*, vol. 49, pp. 29–37.

Leemann, A., Saout, G.L., Winnefeld, F., Rentsch, D. & Lothenbach, B. 2011, 'Alkali–Silica Reaction: the Influence of Calcium on Silica Dissolution and the Formation of Reaction Products', *Journal of American Ceramic Society*, vol. 94, pp. 1243–9

Leng, Y. 2013, *Materials Characterization Introduction to Microscopic and Spectroscopic Methods*, Second edn, Wiley-VCH Verlag GmbH & Co. KGaA, Weinheim, Germany.

Li, C., Sun, H. & Li, L. 2010, 'A review: The comparison between alkali-activated slag (Si+ Ca) and metakaolin (Si+Al) cements', *Cement and Concrete Research*, vol. 40, pp. 1341–9.

Li, Z., Afshinnia, K. & Rangaraju, P.R. 2016, 'Effect of alkali content of cement on properties of high performance cementitious mortar', *Construction and Building Materials*, vol. 102, pp. 631–9.

Lindgård, J., Andiç-Çakır, Ö., Fernandes, I., Rønning, T. & Thomas, M. 2012, 'Alkali–silica reactions (ASR): Literature review on parameters influencing

laboratory performance testing', *Cement and Concrete Research* vol. 42, pp. 223–43.

Lindgård, J., Thomas, M.D.A., Sellevold, E.J., Pedersen, B., Andiç-Çakır, Ö., Justnes, H. & Rønning, T.F. 2013, 'Alkali–silica reaction (ASR)—performance testing: Influence of specimen pre-treatment, exposure conditions and prism size on alkali leaching and prism expansion', *Cement and Concrete Research*, vol. 53, pp. 68–90.

Lollini, F., Redaelli, E. & Bertolini, L. 2014, 'Effects of portland cement replacement with limestone on the properties of hardened concrete', *Cement & Concrete Composites* vol. 46, pp. 32–40.

Lothenbach, B., Saout, G.L., Gallucci, E. & Scrivener, K. 2008, 'Influence of limestone on the hydration of Portland cements', *Cement and Concrete Research* vol. 38, pp. 848–60.

Lothenbach, B., Scrivener, K. & Hooton, R.D. 2011a, 'Supplementary cementitious materials', *Cement and Concrete Research* vol. 41, pp. 1244–56.

Lothenbach, B., Scrivener, K. & Hooton, R.D. 2011b, 'Supplementary cementitious materials', *Cement and Concrete Research*, vol. 41, pp. 1244–56.

Lothenbach, B., Winnefeld, F., Alder, C., Wieland, E. & Lunk, P. 2007, 'Effect of temperature on the pore solution, microstructure and hydration products of Portland cement pastes', *Cement and Concrete Research* vol. 37, pp. 483–91.

Madani, A., Aznar, A., Sanz, J. & Serratosa, J.M. 1990, '29Si and 27Al NMR Study of Zeolite Formation from Alkali-Leached Kaolinites. Influence of Thermal Preactivation', *Journal of Physical Chemistry*, vol. 94, pp. 760-5.

Mahanama, D., Silva, P.D., Kim, T., Castel, A. & Khan, M.S.H. 2019, 'Evaluating Effect of GGBFS in Alkali–Silica Reaction in Geopolymer Mortar with

Accelerated Mortar Bar Test', *Journal of Materials in Civil Engineering*, vol. 31, no. 8.

Matschei, T. & Glasser, F.P. 2010, 'Temperature dependence, 0 to 40°C, of the mineralogy of Portland cement paste in the presence of calcium carbonate', *Cement and Concrete Research*, vol. 40, no. 5, pp. 763-77.

Matschei, T., Lothenbach, B. & Glasser, F.P. 2007, 'Thermodynamic properties of Portland cement hydrates in the system $CaO–Al_2O_3–SiO_2–CaSO_4–CaCO_3–H_2O$', *Cement and Concrete Research* vol. 37, pp. 1379–410.

Mohammadi, I. & South, W. 2016a, 'General purpose cement with increased limestone content in Australia', *ACI Materials Journal*, vol. 113, pp. 335-47.

Mohammadi, J. & South, W. 2016b, 'Effect of up to 12% substitution of clinker with limestone on commercial grade concrete containing supplementary cementitious materials', *Construction and Building Materials* vol. 115, pp. 555–64.

Mohammadi, J., South, W. & Chalmers, D. 2015, 'Towards a More Sustainable Australian Cement and Concrete Industry ', *27th biennial national conference of the concrete institute of Australia in conjunction with the 69th RILEM week conference*, Concrete Institute of Australia, Melbourne, Australia, pp. 596-603.

Monteiro, P.J.M., Wang, K., Sposito, G., Santos, M.C.d. & Andrade, W.P.d. 1997, 'Influence of Mineral Admixtures on Alkali-Aggregate Reaction', *Cement and Concrete Research*, vol. 27, no. 12, pp. 1899-909.

Mota, B., Matschei, T. & Scrivener, K. 2018, 'Impact of NaOH and Na2SO4 on the kinetics and microstructural development of white cement hydration', *Cement and Concrete Research*, vol. 108, pp. 172–85.

Nalbandian-Sugden, H. 2015, *New regulatory trends: effects on coal-fired powerplants and coal demand*, IEA Clean Coal Centre, United Kingdom.

Newlands, K.C., Foss, M., Matchei, T., Skibsted, J. & Macphee, D.E. 2017, 'Early stage dissolution characteristics of aluminosilicate glasses with blast furnace slag- and fly-ash-like compositions', *Journal of American Ceramic Society*, vol. 100, pp. 1941–55.

Palomo, A., Grutzeck, M.W. & Blanco, M.T. 1999, 'Alkali-activated fly ashes: A cement for the future', *Cement and Concrete Research* vol. 29, pp. 1323–9.

Panagiotopoulou, C., Kontori, E., Perraki, T. & Kakali, G. 2007, 'Dissolution of aluminosilicate minerals and by-products in alkaline media', *Journal of Material Science*, vol. 42, pp. 2967–73.

Pane, I. & Hansen, W. 2005, 'Investigation of blended cement hydration by isothermal calorimetry and thermal analysis', *Cement and Concrete Research*, vol. 35, no. 6, pp. 1155-64.

Rajabipour, F., Giannini, E., Dunant, C., Ideker, J. & Thomas, M. 2015, 'Alkali–silica reaction: Current understanding of the reaction mechanisms and the knowledge gaps', *Cement and Concrete Research*, vol. 76, pp. 130–46.

Rajbhandari, N. 2010, 'Determining the Effect of Intergrinding Limestone with Portland Cement on the Durability of Concrete with and without SCM ', The University of New Brunswick.

Ramachandran, V.S., Paroli, R.M., Beaudoin, J.J. & Delgado, A.H. 2002, *Handbook of Thermal Analysis of Construction Materials*, Noyes Publications, United States.

Ramezanianpour, A.M. & Hooton, R.D. 2014, 'A study on hydration, compressive strength, and porosity of Portland-limestone cement mixes containing SCMs', *Cement and Concrete Composites*, vol. 51, pp. 1-13.

Ramezanianpour, A.M. & Hooton, R.D. 2014 'A study on hydration, compressive strength, and porosity of Portland-limestone cement mixes containing SCMs', *Cement & Concrete Composites*, vol. 51, pp. 1–13.

Ramlochan, T., Thomas, M. & Gruber, K.A. 2000, 'The effect of metakaolin on alkali-silica reaction in concrete', *Cement and Concrete Research* vol. 30, pp. 339-44.

Rashad, A.M. 2013, 'Metakaolin as cementitious material: History, scours, production and composition –A comprehensive overview', *Construction and Building Materials* vol. 41, pp. 303–18.

Rasheeduzzafar & Hussain, S.E. 1991, 'Effect of microsilica and blast furnace slag on pore solution composition and alkali-silica reaction', *Cement and Concrete Composites*, vol. 13, no. 3, pp. 219-25.

Rivard, P., Berube, M.A., Ollivier, J.P. & Ballivy, G. 2007, 'Decrease of pore solution alkalinity in concrete tested for alkali-silica reaction', *Materials and Structures* vol. 40, pp. 909-21.

Rossen, J.E., Lothenbach, B. & K.L.Scrivener 2015, 'Composition of C–S–H in pastes with increasing levels of silica fume addition', *Cement and Concrete Research* vol. 75, pp. 14–22.

Saeki, T. & Monteiro, P.J.M. 2005, 'A model to predict the amount of calcium hydroxide in concrete containing mineral admixtures', *Cement and Concrete Research*, vol. 35, no. 10, pp. 1914-21.

Sang, J.C., Jakubik, R.F. & Barkatt, A. 1994, 'The interaction of solutes with silicate glass and its effect on dissolution rates', *Journal of Non-Crystalline Solids* vol. 167, pp. 158-71.

Schmidt, T., Lothenbach, B., Romer, M., Neuenschwander, J. & Scrivener, K. 2009, 'Physical and microstructural aspects of sulfate attack on ordinary and limestone blended Portland cements', *Cement and Concrete Research*, vol. 39, no. 12, pp. 1111-21.

Schöler, A., Lothenbach, B., FrankWinnefeld, Haha, M.B., Zajac, M. & Ludwig, H.-M. 2017, 'Early hydration of SCM-blended Portland cements: A pore solution and isothermal calorimetry study', *Cement and Concrete Research* vol. 93, pp. 71–82.

Scholz, Y., Hübert, C. & Hünger, K.-J. 2016, 'The Influence of Supplementary Cementing Materials on the Dissolution of Aggregates in Alkaline Solutions ', paper presented to the *15th International Conference on Alkali-Aggregate Reaction (ICAAR 2016)*, Brazil.

Scrivener, K., Martirena, F., Bishnoic, S. & Maity, S. 2018, 'Calcined clay limestone cements (LC3)', *Cement and Concrete Research*, vol. 114, pp. 49–56.

Scrivener, K., Snellings, R. & Lothenbach, B. 2016, *A Practical Guide to Microstructural Analysis of Cementitious Materials*, Taylor & Francis Group, LLC, Boca Raton, FL.

Scrivener, K.L., John, V.M. & Gartner, E.M. 2016, *Eco-Efficient Cements: Potential, economically viable solutions for a low CO_2 cement-based materials industry*, United Nations Environment Program.

Scrivener, K.L. & Monteiro, P.J.M. 1994, 'The Alkali-Silica Reaction in a Monolithic Opal', *Journal of American Ceramic Society*, vol. 77, no. 11, pp. 2849-56.

Scrivener, K.L. & Taylor, H.F.W. 1993, 'Delayed ettringite formation: a microstructural and microanalytical study', *Advances in Cement Research*, vol. 5, no. 20, pp. 139 - 46.

Shafaatian, S.M.H., Akhavan, A., Maraghechi, H. & Rajabipour, F. 2013, 'How does fly ash mitigate alkali–silica reaction (ASR) in accelerated mortar bar test (ASTM C1567)?', *Cement & Concrete Composites* vol. 37, pp. 143–53.

Shannon, J., Howard, I.L., Cost, V.T. & Crawley, W. 2017, 'Synergistic Potential of Fly Ash in Concrete Featuring Portland-Limestone Cement', *ACI Materials Journal*, pp. 295-306.

Shayan, A., Diggins, R. & Ivanusec, I. 1996a, 'Effectiveness of Fly Ash in Preventing Deleterious Expansion Due to Alkali-Aggregate in Normal and Steam-Cured Concrete', *Cement and Concrete Research*, vol. 26, no. 1, pp. 153-64.

Shayan, A., Diggins, R. & Ivanusec, I. 1996b, 'Effectiveness of Fly Ash in Preventing Deleterious Expansion due to Alkali-Aggregate Reaction in Normal and Steam-Cured Concrete', *Cement and Cocrete Research*, vol. 26, pp. 153-64.

Shehata, M.H. & Thomas, M.D.A. 2000, 'The effect of fly ash composition on the expansion of concrete due to alkali-silica reaction', *Cement and Concrete Research*, vol. 30, pp. 1063-72.

Shehata, M.H. & Thomas, M.D.A. 2002, 'Use of ternary blends containing silica fume and fly ash to suppress expansion due to alkali–silica reaction in concrete', *Cement and Concrete Research*, vol. 32, pp. 341–9.

Shehata, M.H. & Thomas, M.D.A. 2006, 'Alkali release characteristics of blended cements', *Cement and Concrete Research*, vol. 36, pp. 1166–75.

Shehata, M.H., Thomas, M.D.A. & Bleszynski, R.F. 1999, 'The effects of fly ash composition on the chemistry of pore solution in hydrated cement pastes', *Cement and Concrete Research*, vol. 29, pp. 1915–20.

Shia, Z., Geng, G., Leemann, A. & Lothenbach, B. 2019, 'Synthesis, characterization, and water uptake property of alkali-silica reaction products', *Cement and Concrete Research*, vol. 121, pp. 58–71.

Shimada, Y. & Young, J.F. 2004, 'Thermal stability of ettringite in alkaline solutions at 80ºC', *Cement and Concrete Research* vol. 34, pp. 2261–8.

Siddique, R. & Khan, M.I. 2011, 'Supplementary Cementing Materials', *Engineering Materials*.

Sirivivatnanon, V., Mohammadi, J. & South, W. 2016, 'Reliability of new Australian test methods in predicting alkali silica reaction of field concrete', *Construction and Building Materials*, vol. 126 pp. 868–74.

Skibsted, J. & Andersen, M.D. 2013, 'The Effect of Alkali Ions on the Incorporation of Aluminum in the Calcium Silicate Hydrate (C–S–H) Phase Resulting from Portland Cement Hydration Studied by 29Si MAS NMR', *Journal of American Ceramic Society*, vol. 96, no. 2, pp. 651-6.

Smith, A.S. 1997, 'Quartz Bearing Aggregates and their Role in the Alkali-Silica Reaction in Concrete Prism Test ', Phd thesis, University of Leicester.

Snellings, R. & Scrivener, K.L. 2016, 'Rapid screening tests for supplementary cementitious materials: past and future', *Materials and Structures*, vol. 49, pp. 3265–79.

Standards Australia 2010, *General Purpose and Blended Cements*, AS 3972 SAI Global Limited, Sydney, Australia.

Standards Australia 2015, *Alkali Aggregate Reaction—Guidelines on Minimising the Risk of Damage to Concrete Structures in Australia*, SA HB 79:2015, SAI Global Limited, Sydney, Australia.

Stanton, T.E. 1940, 'Expansion of Concrete through Reaction between Cement and Aggregate', *Proceedings of the American Society of Civil Engineers*, vol. 66, pp. 1781-811.

Suraneni, P. & Weiss, J. 2017, 'Examining the pozzolanicity of supplementary cementitious materials using isothermal calorimetry and thermogravimetric analysis', *Cement and Concrete Composites*, vol. 83, pp. 273-8.

Tanzer, R., Buchwald, A. & Stephan, D. 2015, 'Effect of slag chemistry on the hydration of alkali-activated blast-furnace slag', *Materials and Structures* vol. 48, pp. 629–41.

Taylor, H., Famy, C. & Scrivener, K. 2001, 'Delayed Ettringite Formation', *Cement and Concrete Research*, vol. 31, pp. 683-93.

Taylor, H.F.W. 1997, *Cement Chemistry*, Second Edition edn, Thomas Telford Publishing, Thomas Telford Services Ltd, London.

Taylor, R., Richardson, I.G. & Brydson, R.M.D. 2010, 'Composition and microstructure of 20-year-old ordinary Portland cement–ground granulated blast-furnace slag blends containing 0 to 100% slag', *Cement and Concrete Research*, vol. 40, pp. 971–83.

Teipel, U. 2005, *Energetic Materials*, WILEY-VCH Verlag GmbH & Co. KGaA, Weinheim, Germany.

Tennis, P.D., Thomas, M.D.A. & Weiss, W.J. 2011, *State-of-the-Art Report on Use of Limestone in Cements of up to 15%*, Portland Cement Association.

Thaulow, N., Jakobsen, U.H. & Clark, B. 1996, 'Composition of Alkali Silica Gel and Ettringite in Concrete Railroad Ties: SEM-EDX and X-Ray Diffraction Analyses', *Cement and Concrete Research*, vol. 26, no. 2, pp. 309-18.

Thomas, M. 2011, 'The effect of supplementary cementing materials on alkali-silica reaction: A review', *Cement and Concrete Research*, vol. 41, pp. 1224–31.

Thomas, M., Fournier, B., Folliard, K., Ideker, J. & Shehata, M. 2006, 'Test methods for evaluating preventive measures for controlling expansion due to alkali–silica reaction in concrete', *Cement and Concrete Research* vol. 36, pp. 1842–56.

Thomas, M.D.A. 1996, 'Field studies of fly ash concrete structures containing reactive aggregates ', *Magazine of Concrete Research*, vol. 48, no. 177, pp. 265-79.

Thomas, M.D.A. 2013, *Supplementary Cementing Materials in Concrete*, Taylor & Francis Group, LLC, Boca Raton, Florida.

Thomas, M.D.A., Cail, K., Blair, B., Delagrave, A. & Barcelo, L. 2010, 'Equivalent Performance with Half the Clinker Content using PLC and SCM ', paper presented to the *2010 Concrete Sustainability Conference*.

Thomas, M.D.A., Delagrave, A., Blair, B. & Barcelo, L. 2013, 'Equivalent Durability Performance of Portland Limestone Cement', *Concrete International*, pp. 39-5.

Thomas, M.D.A., Dunster, A., Nixon, P. & Blackwell, B. 2011, 'Effect of fly ash on the expansion of concrete due to alkali-silica reaction – Exposure site studies', *Cement & Concrete Composites*, vol. 33, pp. 359–67.

Thomas, M.D.A., Fournier, B., Folliard, K.J., Shehata, M.H., Jason H. Ideker & Rogers, C. 2007, 'Performance Limits for Evaluating Supplementary Cementing Materials Using Accelerated Mortar Bar Test', *ACI MATERIALS JOURNAL*, pp. 115-22.

Thomson, V.E., Huelsman, K. & Ong, D. 2018, 'Coal-fired power plant regulatory rollback in the United States: Implications for local and regional public health', *Energy Policy*, vol. 123, pp. 558–68.

Tsivilis, S., Batis, G., Chaniotakis, E., Grigoriadis, G. & Theodossis, D. 2000, 'Properties and behavior of limestone cement concrete and mortar', *Cement and Concrete Research*, vol. 30, no. 10, pp. 1679-83.

Tsivilis, S., Tsantilas, J., Kakali, G., Chaniotakis, E. & Sakellariou, A. 2003, 'The permeability of Portland limestone cement concrete', *Cement and Concrete Research*, vol. 33, no. 9, pp. 1465-71.

Turk, K., Kina, C. & Bagdiken, M. 2017, 'Use of binary and ternary cementitious blends of F-Class fly-ash and limestone powder to mitigate alkali-silica reaction risk', *Construction and Building Materials*, vol. 151, pp. 422–7.

Voglis, N., Kakali, G., Chaniotakis, E. & Tsivilis, S. 2005, 'Portland-limestone cements. Their properties and hydration compared to those of other composite cements', *Cement & Concrete Composites* vol. 27 pp. 191–6.

Vollpracht, A., Lothenbach, B., Snellings, R. & Haufe, J. 2016, 'The pore solution of blended cements: a review', *Materials and Structures*, vol. 49, pp. 3341–67.

Wang, H., Wu, D. & Mei, Z. 2019, 'Effect of fly ash and limestone powder on inhibiting alkali aggregate reaction of concrete', *Construction and Building Materials* vol. 210, pp. 620–6.

Weerdt, K.D., Haha, M.B., Saout, G.L., Kjellsen, K.O., Justnes, H. & Lothenbach, B. 2011, 'Hydration mechanisms of ternary Portland cements containing limestone powder and fly ash', *Cement and Concrete Research* vol. 41, pp. 279–91.

Weerdt, K.D., Kjellsen, K.O., Sellevold, E. & Justnes, H. 2011, 'Synergy between fly ash and limestone powder in ternary cements', *Cement & Concrete Composites* vol. 33, pp. 30–8.

Yamada, K., Karasuda, S., Ogawa, S., Sagawa, Y., Osako, M., Hamada, H. & Isneini, M. 2014, 'CPT as an evaluation method of concrete mixture for ASR expansion', *Construction and Building Materials*, vol. 64, pp. 184–91.

Ye, H. & Radlińska, A. 2016, 'Quantitative Analysis of Phase Assemblage and Chemical Shrinkage of Alkali-Activated Slag', *Journal of Advanced Concrete Technology*, vol. 14, pp. 245-60.

Zhang, B., MacKenzie, K.J.D. & Brown, I.W.M. 2009, 'Crystalline phase formation in metakaolinite geopolymers activated with NaOH and sodium silicate', *Journal of Material Science* vol. 44, pp. 4668–76.

Appendix A- Pore Solution Analysis

Table 1-A Low alkali OPC with 25% SCM replacement, 28 days hydration

Binder System (Australian Cement)	Al [mg/L]	Ca [mg/L]	K [mg/L]	Na [mg/L]	S [mg/L]	Si [mg/L]
Low Alkali OPC	3.3	113.1	10650.0	4170.0	133.8	5.2
Low Alkali OPC+25%SL	3.5	90.9	7920.0	3570.0	123.6	5.0
Low Alkali OPC+25%FA	3.4	80.7	5800.0	3540.0	109.2	5.6
Low Alkali OPC+25%MK	17.3	16.6	654.0	487.0	5.2	1.7
Low Alkali OPC+25%SF	0.0	687.0	309.0	330.0	25.5	1.8

Table A-2 High alkali OPC with 25% SCM replacement, 28 days hydration

Binder System (German Cement)	Al [mg/L]	Ca [mg/L]	K [mg/L]	Na [mg/L]	S [mg/L]	Si [mg/L]
High Alkali OPC	6.8	46.5	20130.0	2805.0	699.0	9.3
High Alkali OPC+25%SL	10.9	55.5	14880.0	2730.0	122.4	5.3
High Alkali OPC+25%FA	3.9	57.6	12240.0	2139.0	136.8	5.0
High Alkali OPC+25%MK	88.5	28.9	4320.0	912.0	98.1	14.3
High Alkali OPC+25%SF	0.0	633.0	528.0	195.0	24.2	0.0

Table A-3 Binder Systems for the Simulated Pore Solution, 28 days hydration

Binder System (Australian Cement)	Al [mg/L]	Ca [mg/L]	K [mg/L]	Na [mg/L]	S [mg/L]	Si [mg/L]
Low alkali OPC	3.3	113.1	10650.0	4170.0	133.8	5.2
Low alkali OPC+25%FA	3.4	80.7	5800.0	3570.0	109.2	5.6
Low alkali OPC+25%FA+0.2%Alkali	3.5	75.6	5760.0	5310.0	84.6	5.1
Low alkali OPC+25%FA+0.4% Alkali	5.1	74.7	5550.0	7380.0	115.8	5.8
Low alkali OPC+50%SL	7.6	93.0	4530.0	2724.0	46.5	4.9
Low alkali OPC+50%SL+0.2% Alkali	9.0	80.4	4050.0	3990.0	65.1	5.8
Low alkali OPC+50%SL+0.4% Alkali	9.5	69.0	4050.0	5640.0	81.9	6.2

Table A-4 OPC with 25% limestone substitution, 28 days hydration

Binder System	Al [mg/l]	Ca [mg/l]	K [mg/l]	Na [mg/l]	S [mg/l]	Si [mg/l]
Low Alkali OPC	3.3	113.1	10650.0	4170.0	133.8	5.2
Low Alkali Cement + 25% Limestone	1.8	108.9	7920.0	3450.0	76.5	3.5
High Alkali OPC	6.8	46.5	20130.0	2805.0	699.0	9.3
High Alkali Cement + 25% Limestone	3.4	81.0	13620.0	2100.0	375.0	3.7

Appendix B- ASR gel near paste

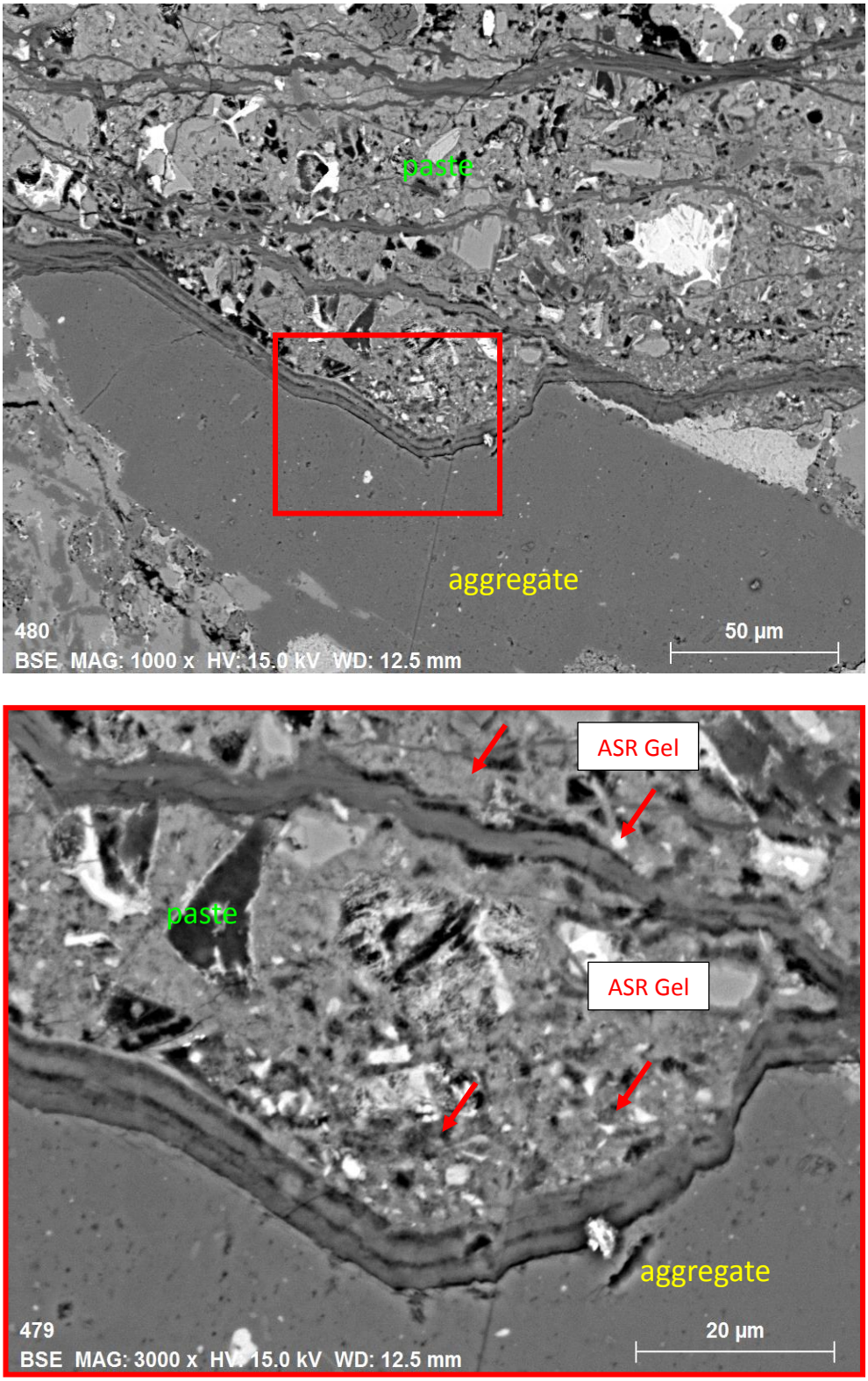

Figure B-1 ASR gel around aggregates and in the cement paste

Appendix C- EDS Maps of ASR gel

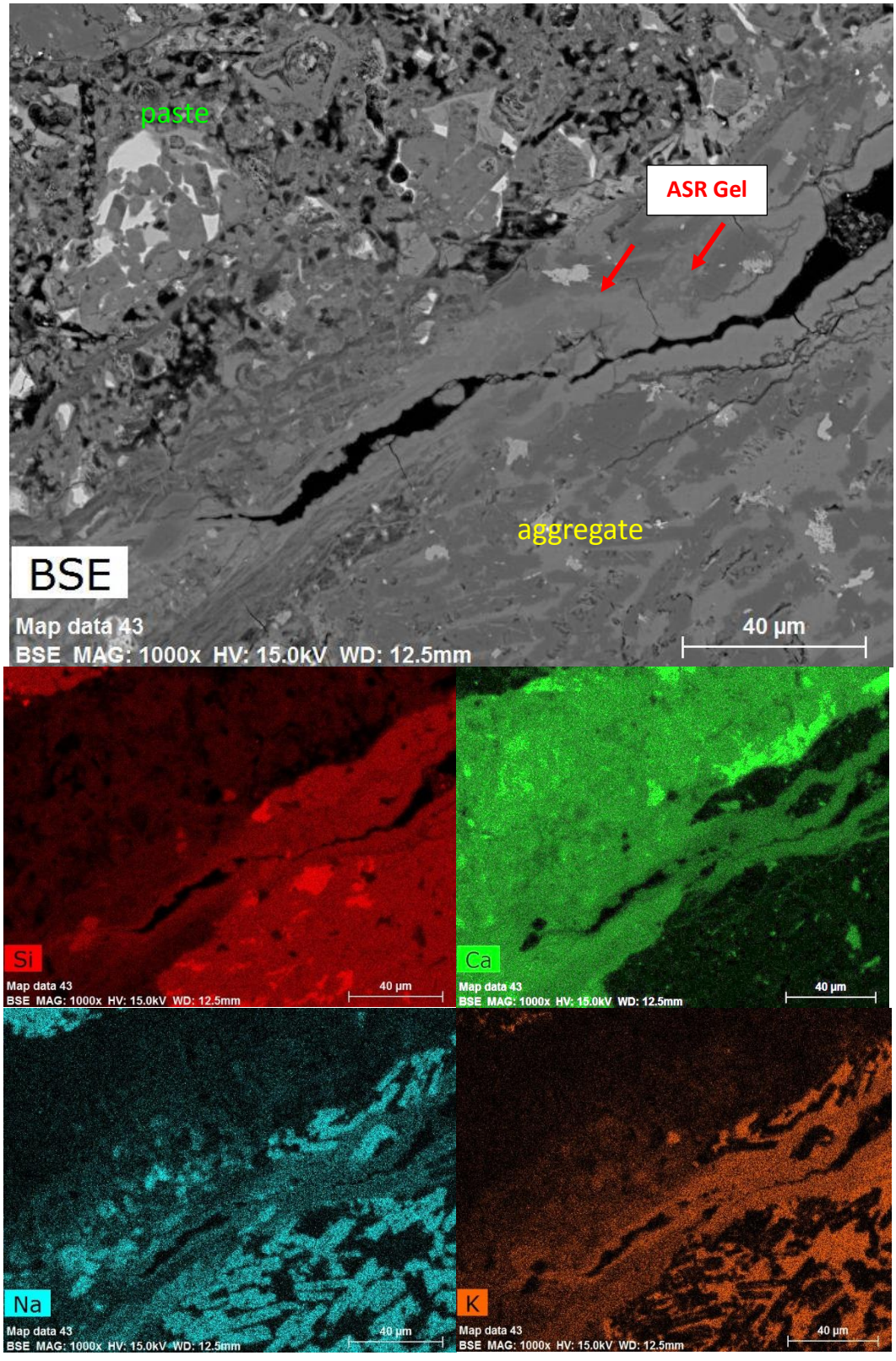

Figure C-1 EDS Map of ASR Gel in Rhyolite Aggregate (CPT, No SCM)

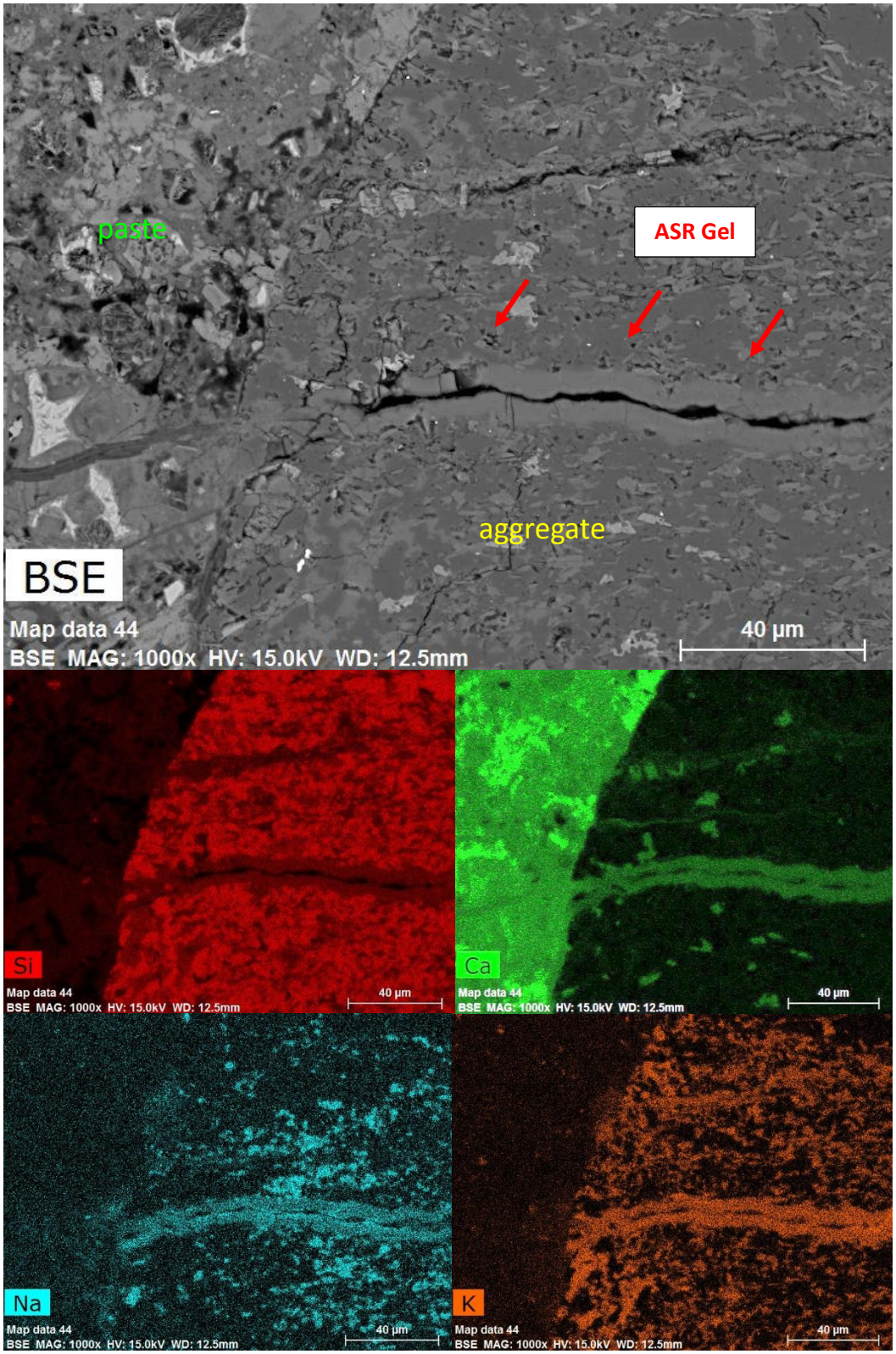

Figure C-2 EDS Map of ASR Gel in Dacite Aggregate (CPT, No SCM)

Appendix D- EDS Maps of Sectioned Mortars

Elemental mapping in Figures D1-D7 show distribution of calcium (Ca)-**green**, silicon (Si)-**red**, aluminium (Al)-**yellow**, sodium (Na)-**light blue** and carbon (C) **(purple)**.in the phases of the sectioned mortars. The denser the color, the more abundant is the element at a particular area. Presence of Na **(light blue)** is likely due to 1M NaOH solution used in AMBT. The presence of carbon (purple regions) in the EDS map confirm the presence of limestone ($CaCO_3$). The carbon however does not register a very dense color as all mortars were subjected to carbon coating prior to SEM EDS analysis.

Ca **(green)** is attributed to the calcium rich cement paste, portlandite, limestone and slag. Si (**red**) is due to aggregates and SCMs (FA, MK, SF, SL). The prominence Al (**yellow)** in the mortars containing slag, fly ash and metakaolin can be observed as well.

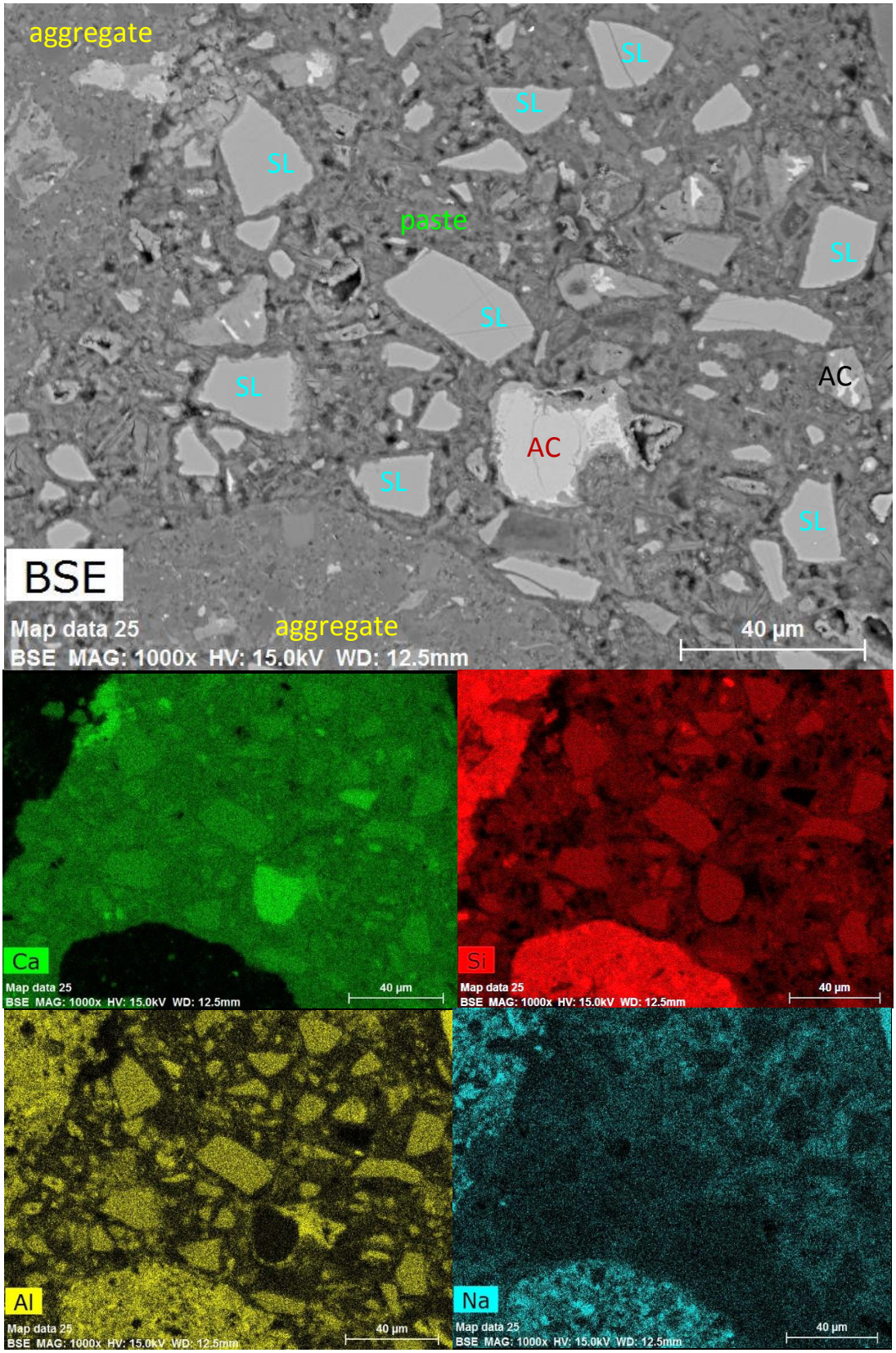

Figure D-1 EDS Map of mortar+65%SL where SL=slag and AC=anhydrous clinker

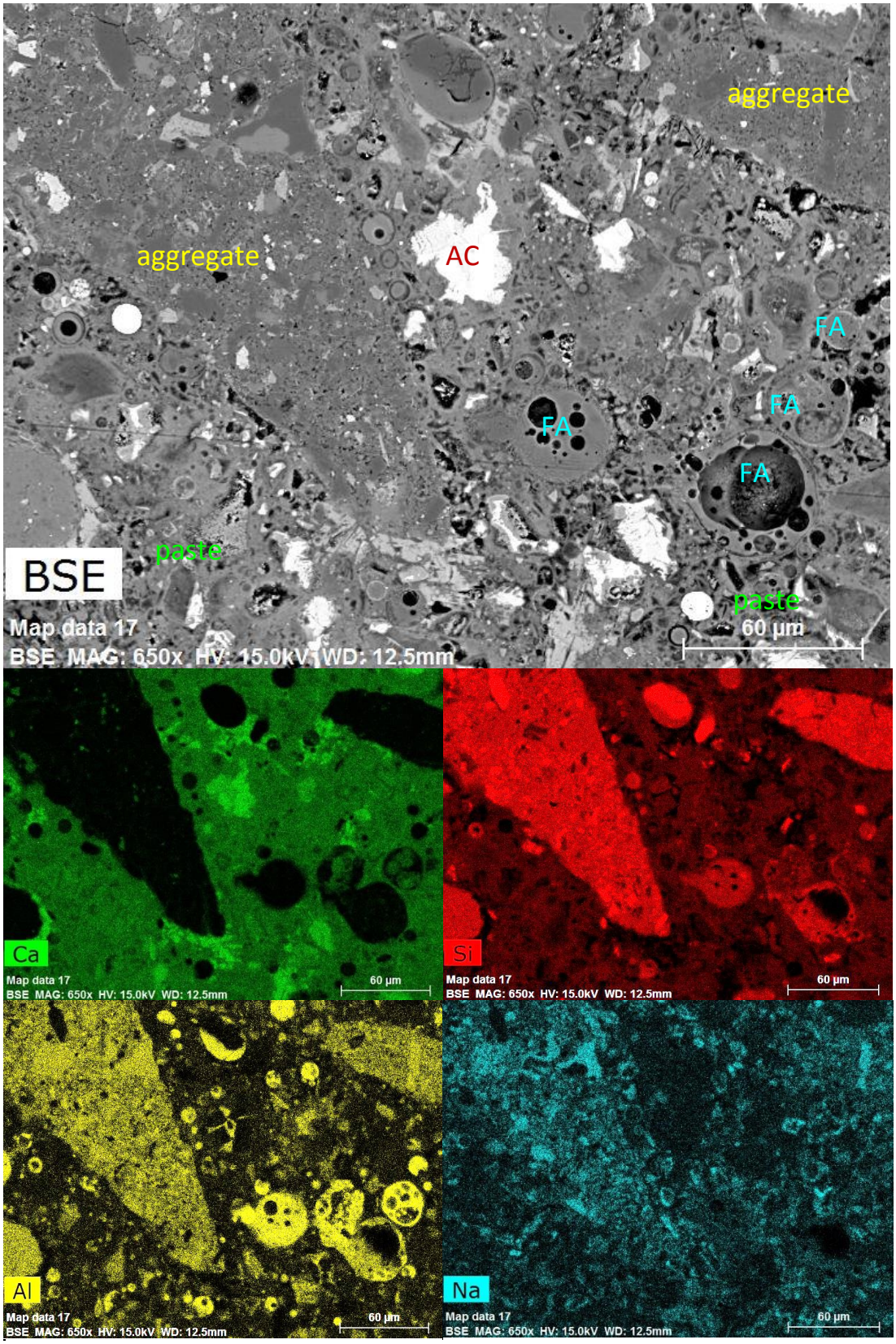

Figure D-2 EDS map of mortar+ 25% FA where FA=fly ash and AC=anhydrous clinker

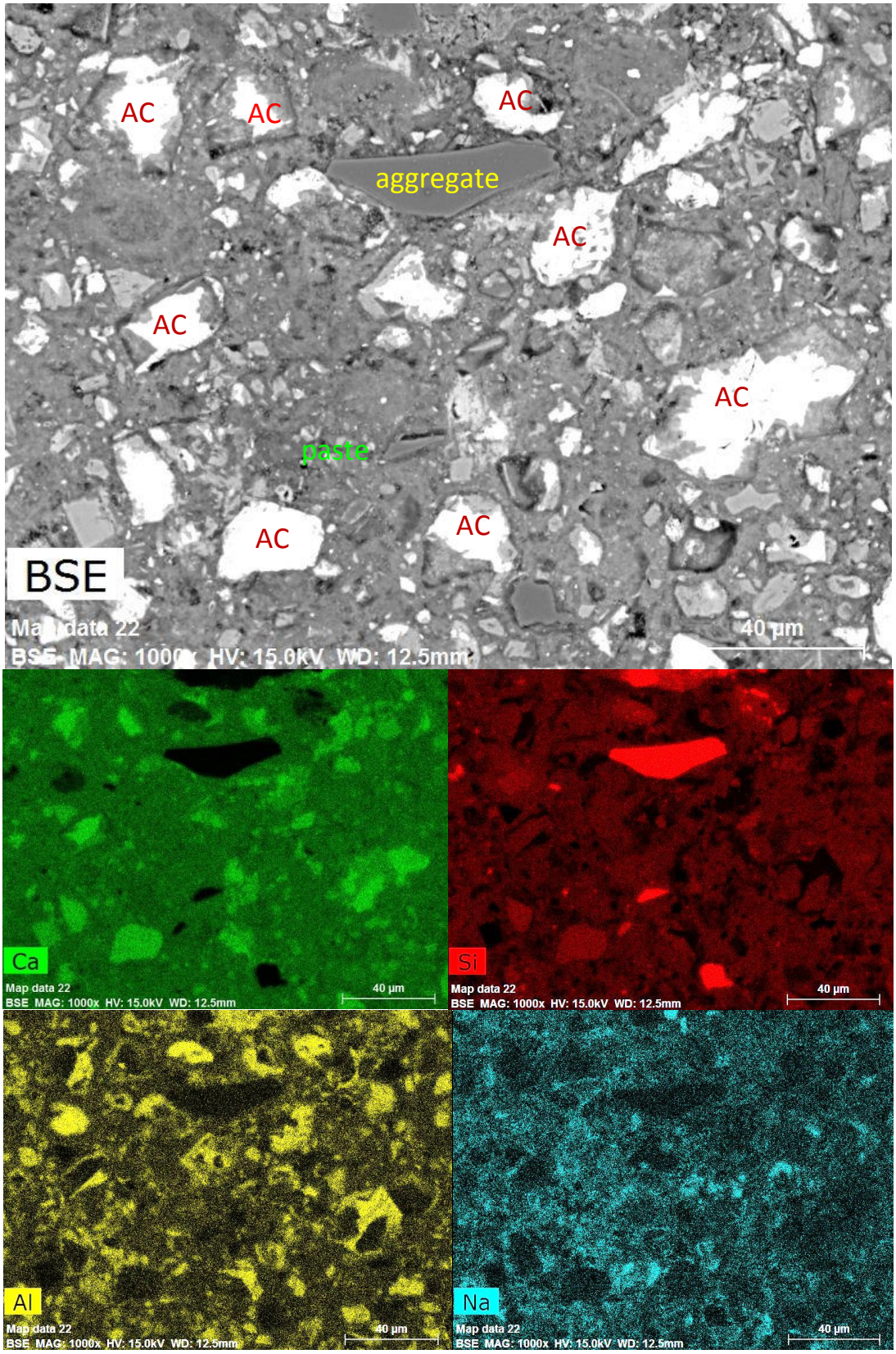

Figure D-3 EDS map of mortar + 15%MK where AC=anhydrous clinker

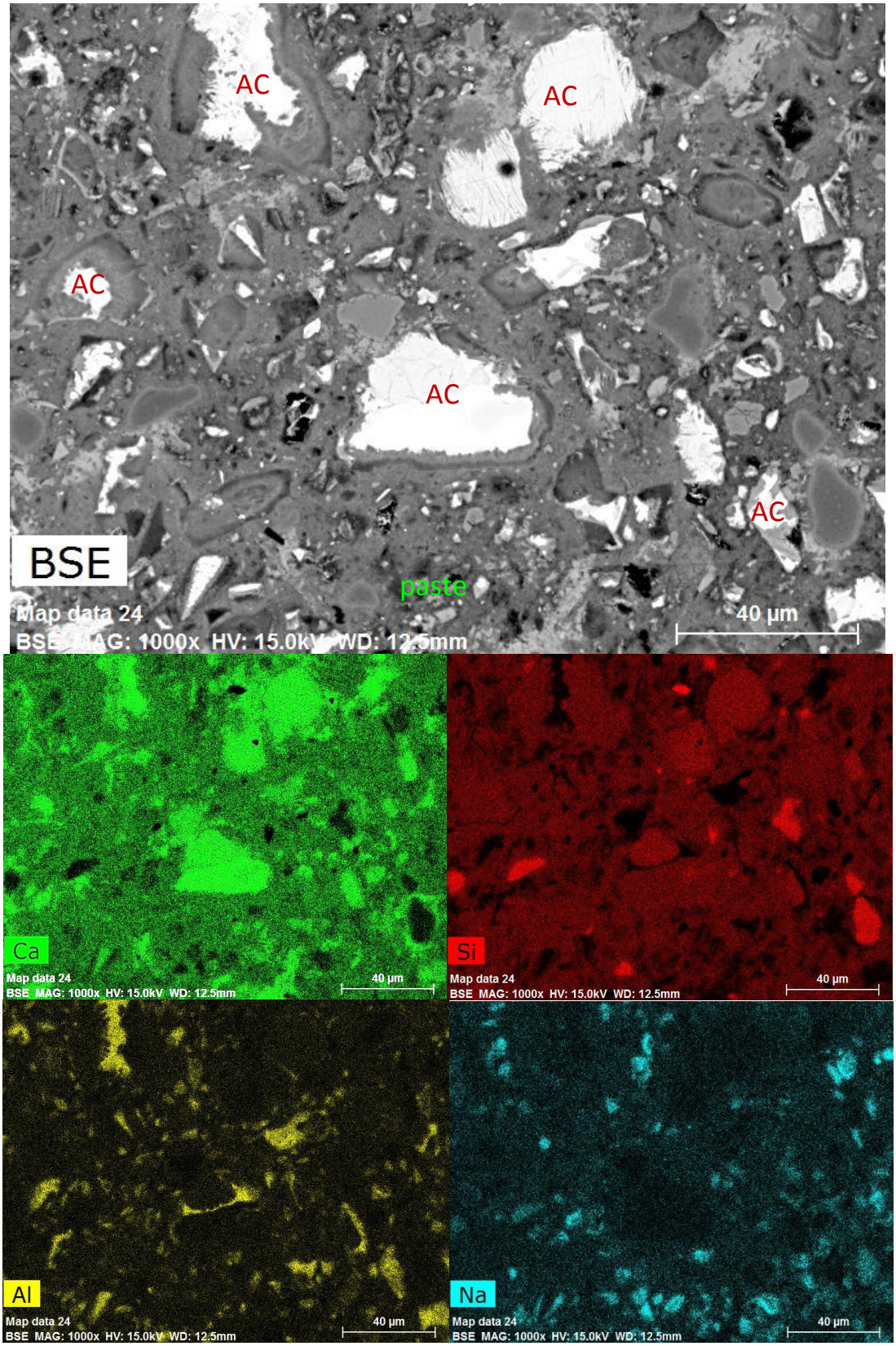

Figure D-4 EDS map of mortar + 10%SF where AC=anhydrous clinker

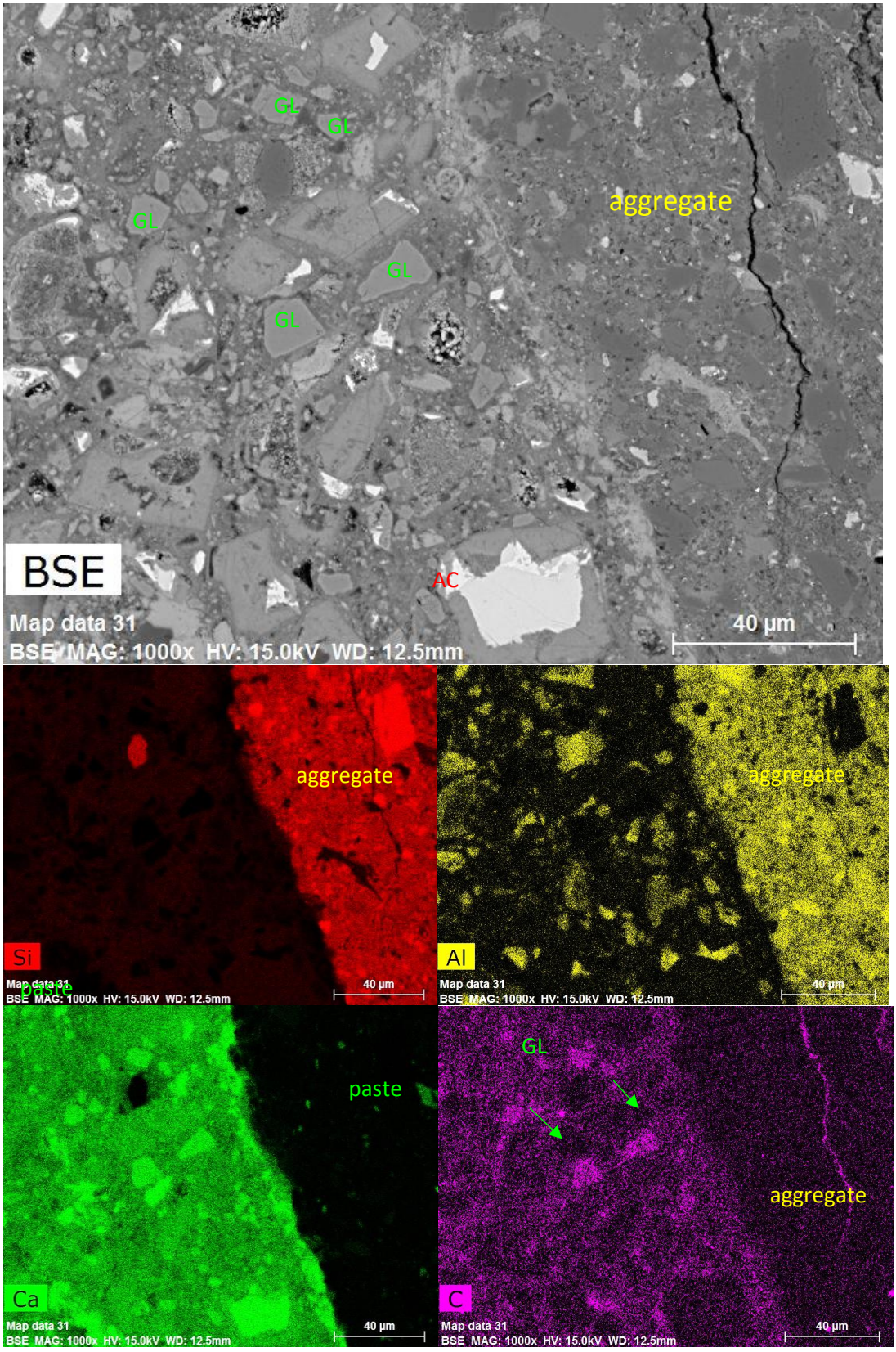

Figure D-5 EDS map of mortar with 17% GL, No SCM where GL=ground limestone and AC=anhydrous clinker

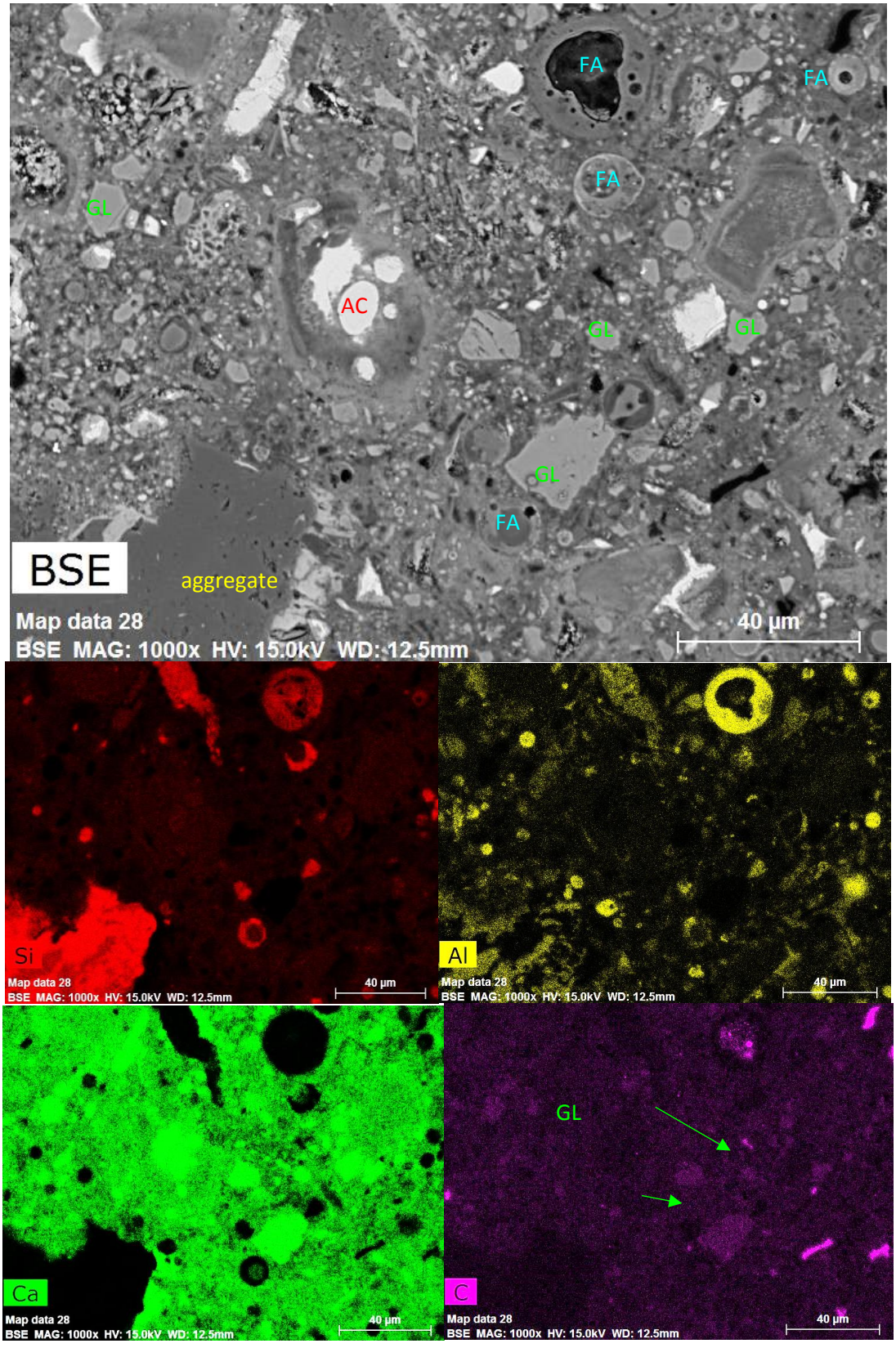

Figure D-6 EDS map of mortar with 17%GL, 25%FA where GL=ground limestone, FA=fly ash and AC=anhydrous clinker

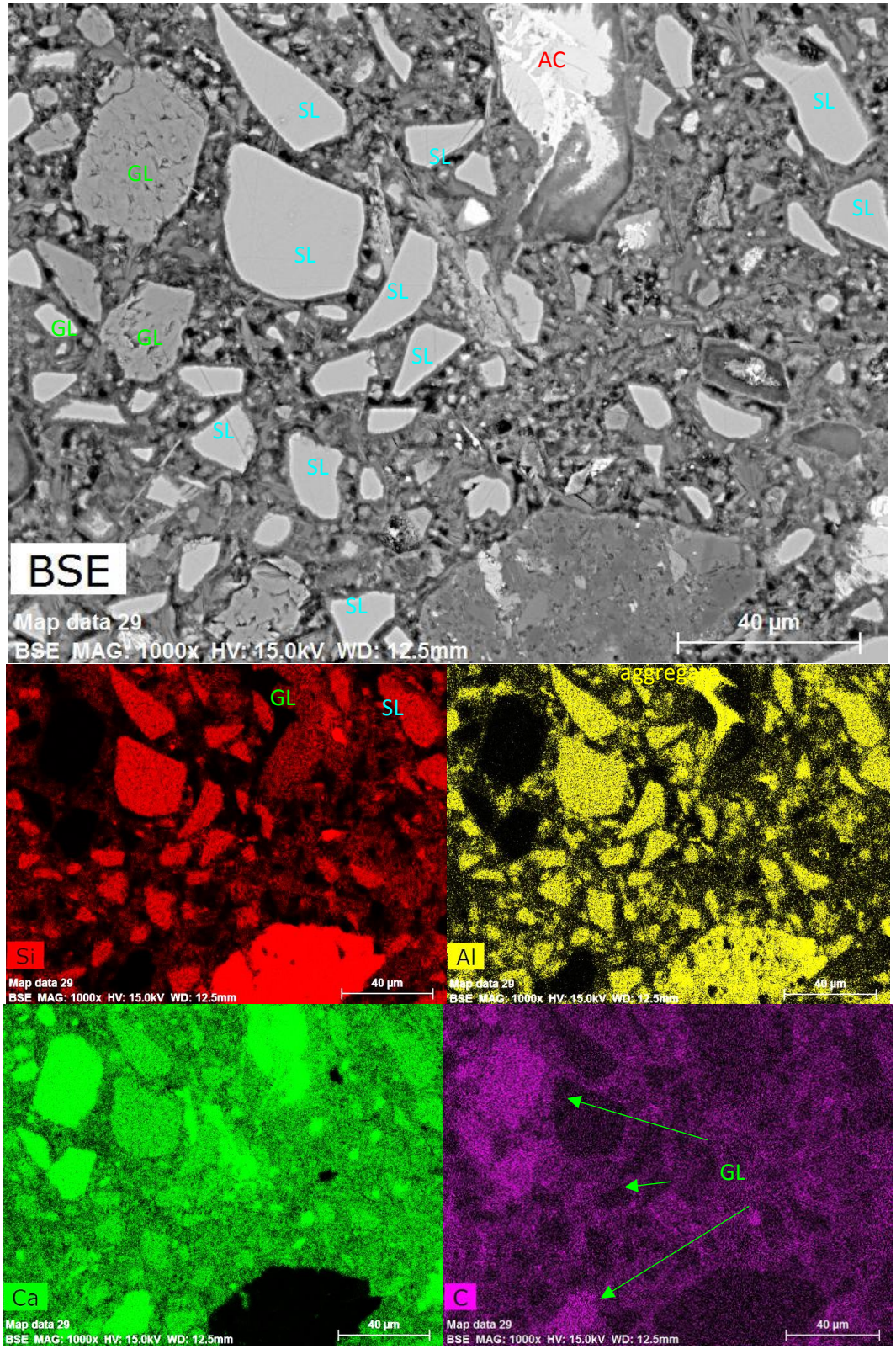

Figure D-7 EDS map of mortar with 17%GL, 65% SL where GL=ground limestone, SL=slag and AC=anhydrous clinker

Appendix E- EDS Analysis of the C-S-H

Table E-1 Limestone blended mortar without SCM (0% GL content)

mortar 0%GL (No SCM)				
Al/Si	**Al/Ca**	**Si/Ca**	**S/Ca**	**Ca/(Si+Al)**
0.0781	0.0426	0.5449	0.0293	1.7021
0.0801	0.0429	0.5349	0.0269	1.7307
0.0810	0.0388	0.4793	0.0263	1.9300
0.0857	0.0504	0.5877	0.0408	1.5673
0.0726	0.0387	0.5327	0.0288	1.7503
0.0875	0.0397	0.4535	0.0230	2.0275
0.0949	0.0583	0.6143	0.0506	1.4867
0.0804	0.0391	0.4859	0.0298	1.9050
0.1071	0.0649	0.6059	0.0368	1.4907
0.0794	0.0469	0.5906	0.0399	1.5686
0.0935	0.0448	0.4794	0.0272	1.9074
0.0839	0.0420	0.5014	0.0260	1.8402
0.0935	0.0521	0.5576	0.0389	1.6400
0.0852	0.0483	0.5667	0.0394	1.6262
0.0810	0.0495	0.6114	0.0377	1.5131
0.0858	0.0495	0.5769	0.0381	1.5963
0.1035	0.0559	0.5407	0.0291	1.6760
0.0914	0.0533	0.5837	0.0310	1.5697
0.0761	0.0384	0.5052	0.0248	1.8396
0.1003	0.0548	0.5466	0.0315	1.6627
0.0672	0.0325	0.4841	0.0230	1.9355
0.0730	0.0370	0.5075	0.0270	1.8365
0.0706	0.0322	0.4556	0.0136	2.0501
0.0681	0.0450	0.6607	0.0318	1.4170
0.0756	0.0453	0.5995	0.0292	1.5508
0.0713	0.0363	0.5091	0.0195	1.8335
0.0777	0.0394	0.5072	0.0287	1.8294
0.0943	0.0487	0.5162	0.0293	1.7703
0.0827	0.0460	0.5559	0.0218	1.6614
0.0784	0.0461	0.5881	0.0347	1.5768
0.0706	0.0330	0.4678	0.0242	1.9968
0.0764	0.0464	0.6070	0.0316	1.5304
0.0887	0.0573	0.6456	0.0367	1.4227
0.0740	0.0446	0.6022	0.0348	1.5461
0.0691	0.0368	0.5325	0.0262	1.7564
0.0802	0.0431	0.5377	0.0286	1.7215
0.0896	0.0581	0.6490	0.0456	1.4142
0.0784	0.0465	0.5936	0.0339	1.5623
0.0747	0.0384	0.5147	0.0274	1.8079

0.1036	0.0582	0.5619	0.0347	1.6125
0.0707	0.0380	0.5382	0.0259	1.7353
0.0857	0.0546	0.6371	0.0418	1.4457
0.0736	0.0339	0.4608	0.0239	2.0211
0.0759	0.0328	0.4319	0.0206	2.1521
0.0827	0.0446	0.5393	0.0314	1.7125
0.0887	0.0516	0.5811	0.0359	1.5806
0.0883	0.0499	0.5646	0.0305	1.6274
0.1001	0.0585	0.5844	0.0307	1.5554
0.1096	0.0694	0.6331	0.0178	1.4235
0.0912	0.0460	0.5046	0.0215	1.8164
0.0914	0.0571	0.6241	0.0347	1.4681
0.0928	0.0608	0.6554	0.0295	1.3963
0.0800	0.0422	0.5269	0.0294	1.7574
0.0651	0.0292	0.4492	0.0230	2.0900
0.0738	0.0368	0.4985	0.0209	1.8683
0.0719	0.0342	0.4756	0.0188	1.9615
0.0765	0.0357	0.4673	0.0185	1.9880
0.0904	0.0570	0.6299	0.0271	1.4558
0.0882	0.0562	0.6376	0.0414	1.4412
0.0827	0.0419	0.5071	0.0275	1.8213
0.0680	0.0397	0.5838	0.0286	1.6037
0.1081	0.0465	0.4301	0.0216	2.0983
0.0925	0.0486	0.5258	0.0279	1.7408
0.0763	0.0358	0.4687	0.0221	1.9824
0.0854	0.0515	0.6032	0.0337	1.5273
0.0731	0.0314	0.4301	0.0167	2.1667
0.0771	0.0422	0.5470	0.0288	1.6972
0.0792	0.0412	0.5197	0.0291	1.7829
0.0827	0.0513	0.6200	0.0353	1.4897
0.0618	0.0301	0.4868	0.0226	1.9349
0.0853	0.0486	0.5694	0.0337	1.6183
0.0844	0.0472	0.5593	0.0276	1.6489
0.0907	0.0566	0.6235	0.0381	1.4704
0.0728	0.0394	0.5415	0.0296	1.7214
0.0906	0.0459	0.5062	0.0268	1.8116
0.0876	0.0485	0.5535	0.0293	1.6612
0.0844	0.0435	0.5159	0.0309	1.7877
0.0696	0.0376	0.5404	0.0290	1.7301
0.0835	0.0407	0.4868	0.0286	1.8960
0.0932	0.0471	0.5049	0.0228	1.8116
0.0762	0.0343	0.4496	0.0181	2.0668
0.0715	0.0336	0.4698	0.0257	1.9865
0.0715	0.0343	0.4795	0.0246	1.9464
0.0659	0.0356	0.5401	0.0231	1.7370
0.0751	0.0424	0.5643	0.0301	1.6484

0.0603	0.0293	0.4858	0.0306	1.9414
0.0684	0.0370	0.5405	0.0365	1.7317
0.0742	0.0356	0.4793	0.0326	1.9422
0.0672	0.0343	0.5106	0.0329	1.8352
0.0566	0.0252	0.4455	0.0294	2.1245
0.0842	0.0476	0.5650	0.0347	1.6325
0.0698	0.0372	0.5332	0.0324	1.7530
0.0764	0.0449	0.5881	0.0401	1.5798
0.0982	0.0501	0.5098	0.0237	1.7860
0.0865	0.0499	0.5770	0.0343	1.5950
0.0806	0.0459	0.5699	0.0277	1.6240
0.0626	0.0311	0.4969	0.0264	1.8939
0.0853	0.0396	0.4644	0.0281	1.9840
0.0655	0.0310	0.4726	0.0252	1.9859
0.0678	0.0375	0.5537	0.0294	1.6915
0.0702	0.0370	0.5272	0.0324	1.7725
0.1156	0.0710	0.6139	0.0409	1.4602
0.0751	0.0403	0.5369	0.0240	1.7325
0.0953	0.0573	0.6017	0.0345	1.5173
0.0940	0.0452	0.4812	0.0269	1.8994
0.0878	0.0486	0.5532	0.0226	1.6619
0.0758	0.0380	0.5012	0.0224	1.8546
0.1054	0.0633	0.6008	0.0225	1.5058
0.0983	0.0581	0.5918	0.0305	1.5387
0.0662	0.0328	0.4960	0.0189	1.8910
0.1039	0.0515	0.4958	0.0240	1.8271
0.0828	0.0492	0.5941	0.0315	1.5546
0.0819	0.0527	0.6441	0.0381	1.4351
0.0858	0.0552	0.6430	0.0159	1.4323
0.0991	0.0655	0.6604	0.0176	1.3778
0.0911	0.0427	0.4682	0.0227	1.9575
0.0820	0.0400	0.4879	0.0288	1.8940
0.0777	0.0460	0.5919	0.0297	1.5677
0.0702	0.0451	0.6424	0.0348	1.4547
0.0985	0.0597	0.6058	0.0351	1.5027
0.0835	0.0495	0.5933	0.0361	1.5557
0.0842	0.0518	0.6153	0.0299	1.4989
0.0894	0.0526	0.5877	0.0291	1.5618
0.0837	0.0448	0.5356	0.0265	1.7229
0.1111	0.0724	0.6520	0.0253	1.3805
0.0895	0.0491	0.5487	0.0219	1.6728
0.0598	0.0325	0.5434	0.0122	1.7363
0.0846	0.0508	0.6001	0.0249	1.5365
0.0818	0.0367	0.4488	0.0213	2.0597
0.1162	0.0631	0.5429	0.0262	1.6503
0.0907	0.0494	0.5444	0.0259	1.6841

0.0958	0.0508	0.5301	0.0265	1.7216
0.0814	0.0383	0.4709	0.0210	1.9639
0.0785	0.0416	0.5305	0.0320	1.7478
0.0706	0.0360	0.5103	0.0202	1.8306
0.0886	0.0563	0.6360	0.0240	1.4444
0.0793	0.0367	0.4634	0.0212	1.9995
0.0829	0.0486	0.5855	0.0333	1.5772
0.0895	0.0392	0.4380	0.0226	2.0958
0.0993	0.0542	0.5459	0.0165	1.6664
0.0805	0.0457	0.5680	0.0294	1.6294
0.0774	0.0400	0.5168	0.0219	1.7960
0.0846	0.0513	0.6055	0.0300	1.5227
0.0768	0.0387	0.5038	0.0177	1.8435
0.0882	0.0564	0.6396	0.0302	1.4368
0.1016	0.0561	0.5520	0.0380	1.6445
0.0901	0.0490	0.5443	0.0323	1.6855
0.0846	0.0416	0.4919	0.0242	1.8743
0.0701	0.0311	0.4434	0.0229	2.1078
0.0706	0.0362	0.5126	0.0270	1.8222
0.0817	0.0473	0.5789	0.0304	1.5970
0.0834	0.0484	0.5802	0.0362	1.5907
0.0823	0.0384	0.4664	0.0236	1.9812
0.0700	0.0388	0.5541	0.0286	1.6866
0.0745	0.0412	0.5530	0.0348	1.6829
0.0795	0.0367	0.4614	0.0240	2.0074
0.1009	0.0543	0.5379	0.0338	1.6886
0.0588	0.0291	0.4938	0.0239	1.9126
0.0631	0.0274	0.4350	0.0174	2.1627
0.0758	0.0414	0.5453	0.0264	1.7044
0.0804	0.0470	0.5843	0.0328	1.5839
0.0861	0.0447	0.5186	0.0293	1.7755
0.0918	0.0562	0.6126	0.0371	1.4953
0.0713	0.0359	0.5040	0.0227	1.8520
0.0805	0.0350	0.4343	0.0181	2.1310
0.1039	0.0670	0.6448	0.0449	1.4049
0.0928	0.0501	0.5396	0.0356	1.6958
0.0784	0.0368	0.4702	0.0265	1.9723
0.0766	0.0417	0.5442	0.0339	1.7069
0.1007	0.0488	0.4845	0.0279	1.8752
0.0627	0.0307	0.4899	0.0269	1.9208
0.0680	0.0368	0.5416	0.0280	1.7288
0.1176	0.0704	0.5987	0.0292	1.4945
0.0809	0.0435	0.5369	0.0331	1.7230
0.0627	0.0327	0.5206	0.0248	1.8073
0.1029	0.0680	0.6608	0.0463	1.3721
0.0809	0.0497	0.6142	0.0315	1.5062

0.0963	0.0490	0.5093	0.0187	1.7911
0.0642	0.0314	0.4897	0.0234	1.9190
0.0733	0.0386	0.5264	0.0232	1.7699
0.0720	0.0432	0.5996	0.0273	1.5557
0.0686	0.0388	0.5656	0.0259	1.6545
0.0838	0.0420	0.5018	0.0282	1.8388
0.0524	0.0244	0.4656	0.0238	2.0408
0.0683	0.0311	0.4551	0.0267	2.0566
0.0631	0.0277	0.4397	0.0240	2.1391
0.0570	0.0271	0.4754	0.0208	1.9903
0.0871	0.0440	0.5058	0.0221	1.8188
0.0712	0.0349	0.4899	0.0256	1.9058
0.0675	0.0398	0.5892	0.0326	1.5900
0.0625	0.0297	0.4749	0.0238	1.9820
0.0675	0.0361	0.5356	0.0323	1.7490
0.0831	0.0422	0.5075	0.0266	1.8191
0.0658	0.0351	0.5339	0.0277	1.7574
0.0820	0.0483	0.5898	0.0291	1.5669
0.0814	0.0473	0.5810	0.0342	1.5915
0.1107	0.0549	0.4956	0.0293	1.8165
0.0859	0.0437	0.5083	0.0253	1.8116
0.0657	0.0334	0.5087	0.0305	1.8445
0.0977	0.0470	0.4810	0.0261	1.8937
0.0662	0.0350	0.5284	0.0293	1.7749
0.0752	0.0384	0.5104	0.0254	1.8221
0.0991	0.0492	0.4968	0.0259	1.8315
0.0968	0.0492	0.5084	0.0274	1.7933
0.0919	0.0613	0.6668	0.0408	1.3735
0.0905	0.0601	0.6637	0.0398	1.3815
0.0622	0.0334	0.5372	0.0287	1.7524
0.0714	0.0365	0.5111	0.0271	1.8261
0.0729	0.0337	0.4621	0.0237	2.0169
0.1015	0.0595	0.5861	0.0294	1.5489
0.0936	0.0457	0.4887	0.0341	1.8712
0.1033	0.0547	0.5298	0.0346	1.7108
0.0743	0.0394	0.5295	0.0283	1.7579
0.0812	0.0429	0.5289	0.0266	1.7487
0.0799	0.0430	0.5379	0.0284	1.7217
0.0699	0.0354	0.5071	0.0305	1.8433
0.0762	0.0507	0.6649	0.0485	1.3975
0.0874	0.0538	0.6156	0.0340	1.4938
0.0718	0.0400	0.5564	0.0327	1.6770
0.0798	0.0373	0.4669	0.0232	1.9835
0.0764	0.0398	0.5204	0.0284	1.7853
0.0730	0.0353	0.4835	0.0294	1.9275
0.0695	0.0330	0.4752	0.0260	1.9676

	0.0826	0.0462	0.5596	0.0367	1.6506
	0.0751	0.0403	0.5369	0.0304	1.7323
	0.0925	0.0550	0.5939	0.0233	1.5413
	0.0867	0.0512	0.5904	0.0273	1.5587
	0.0895	0.0459	0.5126	0.0238	1.7905
	0.0964	0.0645	0.6691	0.0457	1.3631
	0.0931	0.0578	0.6207	0.0427	1.4739
	0.0804	0.0409	0.5089	0.0286	1.8188
	0.0837	0.0535	0.6391	0.0461	1.4439
	0.0731	0.0398	0.5445	0.0312	1.7113
	0.0982	0.0531	0.5407	0.0324	1.6842
	0.1034	0.0622	0.6013	0.0327	1.5072
	0.0813	0.0382	0.4698	0.0324	1.9685
	0.0772	0.0402	0.5208	0.0243	1.7825
	0.0848	0.0484	0.5708	0.0310	1.6151
	0.0686	0.0332	0.4839	0.0232	1.9339
Average	0.0819	0.0445	0.5404	0.0288	1.7310
STDEV	0.0123	0.0096	0.0582	0.0065	0.1929

Table E-2 Limestone blended mortar without SCM (17% GL content)

mortar 17%GL (No SCM)				
Al/Si	**Al/Ca**	**Si/Ca**	**S/Ca**	**Ca/(Si+Al)**
0.0847	0.0516	0.6090	0.0276	1.5138
0.1137	0.0644	0.5664	0.0343	1.5853
0.0673	0.0288	0.4282	0.0170	2.1880
0.0955	0.0506	0.5299	0.0261	1.7226
0.0945	0.0528	0.5582	0.0254	1.6367
0.1005	0.0590	0.5873	0.0316	1.5472
0.1015	0.0643	0.6337	0.0300	1.4326
0.0832	0.0360	0.4319	0.0189	2.1373
0.0889	0.0397	0.4466	0.0188	2.0565
0.0912	0.0436	0.4778	0.0196	1.9180
0.1069	0.0623	0.5827	0.0262	1.5505
0.0900	0.0477	0.5299	0.0268	1.7312
0.0976	0.0524	0.5367	0.0270	1.6975
0.1103	0.0577	0.5232	0.0277	1.7214
0.0916	0.0490	0.5350	0.0193	1.7124
0.0913	0.0461	0.5049	0.0177	1.8148
0.1069	0.0670	0.6274	0.0306	1.4400
0.1039	0.0630	0.6065	0.0298	1.4936
0.0896	0.0481	0.5364	0.0280	1.7110
0.0823	0.0452	0.5499	0.0249	1.6802

0.0900	0.0524	0.5825	0.0301	1.5750
0.0795	0.0375	0.4709	0.0229	1.9671
0.1262	0.0631	0.4997	0.0281	1.7769
0.0823	0.0438	0.5315	0.0236	1.7383
0.0904	0.0492	0.5448	0.0237	1.6833
0.0865	0.0398	0.4604	0.0164	1.9990
0.0781	0.0382	0.4892	0.0193	1.8960
0.0859	0.0511	0.5944	0.0324	1.5491
0.0917	0.0501	0.5460	0.0256	1.6777
0.0893	0.0432	0.4843	0.0209	1.8955
0.1002	0.0533	0.5322	0.0337	1.7077
0.1044	0.0693	0.6644	0.0408	1.3629
0.0944	0.0394	0.4173	0.0225	2.1894
0.0894	0.0449	0.5018	0.0213	1.8295
0.0903	0.0414	0.4585	0.0192	2.0006
0.1015	0.0580	0.5715	0.0312	1.5886
0.0812	0.0375	0.4625	0.0219	1.9998
0.1038	0.0534	0.5142	0.0260	1.7619
0.0889	0.0467	0.5249	0.0280	1.7495
0.0953	0.0623	0.6543	0.0392	1.3955
0.1011	0.0706	0.6987	0.0406	1.2998
0.0897	0.0479	0.5336	0.0297	1.7197
0.1147	0.0595	0.5182	0.0264	1.7312
0.1067	0.0596	0.5581	0.0299	1.6191
0.0889	0.0526	0.5916	0.0317	1.5523
0.0862	0.0488	0.5659	0.0387	1.6268
0.0755	0.0353	0.4673	0.0235	1.9899
0.0837	0.0442	0.5281	0.0300	1.7472
0.0793	0.0423	0.5328	0.0270	1.7389
0.0897	0.0401	0.4465	0.0205	2.0554
0.0903	0.0464	0.5131	0.0213	1.7874
0.0777	0.0381	0.4895	0.0225	1.8957
0.0796	0.0369	0.4638	0.0132	1.9972
0.0706	0.0348	0.4924	0.0150	1.8969
0.0823	0.0402	0.4882	0.0131	1.8928
0.0867	0.0492	0.5672	0.0145	1.6224
0.0941	0.0632	0.6718	0.0177	1.3604
0.0768	0.0383	0.4989	0.0098	1.8613
0.0934	0.0607	0.6504	0.0193	1.4061
0.0823	0.0492	0.5985	0.0191	1.5439
0.1036	0.0646	0.6234	0.0340	1.4535
0.0728	0.0402	0.5514	0.0135	1.6904
0.1015	0.0587	0.5782	0.0261	1.5701
0.0888	0.0509	0.5729	0.0217	1.6033
0.0739	0.0400	0.5411	0.0234	1.7209
0.1175	0.0698	0.5938	0.0234	1.5069

0.0763	0.0378	0.4959	0.0159	1.8735
0.0914	0.0473	0.5170	0.0182	1.7721
0.0684	0.0309	0.4522	0.0154	2.0699
0.0834	0.0461	0.5530	0.0212	1.6693
0.0709	0.0320	0.4510	0.0141	2.0704
0.0895	0.0574	0.6409	0.0306	1.4321
0.0835	0.0394	0.4717	0.0254	1.9568
0.0649	0.0282	0.4338	0.0161	2.1648
0.0916	0.0537	0.5865	0.0291	1.5620
0.0971	0.0603	0.6211	0.0300	1.4675
0.0837	0.0526	0.6286	0.0298	1.4679
0.0947	0.0479	0.5060	0.0196	1.8055
0.0860	0.0419	0.4868	0.0209	1.8915
0.1039	0.0547	0.5259	0.0188	1.7226
0.1141	0.0803	0.7036	0.0213	1.2757
0.1023	0.0688	0.6726	0.0300	1.3488
0.0868	0.0465	0.5355	0.0169	1.7182
0.0974	0.0568	0.5833	0.0274	1.5622
0.0995	0.0601	0.6038	0.0273	1.5064
0.0846	0.0379	0.4484	0.0234	2.0561
0.0795	0.0397	0.4998	0.0226	1.8533
0.1240	0.0769	0.6202	0.0331	1.4344
0.1184	0.0662	0.5592	0.0157	1.5988
0.0821	0.0475	0.5788	0.0147	1.5966
0.0942	0.0543	0.5767	0.0176	1.5847
0.0931	0.0641	0.6890	0.0303	1.3278
0.0755	0.0419	0.5554	0.0197	1.6742
0.0556	0.0412	0.7412	0.0063	1.2781
0.0894	0.0450	0.5030	0.0173	1.8250
0.1080	0.0536	0.4965	0.0159	1.8178
0.0815	0.0449	0.5502	0.0251	1.6804
0.0873	0.0697	0.7986	0.0200	1.1516
0.0857	0.0538	0.6276	0.0428	1.4677
0.0925	0.0508	0.5499	0.0346	1.6646
0.0699	0.0342	0.4895	0.0351	1.9095
0.1225	0.0882	0.7198	0.0543	1.2377
0.1076	0.0578	0.5368	0.0339	1.6818
0.0724	0.0341	0.4709	0.0310	1.9801
0.0785	0.0424	0.5403	0.0363	1.7163
0.2756	0.1301	0.4720	0.0315	1.6608
0.0998	0.0516	0.5167	0.0293	1.7597
0.0711	0.0375	0.5274	0.0327	1.7703
0.0765	0.0402	0.5256	0.0298	1.7673
0.0748	0.0340	0.4549	0.0251	2.0453
0.0938	0.0509	0.5431	0.0280	1.6834
0.0902	0.0413	0.4580	0.0259	2.0029

0.0910	0.0432	0.4748	0.0293	1.9304
0.0955	0.0585	0.6125	0.0423	1.4905
0.0802	0.0411	0.5123	0.0387	1.8072
0.0886	0.0501	0.5651	0.0501	1.6254
0.1168	0.0667	0.5709	0.0432	1.5683
0.0786	0.0393	0.4997	0.0287	1.8553
0.0927	0.0558	0.6026	0.0287	1.5189
0.0950	0.0445	0.4684	0.0291	1.9499
0.1273	0.0671	0.5274	0.0321	1.6820
0.0859	0.0446	0.5196	0.0309	1.7724
0.0946	0.0584	0.6169	0.0414	1.4807
0.0880	0.0423	0.4811	0.0231	1.9104
0.0895	0.0422	0.4716	0.0263	1.9461
0.0730	0.0348	0.4771	0.0275	1.9534
0.0830	0.0473	0.5694	0.0360	1.6216
0.0847	0.0463	0.5473	0.0360	1.6845
0.1037	0.0616	0.5934	0.0388	1.5268
0.0866	0.0485	0.5600	0.0403	1.6435
0.1112	0.0708	0.6362	0.0465	1.4144
0.0995	0.0582	0.5854	0.0339	1.5538
0.0804	0.0363	0.4519	0.0244	2.0483
0.0962	0.0509	0.5292	0.0320	1.7237
0.0994	0.0534	0.5373	0.0293	1.6927
0.0764	0.0379	0.4963	0.0318	1.8717
0.0876	0.0525	0.5992	0.0339	1.5345
0.0861	0.0543	0.6310	0.0384	1.4590
0.0936	0.0622	0.6647	0.0316	1.3756
0.0888	0.0492	0.5542	0.0252	1.6573
0.1018	0.0591	0.5803	0.0242	1.5639
0.0783	0.0407	0.5201	0.0167	1.7831
0.0908	0.0520	0.5723	0.0254	1.6019
0.0785	0.0444	0.5657	0.0262	1.6390
0.0784	0.0381	0.4865	0.0193	1.9062
0.0769	0.0428	0.5564	0.0263	1.6690
0.0849	0.0444	0.5231	0.0281	1.7623
0.0885	0.0440	0.4968	0.0288	1.8492
0.0944	0.0421	0.4453	0.0241	2.0520
0.0870	0.0446	0.5122	0.0310	1.7961
0.0767	0.0380	0.4957	0.0293	1.8737
0.0972	0.0509	0.5240	0.0294	1.7392
0.0836	0.0425	0.5084	0.0276	1.8151
0.0906	0.0433	0.4783	0.0291	1.9171
0.0788	0.0490	0.6213	0.0431	1.4921
0.0853	0.0413	0.4840	0.0293	1.9035
0.1153	0.0689	0.5977	0.0479	1.5002
0.0983	0.0668	0.6799	0.0487	1.3392

0.0990	0.0529	0.5338	0.0353	1.7046
0.0847	0.0494	0.5841	0.0359	1.5784
0.1514	0.0849	0.5610	0.0394	1.5481
0.0982	0.0640	0.6511	0.0420	1.3985
0.0789	0.0395	0.5013	0.0298	1.8491
0.0963	0.0540	0.5605	0.0407	1.6273
0.0839	0.0518	0.6171	0.0502	1.4951
0.0767	0.0408	0.5321	0.0270	1.7456
0.0858	0.0423	0.4931	0.0314	1.8676
0.0772	0.0380	0.4915	0.0319	1.8889
0.1016	0.0549	0.5403	0.0403	1.6801
0.1212	0.0601	0.4957	0.0308	1.7992
0.0957	0.0514	0.5369	0.0357	1.6998
0.0796	0.0439	0.5513	0.0408	1.6803
0.1172	0.0699	0.5961	0.0360	1.5015
0.0936	0.0594	0.6346	0.0422	1.4410
0.0926	0.0546	0.5898	0.0376	1.5517
0.0828	0.0398	0.4807	0.0202	1.9214
0.0830	0.0468	0.5639	0.0342	1.6375
0.0825	0.0392	0.4753	0.0211	1.9436
0.0850	0.0466	0.5481	0.0360	1.6814
0.0885	0.0424	0.4787	0.0275	1.9189
0.0825	0.0397	0.4809	0.0249	1.9210
0.0883	0.0509	0.5762	0.0343	1.5947
0.0846	0.0514	0.6073	0.0457	1.5182
0.0807	0.0412	0.5103	0.0310	1.8132
0.0874	0.0493	0.5649	0.0356	1.6281
0.1073	0.0557	0.5196	0.0326	1.7382
0.0950	0.0470	0.4950	0.0317	1.8449
0.0687	0.0293	0.4268	0.0182	2.1925
0.0789	0.0370	0.4682	0.0231	1.9795
0.0903	0.0564	0.6244	0.0431	1.4690
0.0770	0.0368	0.4788	0.0287	1.9394
0.0797	0.0453	0.5686	0.0368	1.6288
0.0842	0.0414	0.4916	0.0264	1.8760
0.0709	0.0334	0.4715	0.0265	1.9806
0.0904	0.0452	0.4998	0.0345	1.8348
0.0741	0.0319	0.4302	0.0242	2.1643
0.0885	0.0429	0.4850	0.0300	1.8941
0.0914	0.0525	0.5737	0.0377	1.5971
0.0840	0.0521	0.6199	0.0366	1.4880
0.0834	0.0461	0.5531	0.0356	1.6690
0.0887	0.0546	0.6157	0.0389	1.4919
0.0890	0.0483	0.5425	0.0310	1.6928
0.0924	0.0594	0.6432	0.0405	1.4232
0.0751	0.0352	0.4688	0.0240	1.9842

	0.1893	0.0972	0.5133	0.0363	1.6380
	0.1122	0.0528	0.4705	0.0300	1.9109
	0.0842	0.0440	0.5227	0.0310	1.7646
	0.1098	0.0604	0.5501	0.0282	1.6380
	0.1144	0.0636	0.5563	0.0311	1.6131
	0.1022	0.0482	0.4718	0.0209	1.9230
	0.0653	0.0298	0.4569	0.0241	2.0546
	0.0942	0.0499	0.5297	0.0292	1.7255
	0.0949	0.0538	0.5668	0.0352	1.6114
	0.0841	0.0427	0.5074	0.0333	1.8180
	0.0839	0.0507	0.6038	0.0346	1.5279
	0.0717	0.0369	0.5143	0.0352	1.8144
	0.0997	0.0472	0.4731	0.0265	1.9222
	0.0841	0.0451	0.5359	0.0358	1.7212
	0.0676	0.0317	0.4689	0.0230	1.9978
	0.0918	0.0574	0.6257	0.0414	1.4638
	0.1186	0.0820	0.6912	0.0425	1.2933
	0.0927	0.0528	0.5703	0.0336	1.6048
	0.0882	0.0478	0.5415	0.0324	1.6970
	0.0805	0.0349	0.4340	0.0186	2.1324
	0.0830	0.0384	0.4624	0.0198	1.9971
	0.0770	0.0342	0.4435	0.0255	2.0934
	0.0907	0.0498	0.5491	0.0293	1.6697
	0.0803	0.0426	0.5306	0.0322	1.7446
	0.0690	0.0345	0.4997	0.0246	1.8721
	0.0920	0.0537	0.5837	0.0360	1.5687
	0.0806	0.0432	0.5364	0.0303	1.7252
	0.0836	0.0473	0.5654	0.0301	1.6323
	0.0861	0.0479	0.5559	0.0363	1.6564
	0.0847	0.0511	0.6029	0.0341	1.5292
	0.1114	0.0523	0.4696	0.0291	1.9160
	0.0857	0.0441	0.5141	0.0301	1.7915
	0.0744	0.0359	0.4823	0.0231	1.9300
	0.1223	0.0667	0.5451	0.0294	1.6346
	0.1186	0.0820	0.6912	0.0425	1.2933
Average	0.0914	0.0498	0.5420	0.0289	1.7156
STDEV	0.0189	0.0125	0.0656	0.0081	0.2076

Table E-3 Limestone blended mortar with 0%GL and 25%FA

mortar 0%GL+25%FA				
Al/Si	**Al/Ca**	**Si/Ca**	**S/Ca**	**Ca/(Si+Al)**
0.1537	0.1030	0.6702	0.0247	1.2934
0.1544	0.0928	0.6009	0.0177	1.4416
0.1877	0.1162	0.6189	0.0106	1.3604

0.1305	0.1004	0.7692	0.0229	1.1500
0.1620	0.1058	0.6532	0.0194	1.3175
0.1306	0.0895	0.6851	0.0206	1.2911
0.1474	0.0859	0.5824	0.0144	1.4964
0.1451	0.0985	0.6787	0.0222	1.2866
0.1480	0.0788	0.5325	0.0154	1.6358
0.1424	0.0824	0.5787	0.0108	1.5126
0.1423	0.1137	0.7989	0.0268	1.0958
0.1563	0.1083	0.6931	0.0181	1.2479
0.1504	0.0877	0.5828	0.0126	1.4916
0.1595	0.1019	0.6387	0.0215	1.3503
0.1463	0.1050	0.7181	0.0320	1.2149
0.1663	0.0946	0.5691	0.0182	1.5067
0.1794	0.1249	0.6963	0.0223	1.2177
0.1495	0.1010	0.6756	0.0293	1.2877
0.1329	0.0791	0.5957	0.0144	1.4818
0.1327	0.0833	0.6272	0.0112	1.4076
0.1352	0.0864	0.6390	0.0179	1.3785
0.1350	0.0839	0.6213	0.0074	1.4180
0.1219	0.0639	0.5238	0.0087	1.7018
0.1494	0.1052	0.7038	0.0093	1.2361
0.1606	0.1138	0.7086	0.0213	1.2160
0.1543	0.1071	0.6943	0.0248	1.2478
0.1745	0.1199	0.6868	0.0161	1.2396
0.1468	0.1049	0.7146	0.0189	1.2204
0.1295	0.0701	0.5414	0.0123	1.6353
0.1854	0.1231	0.6641	0.0164	1.2702
0.1329	0.0882	0.6635	0.0184	1.3303
0.1711	0.1212	0.7084	0.0193	1.2054
0.1408	0.0871	0.6185	0.0173	1.4172
0.1439	0.1081	0.7512	0.0259	1.1638
0.1715	0.1135	0.6615	0.0274	1.2904
0.1460	0.0952	0.6517	0.0275	1.3388
0.1479	0.1118	0.7555	0.0313	1.1530
0.1568	0.1121	0.7149	0.0179	1.2092
0.1454	0.0943	0.6486	0.0106	1.3461
0.1633	0.0883	0.5409	0.0086	1.5894
0.1626	0.1100	0.6766	0.0144	1.2712
0.1532	0.1161	0.7580	0.0191	1.1441
0.1458	0.0859	0.5890	0.0114	1.4818
0.1418	0.0887	0.6252	0.0060	1.4007
0.1911	0.1156	0.6048	0.0250	1.3882
0.1649	0.1225	0.7426	0.0215	1.1559
0.1725	0.0989	0.5732	0.0170	1.4879
0.1574	0.1103	0.7004	0.0093	1.2336
0.1740	0.1165	0.6694	0.0187	1.2725

0.1670	0.1189	0.7118	0.0285	1.2039
0.1279	0.0723	0.5651	0.0160	1.5688
0.1294	0.0850	0.6565	0.0218	1.3487
0.1227	0.0751	0.6120	0.0198	1.4554
0.1954	0.1152	0.5897	0.0326	1.4186
0.1691	0.1147	0.6785	0.0262	1.2607
0.1768	0.1055	0.5970	0.0253	1.4235
0.1413	0.0832	0.5891	0.0225	1.4873
0.1477	0.0977	0.6617	0.0269	1.3169
0.1351	0.0845	0.6253	0.0187	1.4088
0.1389	0.0970	0.6981	0.0285	1.2577
0.1538	0.0976	0.6348	0.0232	1.3653
0.1446	0.0908	0.6280	0.0200	1.3912
0.1502	0.1123	0.7475	0.0177	1.1631
0.1488	0.0907	0.6093	0.0103	1.4285
0.1804	0.1249	0.6924	0.0096	1.2235
0.1472	0.0881	0.5985	0.0186	1.4565
0.1508	0.1065	0.7063	0.0245	1.2304
0.1575	0.1072	0.6809	0.0119	1.2689
0.1570	0.1098	0.6992	0.0187	1.2360
0.1519	0.0834	0.5491	0.0092	1.5810
0.1745	0.1121	0.6423	0.0172	1.3257
0.1522	0.0985	0.6472	0.0206	1.3409
0.1522	0.0888	0.5833	0.0086	1.4878
0.1782	0.1214	0.6811	0.0148	1.2461
0.1355	0.0802	0.5919	0.0130	1.4878
0.1472	0.1016	0.6906	0.0194	1.2622
0.1835	0.1089	0.5933	0.0159	1.4241
0.1469	0.0925	0.6298	0.0158	1.3845
0.1969	0.1260	0.6397	0.0339	1.3061
0.1544	0.0951	0.6156	0.0225	1.4071
0.1461	0.0892	0.6106	0.0133	1.4290
0.1465	0.1158	0.7905	0.0167	1.1034
0.1437	0.0910	0.6335	0.0071	1.3801
0.1457	0.0810	0.5558	0.0134	1.5704
0.1618	0.0973	0.6014	0.0187	1.4312
0.1434	0.0777	0.5418	0.0132	1.6143
0.1640	0.1101	0.6713	0.0157	1.2798
0.1562	0.1222	0.7821	0.0278	1.1059
0.1544	0.1035	0.6701	0.0205	1.2927
0.1384	0.0832	0.6014	0.0151	1.4607
0.1565	0.0975	0.6232	0.0212	1.3874
0.1599	0.0934	0.5841	0.0175	1.4760
0.1705	0.0993	0.5822	0.0202	1.4673
0.1567	0.0992	0.6330	0.0214	1.3657
0.1555	0.1177	0.7566	0.0319	1.1437

0.1738	0.1191	0.6851	0.0168	1.2435
0.1533	0.0953	0.6217	0.0264	1.3947
0.1470	0.0928	0.6318	0.0269	1.3799
0.1558	0.0814	0.5224	0.0199	1.6562
0.1745	0.0976	0.5593	0.0218	1.5224
0.1646	0.1003	0.6091	0.0118	1.4098
0.1672	0.1023	0.6118	0.0095	1.4004
0.1626	0.1045	0.6423	0.0133	1.3391
0.1750	0.1200	0.6859	0.0166	1.2408
0.1564	0.0929	0.5943	0.0187	1.4550
0.1594	0.0933	0.5855	0.0200	1.4731
0.1500	0.1127	0.7516	0.0271	1.1570
0.1557	0.0810	0.5201	0.0154	1.6636
0.1506	0.0814	0.5404	0.0084	1.6083
0.1467	0.0854	0.5822	0.0153	1.4979
0.1518	0.1111	0.7318	0.0251	1.1864
0.1516	0.1001	0.6603	0.0172	1.3151
0.1562	0.1010	0.6466	0.0159	1.3375
0.1690	0.1006	0.5953	0.0208	1.4369
0.1641	0.1013	0.6172	0.0134	1.3918
0.1583	0.1012	0.6390	0.0196	1.3510
0.1621	0.1161	0.7159	0.0285	1.2020
0.1456	0.0943	0.6473	0.0196	1.3485
0.1398	0.0905	0.6472	0.0247	1.3556
0.1404	0.0872	0.6211	0.0154	1.4118
0.1300	0.0910	0.7001	0.0162	1.2641
0.1668	0.1304	0.7814	0.0192	1.0968
0.1694	0.1271	0.7506	0.0164	1.1393
0.1460	0.0885	0.6061	0.0058	1.4396
0.1444	0.1018	0.7048	0.0265	1.2398
0.1579	0.1030	0.6522	0.0117	1.3242
0.1531	0.0870	0.5686	0.0356	1.5251
0.1469	0.0878	0.5975	0.0269	1.4592
0.1504	0.0988	0.6568	0.0181	1.3235
0.1798	0.1014	0.5638	0.0200	1.5035
0.1418	0.0794	0.5594	0.0176	1.5655
0.1587	0.0874	0.5507	0.0195	1.5674
0.1644	0.1031	0.6267	0.0229	1.3703
0.1451	0.0998	0.6878	0.0292	1.2697
0.1353	0.0740	0.5471	0.0233	1.6101
0.1555	0.0962	0.6186	0.0235	1.3989
0.1659	0.1018	0.6139	0.0262	1.3972
0.1664	0.1017	0.6114	0.0243	1.4023
0.1489	0.0944	0.6339	0.0203	1.3731
0.1422	0.0816	0.5734	0.0211	1.5269
0.1514	0.0904	0.5972	0.0200	1.4542

0.1370	0.0864	0.6307	0.0178	1.3944
0.1410	0.0836	0.5931	0.0209	1.4778
0.1492	0.1015	0.6802	0.0326	1.2792
0.1350	0.0781	0.5785	0.0244	1.5232
0.1448	0.0824	0.5690	0.0254	1.5352
0.1619	0.0911	0.5630	0.0226	1.5287
0.1496	0.0816	0.5456	0.0213	1.5942
0.1534	0.0941	0.6136	0.0318	1.4129
0.1620	0.0879	0.5424	0.0364	1.5867
0.1786	0.1172	0.6563	0.0292	1.2929
0.1491	0.0891	0.5973	0.0201	1.4570
0.1643	0.0975	0.5933	0.0251	1.4476
0.1916	0.1251	0.6531	0.0160	1.2850
0.1600	0.0922	0.5758	0.0170	1.4970
0.1816	0.1242	0.6842	0.0156	1.2370
0.1689	0.1105	0.6544	0.0167	1.3073
0.1660	0.1153	0.6947	0.0288	1.2346
0.1923	0.1049	0.5456	0.0227	1.5373
0.1688	0.0997	0.5907	0.0212	1.4484
0.1835	0.1107	0.6036	0.0159	1.3999
0.1445	0.0790	0.5471	0.0143	1.5972
0.1583	0.1093	0.6904	0.0202	1.2504
0.1642	0.1081	0.6584	0.0145	1.3047
0.1719	0.1159	0.6739	0.0235	1.2662
0.1504	0.0895	0.5949	0.0142	1.4612
0.1664	0.1048	0.6297	0.0227	1.3615
0.1463	0.0797	0.5449	0.0180	1.6010
0.1524	0.0994	0.6520	0.0175	1.3308
0.1614	0.1153	0.7144	0.0240	1.2052
0.1748	0.1224	0.7004	0.0264	1.2153
0.1952	0.1126	0.5768	0.0159	1.4504
0.1787	0.1287	0.7199	0.0177	1.1785
0.1644	0.1034	0.6287	0.0123	1.3660
0.1845	0.1362	0.7379	0.0222	1.1441
0.1585	0.0903	0.5696	0.0206	1.5153
0.1628	0.1100	0.6757	0.0177	1.2728
0.1784	0.1250	0.7006	0.0191	1.2113
0.1792	0.1368	0.7635	0.0195	1.1108
0.1381	0.0775	0.5613	0.0151	1.5655
0.1795	0.1351	0.7529	0.0240	1.1260
0.1668	0.1101	0.6600	0.0146	1.2987
0.1430	0.0765	0.5347	0.0107	1.6362
0.1444	0.1018	0.7052	0.0255	1.2391
0.1725	0.1245	0.7213	0.0266	1.1823
0.1509	0.0826	0.5475	0.0149	1.5871
0.1730	0.1376	0.7953	0.0224	1.0720

0.1765	0.1254	0.7104	0.0249	1.1965
0.1634	0.0948	0.5801	0.0195	1.4818
0.1701	0.1245	0.7317	0.0146	1.1680
0.1833	0.1339	0.7305	0.0195	1.1569
0.1742	0.1264	0.7255	0.0200	1.1738
0.1614	0.1214	0.7520	0.0269	1.1450
0.1693	0.0927	0.5475	0.0074	1.5621
0.1657	0.1016	0.6136	0.0170	1.3982
0.1675	0.0958	0.5719	0.0137	1.4978
0.1712	0.1157	0.6755	0.0198	1.2640
0.1629	0.1058	0.6494	0.0155	1.3242
0.1556	0.0986	0.6335	0.0173	1.3661
0.1626	0.1185	0.7292	0.0271	1.1796
0.1878	0.1299	0.6917	0.0180	1.2172
0.1508	0.0959	0.6361	0.0206	1.3662
0.1598	0.1201	0.7512	0.0370	1.1477
0.1469	0.0801	0.5451	0.0221	1.5994
0.1630	0.0951	0.5839	0.0139	1.4727
0.1592	0.1035	0.6500	0.0156	1.3272
0.1552	0.1041	0.6705	0.0223	1.2911
0.1598	0.1179	0.7373	0.0244	1.1694
0.1516	0.0954	0.6294	0.0146	1.3797
0.1704	0.1141	0.6693	0.0238	1.2765
0.1773	0.1159	0.6536	0.0184	1.2996
0.1494	0.0847	0.5672	0.0242	1.5339
0.1725	0.1064	0.6164	0.0175	1.3835
0.1723	0.0953	0.5533	0.0190	1.5417
0.1603	0.0879	0.5486	0.0134	1.5711
0.1875	0.1327	0.7078	0.0294	1.1897
0.1672	0.1075	0.6425	0.0238	1.3334
0.1796	0.1268	0.7059	0.0287	1.2009
0.1540	0.0850	0.5520	0.0079	1.5697
0.1698	0.1206	0.7105	0.0208	1.2032
0.1529	0.0888	0.5806	0.0191	1.4940
0.1477	0.0885	0.5995	0.0202	1.4535
0.1646	0.0989	0.6009	0.0077	1.4289
0.1776	0.1127	0.6344	0.0247	1.3385
0.1704	0.1113	0.6535	0.0215	1.3075
0.1935	0.1072	0.5540	0.0222	1.5123
0.1582	0.1167	0.7378	0.0244	1.1702
0.1537	0.0979	0.6366	0.0216	1.3615
0.1568	0.1084	0.6915	0.0215	1.2501
0.1640	0.1007	0.6139	0.0158	1.3993
0.1755	0.1192	0.6792	0.0191	1.2524
0.1642	0.1114	0.6784	0.0219	1.2660
0.1435	0.1114	0.7762	0.0266	1.1266

	0.1550	0.1004	0.6474	0.0208	1.3373
	0.1610	0.1095	0.6800	0.0249	1.2667
	0.1612	0.1101	0.6829	0.0190	1.2610
	0.1548	0.0870	0.5620	0.0108	1.5408
	0.1653	0.1003	0.6065	0.0087	1.4149
	0.1986	0.1327	0.6683	0.0139	1.2485
Average	0.1584	0.1018	0.6420	0.0195	1.3585
STDEV	0.0150	0.0150	0.0640	0.0061	0.1388

Table E-4 Limestone blended mortar with 17%GL and 25%FA

mortar 17%GL + 25%FA				
Al/Si	**Al/Ca**	**Si/Ca**	**S/Ca**	**Ca/(Si+Al)**
0.1454	0.1037	0.7131	0.0217	1.2244
0.1476	0.0962	0.6518	0.0137	1.3368
0.1511	0.1045	0.6920	0.0189	1.2554
0.1726	0.1283	0.7435	0.0191	1.1471
0.1430	0.1100	0.7697	0.0112	1.1367
0.1679	0.1160	0.6906	0.0096	1.2398
0.1798	0.1283	0.7135	0.0165	1.1880
0.1425	0.0936	0.6568	0.0114	1.3327
0.1705	0.1263	0.7406	0.0255	1.1535
0.1469	0.1094	0.7449	0.0238	1.1706
0.1679	0.1253	0.7458	0.0245	1.1481
0.1365	0.0884	0.6477	0.0096	1.3584
0.1674	0.1252	0.7474	0.0100	1.1460
0.1636	0.1173	0.7169	0.0090	1.1988
0.1416	0.0839	0.5927	0.0035	1.4780
0.1574	0.1074	0.6821	0.0228	1.2666
0.1527	0.1020	0.6681	0.0184	1.2986
0.1718	0.0920	0.5356	0.0080	1.5933
0.1604	0.1046	0.6520	0.0253	1.3217
0.1771	0.1132	0.6396	0.0254	1.3284
0.1990	0.1393	0.7000	0.0087	1.1914
0.1896	0.1426	0.7521	0.0152	1.1176
0.1528	0.0839	0.5490	0.0138	1.5802
0.1767	0.1336	0.7562	0.0241	1.1239
0.1474	0.0994	0.6745	0.0170	1.2921
0.1738	0.1266	0.7280	0.0240	1.1702
0.1653	0.0994	0.6015	0.0218	1.4266
0.1616	0.0963	0.5956	0.0053	1.4454
0.1613	0.1071	0.6640	0.0141	1.2969
0.1709	0.1263	0.7388	0.0188	1.1560
0.1718	0.1093	0.6361	0.0203	1.3415
0.1743	0.1171	0.6720	0.0252	1.2672
0.1484	0.0759	0.5111	0.0118	1.7035

0.1725	0.1355	0.7856	0.0176	1.0856
0.1720	0.1149	0.6680	0.0180	1.2773
0.1708	0.0991	0.5804	0.0059	1.4716
0.1836	0.1404	0.7648	0.0203	1.1047
0.1896	0.1113	0.5870	0.0100	1.4320
0.1469	0.0885	0.6024	0.0123	1.4475
0.1333	0.0755	0.5665	0.0121	1.5577
0.1368	0.0817	0.5975	0.0178	1.4723
0.1494	0.0884	0.5917	0.0060	1.4703
0.1590	0.1192	0.7495	0.0200	1.1511
0.1444	0.0856	0.5927	0.0081	1.4743
0.1562	0.1221	0.7816	0.0219	1.1065
0.1541	0.0984	0.6387	0.0133	1.3567
0.1657	0.1213	0.7319	0.0069	1.1720
0.1680	0.1137	0.6766	0.0113	1.2654
0.1976	0.1296	0.6559	0.0170	1.2731
0.1559	0.0900	0.5771	0.0149	1.4990
0.1707	0.0957	0.5606	0.0217	1.5238
0.1478	0.0952	0.6438	0.0164	1.3533
0.1521	0.1051	0.6911	0.0196	1.2559
0.1469	0.1009	0.6866	0.0247	1.2699
0.1544	0.0842	0.5449	0.0023	1.5897
0.1983	0.1524	0.7686	0.0107	1.0858
0.1598	0.1229	0.7689	0.0103	1.1214
0.1906	0.1254	0.6581	0.0114	1.2763
0.1565	0.1108	0.7077	0.0120	1.2218
0.1966	0.1083	0.5509	0.0067	1.5170
0.1618	0.1023	0.6322	0.0071	1.3616
0.1954	0.1468	0.7513	0.0098	1.1135
0.1813	0.1315	0.7251	0.0156	1.1674
0.1816	0.1096	0.6035	0.0069	1.4023
0.1851	0.1124	0.6072	0.0088	1.3897
0.1468	0.0974	0.6637	0.0054	1.3139
0.1455	0.1020	0.7011	0.0229	1.2451
0.1707	0.1054	0.6173	0.0143	1.3837
0.1515	0.1079	0.7125	0.0165	1.2189
0.1649	0.0933	0.5657	0.0100	1.5174
0.1817	0.1197	0.6584	0.0131	1.2853
0.1539	0.0917	0.5957	0.0064	1.4549
0.1804	0.1302	0.7216	0.0113	1.1741
0.1775	0.1120	0.6308	0.0138	1.3462
0.1612	0.0973	0.6036	0.0193	1.4269
0.1923	0.1274	0.6627	0.0268	1.2656
0.1537	0.1199	0.7802	0.0105	1.1111
0.1617	0.1253	0.7749	0.0167	1.1109
0.1642	0.0940	0.5723	0.0043	1.5009

0.1461	0.0826	0.5652	0.0082	1.5437
0.1787	0.1277	0.7143	0.0141	1.1877
0.1848	0.1423	0.7700	0.0384	1.0962
0.1547	0.1114	0.7202	0.0215	1.2025
0.1825	0.1261	0.6911	0.0149	1.2237
0.1864	0.1032	0.5536	0.0021	1.5226
0.1770	0.1067	0.6031	0.0108	1.4087
0.1593	0.1092	0.6854	0.0186	1.2585
0.1738	0.1231	0.7081	0.0075	1.2031
0.1301	0.0669	0.5147	0.0007	1.7192
0.1799	0.1276	0.7089	0.0180	1.1956
0.1542	0.1112	0.7215	0.0146	1.2008
0.1496	0.0808	0.5402	0.0059	1.6104
0.1473	0.0970	0.6586	0.0162	1.3235
0.1427	0.0863	0.6044	0.0069	1.4479
0.1421	0.0986	0.6935	0.0133	1.2625
0.1703	0.1078	0.6332	0.0127	1.3494
0.1983	0.1489	0.7512	0.0153	1.1109
0.1888	0.1433	0.7590	0.0171	1.1083
0.1582	0.0845	0.5340	0.0174	1.6167
0.1311	0.0716	0.5461	0.0201	1.6189
0.1488	0.0889	0.5977	0.0089	1.4564
0.1722	0.1269	0.7371	0.0141	1.1574
0.1609	0.1050	0.6522	0.0115	1.3207
0.1723	0.1045	0.6065	0.0087	1.4065
0.1806	0.1167	0.6462	0.0115	1.3108
0.1663	0.1129	0.6790	0.0133	1.2628
0.1538	0.0980	0.6368	0.0173	1.3610
0.1572	0.0855	0.5438	0.0184	1.5890
0.1640	0.0984	0.6001	0.0152	1.4315
0.1680	0.1038	0.6179	0.0206	1.3857
0.1381	0.0735	0.5319	0.0140	1.6518
0.1694	0.1130	0.6673	0.0104	1.2816
0.1585	0.1150	0.7254	0.0212	1.1899
0.1519	0.0934	0.6147	0.0071	1.4123
0.1578	0.1007	0.6380	0.0137	1.3537
0.1376	0.0801	0.5821	0.0068	1.5103
0.1680	0.1209	0.7197	0.0162	1.1896
0.1623	0.1091	0.6721	0.0165	1.2801
0.1822	0.1303	0.7155	0.0106	1.1823
0.1703	0.1090	0.6400	0.0101	1.3352
0.1707	0.0948	0.5554	0.0065	1.5379
0.1531	0.1010	0.6593	0.0118	1.3154
0.1652	0.0999	0.6046	0.0040	1.4196
0.1938	0.1428	0.7370	0.0173	1.1365
0.1755	0.1195	0.6810	0.0082	1.2492

0.1576	0.0950	0.6031	0.0058	1.4323
0.1573	0.1161	0.7386	0.0108	1.1699
0.1692	0.1011	0.5978	0.0058	1.4306
0.1975	0.1273	0.6446	0.0061	1.2956
0.1893	0.1061	0.5602	0.0099	1.5010
0.1862	0.1288	0.6919	0.0286	1.2185
0.1875	0.1340	0.7146	0.0214	1.1784
0.1965	0.1211	0.6162	0.0133	1.3563
0.1701	0.0953	0.5603	0.0116	1.5253
0.1564	0.0889	0.5688	0.0143	1.5204
0.1483	0.0812	0.5476	0.0110	1.5902
0.1685	0.1190	0.7064	0.0174	1.2115
0.1686	0.1196	0.7091	0.0271	1.2067
0.1901	0.1284	0.6752	0.0098	1.2445
0.1793	0.1400	0.7810	0.0127	1.0858
0.1837	0.1348	0.7338	0.0112	1.1513
0.1629	0.1225	0.7523	0.0119	1.1431
0.1714	0.1354	0.7901	0.0128	1.0805
0.1664	0.1143	0.6872	0.0096	1.2476
0.1671	0.0907	0.5427	0.0000	1.5788
0.1709	0.1237	0.7240	0.0120	1.1796
0.1585	0.0892	0.5628	0.0043	1.5339
0.1569	0.0828	0.5279	0.0110	1.6373
0.1689	0.1025	0.6071	0.0126	1.4093
0.1766	0.1311	0.7426	0.0259	1.1445
0.1376	0.0745	0.5414	0.0138	1.6237
0.1583	0.1025	0.6475	0.0249	1.3333
0.1695	0.1053	0.6211	0.0106	1.3767
0.1686	0.0906	0.5373	0.0037	1.5925
0.1557	0.1179	0.7570	0.0088	1.1430
0.1660	0.1228	0.7396	0.0101	1.1595
0.1586	0.0888	0.5599	0.0119	1.5417
0.1597	0.0986	0.6174	0.0137	1.3966
0.1498	0.0851	0.5680	0.0092	1.5313
0.1458	0.0803	0.5507	0.0118	1.5848
0.1971	0.1226	0.6220	0.0136	1.3431
0.1599	0.1180	0.7377	0.0086	1.1687
0.1670	0.1281	0.7672	0.0141	1.1169
0.1705	0.1232	0.7226	0.0173	1.1823
0.1278	0.0721	0.5639	0.0107	1.5724
0.1548	0.0983	0.6351	0.0083	1.3634
0.1422	0.0919	0.6462	0.0028	1.3548
0.1475	0.0859	0.5828	0.0129	1.4953
0.1339	0.0777	0.5806	0.0109	1.5190
0.1968	0.1136	0.5772	0.0138	1.4476
0.1822	0.1299	0.7128	0.0159	1.1868

0.1684	0.1253	0.7444	0.0122	1.1498
0.1559	0.0964	0.6184	0.0111	1.3990
0.1640	0.1094	0.6671	0.0082	1.2879
0.1620	0.1078	0.6652	0.0154	1.2936
0.1645	0.1068	0.6493	0.0174	1.3226
0.1665	0.1233	0.7403	0.0134	1.1580
0.1803	0.1271	0.7049	0.0117	1.2021
0.1536	0.0976	0.6354	0.0095	1.3643
0.1517	0.0891	0.5871	0.0141	1.4790
0.1392	0.0813	0.5836	0.0118	1.5040
0.1973	0.1118	0.5667	0.0217	1.4738
0.1614	0.1102	0.6831	0.0183	1.2605
0.1801	0.1043	0.5788	0.0215	1.4639
0.1585	0.1118	0.7053	0.0109	1.2239
0.1399	0.0741	0.5299	0.0068	1.6557
0.1595	0.0896	0.5617	0.0089	1.5355
0.1834	0.1317	0.7182	0.0153	1.1766
0.1413	0.0953	0.6749	0.0157	1.2984
0.1437	0.1088	0.7569	0.0119	1.1551
0.1507	0.0846	0.5616	0.0008	1.5476
0.1597	0.0952	0.5961	0.0092	1.4466
0.1438	0.0850	0.5911	0.0116	1.4791
0.1571	0.1005	0.6398	0.0127	1.3507
0.1698	0.0997	0.5874	0.0098	1.4554
0.1493	0.1002	0.6709	0.0053	1.2968
0.1853	0.1375	0.7423	0.0118	1.1366
0.1458	0.0987	0.6769	0.0097	1.2892
0.1522	0.1099	0.7218	0.0206	1.2024
0.1616	0.1148	0.7104	0.0150	1.2119
0.1730	0.1141	0.6596	0.0065	1.2925
0.1431	0.0944	0.6601	0.0098	1.3253
0.1595	0.1009	0.6327	0.0040	1.3632
0.1860	0.1311	0.7050	0.0122	1.1960
0.1400	0.0895	0.6392	0.0038	1.3722
0.1905	0.1496	0.7854	0.0318	1.0695
0.1667	0.1145	0.6866	0.0163	1.2482
0.1512	0.0807	0.5339	0.0105	1.6271
0.1881	0.1418	0.7538	0.0162	1.1166
0.1912	0.1194	0.6244	0.0180	1.3444
0.1506	0.1071	0.7110	0.0081	1.2223
0.1576	0.1260	0.7998	0.0167	1.0801
0.1503	0.0897	0.5966	0.0055	1.4571
0.1413	0.0913	0.6461	0.0081	1.3562
0.1795	0.1333	0.7424	0.0119	1.1419
0.1727	0.1296	0.7502	0.0187	1.1367
0.1578	0.1132	0.7171	0.0124	1.2044

	0.1611	0.1054	0.6542	0.0180	1.3165
	0.1648	0.1013	0.6145	0.0179	1.3970
	0.1866	0.1212	0.6494	0.0192	1.2977
	0.1581	0.1181	0.7472	0.0181	1.1556
	0.1729	0.1108	0.6407	0.0044	1.3308
	0.1622	0.1058	0.6521	0.0124	1.3193
	0.1601	0.1103	0.6885	0.0191	1.2520
	0.1554	0.1156	0.7438	0.0123	1.1636
	0.1701	0.1156	0.6799	0.0103	1.2571
	0.1680	0.0924	0.5503	0.0096	1.5558
	0.1752	0.1114	0.6362	0.0143	1.3375
	0.1619	0.1115	0.6886	0.0129	1.2499
	0.1638	0.1061	0.6481	0.0138	1.3259
	0.1725	0.1183	0.6858	0.0150	1.2436
	0.1509	0.1072	0.7101	0.0101	1.2235
	0.1738	0.1227	0.7060	0.0228	1.2067
	0.1678	0.1166	0.6946	0.0178	1.2328
	0.1666	0.1265	0.7597	0.0183	1.1284
	0.1621	0.0985	0.6078	0.0197	1.4159
	0.1492	0.0936	0.6271	0.0207	1.3876
	0.1634	0.1255	0.7683	0.0159	1.1188
	0.1672	0.0834	0.4988	0.0028	1.7176
Average	0.1643	0.1084	0.6578	0.0135	1.3226
STDEV	0.0157	0.0176	0.0716	0.0060	0.1543

Table E-5 Limestone blended mortar with 0%GL and 65%SL

mortar 0%GL + 65%SL				
Al/Si	**Al/Ca**	**Si/Ca**	**S/Ca**	**Ca/(Si+Al)**
0.1970	0.1203	0.6107	0.0167	1.3680
0.2040	0.1382	0.6778	0.0198	1.2255
0.2356	0.1522	0.6459	0.0237	1.2529
0.1942	0.1138	0.5862	0.0202	1.4285
0.2023	0.1479	0.7308	0.0224	1.1380
0.1963	0.1262	0.6430	0.0140	1.3000
0.2324	0.1639	0.7052	0.0253	1.1507
0.2061	0.1398	0.6786	0.0255	1.2219
0.1999	0.1302	0.6511	0.0182	1.2799
0.2866	0.1831	0.6389	0.0213	1.2166
0.2071	0.1134	0.5474	0.0172	1.5133
0.2337	0.1328	0.5680	0.0201	1.4271
0.2011	0.1413	0.7025	0.0241	1.1852
0.1854	0.1264	0.6815	0.0182	1.2378
0.1870	0.1279	0.6837	0.0107	1.2322
0.2227	0.1266	0.5684	0.0095	1.4389
0.1905	0.1198	0.6289	0.0166	1.3357

0.2214	0.1493	0.6741	0.0145	1.2145
0.1950	0.1322	0.6781	0.0095	1.2341
0.2860	0.1492	0.5218	0.0188	1.4901
0.2026	0.1647	0.8126	0.0225	1.0233
0.1935	0.1470	0.7596	0.0213	1.1029
0.1860	0.1262	0.6783	0.0141	1.2431
0.2002	0.1653	0.8257	0.0224	1.0090
0.2024	0.1321	0.6526	0.0166	1.2744
0.2376	0.1242	0.5226	0.0135	1.5461
0.2540	0.1879	0.7398	0.0272	1.0779
0.2171	0.1482	0.6827	0.0182	1.2034
0.2868	0.1972	0.6877	0.0392	1.1300
0.2076	0.1289	0.6209	0.0114	1.3339
0.2300	0.1845	0.8022	0.0275	1.0135
0.1893	0.1494	0.7891	0.0196	1.0655
0.2113	0.1553	0.7349	0.0180	1.1234
0.2214	0.1524	0.6884	0.0163	1.1893
0.2388	0.1729	0.7242	0.0194	1.1146
0.2581	0.1673	0.6483	0.0321	1.2260
0.2745	0.1810	0.6593	0.0361	1.1901
0.2869	0.1829	0.6375	0.0338	1.2190
0.2341	0.1591	0.6799	0.0290	1.1918
0.1913	0.1209	0.6322	0.0157	1.3278
0.1977	0.1381	0.6983	0.0251	1.1957
0.2130	0.1477	0.6935	0.0207	1.1888
0.2026	0.1351	0.6668	0.0201	1.2470
0.1862	0.1440	0.7735	0.0253	1.0899
0.1892	0.1101	0.5820	0.0137	1.4450
0.2066	0.1486	0.7192	0.0352	1.1523
0.2276	0.1462	0.6423	0.0268	1.2684
0.2157	0.1379	0.6392	0.0260	1.2868
0.2176	0.1462	0.6718	0.0312	1.2225
0.2630	0.1539	0.5850	0.0293	1.3534
0.1851	0.1484	0.8015	0.0167	1.0527
0.1767	0.1302	0.7367	0.0112	1.1536
0.1950	0.1318	0.6760	0.0139	1.2379
0.2063	0.1334	0.6465	0.0157	1.2822
0.1788	0.1154	0.6452	0.0103	1.3149
0.2196	0.1865	0.8491	0.0224	0.9656
0.1907	0.1448	0.7594	0.0202	1.1060
0.1985	0.1629	0.8209	0.0241	1.0165
0.1986	0.1485	0.7477	0.0229	1.1159
0.2240	0.1571	0.7014	0.0204	1.1647
0.1859	0.1571	0.8450	0.0246	0.9980
0.1909	0.1193	0.6250	0.0120	1.3435
0.1962	0.1303	0.6639	0.0123	1.2591

0.2186	0.1488	0.6807	0.0139	1.2056
0.1866	0.1217	0.6522	0.0183	1.2922
0.2410	0.1898	0.7874	0.0265	1.0233
0.1997	0.1555	0.7789	0.0196	1.0702
0.1848	0.1357	0.7340	0.0177	1.1499
0.2070	0.1400	0.6765	0.0189	1.2248
0.2749	0.1887	0.6864	0.0252	1.1428
0.1778	0.1320	0.7425	0.0231	1.1434
0.2009	0.1585	0.7889	0.0232	1.0555
0.1991	0.1426	0.7159	0.0202	1.1649
0.2415	0.1329	0.5502	0.0123	1.4639
0.1876	0.1157	0.6164	0.0166	1.3660
0.2284	0.1790	0.7838	0.0175	1.0387
0.1815	0.1209	0.6660	0.0183	1.2709
0.1791	0.1131	0.6318	0.0069	1.3424
0.2371	0.1688	0.7118	0.0140	1.1356
0.2780	0.1752	0.6303	0.0166	1.2414
0.2136	0.1624	0.7604	0.0255	1.0836
0.1822	0.1422	0.7804	0.0201	1.0839
0.1807	0.1337	0.7403	0.0197	1.1442
0.1876	0.1339	0.7135	0.0165	1.1801
0.2138	0.1629	0.7620	0.0214	1.0811
0.2083	0.1326	0.6367	0.0174	1.2998
0.2119	0.1267	0.5980	0.0097	1.3799
0.2199	0.1478	0.6721	0.0187	1.2197
0.2504	0.1522	0.6076	0.0142	1.3162
0.2985	0.1760	0.5895	0.0199	1.3064
0.1894	0.1326	0.7002	0.0186	1.2007
0.2488	0.1701	0.6839	0.0161	1.1709
0.1990	0.1495	0.7514	0.0163	1.1100
0.1886	0.1485	0.7872	0.0177	1.0687
0.2953	0.2087	0.7066	0.0364	1.0925
0.2042	0.1632	0.7991	0.0270	1.0391
0.2167	0.1463	0.6754	0.0202	1.2170
0.1901	0.1333	0.7014	0.0199	1.1979
0.2979	0.1772	0.5948	0.0391	1.2954
0.1945	0.1346	0.6921	0.0155	1.2096
0.2798	0.1973	0.7050	0.0240	1.1084
0.2643	0.1626	0.6152	0.0196	1.2856
0.2282	0.1777	0.7788	0.0222	1.0454
0.2026	0.1204	0.5945	0.0061	1.3987
0.2635	0.1934	0.7340	0.0278	1.0782
0.2339	0.1947	0.8326	0.0218	0.9734
0.2623	0.1726	0.6579	0.0212	1.2041
0.2388	0.1258	0.5267	0.0114	1.5327
0.2330	0.1543	0.6624	0.0229	1.2244

0.2659	0.1653	0.6217	0.0225	1.2707
0.2522	0.1730	0.6857	0.0167	1.1645
0.2132	0.1560	0.7316	0.0130	1.1267
0.2251	0.1731	0.7690	0.0164	1.0614
0.2098	0.1393	0.6641	0.0129	1.2447
0.2221	0.1778	0.8005	0.0252	1.0222
0.1936	0.1297	0.6698	0.0086	1.2508
0.2542	0.1855	0.7295	0.0187	1.0930
0.1924	0.1332	0.6922	0.0153	1.2116
0.2926	0.1967	0.6724	0.0258	1.1505
0.1812	0.0959	0.5292	0.0087	1.5997
0.2034	0.1565	0.7694	0.0264	1.0801
0.2234	0.1387	0.6208	0.0188	1.3167
0.2534	0.1465	0.5782	0.0180	1.3798
0.1812	0.1294	0.7140	0.0247	1.1857
0.1751	0.1090	0.6224	0.0182	1.3672
0.1730	0.0925	0.5345	0.0086	1.5949
0.2401	0.1716	0.7148	0.0435	1.1281
0.2446	0.1755	0.7175	0.0199	1.1198
0.2731	0.1759	0.6441	0.0147	1.2195
0.2038	0.1706	0.8374	0.0253	0.9920
0.2025	0.1450	0.7164	0.0238	1.1609
0.2438	0.1769	0.7255	0.0258	1.1082
0.2145	0.1363	0.6356	0.0271	1.2955
0.2204	0.1557	0.7064	0.0220	1.1598
0.2465	0.1898	0.7699	0.0376	1.0420
0.2351	0.1576	0.6704	0.0198	1.2078
0.2267	0.1707	0.7530	0.0242	1.0826
0.1974	0.1267	0.6420	0.0150	1.3009
0.1888	0.1048	0.5552	0.0112	1.5152
0.2115	0.1570	0.7425	0.0212	1.1116
0.2299	0.1424	0.6194	0.0149	1.3126
0.2007	0.1562	0.7782	0.0295	1.0703
0.2000	0.1415	0.7077	0.0268	1.1775
0.2113	0.1383	0.6543	0.0241	1.2617
0.1756	0.1414	0.8052	0.0317	1.0565
0.1756	0.1369	0.7800	0.0236	1.0906
0.1674	0.1243	0.7422	0.0306	1.1541
0.1812	0.1383	0.7637	0.0214	1.1086
0.2475	0.1922	0.7767	0.0276	1.0320
0.1587	0.1098	0.6914	0.0131	1.2482
0.1995	0.1530	0.7671	0.0331	1.0868
0.1945	0.1431	0.7355	0.0236	1.1382
0.1650	0.1171	0.7096	0.0189	1.2097
0.1929	0.1429	0.7407	0.0264	1.1318
0.1852	0.1428	0.7707	0.0228	1.0947

	0.1888	0.1456	0.7709	0.0159	1.0912
	0.1912	0.1568	0.8201	0.0221	1.0237
	0.2574	0.1799	0.6987	0.0137	1.1382
	0.1961	0.1150	0.5865	0.0164	1.4255
	0.2424	0.2030	0.8375	0.0296	0.9611
	0.2311	0.1615	0.6990	0.0132	1.1621
	0.2518	0.1454	0.5776	0.0141	1.3831
	0.2152	0.1347	0.6257	0.0125	1.3152
	0.2964	0.1742	0.5878	0.0175	1.3122
	0.2359	0.1661	0.7042	0.0204	1.1491
	0.2177	0.1833	0.8422	0.0288	0.9751
	0.2028	0.1251	0.6167	0.0123	1.3482
	0.2055	0.1597	0.7771	0.0323	1.0675
	0.2382	0.1328	0.5576	0.0351	1.4484
	0.2815	0.1927	0.6844	0.0285	1.1401
	0.2760	0.2262	0.8195	0.0675	0.9563
	0.2614	0.1539	0.5886	0.0233	1.3469
	0.2465	0.1507	0.6112	0.0340	1.3126
	0.2934	0.1560	0.5317	0.0454	1.4540
	0.1985	0.1184	0.5964	0.0302	1.3989
	0.2213	0.1345	0.6080	0.0413	1.3467
	0.2150	0.1580	0.7347	0.0354	1.1203
	0.2283	0.1448	0.6342	0.0218	1.2838
	0.2071	0.1373	0.6629	0.0218	1.2497
	0.2097	0.1464	0.6983	0.0219	1.1838
	0.2720	0.1603	0.5896	0.0317	1.3335
	0.2281	0.1219	0.5344	0.0246	1.5238
	0.2869	0.1850	0.6448	0.0285	1.2051
	0.2220	0.1501	0.6762	0.0358	1.2102
	0.1990	0.1094	0.5496	0.0208	1.5176
	0.1998	0.1044	0.5225	0.0256	1.5953
	0.2075	0.1511	0.7283	0.0353	1.1371
	0.2014	0.1196	0.5941	0.0319	1.4010
	0.1996	0.1153	0.5779	0.0314	1.4426
	0.1871	0.1062	0.5677	0.0276	1.4838
	0.2111	0.1518	0.7190	0.0155	1.1484
	0.2381	0.1308	0.5496	0.0229	1.4697
	0.2459	0.1747	0.7107	0.0179	1.1294
	0.2467	0.1621	0.6574	0.0114	1.2202
	0.2761	0.2005	0.7261	0.0199	1.0792
	0.2827	0.2123	0.7512	0.0480	1.0379
	0.2947	0.1997	0.6776	0.0295	1.1398
	0.2067	0.1708	0.8265	0.0255	1.0027
	0.2154	0.1613	0.7486	0.0194	1.0991
Average	0.2195	0.1499	0.6854	0.0219	1.2128
STDEV	0.0323	0.0247	0.0781	0.0082	0.1406

Table E-6 Limestone blended mortar with 17%GL and 65%SL

mortar 17%GL + 65% SL				
Al/Si	**Al/Ca**	**Si/Ca**	**S/Ca**	**Ca/(Si+Al)**
0.2624	0.1593	0.6070	0.0463	1.3050
0.2228	0.1457	0.6542	0.0299	1.2500
0.2776	0.2000	0.7207	0.0251	1.0861
0.2072	0.1254	0.6052	0.0156	1.3687
0.2080	0.1609	0.7736	0.0282	1.0700
0.2460	0.1389	0.5647	0.0181	1.4212
0.1958	0.1226	0.6264	0.0215	1.3350
0.2003	0.1123	0.5606	0.0230	1.4861
0.2068	0.1500	0.7255	0.0293	1.1422
0.2553	0.1739	0.6809	0.0323	1.1699
0.2305	0.1418	0.6155	0.0214	1.3205
0.2251	0.1636	0.7268	0.0351	1.1230
0.2267	0.1674	0.7383	0.0292	1.1041
0.2115	0.1113	0.5261	0.0214	1.5688
0.2648	0.1909	0.7210	0.0482	1.0966
0.2131	0.1544	0.7243	0.0346	1.1381
0.2066	0.1271	0.6154	0.0175	1.3468
0.2290	0.1197	0.5226	0.0161	1.5571
0.2364	0.1669	0.7059	0.0330	1.1457
0.2090	0.1204	0.5760	0.0204	1.4361
0.2904	0.1726	0.5944	0.0388	1.3037
0.2581	0.1527	0.5917	0.0392	1.3432
0.2609	0.1820	0.6975	0.0331	1.1370
0.2574	0.1762	0.6846	0.0267	1.1616
0.2617	0.1751	0.6690	0.0222	1.1847
0.2107	0.1088	0.5163	0.0283	1.5997
0.2244	0.1722	0.7676	0.0352	1.0640
0.2134	0.1224	0.5736	0.0251	1.4368
0.2016	0.1380	0.6845	0.0294	1.2157
0.2358	0.1406	0.5961	0.0204	1.3574
0.2664	0.1877	0.7046	0.0336	1.1208
0.2370	0.1576	0.6649	0.0247	1.2158
0.2239	0.1509	0.6739	0.0260	1.2124
0.2999	0.2198	0.7327	0.0299	1.0500
0.2533	0.1314	0.5186	0.0221	1.5386
0.2294	0.1292	0.5631	0.0163	1.4446
0.2639	0.1518	0.5750	0.0270	1.3759
0.2604	0.1646	0.6321	0.0274	1.2551
0.2247	0.1682	0.7487	0.0365	1.0906
0.2492	0.1813	0.7273	0.0316	1.1007
0.2434	0.1802	0.7402	0.0341	1.0864

0.2139	0.1458	0.6816	0.0187	1.2087
0.2598	0.1495	0.5753	0.0210	1.3798
0.2475	0.1768	0.7141	0.0263	1.1225
0.2176	0.1511	0.6946	0.0230	1.1824
0.2543	0.1798	0.7071	0.0256	1.1275
0.2355	0.1590	0.6753	0.0185	1.1985
0.2575	0.1542	0.5987	0.0150	1.3282
0.2272	0.1635	0.7197	0.0261	1.1322
0.2071	0.1156	0.5584	0.0155	1.4837
0.2031	0.1490	0.7336	0.0259	1.1330
0.2096	0.1561	0.7445	0.0277	1.1104
0.1921	0.1156	0.6015	0.0252	1.3944
0.2010	0.1517	0.7544	0.0275	1.1037
0.2094	0.1594	0.7612	0.0273	1.0862
0.2314	0.1659	0.7168	0.0241	1.1329
0.2221	0.1528	0.6879	0.0265	1.1895
0.1837	0.1088	0.5921	0.0120	1.4267
0.1871	0.1330	0.7108	0.0198	1.1851
0.2082	0.1171	0.5622	0.0114	1.4721
0.2171	0.1286	0.5921	0.0112	1.3876
0.2809	0.2174	0.7741	0.0255	1.0085
0.1977	0.1236	0.6254	0.0106	1.3350
0.1991	0.1430	0.7180	0.0183	1.1615
0.2265	0.1713	0.7563	0.0340	1.0780
0.2153	0.1564	0.7265	0.0235	1.1327
0.2266	0.1807	0.7974	0.0273	1.0224
0.2562	0.1600	0.6247	0.0214	1.2743
0.2245	0.1528	0.6806	0.0215	1.1998
0.2256	0.1269	0.5628	0.0189	1.4499
0.2353	0.1470	0.6249	0.0221	1.2954
0.2385	0.1658	0.6951	0.0313	1.1617
0.2180	0.1499	0.6875	0.0239	1.1941
0.2190	0.1534	0.7008	0.0192	1.1707
0.2120	0.1608	0.7587	0.0185	1.0875
0.2207	0.1611	0.7296	0.0194	1.1227
0.2057	0.1454	0.7069	0.0163	1.1733
0.2061	0.1623	0.7877	0.0181	1.0526
0.2981	0.2125	0.7130	0.0318	1.0805
0.2428	0.1839	0.7574	0.0257	1.0623
0.2389	0.1681	0.7039	0.0199	1.1468
0.2540	0.1581	0.6226	0.0197	1.2809
0.2391	0.1422	0.5946	0.0162	1.3572
0.2303	0.1339	0.5814	0.0139	1.3981
0.2198	0.1308	0.5953	0.0131	1.3771
0.2615	0.2078	0.7947	0.0287	0.9975
0.2597	0.1490	0.5738	0.0130	1.3834

0.2405	0.1814	0.7542	0.0272	1.0689
0.2689	0.1937	0.7204	0.0230	1.0939
0.2386	0.1831	0.7674	0.0269	1.0521
0.2437	0.1761	0.7227	0.0279	1.1125
0.2377	0.1507	0.6339	0.0165	1.2746
0.2563	0.1736	0.6774	0.0182	1.1752
0.2533	0.1455	0.5746	0.0198	1.3886
0.2723	0.1667	0.6124	0.0227	1.2835
0.2415	0.1523	0.6307	0.0226	1.2772
0.2377	0.1724	0.7254	0.0317	1.1138
0.1969	0.1273	0.6465	0.0218	1.2922
0.2283	0.1141	0.5000	0.0220	1.6282
0.2067	0.1302	0.6299	0.0227	1.3157
0.1877	0.1332	0.7098	0.0245	1.1863
0.2005	0.1539	0.7675	0.0272	1.0853
0.2662	0.1740	0.6536	0.0220	1.2083
0.2151	0.1333	0.6199	0.0392	1.3275
0.2348	0.1835	0.7812	0.0260	1.0366
0.2227	0.1673	0.7511	0.0255	1.0889
0.2715	0.2167	0.7982	0.0212	0.9853
0.2425	0.1748	0.7211	0.0242	1.1162
0.2245	0.1763	0.7855	0.0249	1.0397
0.2232	0.1564	0.7008	0.0199	1.1666
0.2443	0.1529	0.6258	0.0142	1.2841
0.2160	0.1442	0.6678	0.0140	1.2314
0.2045	0.1392	0.6807	0.0098	1.2196
0.1927	0.1161	0.6027	0.0094	1.3911
0.1896	0.1407	0.7421	0.0168	1.1328
0.1770	0.1068	0.6034	0.0075	1.4082
0.1960	0.1289	0.6574	0.0102	1.2718
0.2015	0.1122	0.5571	0.0082	1.4941
0.1869	0.1159	0.6203	0.0038	1.3582
0.1874	0.0967	0.5160	0.0085	1.6323
0.2124	0.1362	0.6410	0.0164	1.2867
0.1988	0.1238	0.6229	0.0113	1.3392
0.1798	0.1344	0.7472	0.0186	1.1344
0.1708	0.1056	0.6183	0.0101	1.3813
0.2585	0.1597	0.6178	0.0150	1.2862
0.1772	0.1049	0.5921	0.0125	1.4346
0.1972	0.1241	0.6293	0.0142	1.3273
0.1957	0.1493	0.7626	0.0156	1.0966
0.2038	0.1089	0.5343	0.0111	1.5546
0.2131	0.1207	0.5666	0.0108	1.4550
0.2046	0.1265	0.6183	0.0095	1.3427
0.1910	0.1411	0.7388	0.0184	1.1365
0.1982	0.1231	0.6209	0.0073	1.3441

	0.1929	0.0983	0.5094	0.0126	1.6455
	0.1808	0.1253	0.6930	0.0169	1.2220
	0.1708	0.0994	0.5820	0.0146	1.4674
	0.1853	0.1422	0.7676	0.0207	1.0991
	0.2016	0.1443	0.7156	0.0189	1.1629
	0.2143	0.1352	0.6306	0.0168	1.3059
	0.1944	0.1286	0.6614	0.0196	1.2659
	0.1821	0.0987	0.5422	0.0130	1.5603
	0.2240	0.1655	0.7386	0.0286	1.1061
	0.2114	0.1180	0.5579	0.0151	1.4795
	0.2413	0.1594	0.6604	0.0212	1.2198
	0.1766	0.1157	0.6554	0.0160	1.2968
	0.1828	0.1209	0.6612	0.0202	1.2787
	0.1855	0.1185	0.6387	0.0108	1.3208
	0.1687	0.1226	0.7266	0.0204	1.1775
	0.1730	0.1273	0.7357	0.0173	1.1587
	0.2307	0.1552	0.6729	0.0250	1.2075
	0.2062	0.1470	0.7128	0.0184	1.1631
	0.1979	0.1495	0.7558	0.0220	1.1046
	0.1872	0.1094	0.5845	0.0148	1.4410
Average	0.2226	0.1480	0.6640	0.0217	1.2490
STDEV	0.0282	0.0262	0.0740	0.0078	0.1510